The ecotoxicological and environmental behaviour and transformations of silver nanoparticles

By

Isabella Romer Roche

School of Geography, Earth and Environmental Sciences

College of Life and Environmental Sciences

The University of Birmingham, UK

September 2012

Abstract

Silver nanoparticles (AgNPs) are currently widely used and of special interest due to their anti-microbial properties. They have been used extensively in commercial applications in cosmetics and as bacteriocides in fabrics and other consumer products and they also show great potential in medicine and health-related areas. AgNPs might be the most worrying of the manufactured nanoparticles because of their inherent toxicity and the many different consumer products used will undoubtedly lead to wide exposure in the environment.

Synthesizing silver nanoparticles that are both uniform and stable and to be able to control their size distribution is a difficult task. Citrate reduction is a widely used method, but the nanoparticles synthesized with it have a broad size distribution and different morphologies. Coating the NP surface with layers of neutral organic molecules can efficiently protect them from aggregation by steric repulsion. Monodisperse and stable AgNPs, with citrate and PEG as capping agents, of three different sizes (7, 10 and 20nm) have been synthesised and fully characterised (using DLS, AFM, UV-Vis, FFF, TEM, and a range of other methods).

Once released into the environment, the mobility, bioavailability, and toxicity of AgNPs in any ecosystem are dominated by colloidal stability. There have been studies on the stability or the aggregation of various NPs under a range of environmental conditions, but there is little information on fully characterised AgNPs in media used in (eco) toxicity studies.

Stability of AgNPs (7, 10 and 20nm citrate capped) was assessed over 24 or 48 hours or 21 days (similar time periods to acute and chronic OECD tests) in different dilutions of media recommended by OECD for *Daphnia magna* toxicity testing. The particles aggregated quickly in the media. After diluting the media by a factor of 2, 5 or 10, aggregation was reduced, although the smallest NPs were unstable under all media conditions. Media diluted up to 10-fold in the absence of AgNPs did not induce any loss of either viability or mobility in the daphnids. A brief range finding experiment in a 10-fold dilution of the media indicated the concentration at which 7nm particles caused 50% immobilisation (LC_{50}) of *D. magna* neonates (<24hrs) to be 5.36 $\mu g\ L^{-1}$, LC_{50} couldn't be calculated for

the particles in media1. In the case of $AgNO_3$, LC_{50} values for media1 and media10 were 1.43 and 0.87 $\mu g\ L^{-1}$, respectively. AgNPs aggregate in high ionic strength media and aggregated forms are much less toxic, the reason is mostly due to change in nature of toxicant (aggregate dispersed). We recommend the use of a 10-fold diluted OECD media to perform ecotoxicology experiments to obtain disperse and stable citrate capped AgNPs.

AgNPs of 20nm in size and citrate capped were exposed to different environmentally relevant conditions, i.e. sunlight, synthetic waters, presence of natural organic matter, etc, and the changes were followed by DLS and UV-vis. The addition of fulvic acid (FA) improves particle stability, while sunlight makes particles more unstable. Solutions with high ionic strength induce aggregation. By using HR-STEM and electron energy-loss spectroscopy (EELS) surface changes of citrate stabilized AgNPs prepared in the lab were assessed after being exposed to different conditions. No oxidation was observed on any of the conditions, only aggregation and dissolution.

Para mi abuelo, donde quiera que estes, Dr Marcel Roche.

Para mi mamá, que siempre ha creido en mi, Noelle Roche.

Mojej babci dziękuję za wszystko, Irene de Romer.

Finalmente, para Vladimir Peña, gracias por ayudarme a mantener mi cordura, eres el amor de mi vida.

Acknowledgements

I would like to thank the University of Birmingham, School of Geography, Earth and Environmental Sciences and CEFAS for the financial support which made this research possible. I would like to thank my supervisor, Prof. Jamie Lead for giving me the opportunity to do my PhD work in his group and for all his support and help. I would also like to thank my co-supervisors Prof. Mark Viant and Dr. Brett Lyons (from CEFAS), and also Prof. Kevin Chipman, for all their support.

Many people helped me in my work, through their expertise or technical support. I would like to thank Dr. Steve Baker for the ICP-MS element analyses and Dr. James Bowen for his help with the Rheometer. I want to acknowledge the people from the microscopy centre, Paul Stanley, Theresa Morris and Ming Chu, for their help with the TEM. I would like to thank Zhiwei Wang, from the Nanoscale Physics Research Laboratory, for all his help with the STEM, and Richard Palmer. Many thanks go to Sue for her help with nanoparticle synthesis and to Mohammed for all his help with the FFF, TEM, AFM and nanoparticles in general. I would like to thank especially Ruth for all the coffees and her help with AFM, TEM, physics and my dissertation; this past 3 years would have been very hard if it wasn't for your help and friendship.

Special thanks go to all the people in the group, for the great atmosphere in the lab, and all the people in office 325. Thanks Laura for all the lunch breaks and good times, thanks Marie for all the talks about food (our shared passion) and all the times that we went to the cinema. I would also like to thank Mila, for all her support with work and all the smiles she shares with everyone. Special thanks go to the wonderful Daphnia workers, Tom White and Alex Gavin, without whom I wouldn't have been able to finish this thesis; I hope your Daphnia babies are always happy ☺

Last but not least, I want to acknowledge everyone that gave me support directly or indirectly, my flatmate Paulo, another PhD survivor and great friend; Santi, the best friend one can ask for; Diana, that was going through this process at the same time as me; my family, my sister Paula, who has also been through this process at the same time as me and has been a great support throughout the years, my brother Gonzalo, who I miss very much, my mother, a great woman that has been an

inspiration to all her children, my father, always there to listen, my grandmother, who has also been my rock and a very special person in my life, my uncle Bobby, for all the laughs and good times, and the friends that have always been there for me, even if they are one ocean away. Thanks for believing in me.

I'm also grateful for all the distraction that dateline MSNBC, Channel 4 documentaries, Crime shows, Ghost Whisperer and many musicians and bands have given me in this stressful period of time, it wouldn't have been the same without them.

Finally I want to thank my boyfriend, Vlad, who has helped me keep my cool and has been there in the good, the bad and the stressful times. Thank you, lovely, for believing in me, these times would have been much harder if it wasn't for your support.

Table of Contents

List of Figures

Chapter 1

Chapter 2

Chapter 3

Chapter 4

Chapter 5

List of tables

Chapter 1

Chapter 2

Chapter 3

Chapter 4

Chapter 5

Common abbreviations

AFM	Atomic force microscopy
Ag	Silver
Ag+	Silver ions, ionic silver
$AgNO_3$	Silver nitrate
AgNPs	Silver nanoparticles
ca.	from the Latin *circa* (around, about)
d_H	Hydrodynamic diameter
dp, dn, dw	The peak, number, and weight average hydrodynamic diameters
D. magna	*Daphnia magna*
DLS	Dynamic light scattering
DLVO	Derjaguin-Landau-Verwey-Overbeek theory
EDX	Energy dispersive x-rays
EELs	Electron energy loss spectroscopy
EM	Electron microscopy
ENMs	Engineered nanomaterials
FA	Fulvic Acid
FCC	Face-centered cubic
FlFFF	Flow-Field Flow Fractionation
FFF	Fild Flow Fractionation
HAADF	High angle annular dark field detector
HA	Humic acid
HNO_3	Nitric acid
HR- STEM	High resolution scanning transmission electron microscopy
HS	Humic substances
ICP-MS	Inductively coupled plasma mass spectrometry
LC_{50}	Concentration at which particles cause 50% immobilisation
$NaBH_4$	Sodium borohydride

NM / NMs	Nanomaterial(s)
NOM	Natural organic matter
NP/ NPs	Nanoparticle(s)
OECD	The Organisation for Economic Co-operation and Development
PdI	Polydispersity index width
PEG	poly(ethylene glycol)
PEG-SH	thiolated poly(ethylene glycol)
PVP	poly(*N*-vinyl-2-pyrrolidone)
SPR	Surface plasmon resonance
SRFA	Suwannee River fulvic acid
STEM	Scanning transmission electron microscopy
TEM	Transmission Electron Microscopy
UHP	Ultra high purity

1

Introduction

1.1 Introduction to nanotechnology and nanoparticles

Nanoscience explores the nature of matter, between atoms and molecules as defined by quantum mechanics, and the condensed matter, as defined by solid state chemistry and physics (Klabunde et al. 2009). It involves the study of how to control the formation of well-defined nanostructures or nanomaterials (NMs), starting from molecular scale building blocks of two- and three-dimensions (Ju-Nam et al. 2008). Important questions arise in nanoscience, from the decrease in the size of a material will make it behave more like an atom or molecule? And how many atoms in a NM will induce bulk-like behaviour? Nanoscience has led to the discovery of surprising material properties that can be very different from those of the bulk, such as an increased surface area and increased reactivity when size is decreased. It has also led to the birth of nanotechnology, that can be defined as the discovery and patenting of new products and processes based on nanostructure control of materials (Hannink et al. 2006).

A nanometre (nm) is one thousand millionth of a meter, 10^{-9} nm. To illustrate this, the size of a human hair ranges between 25000 nm and 180000 nm wide and viruses are around 100 nm in diameter (Figure 1.1). About ten hydrogen atoms in a line make up one nanometre. The size range size from approximately 1 nm to 100 nm has been defined as nanoscale by the Bristish standards Institution (BSI) (BSI 2007).

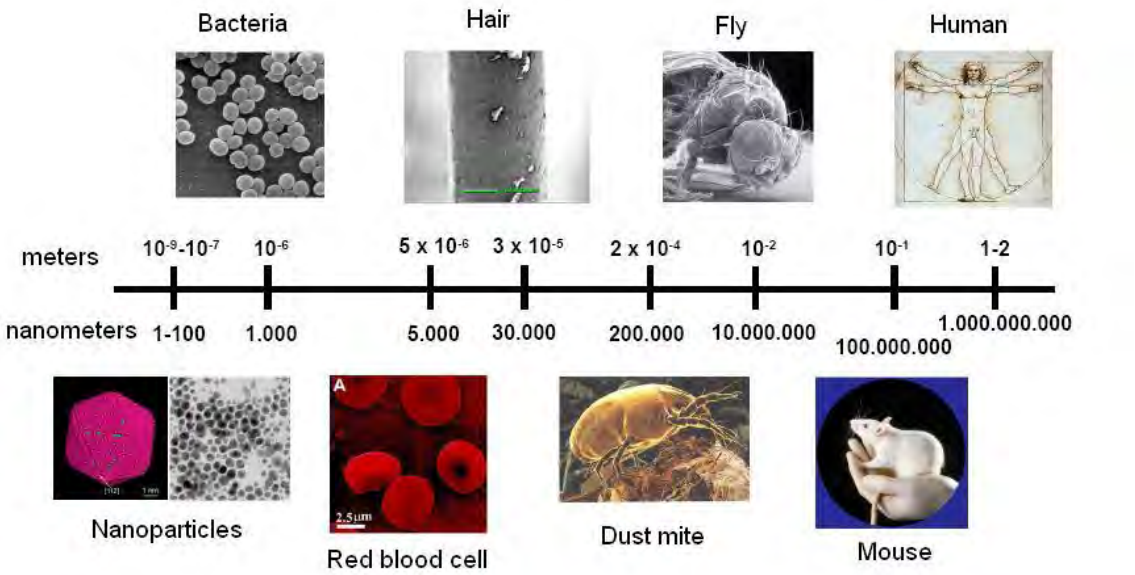

Figure 1.1 Scale in nanometres and meters comparing the size of nanoparticles with different things found in nature. Adapted from (Monge 2008).

Nanoparticles (NPs) are usually defined as the particles that range between 1 and 100nm in size (Hosokawa 2007; Klabunde et al. 2009). BSI has defined nanoparticles as a nano-object with all three external dimensions in the nanoscale (BSI 2007). The European Union has defined the term NM as a natural, incidental or manufactured material containing particles, in an unbound state or as an aggregate or as an agglomerate and where, for 50 % or more of the particles in the number size distribution, one or more external dimensions is in the size range 1 nm-100 nm (EuropeanComission 2011).

Although a variety of terms are used to define NPs and NMs, the nature and type of particle (e.g. size, shape and associated toxicity) can help to determine the terminology (Section 1.2). The sources of NPs are varied, from natural to manufactured, and their impacts will be diverse. These changes in NP effects complicate the terminology and the definitions currently used for NPs. A particle's dimension must therefore be determined by the individual, prior to NP studies, for future reference.

Some NP properties will be predictable (e.g. specific surface area, reactivity, crystal structure) and others will be unpredictable (e.g. surface plasmon resonance, solubility, photochemistry, surface properties). Some properties are associated with the bulk material, and are averaged properties, such as resistivity and magnetisation, density and the dielectric constant (Ju-Nam et al. 2008). The production of nanoscale

materials has accelerated in the past years due to their properties, including high surface area, small size and large number of surface atoms of the particles; and also due to the technological advances that have allowed us to manipulate matter at this spatial scale. There has also been a rapid increase in the applications of NMs in many areas. NMs have captured the attention of researchers, government, and the industry in a worldwide scale (Ju-Nam et al. 2008). According to the Woodrow Wilson Database, there is a total of 1317 products containing NMs as of March 2011, the number has increased 56% since March 2006 (Woodrow_Wilson_database 2011), see Figure 1.2. Europe has overtaken East Asia as the second greatest contributor of manufacturer-identified nanotechnology-enabled consumer products, the USA being the largest contributor.

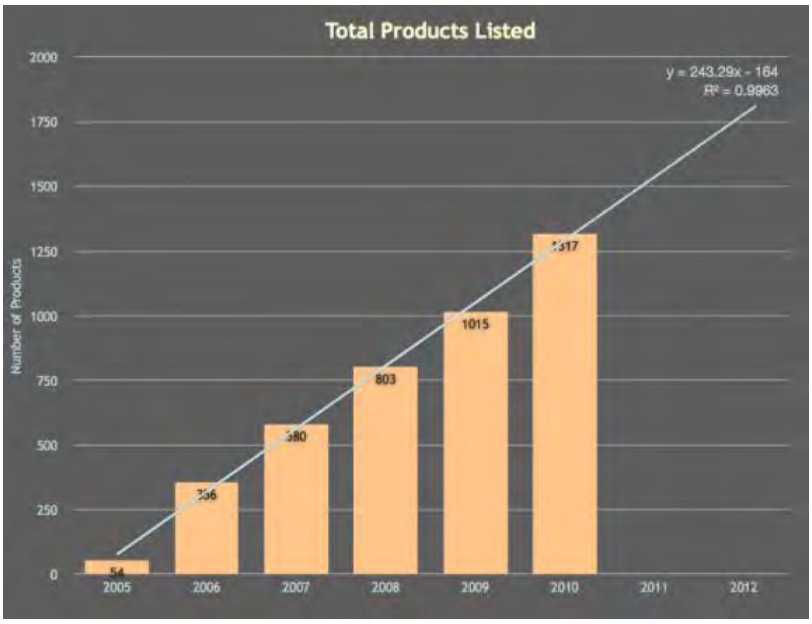

Figure 1.2 Number of total products listed, by date of inventory update, with regression analysis, courtesy of (Woodrow_Wilson_database 2011).

In the nanoscale, the properties change (Domínguez-Vera et al. 2007). NPs differ from larger materials in that the number of atoms at the surface and their physical properties are different from those of bulk materials (Poole et al. 2003; Ju-Nam et al. 2008). One of the most important attributes of all NPs is their high surface area per unit mass. The unique physico-chemical properties of NPs that manufacturers seek

to exploit, may have unforeseen consequences in terms of ecotoxicity and environmental impact (Colvin 2003) and describing these impacts has become an active focus for regulatory (OECD 2009; PROSPECT 2010; OECD 2010a) as well as peer-reviewed research (Stone et al. 2010) in the past decade.

Metal NPs in general have the advantage of easy preparation and the possibility of chemical modification of the surface by a variety of capping agents (Haick 2007). An important property which metal NPs exhibit is the resonance effect, the surface plasmon resonance (SPR) explained in chapter 2, section 2.3.4, which is caused by the interaction with the incident light and the free electrons in the materials. Aqueous solutions of AgNPs stabilised with citrate are yellow colloidal solutions which present a surface plasmon band (SPB) at 400 nm (Doty et al. 2005; Ju-Nam et al. 2008). Size and shape of nanoparticles can have an effect on the SPR and the colour of the suspension (Huang et al. 2010).

In the past, gold NPs (AuNPs) and silver NPs (AgNPs) were used to stain glass, Figure 1.3 shows the Lycurgus Cup, which dates back to Roman times and is currently at the British Museum, it has gold and silver NPs embedded in glass.

Figure 1.3 Lycurgus Cup that contains silver and gold nanoparticles. When light is shone through the cup it changes colour, from green to red. Source http://news.bbc.co.uk/1/hi/sci/tech/7722620.stm

1.2 Type of nanomaterials

Nanomaterials (NMs) currently in commercial production can be grouped into five broad categories, although there is clearly some overlap in classifications:

1. Carbonaceous. Including carbon nanotubes (CNTs), fullerenes and graphene.
2. Metals. Including zerovalent iron (nZVI), silver (AgNPs), gold (AuNPs), etc.
3. Metal oxides. Including zinc oxide (ZnO), titanium dioxide (TiO_2) and cerium oxide (CeO_2).
4. Nanopolymers. Including polystyrene and polymethylmethacrylate (PMMA).
5. Quantum dots. Including selenides, sulphides, tellurides, zinc, amongst others, including core-shell quantum dots.

These five categories are based on the material that the NMs are made from. However, this does not necessarily reflect their physico-chemistry. Size, shape (i.e. rods, prisms, tubes, and spheres) (Sun et al. 2002; Wiley et al. 2005) and crystal structure are important factors that influence their physical and chemical properties. Capping agents and coating (i.e. core-shell particles, functionalising the surface) can also have an influence on the NMs and its properties. Thus, two particles of the same material but of different size and shape may have different physical and chemical properties, stability and potential uses (Ju-Nam et al. 2008).

Of these five categories, carbonaceous, metals and metal oxides contribute most to current production volumes (Dair et al. 2010) and have a range of uses based on high tensile strength and conductivity (e.g. CNTs) and catalytic activity (TiO_2 and CeO_2). Two of the most widely used metals and metal oxides in consumer products are AgNPs and TiO_2 (see Figure 1.4) (Mueller et al. 2008). Titanium oxide NPs (TiO_2 NPs) are produced on a large scale for applications in paints and coatings, they have self-cleaning, antifouling, and antimicrobial properties (NanoScale 2011) due to their improved photocatalytic reactivity because of their small particle size, faster kinetics due to high surface area, better transparency as opacity is decreased with small particle size, enhanced biocidal characteristics due to higher surface area

and higher coverage per unit mass due to lower density. They are also used in cosmetics as a UV-absorber, due to their improved UV protection and low opacity.

Applications for TiO_2 NPs have not been developed rapidly, even though they have a large specific surface area (as all NMs do), due to their tendency to aggregate very easily forming larger particles. Aggregation can hinder catalyst efficiency. TiO_2 NPs are hard to separate and recover during the reaction process from the reactant mixture (Zhao et al. 2011). But because of its photoactivity, it is widely used, sometimes in combination with ZnO, in sunscreens (Klaine et al. 2008).

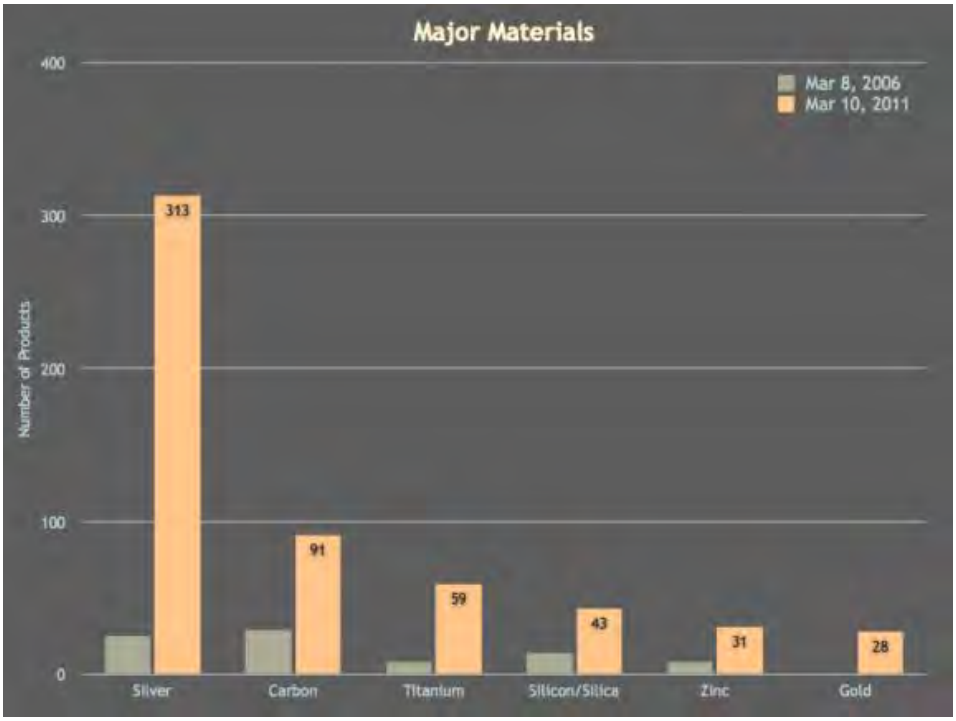

Figure 1.4 Number of products associated with specific materials (Woodrow_Wilson_database 2011).

1.3 Silver nanoparticles

Silver NPs (AgNPs) are the main NP type in use currently (see Figure 1.4) (Henglein et al. 1998) and are used in increasing quantities for industrial applications as they have powerful anti-microbial properties (Sondi et al. 2004). AgNPs are used as antibacterial agent when free or incorporated into coatings, fibres, bandages, dressings, sticking plasters, plastics, soap and textiles, in fabrics or other goods (AmericanElements 2011). They have been widely used in commercial applications in cosmetics and as bacteriocides in fabrics (Ju-Nam et al. 2008).

Silver has been known to be used in wound management, this can be traced back to the 18th century, at this time silver nitrate ($AgNO_3$) was used to treat ulcers (Klasen 2000; Chopra 2007). Silver ions and their antimicrobial activity were identified in the 19th century, and in the 1920s colloidal silver was accepted by the US Food and Drug Administration (FDA) as being an effective treatment for wound management (Hugo et al. 1982; Demling et al. 2001; Chopra 2007). After penicillin was introduced in the 1940s, the use of silver diminished because antibiotics became the standard treatment for bacterial infections. In the 60's silver became popular again, it was used for the management of burn patients, this time in the form of 0.5% $AgNO_3$ solution (Moyer et al. 1965). It has been demonstrated that, in low concentrations and short contact times, silver is non toxic to human cells (Martinez-Castanon et al. 2008).

Because some bacterial strains have demonstrated recently an increasing resistance toward antibiotics silver has received renewed interest. The powerful antimicrobial activity of silver is known to be effective against nearly 650 types of bacteria (Perelshtein et al. 2008). Reducing the size of materials by using nanoparticles and thus increasing the surface area is an efficient and reliable tool for improving their properties (Kim et al. 2007).

The mode of action of AgNPs as antibacterial agents is not understood completely. The antibacterial effect might come from the catalytic oxidation of the NPs by metallic silver and the subsequent reaction with dissolved silver ion (Ag+). Long term release of these silver ions (Ag+) by oxidation of zero-valent metallic silver Ag^0 in contact with water might be the end mechanism of products that contain AgNPs (Kumar et al. 2005). It has also been shown that size and shape of NPs will have an influence on their effects and toxicity (Morones et al. 2005; Pal et al. 2007). Small NPs have more antibacterial effect, compared to larger ones. It has also been shown that triangular plates NPs are more efficient antibacterial agents compared with spherical and rod-shaped NPs (Ju-Nam et al. 2008).

1.4 Synthesis of metal nanoparticles

The two most common methods used to manufacture NMs are the top-down bottom-up. Top-down starts with a large structure that becomes smaller through successive cuttings (generally grinding, milling, etc); bottom-up starts from atoms that will react to form a NM (Helland 2004) (See Figure 1.5). It has been the development of advanced measurement and manipulation instrumentation, such as atomic force microscopes (AFM) and transmission electron microscopes (TEM), that has allowed scientists to see and manipulate structures in the nanometre scale.

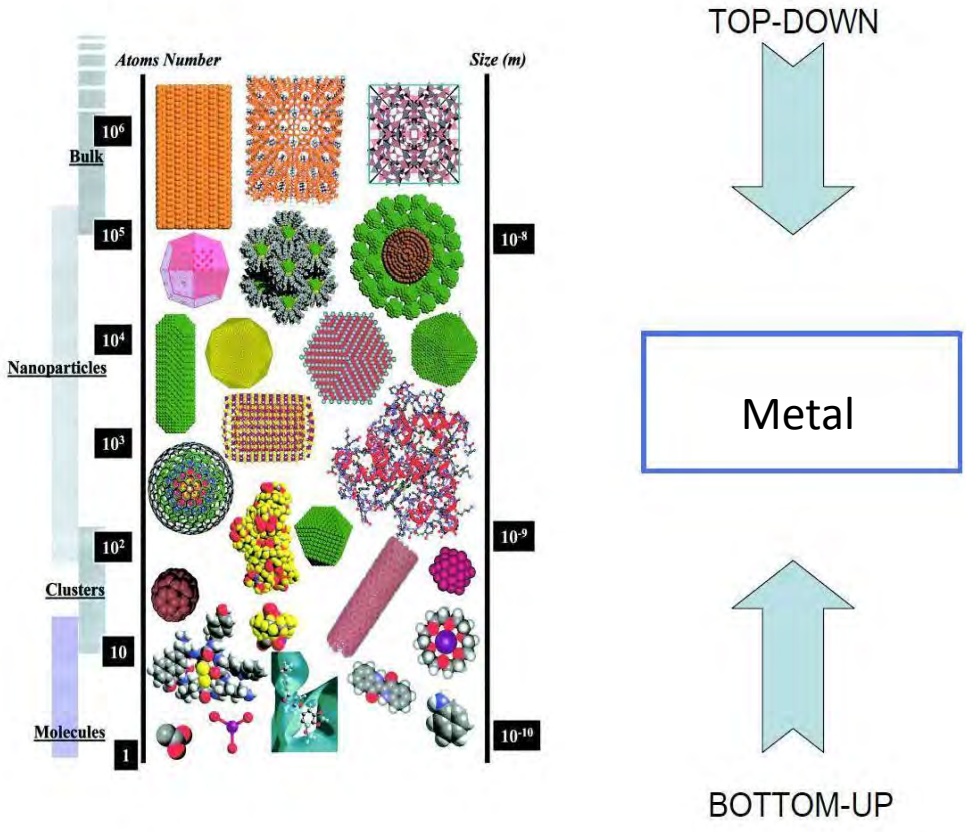

Figure 1.5 Size comparison of nanoparticles with different chemical species. Illustration of the bottom-up and top-down method of synthesis. Adapted from (Monge 2008).

Top-down nanofabrication can be achieved by high-energy milling, chemical mechanical milling, electro-explosion, laser ablation or spluttering. A common top down fabrication technique is nanolithography, which is used to manufacture computer chips. Top-down is useful when making surface imprints that need to be replicated. The disadvantages of this method are that bulky instruments are usually needed; it is also not very useful for single NP production due to the fact that there will be imperfections on the surface of the structure, there will probably be contamination, and the NPs obtained will be polydisperse.

Bottom-up approaches generate NPs from the atomic or molecular level and thus are predominantly chemical processes. Commonly used techniques are crystallisation/precipitation, sol-gel methods,

chemical vapour deposition, gas-phase aggregation and self-assembly routes, such as wet chemistry synthesis (Hannink et al. 2006; Klabunde et al. 2009). This type of approach is cleaner than the top-down method to produce NPs, the NPs obtained will have fewer defects, will have a more homogenous chemical composition, will be closer to thermodynamic equilibrium and will be more monodisperse. Bottom-up synthesis involves chemical reactions, nucleation and growth process as a starting point to induce the formation of more complex NMs (Rotello 2003).

We are interested in obtaining well defined and monodisperse AgNPs, hence we chose to use bottom-up methods in mild conditions. Chemical synthesis of this type of particles consists of dissolving a silver salt in the correct solvent, and then to induce a reduction to the zero valent state. The lifetime of the atomic clusters in the solution is short, and they tend to aggregate (Ju-Nam et al. 2008). By using the appropriate ligand the formation of larger particles can be stopped and aggregation can be avoided. The most common ligands used are sodium citrate (Lee et al. 1982; Henglein et al. 1999; Pillai et al. 2004; Doty et al. 2005; Cumberland and Lead 2009; Römer et al. 2011) and different polymers (PVP, PEG, etc) (Silvert et al. 1996; Hoppe et al. 2006; Christian et al. 2010).

One of the most common synthesis of NPs is the hydrothermal method. This type of synthesis is interesting to us due to its simplicity and mild conditions used. The chemical reduction was first published by Faraday in 1857 (Faraday 1857) and later on improved by Turkevich and colleagues in the 1950s for the preparation of AuNPs (Turkevich et al. 1951). This reaction involves the heating of a solution of chloroauric acid ($HAuCl_4$) to its boiling point, followed by reduction with sodium citrate; the resultant nanoparticles were very uniform with a diameter of 20nm. Other groups further studied this method (Fujita et al. 1962; Berry et al. 1963; Wilenzick et al. 1967; Frens 1973) which by varying the reaction conditions (e.g. the ratio of trisodium citrate to gold salt, temperature, time, etc) were able to achieve a degree of control over the diameter of the resultant nanoparticles (Kumar 2009). This reaction can be used to obtain AgNPs, but yielding more polydisperse, larger and less uniform particles. Table 1.1 shows different reactions that yielded stable AgNPs with different capping agents.

We can obtain NPs easily by using a reducing agent, a common strong reducing agent is sodium borohydride ($NaBH_4$) (Glavee et al. 1992), a large number of nuclei are formed when it is used to reduce metal salts and therefore the resulting particles are small (<10nm). In the case AgNPs, a silver nitrate salt ($AgNO_3$) can be reduced by using $NaBH_4$ in the presence of sodium citrate, where the citrate acts only as a capping agent. These particles are electrostatically stabilized (see Figure 1.6, left). Capping agents improve particle stability. When the NP surface is not protected by a molecule the interactions between NPs will occur to reduce their surface energy and will lead to aggregation (Ju-Nam et al. 2008) (discussed in section 1.5.3).

Figure 1.6 An example of electrostatically (a) and sterically (b) stabilized AgNPs. In the case of the citrate capped NPs, the negatively charged citrate caps the positively charged surface of the NP. Based on (Dumur et al. 2011).

Table 1.1 Examples of reactions published where AgNPs with different capping agents were obtained.

Capping agent	Reaction conditions	Size (nm)	Shape	Other details	Reference
Sodium citrate	1mM $AgNO_3$ boiling and 1% sodium citrate. The solution was kept on boiling for ca.1 h.	-	-	Solution was greenish yellow and had absorbed at 420 nm.	(Lee et al. 1982)
	The solution contains 1.0 X 10^{-4} M $AgClO_4$, 2.5 X10^{-2} M N_2O, 0.3 M 2-propanol, and citrate in various concentrations (5.0 X10^{-5} to 1.5 X 10^{-3} M)	10 to 20	Spherical	Well-separated NPs with a narrow size distribution are produced in a narrow range of citrate concentration, about (1-5) X 10^{-4} M	(Henglein et al. 1999)
	20 ml of $AgNO_3$ (0.25 mM) and 0.25 mM trisodium citrate. 0.6 ml of 10 mM NaBH4 was added all at once. Stirring was stopped after 30 s	4 $\pm$ 2	Spherical	Seed was used after 2 hours	(Jana et al. 2001)
	A solution of $AgNO_3$ (1.0 X 10-3 M) was heated until it began to boil. Sodium citrate solution was added dropwise to the $AgNO_3$ solution as soon as the boiling commenced and heated for 15min more.	50-100	crystallites	The color of the solution slowly turned into grayish yellow	(Pillai et al. 2004)
	$NaBH_4$ (6 ml, 10 mM), 200 ml of $AgNO_3$ (0.25 mM) and trisodium citrate (0.25 mM). The reaction was stirred for 30 min.	8.1 $\pm$ 1.6; 15.3 $\pm$ 6.4	Spherical	yellow colloidal silver	(Doty et al. 2005)
	100ml sodium citrate (0.31 mM), 100ml $AgNO_3$ (0.25mM) and 6ml $NaBH_4$ (0.25mM). After 10 min of stirring the cold solution, it was was heated slowly to boiling and heated for a further 90 min	13.7± 6.2	Spherical	Solutions were prepared in pure water and kept at 4 ◦C in the dark for 30 min before the reaction	(Cumberland and Lead 2009)
	400 ml of boiling water, 1.690 ml of 58.8 mmol L^{-1} $AgNO_3$ and 2.920 ml of 34 mmol L^{-1} sodium citrate stirring, before dropwise addition of 2.000 ml of 100 mmol L^{-1} $NaBH_4$	22.5 ± 0.6 (DLS)	Spherical	-	(MacCuspie et al. 2011)
PVP	3 mL of $AgNO_3$ (0.23-2.3 mM) containing 0.25-1 wt % PVP was placed in a rectangular quartz vessel. The sample was irradiated by 254 nm UV light at room temperature.	15 to 22	Spherical	The rate of the photoreduction process was observed to increase with the PVP concentration	(Huang et al. 1996)
	PVP (15 and 20 g) in *75* ml ethylene glycol at room temperature, $AgNO_3$ was added (1 and 3.2 mg). Stirred at room temperature until complete dissolution. The system was heated to 120°C at a constant rate of 1 ^{o}C min, left for 1 h at this temperature.	25 $\pm$ 6 and 36 $\pm$ 11	Spherical	Known as polyol process	(Silvert et al. 1996)
	Polyol process (Silvert et al., 1996) changing the PVP to $AgNO_3$ ratio	50 to 100	Nanocubes	morphology of the product had a strong dependence on the reaction conditions.	(Sun et al. 2002)
	2.9 mM $AgNO_3$ and PVP K15 0.02 M at room temperature were mixed. After the solution was shaken, samples were heated to the selected reaction temperature (between 25 and 70 °C) and left standing for the reaction to proceed.	18.8 $\pm$ 3	Spherical	Different shapes and sizes were obtained with PVP 10 and different concentrations.	(Hoppe et al. 2006)

Capping agent	Reaction conditions	Size (nm)	Shape	Other details	Reference
PVP	10 ml of $AgNO_3$ (1.0 mM) was added dropwise (about 1 drop/second) to 30 ml of $NaBH_4$ (2.0 mM) that had been chilled in an icebath. 0.3% PVP was added to prevent aggregation.	12 ± 2	Spherical	The solution turned light yellow after the addition of 2 ml of $AgNO_3$ and a brighter yellow when all of it had been added	(Solomon et al., 2007)
	Sodium citrate (3.68 ml, 30 mM), PVP (3.68 ml, 2% w/w), and H_2O_2 (120 ml, 30% w/w) were added into $AgNO_3$ (43 ml, 0.11 mM) under stirring. After 3 min, 100 mM $NaBH_4$ of 150, 160, 170, 180, 200, 220, 250, 280, 300, 330, 360, or 500 ml was added into each mixture, to synthesize twelve colloids of Ag NPs.	2.6 ± 0.8; 4.6 ± 1.1; 9.5 ± 3.2; 10.0 ± 3.8; 16.1 ± 5.4; 18.0 ± 6.7; 16.7 ± 5.6; 17.1 ± 6.2; 19.0 ± 5.9; 20.3 ± 7.2; 27.0 ± 9.7; 29.1 ± 9.5	Spherical, rods, triangles, cookie	Solutions turned light yellow, yellow, light orange, orange red, red, dark red, purple, purple violet, violet, blue, light blue, and green, respectively	(Huang et al. 2010)
PEG-OH	A methanolic solution of PEG-OH (12.5 mg ml^{-1}), 4 ml of dodecanethiol-stabilized Ag NPs in hexane and the mixture was gently shaken.	5.3 + 1.0	Spherical	-	(Doty et al. 2005)
PEG-NH_2	A methanolic solution of PEG-NH_2 (15 mg ml^{-1}),1 ml of decanethiol-stabilized AgNPs in hexane.	5.3 + 1.0	Spherical	-	
PEG	AgNO3 (400 mg, 2.4 mmol) was dissolved in 50 ml PEG at room temperature. The suspension was stirred at 23 ◦C until dissolution and heated, with a constant rate of 1 ◦C/min, up to 30, 60, 90 and 120 ◦C at successive steps, the reaction was left in the last temp. for 3 h.	4 ± 2; 4 and 20; 10 and 20 (with triangles); polydisperse	Spherical and a mix of spheres and triangles	120 ◦C generated spheres, triangles and pentagons	(Popa et al. 2007)
PEG-SH	4 ml of an ethanolic $AgNO_3$ solution (0.0075 M) were mixed with 0.075 g of PEG-SH (under N_2) and sonicated. 1.3 mL of 0.09 M NaBH4 in ethanol was added dropwise. The suspension was kept at room temperature for 2 h.	10-20 and 1-5	Spherical	Particles were stable in chloride solution	(Shkilnyy et al. 2009)
	AgNO3 0.3 mol and MPEGSH 590 mg in methanol (50 ml) with a solution of sodium borohydride (0.942 mmol) in 4 ml methanol.	5.6 ± 1.4	Spherical	Yield was 49%	(Christian et al. 2010)

Small nanoparticles can be used as seeds or nucleation centres for the preparation of nanoparticles with larger sizes and different shapes, giving us better control on the growth of the particle. The seeds act as catalysts for the reduction of silver ion by weaker reducing agents, like ascorbic acid. The stabilization of the particles can occur in many different ways but primarily based on electrostatic repulsion or steric hindrance as with many metal oxides (Figure 1.6) (Ju-Nam et al. 2008).

Poly(*N*-vinyl-2-pyrrolidone) (PVP) (Hoppe et al. 2006) is a water-soluble polymer that has been used as protecting agent against agglomeration of metal colloids in the well-known polyol process (Silvert et al. 1996; Silvert et al. 1997) to obtain sterically stabilized NPs (see Figure 1.6, right). It has been reported that PVP may serve as a reducing agent (see Figure 1.7) and that by varying the ratio of metal salt to PVP, the size and shape of the nanoparticle can be tuned. The reduction process can be explained by two main reactions:

(1) direct abstraction of hydrogen atoms from the polymer by the metal ion

(2) reduction of the metal precursor by organic macroradicals formed by degradation of PVP

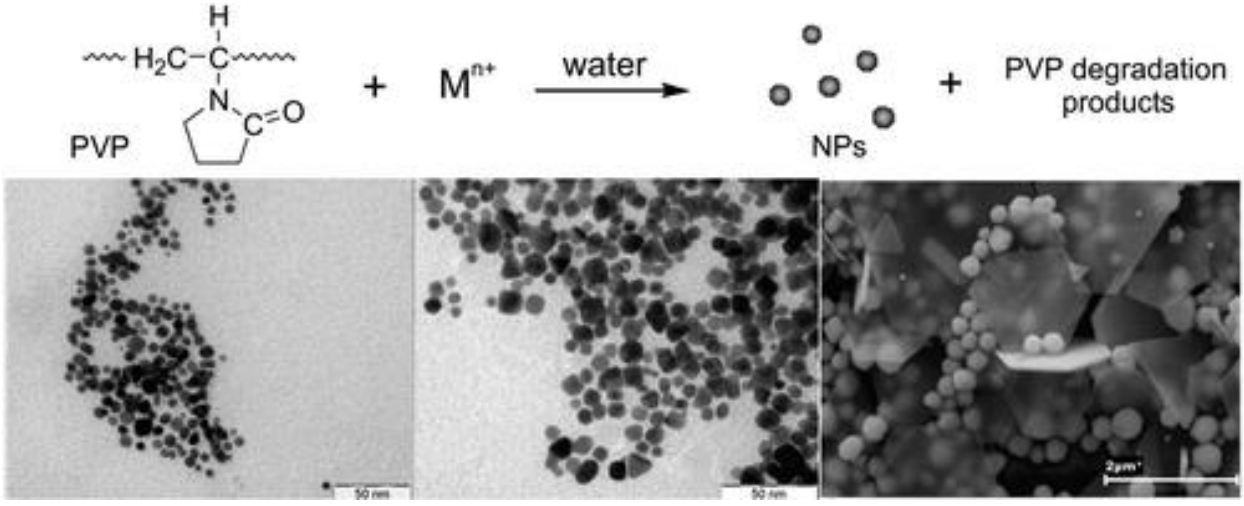

Figure 1.7 Reduction of nanoparticles by using PVP as capping and reducing agent, including some images of the particles obtained (Hoppe et al. 2006).

Other common capping agents used to make sterically stabilized nanoparticles are poly(ethylene glycols) (PEG) (Doty et al. 2005), which works better when functionalized by thiol (Fernandez-Lopez et al. 2009; Shkilnyy et al. 2009; Christian et al. 2010) and amine groups (Li et al. 2006). PEG as a capping agent is very widely used in commercial applications because of its solubility in a wide range of solvents (Christian et al. 2010), when using a functionalized group we can obtain particles in an easier way and with additional properties. Other polymers used are poly(ethylene oxide) (PEO) (Rujitanaroj et al. 2007), poly(sodium acrylate) (Hussain et al. 2003), poly(ethylene alcohol) (PEG-OH) (Doty et al. 2005), Poly(vinyl alcohols) (Longenberger et al. 1995), amongst others.

1.4.1 Nucleation and Growth

The shape of the size distribution curve of the nanoparticles synthesized depends largely on the relative rates of two separate processes, nucleation and growth. Nucleation can be defined as the process whereby a discrete particle of a new phase forms in a previously single-phase system, usually a homogeneous solution. Growth can be defined as a process in which additional material deposits on this particle causing it to increase in size (Turkevich et al. 1951).

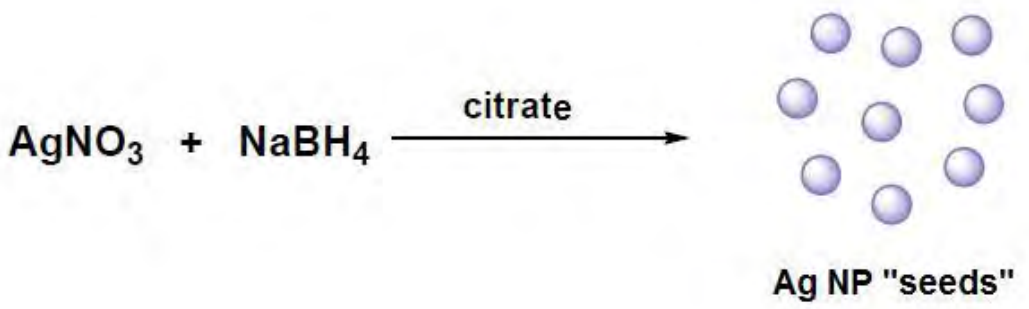

Figure 1.8 Nucleation process for AgNPs stabilized with citrate, formation of seeds (García-Barrasa et al. 2011).

Reduction of metal ion precursors produce Ag seeds (see Figure 1.8) (Pillai et al. 2004). Small Ag clusters are formed through the agglomeration of the seeds; these small clusters further grow into larger clusters (Figure 1.9). The growth is dictated by the presence of a stabilizer or complexing agent (Belloni et al. 1998). When an organic molecule is added at an early stage of cluster growth, covalent linkage or surface capping tends to yield smaller-sized NPs. Even though citrate ions complex strongly during early growth stages, these reactions will yield larger clusters with different shapes and sizes (Pillai et al. 2004).

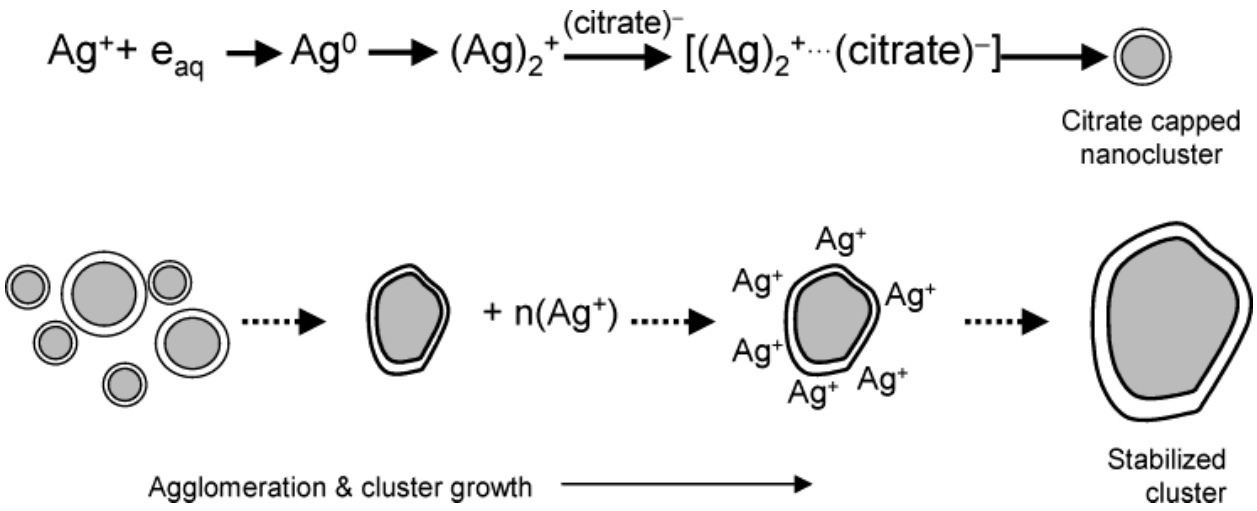

Figure 1.9 Primary and Secondary Growth Steps in the Formation of Silver Nanoparticles (Pillai et al. 2004).

In the citrate reduction procedure, shown in Figure 1.9, few seeds of Ag NPs are formed in the beginning, and a strong complex with the citrate anions is formed. As citrate is lost from the solution, fewer new seeds are produced. The complex will grow slowly by aggregation and will reach an optimal size, at this stage the layer of citrate, which is very strong and repelling, will prevent further aggregation. Ostwald ripening will induce further growth (Figure 1.10), larger particles grow at the expense of smaller ones (Boistelle et al. 1988; Pillai et al. 2004). Ostwald ripening is defined by equation (1.1) (Boistelle et al. 1988) and explained in Figure 1.10:

$$\bar{r}^3 - \bar{r}_0^3 = \frac{3\, D_v\, m\ \ C_s}{4\, k_B\, T\ \ ^2}\ (t - t_0) \qquad (1.1)$$

Where $\bar{r}$ is the average radius of all particles, r_0 is the radius of the particle at time zero (often negligible), Dv is the coefficient for volume diffusion, m is molecular weight, is the particle surface tension or surface energy, C_s is the solubility of a large crystal of infinite size, K_B is the Boltzmann constant, T is absolute temperature, is density, t is time and t_o is time zero.

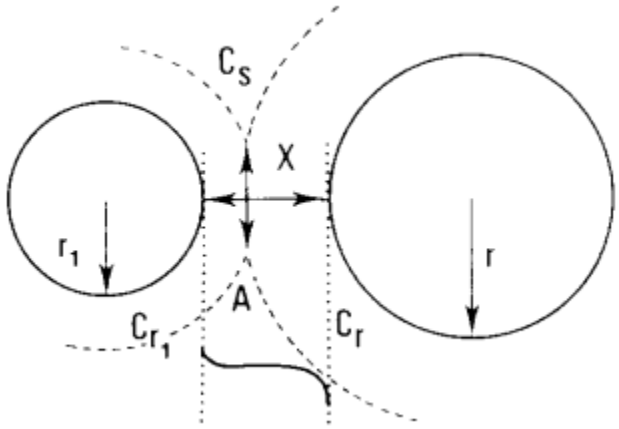

Figure 1.10 Schematic representation of the solute transfer from the smallest to the largest crystal during Ostwald ripening. The crystals are separated by the distance X and their concentration spheres interact with the cross section A. Since they are not of infinite size and since equilibrium must be achieved, the crystals must (slightly) dissolve in order to restore the proper concentrations. When the distance X between the crystals is not too large, the two concentration spheres intersect with a cross section of area A (Boistelle et al. 1988).

As the smaller particles are oxidized, the Ag+ ions readsorb on the larger silver crystallites and undergo reduction at the metal surface. Such a reduction of Ag+ ions at the silver surface is facilitated by the decrease in the reduction potential at the metal surface compared to the bulk solution. Greater reaction time (refluxing time) is needed to achieve almost complete reduction in a citrate reduction method (Pillai et al. 2004).

The particles formed at lower citrate concentrations have many imperfections and often consist of several crystallites. At a very high citrate concentration, large lumps often are formed because of the coalescence of destabilized particles (Henglein et al. 1998).

1.5 Nanoparticle characteristics and properties

Nanoparticles can have very different characteristics, like different core material, size, shape, crystal shape or amorphous structure, have different coatings or surface chemistry (Hassellöv et al. 2009), like seen in Table 1.1. Coatings and surface chemistry are parameters that can control particle behaviour and their stability in different media (Tejamaya et al. 2012). Figure 1.11 shows the complexity of NPs, showing their different properties, which will have an influence in their stability and toxicity. A multi-method approach, combining sophisticated methods, like field flow fractionation (FFF), inductively coupled plasma mass spectrometry (ICP-MS) and transmission electron microscopy (TEM), is the best approach to determine the presence of NPs in the environment. The different methods used in this work are discussed in detail in Chapter 2.

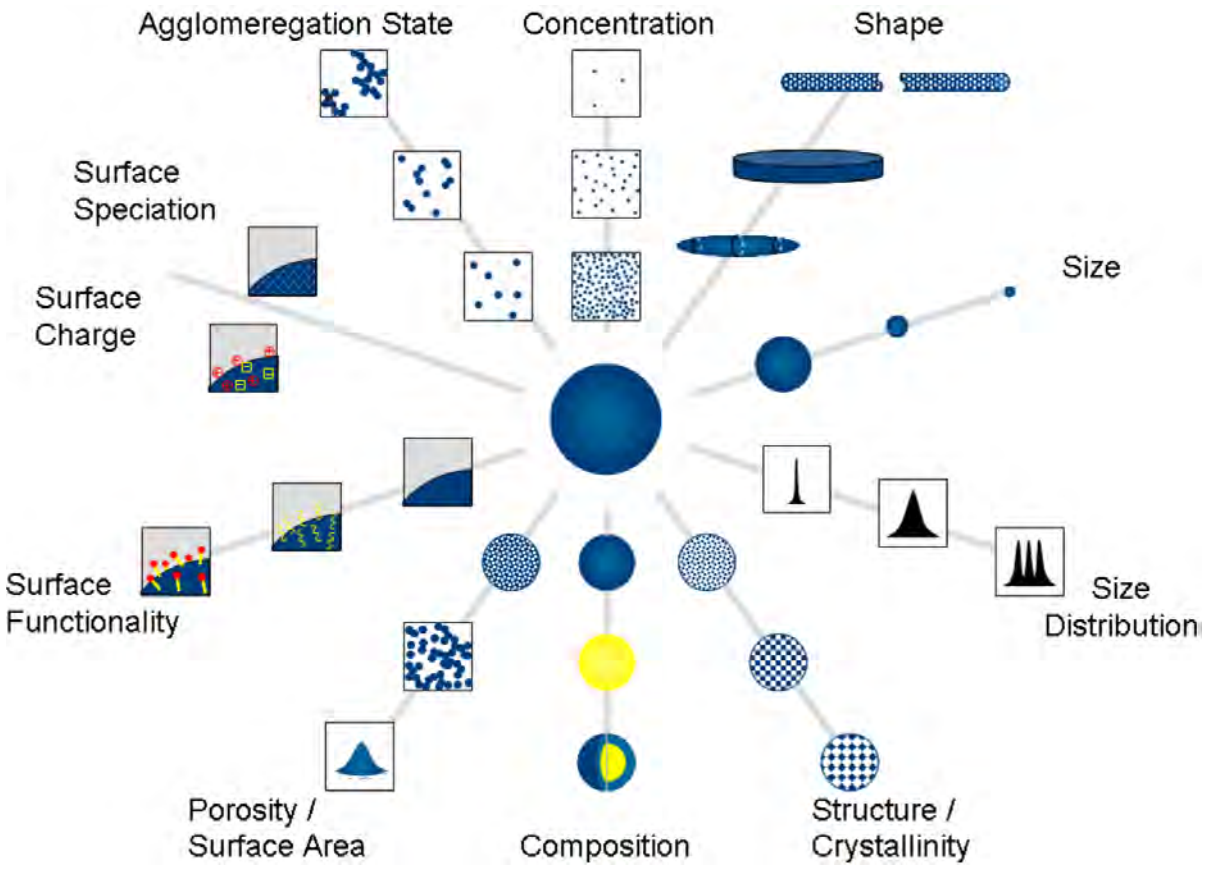

Figure 1.11 The important properties of manufactured NPs in aqueous media are shown, indicating that a homogeneous solid sphere with a clean surface can't be assumed. These properties are important to understand the fate and behaviour of these NPs in the environment or for ecotoxicology experiments. Therefore, we need a multi-method approach to obtain a complete characterisation (Hassellöv et al. 2009).

1.5.1 Size of nanoparticles

Nanoparticles have properties that differ from the bulk, such as their atypical surface structure and their reactivity, when their size is smaller than 100 nm (Auffan et al. 2009). The number of atoms localized at the surface increases related to the area and volume of the NP as the size decreases, in particles smaller than 20-30nm. These smaller nanoparticles have a size-dependent crystallinity and will differ drastically

from the bulk. Crystallographic changes may occur to stabilize them. Bandgap energy increases as diameter decreases below 6–8 nm, (see section 1.5.2), which is related to fluorescence wavelength (Auffan et al. 2009). Melting point can also be reduced by reducing size. Particle size can also affect the reactivity, enhancing processes such as dissolution, catalytic properties, redox reactions or the generation of reactive oxygen species, differing from the effects obtained by the bulk. These changes are important in an environmental health point of view, due to the fact that toxicity and environmental effects will change with the size of NPs.

1.5.2 Shape and crystallinity of nanoparticles

The shape of a NP determines its surface atomic arrangement and coordination. A cubic NP will be bounded by six [100] facets, on which surface atoms are arranged in 4-fold symmetry with an eight coordination number (Tian et al. 2008). Metal NPs tend to be face-centered cubic (FCC) and will nucleate and grow into twinned and multiply twinned particles, with their surfaces bounded by the lowest-energy [111] facets (Sun et al. 2002). The different surface lattice planes for an FCC nanoparticle are shown in Figure 1.12. It has been shown that [111] facets have high reactivity and were very toxic to bacteria (Morones et al. 2005). In other studies, truncated triangular NPs have shown higher biocidal capacity than spherical or triangular NPs (Pal et al. 2007).

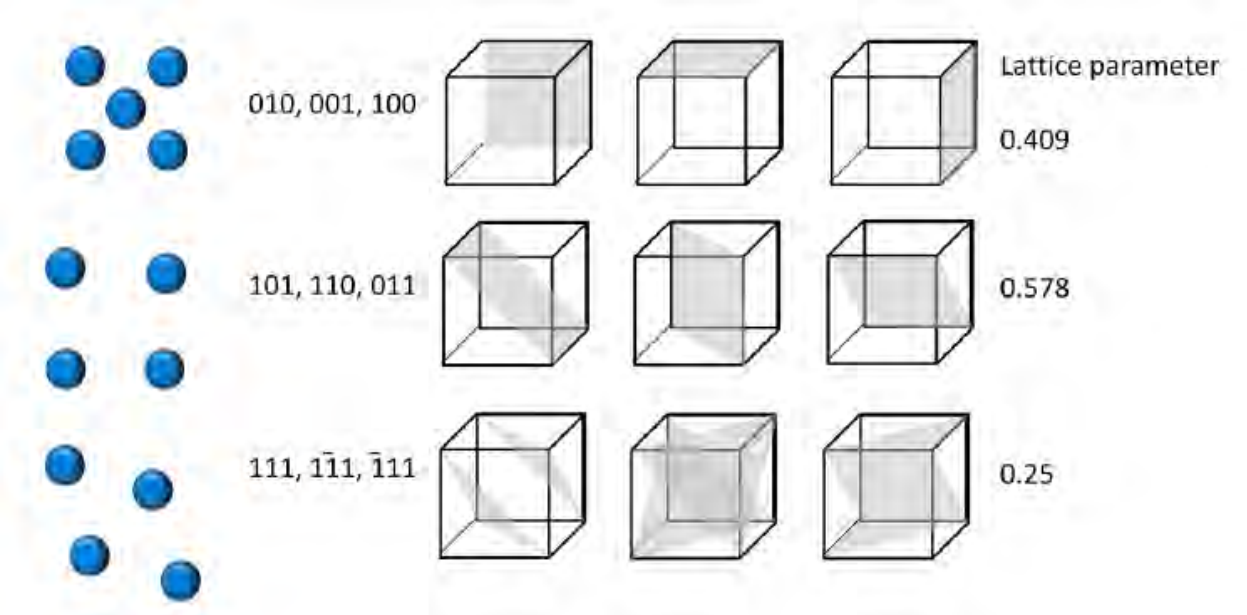

Figure 1.12 Surface lattice planes of the FCC system for a single crystal in the case of Ag. The most frequently studied surface planes are [100], [110] and [111]. The lattice parameter is explained in Figure 1.14. Courtesy of Ruth Merrifield.

Figure 1.13 shows the surface lattice planes of the FCC system for Ag looked from different planes. By using Scanning Transmission Electron microscopy (STEM), explained in chapter 2, section 2.3.9, we can image NPs with atomic resolution, and we can obtain the lattice fringes. These numbers will correspond with certain lattice parameters, and this way we can say in which plane we are imaging the particle. Lattice parameters are related to interatomic distances.

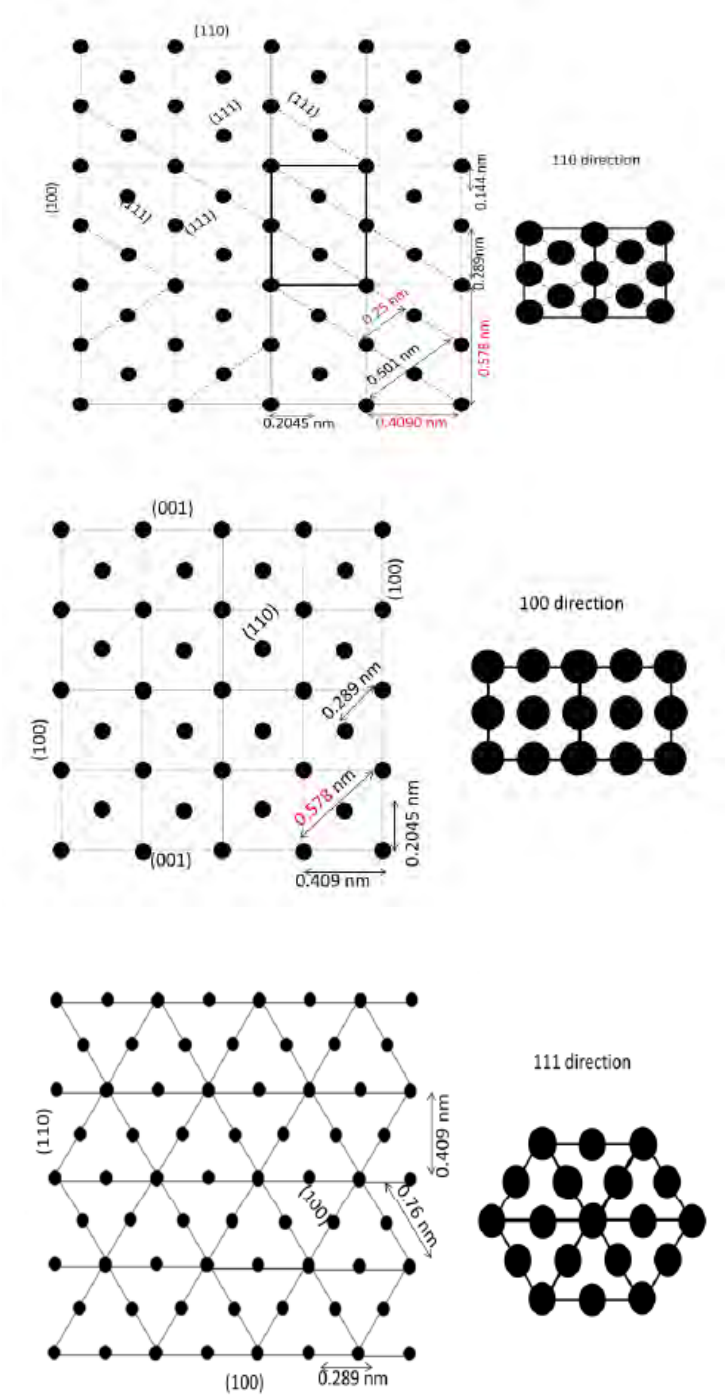

Figure 1.13 Surface lattice planes of the FCC system for Ag, looked from different planes. Interatomic distances are shown in red in the different images. Images courtesy of Ruth Merrifield.

The shape of NPs will be influenced by the different lattice planes present, as seen in Figure 1.14. A seed would tend to be in octahedral or tetrahedral shape to minimize the total surface energy and thus will

have [111] facets. However, when in these shapes they will have a larger surface area than a cube of the same volume and are expected to exist as truncated octahedrons enclosed by a mix of [111] and [100] facets. This shape is nearly spherical and thus the smallest surface area to minimize the total interfacial free energy (Xia et al. 2009). The shape of the particle will then depend of the shape of these seeds. Small metal NPs tend to exist in the form of decahedral and icosahedral multiply twinned particles consisting of five and twenty tetrahedral, respectively, with twinning on their [111] planes.

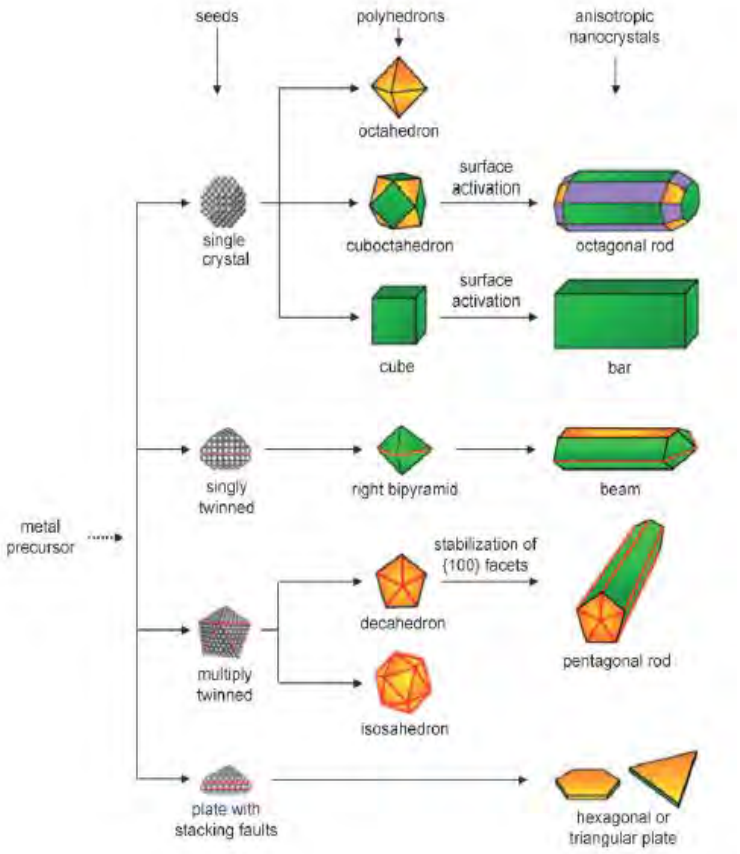

Figure 1.14 Pathways that lead to FCC metal NPs with different shapes. First, a precursor is reduced or decomposed to form seeds with a single-crystal, singly twinned, or multiply twinned structure. Plate-like seeds will form if stacking faults are introduced. The green, orange, and purple represent the [100], [111], and [110] facets, respectively. Twin planes are delineated in the drawing with red lines (Xia et al. 2009).

1.5.3 Nanoparticle aggregation, DLVO theory and fractal dimensions

The stability of NPs is determined by the net electrostatic surface interactions of the particles, according to classic Dejaguin–Landau–Verwey–Overbeek (DLVO) theory (Stebounova et al. 2011). DLVO theory explains aggregation behaviour of nanoparticles in the presence of electrolytes, which induce aggregation by screening the surface charge (Li et al. 2011). The total interaction energy between nanoparticles consists of the total interaction energy ($V_T = V_A + V_R$) between the van der Waals attraction (Eq. 1.2) and electrostatic repulsion (Eq. 1.3) (Baalousha et al. 2008):

$$V_A(h) = -\frac{A}{6}\left[\frac{2R^2}{h^2+4Rh} + \frac{2R^2}{(h+2R)^2} + ln\left(1 - \frac{4R^2}{(h+2R)^2}\right)\right] \quad (1.2)$$

$$V_R(h) = 32\pi\epsilon R\left(\frac{kT}{ze}\right)^2 \gamma^2 exp(-\kappa h) \quad (1.3)$$

Where ε is the permittivity of the medium; R is the particle radius; is the surface potential (dimensionless); k is the Boltzmann Constant; T is the absolute temperature; h is the surface separation between particles; e is the electron charge; A is the Hamaker Constant; κ is the inverse-Debye Huckel screening length and can be calculated for electrolyte solutions containing different salts (Baalousha et al. 2008):

$$\kappa = \sqrt{\frac{e^2 \Sigma n_i z_i^2}{\epsilon kT}} \quad (1.4)$$

where, *n,* is the number concentration of ion, *i,* and z, is the valence of the ions.

In the case of two particles of the same type in suspension, the particle will have the same charge; the forces due to these charges will be identical and hence repulsive, leading to a stable suspension. In this type of suspensions aggregation is prevented when the particle charge doesn't allow van der Waal's forces to act. When the pH or ionic strength of a solution is changed, particle charge will be affected, becoming weaker, and prevention of aggregation will require further stabilisation, like adding a surface coating or ligand (steric stabilisation) (Christian et al. 2008). In most cases, these changes in the solution will lead to aggregation. DLVO theory has some limitations, it does not include the effects of particle shape, charge, heterogeneity, and surface roughness which can influence the collision efficiency of NPs (Bhattacharjee et al. 2000; Handy et al. 2008).

There are two limiting regimes of colloid aggregation; they correspond to rapid and slow aggregation. In diffusion-limited aggregation, which is the rapid type, the aggregation rate is limited by the time between the collisions of the NPs and depends on their diffusion (Lin et al. 1990a). Rate-limited aggregation, which is a much slower aggregation, will happen when the reaction rate of two particles is slower than the collision rate, in this way a large number of collisions will be needed before two particles can stick together (Lin et al. 1990b).

Aggregation and the structure of these aggregates is an important factor in the fate and behaviour of NPs as well as their interaction with contaminants (Christian et al. 2008). This structure of aggregates can be described by fractal dimension (Lee et al. 2004; Rizzi et al. 2004). Fractal dimension is a ratio that compares statistically how fractal patterns change with the scale in which they were measured. Information about the morphology of the aggregate related to the irregularity, mass distribution in an aggregate, and porosity and compactness of the aggregate, can be obtained by using fractal dimension (Christian et al. 2008). They can be calculated by using a geometric power–law scaling relationships between each dimensional geometry (mass or volume in the case of three dimensions, projected area for two dimensions, or perimeter for only one dimension) and length scales of the aggregate, as seen in

Figure 1.15 (Lee et al. 2004; Baalousha et al. 2008). The value range for fractal dimension is between 1 and 3: 1 for a linear aggregate and 3 for a compact sphere. When the aggregates are very porous, the fractal dimension will be lower, which results in faster sedimentation compared to aggregates with a higher fractal dimension or impermeable spheres (Christian et al. 2008).

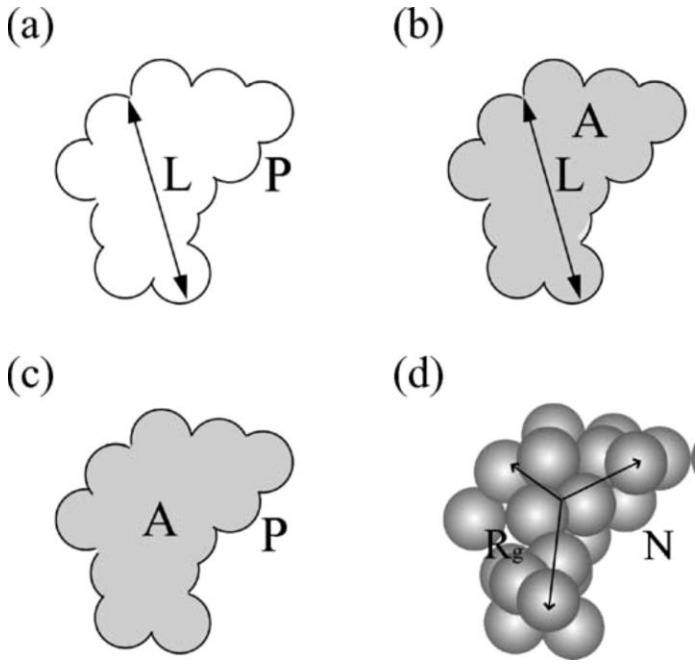

Figure 1.15 Measurements of aggregate fractal dimensions. (a) One-dimensional fractal dimension power–law scaling with perimeter and the maximum length of an aggregate. (b) Two-dimensional fractal dimensions power–law scaling with area and the maximum length of an aggregate. (c) Perimeter based fractal dimension power–law scaling with area and perimeter. (d) Three-dimensional fractal dimensions power–law scaling with the number of primary particles and the radius of gyration (Lee et al. 2004).

Fractal dimension was calculated by analysing the TEM images with Image J and the program Fractalyse. The value used was the two-dimensional fractal which provides information about the projected area of an aggregate (Lee et al. 2004; Baalousha et al. 2008).

1.5.4 Non-DLVO interactions

A number of non-DLVO forces can also influence the stability of NPs suspensions in aqueous environments. The most significant forces include steric interactions, magnetic forces (for iron-based NMs), and hydration forces (Petosa et al. 2010).

Equation 1.2 shows the extent of steric forces (F_{ST}) for particles with adsorbed layers of polymers or surfactants that might lead to steric repulsion between two particles (Petosa et al. 2010).

$$F_{ST}(h) = 2\pi\left(\frac{a_1 a_2}{a_1 + a_2}\right)\left(\frac{k_B T}{s^3}\right)\left\{\frac{8l}{5}\left[\left(\frac{2l}{h}\right)^{5/4} - 1\right] + \frac{8l}{7}\left[\left(\frac{h}{2l}\right)^{7/4}\right.\right. \quad (1.2)$$

Where a is particle radius, i = 1, 2, K_B is the Boltzmann constant, 1.3805 × 10^{-23} J K^{-1}, s is the distance between polymer chains on a surface, T is the absolute temperature, l is film thickness, and h is the surface-to-surface separation distance.

This expression is based on the Alexander-de Gennes theory that is used to evaluate the repulsive steric force and the Derjaguin approximation. Steric interactions can be particularly important for NPs in aquatic environments, as most particles adsorb natural organic matter (NOM) that is known to stabilize colloids (Baalousha et al 2008).

1.6 Discharge and Release

Release of NMs into the environment may occur during the production, the manufacture of NM-containing products, disposal, and the use and re-use of these products (Klaine et al. 2008). Recent studies have shown the processes through which NMs can enter aquatic systems. Kaegi *et al.* (Kaegi et al. 2008;

Kaegi et al. 2010), for example, demonstrated how Ag and TiO_2 NPs can be weathered or washed off from painted building facades into storm drains and surface waters. For the TiO_2, they studied three types of samples, one collected on a new facade, an aged one (2 years old) and urban runoff coming from a greater urban catchment. It was found that the concentrations of Ti in the runoff of the new facade were as high as 600 μg L^{-1}, the aged facade contained around 10 μg L^{-1}, and the runoff had 15 μg L^{-1}. For AgNPs, a substantial leaching was observed during the initial runoff events with a maximum concentration of 145 μg L^{-1}. More than 30% of the AgNPs were released to the environment after one year. Particles were small in size, mostly <15 nm, and were released attached to the organic binders of the paint. AgNPs seem to be transformed to considerably less toxic forms such as silver sulphide (Ag_2S), according to microscopic results (Kaegi et al. 2010).

Other recent studies (Benn et al. 2008) reported AgNPs emissions into water from NM containing textiles after washing and subsequently into the waste water treatment system. Kim *et al*. (2010) have identified nanosized Ag_2S particles in the final stage sewage sludge materials, which has shown reduced toxicity to nitrifying bacteria than AgNPs, although the provenance of these Ag_2S NPs is not clear. Focusing on waste water treatment works, Westerhoff *et al*. (2011) have shown that TiO_2 NPs can pass through waste water treatment plants and enter aquatic systems; while other studies have shown partitioning to solid or liquid phases depends largely on NM surface chemistry. Jarvie *et al.* (Jarvie et al. 2009; Jarvie et al. 2010) found that surfactant coated silicon oxide (SiO_2) NPs rapidly aggregated and sedimented out to form part of the solid sewage sludge; interactions between the adsorbed surfactant molecules and organic matter in the sewage induced aggregation. Uncoated NPs remained dispersed in the sewage and could continue through the effluent stream, this way they can end up in surface waters due to discharge. It was also found that some NMs had the ability to lose, change or gain new coatings, including NOM, during their transit through aquatic environments.

Exposure scenarios, potential adverse effects and opportunities for novel applications, will depend strongly on the life cycle of products containing engineered nanomaterials (ENMs). NM production, transport, manufacture of NM-containing product(s), use of the product(s) and any waste streams generated including at the point of recycling or final disposal are key in this regard (Som et al. 2010).

At this moment it is very hard to estimate the current production, release and flow coefficients of NMs into the environment (Mueller et al. 2008). Many times NM-containing products are not reported, there is also no monitoring of the registered products and little information on transport. Environmental exposure modelling of NMs can be very challenging due to the lack of analytical and in situ techniques and instruments that have the ability to detect, quantify and characterise NMs in complex environmental or biological media (Gottschalk et al. 2009). A multi-method approach, as mentioned before, is the best way to detect the presence and measure NMs in natural samples.

1.7 Fate, behaviour and transport

The use of NMs may result in several types of effects such as (eco)toxicological effects, bioaccumulation or carrier effects on pollutants in the environmental compartments (Som et al. 2010). Risks from NMs emissions may emerge if both exposure (due to NMs presence in the environment) and hazards (in the form of toxic effects) are observed (Klaine et al. 2008). NMs will go through loss mechanisms in the environment, dissolution may remove NMs, while aggregation may reduce surface water concentrations, but increase sediment concentrations. Interaction with NOM and reformation into other chemicals under environmental conditions are also key processes (Klaine et al. 2008; Alvarez et al. 2009). There are indications that these processes will happen and soils and surface waters are likely major pathways, with ultimate sink being sediments.

Mechanisms such as aggregation (explained in section 1.5.3) may occur and greatly influence NM fate and behaviour (Levard et al. 2012). All NMs have a tendency to aggregate; studies have demonstrated

that bare NMs form aggregates to reduce their free interfacial energy resulting from their high surface area once dispersed in an aqueous solution and collide with each other (Jiang et al. 2009; Yang et al. 2009; Mukherjee et al. 2010). Increases in ionic strengths which occur for instance when moving through an estuarine transect form the freshwater side, will cause increased aggregation in charge stabilised NMs. AgNPs aggregate in environmentally relevant conditions when charge stabilized or bare (Cumberland and Lead 2009; El Badawy et al. 2010; Römer et al. 2011), although this aggregation is reduced and even reversed in the presence of some NOM (Cumberland and Lead 2009; Fabrega et al. 2009; Fabrega et al. 2011). Changes in particle size and shape resulting from aggregation may significantly alter transport potential as well as NM reactivity and toxicity, and can lead to particle deposition (Petosa et al. 2010). For NPs which are sterically stabilised, rather than charge stabilised, for example PVP or PEG coated NPs, little or no aggregation occurs (Jiang et al. 2009).

Previous studies have shown that addition of low and environmentally relevant concentrations of humic substances (HS) stabilise NMs and reduce losses from surface water by aggregation/sedimentation. Cumberland and Lead (2009) showed that AgNPs are stable and show no aggregation in environmentally relevant conditions when stabilized with HS, although high concentrations of Ca^{2+} still causes loss. Gao *et al.* (2009) found that AgNPs were less toxic to the freshwater *zooplankton Ceriodaphnia dubia* in waters rich in NOM compared to waters with low organic content. They believe that NOM coats the NPs and the rate of Ag+ release is reduced; there is a reduced solubility and a reduction in bioavailability. Huynh *et al.* 2011 found that PVP coated AgNPs were significantly more stable than citrate-coated AgNPs in both NaCl and $CaCl_2$, which is likely due to steric repulsion. The adsorption of humic acid (HA) induced additional electrosteric repulsion that elevated the stability of both nanoparticles in suspensions containing NaCl or low concentrations of $CaCl_2$. Conversely, enhanced aggregation occurred for both nanoparticles at high $CaCl_2$ concentrations due to interparticle bridging by HA aggregates. Fabrega *et al*. (2009) found that NOM such as HS can cause disaggregation and mitigate short term bacterial toxicity through the formation of nanoscale films, with individual AgNPs stabilized by charge and entropically driven steric effects. The fate of ENMs will depend on their behaviour when in contact with natural HS and

other colloids and the repercussions of these interactions on ecosystem fate, behaviour and bioavailability of NPs must be characterised (Klaine et al. 2008). Factors such as pH, calcium ion concentration, and the presence of other types of natural colloids (Lead et al. 2006; Baalousha et al. 2008; Jiang et al. 2009; El Badawy et al. 2010; Petosa et al. 2010), will be important, and sediments (via aggregation and settling) are the likely final sink of NMs despite the stabilization effect of HS. Figure 1.16 shows the effect on ENMs of natural water components.

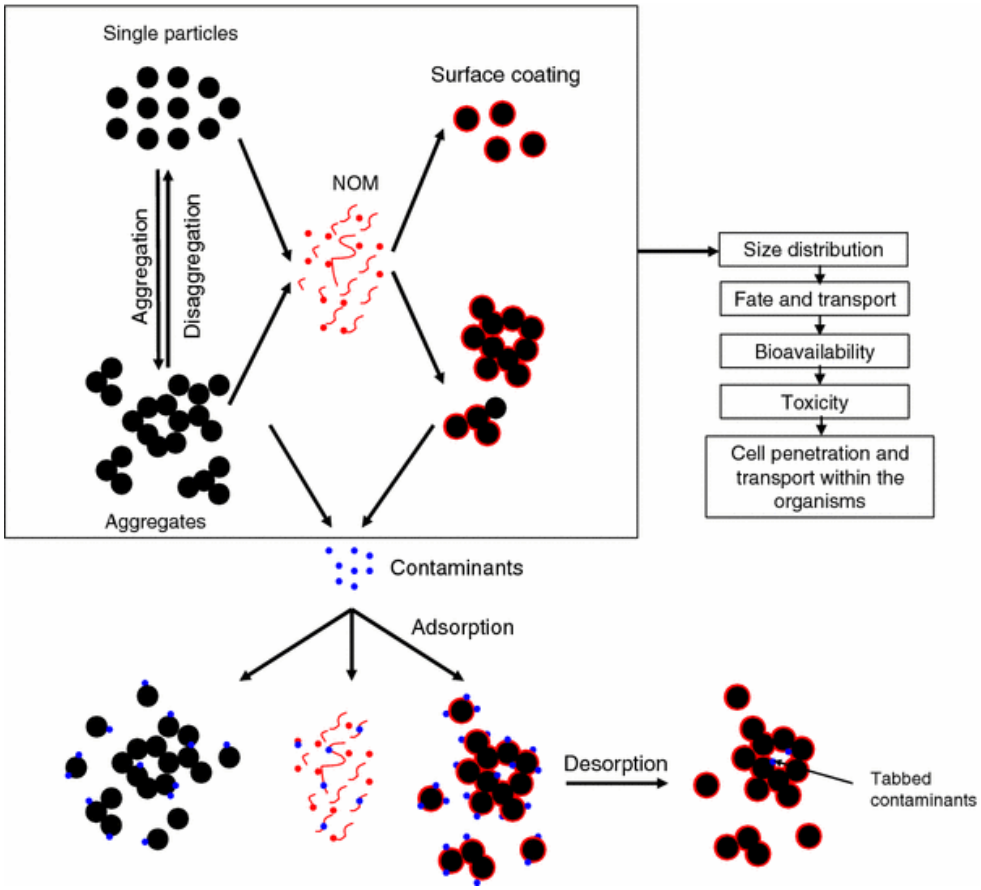

Figure 1.16 Interaction of NPs with natural water components. From Christian *et al.* (2008).

AgNPs products may release Ag+ ions which causes loss of the NP and these could be transported though waste waters and sewage from textiles and washing machines (Benn et al. 2008; Mueller et al. 2008; Kittler et al. 2010; Zhang et al. 2011). Dissolution is a final sink for NMs resulting in the loss of the

NM and the production of dissolved species, unlike aggregation where NMs are likely to be reversibly changed and move to a different environmental compartment. Zhang *et al.* (2011) studied the ion release kinetics of citrate stabilized AgNPs with different diameters in Hoagland medium (used for hydroponics) and suggest that the primary particle size of citrate-coated AgNPs, rather than the aggregated sizes, will govern the release. Kittler *et al.* (2010) also studied surface coating effects on the kinetics of Ag+ release, and developed an empirical model using first-order reaction kinetics. It was found that there was a limiting value of the released silver, i.e., the particles did not completely dissolve, and "aged" (i.e., immersed) PVP coated AgNPs were much more toxic to cells than freshly prepared particles.

Exposure to light can also lead to NP changes. Sunlight irradiation is thought to influence the toxicity of AgNPs in the environment, particularly since AgNPs and NOM are UV light sensitive (Li et al. 2011). It can also alter their dispersion in aquatic environments by inducing morphological changes on NPs. Cheng *et al.* (2011) observed that AgNPs (coated with gum arabic and PVP) exposed to sunlight and UV-light were very unstable, clearing after 2 days. NPs coated with PVP aggregated and NPs with gum arabic precipitated to the bottom of the vial. Their results also show toxicity of the AgNPs is significantly reduced after the sunlight treatment. Li et al. (2012) found that Ag+ release was not impacted by the artificial sunlight; but the light and citrate imparted morphological changes to the particles.

Understanding the eventual fate and behaviour of NMs upon reaching the environment is critical as this will determine their environmental distributions and concentration, pathways, sinks and ultimately control ecotoxicology, human health effects and the extent to which organisms are exposed. The precise fate of NMs over relevant timescales is uncertain because of the complexity of a) types NMs and b) different environmental systems. One has to consider the whole life cycle of NMs to ensure that possible impacts can be systematically discovered. It is obvious that much research is needed in freshwater, marine, atmosphere, sediment and soil ecosystems (Klaine et al. 2008).

1.8 Predicted environmental concentrations (PEC)

Due to the lack of methodologies to measure and quantify NMs in the environment there is no direct data for concentrations of manufactured NMs present in the environment. Therefore, modelling is required to produce predicted environmental concentrations (PEC) in different compartments (Gottschalk et al. 2010) and this modelling has been performed by a number of research groups, especially for Ag NMs (Blaser et al. 2008; Johnson et al. 2011). For instance, Gottschalk et al. (2010) modelled the PEC for TiO_2 NPs, CNTs and AgNPs for Switzerland. The model was generated considering different input parameters, such as production volumes of the NMs, manufacturing and consumption quantities of NM containing products, and the fate and pathways of the NMs in different environments, such as natural and manmade. All parameters were treated as probability distributions, due to the lack of data, and a probabilistic material flow analysis model was used. Using published data and to estimate potential risks, the PEC values were compared to the predicted no-effect concentrations (PNEC). In a regulatory context in the EU, risk is defined as the ratio PEC/ PNEC, for which numbers larger than 1 indicate cause for concern. The risk quotients for AgNPs were larger than 1 for treated wastewater and much smaller for all other environmental compartments (lower atmosphere, soil, surface water, groundwater, and sediments). It is worth noting that there is large uncertainty in the estimated PEC values, given the lack of data, especially concentrations measured in the environment which could validate the model predictions. In addition, considerable uncertainty in PNEC stems from poorly constrained dose quantification (Fabrega et al. 2011).

1.9 Quantifying dose

The primary practical challenge when undertaking ecotoxicity and toxicity studies on NPs, is administering dose and determining the form of the NP at the point of exposure; i.e. describing what the test organism is subjected to in reality. As it has been mentioned before, in media with high ionic strength or in contact with NOM NPs will aggregate or behave differently. The initial step in many ecotoxicity assays requires an even distribution of the toxicant in a stock suspension for subsequent application in the exposure medium. Adding dispersing agents or solvents can add toxicity, they could be either independently toxic or in combination with the NP (Henry et al. 2007). Physical dispersion, such as sonication, has the potential to damage some NPs, notably causing breakage of CNTs thereby altering their aspect ratio and potentially their toxicity profile (Kennedy et al. 2009). The choice of dispersion methods will depend on the dispersive properties of the NP and tolerance of the test organism to dispersing agents, but to obtain an accurate result it would be preferable not to add any external disturbance.

The concentration of a colloidal dispersion of particles can alter substantially during the course of ecotoxicity assays, even during acute exposures. This dynamic process is primarily attributable to particle aggregation and dissolution. Aggregation has implications for a classic dose-response assay in that at higher nominal doses a greater proportion of NPs will be present as aggregates. If those aggregates are sufficiently large or dense to sediment in a static culture, this will alter the NP dose received by the test organism; the actual exposure. The nature of the toxicant is also changed by aggregation, via changes in particle bioavailability (Lovern et al. 2006). Large aggregates may reduce membrane permeability but facilitate capture efficiency for filter or suspension feeding organisms (Ward et al. 2009; Petosa et al. 2010). Diluting culture media, and thus reducing the ionic strength, may reduce aggregation over time scales relevant for ecotoxicity assays, without causing physiological stress to the test organism (Römer et al. 2011).

Solubility will be influenced by particle size and shape, as a function of changing surface area (Borm et al. 2006; Zhang et al. 2011), and especially by functionalization or particle coating, which can limit surface oxidation and dissolution (Kittler et al. 2010; Zhao et al. 2012). Availability of free Ag+ will be influenced by the composition of the exposure media, as they can complex with inorganic and organic ligands that may be present. Ag^{+} ions easily form chloride and sulfide complexes which may alter the toxicity observed (Choi et al. 2009).

To describe actual organism exposure, NP characterisation must be performed *in situ* in media or exposure water. It must also be performed repeatedly, at the beginning and end of an assay as a minimum, in order to capture dynamic changes in physico-chemical parameters during the assay. Characterisation and quantification of NPs is a complex technical challenge, and the most appropriate methods will depend on a number of variables including nominal average particle size, particle concentration, chemical environment of the exposure media and the underlying principles of the characterisation technique. Even for a single NP property (e.g. size) all techniques will have advantages, biases and limitations.

1.10 Toxicity of silver nanoparticles

Silver toxicity to many organisms has long been known in the dissolved or ionic form (Reinfelder et al. 1999; Lubick 2008), with concerns previously due to discharges from photographic industry and mining (Eckelman et al. 2007). Recently, AgNPs are of great concern, due to the current and projected high exposure (Mueller et al. 2008). It is widely predicted that, due to their specific applications, AgNPs will be released primarily to aquatic environments (Mueller et al. 2008; Kaegi et al. 2010; Nowack et al. 2011). Pelagic organisms are initially at risk, and the potential toxicity of AgNPs has been demonstrated for a

number of freshwater species: *Lemna minor*, *Daphnia magna*, algae (for example, *Chlamydomonas reinhardtii*), brown trout and Zebrafish. A number of studies have also been conducted on bacteria, plants and humans. Figure 1.17 shows some examples of different organisms exposed to AgNPs, and a summary of the work done in recent years on toxicity is shown in Table 1.2.

Some toxicological effects of AgNPs found during *in vitro* studies are oxidative stress, cytotoxicity and chromosome instability, intracellular calcium transients, cell cycle arrest, apoptosis, interference with DNA replication fidelity, amongst others. In vivo studies have also shown oxidative stress and alteration of gene expression produced by free radical. These free radicals have also shown the ability to produce blood–brain barrier destruction and astrocyte swelling, neuronal degeneration; and to induce brain edema formation (Dhawan et al. 2010).

Accurate dose measurement is very important, as well as appropriate characterisation. In most studies commercially available NPs which are polydisperse, heterogeneous and not easily dispersible are used, which can alter dose. Also, studies tend to use short exposure periods and high concentrations of NPs, which is not environmentally relevant (Cumberland and Lead 2009).

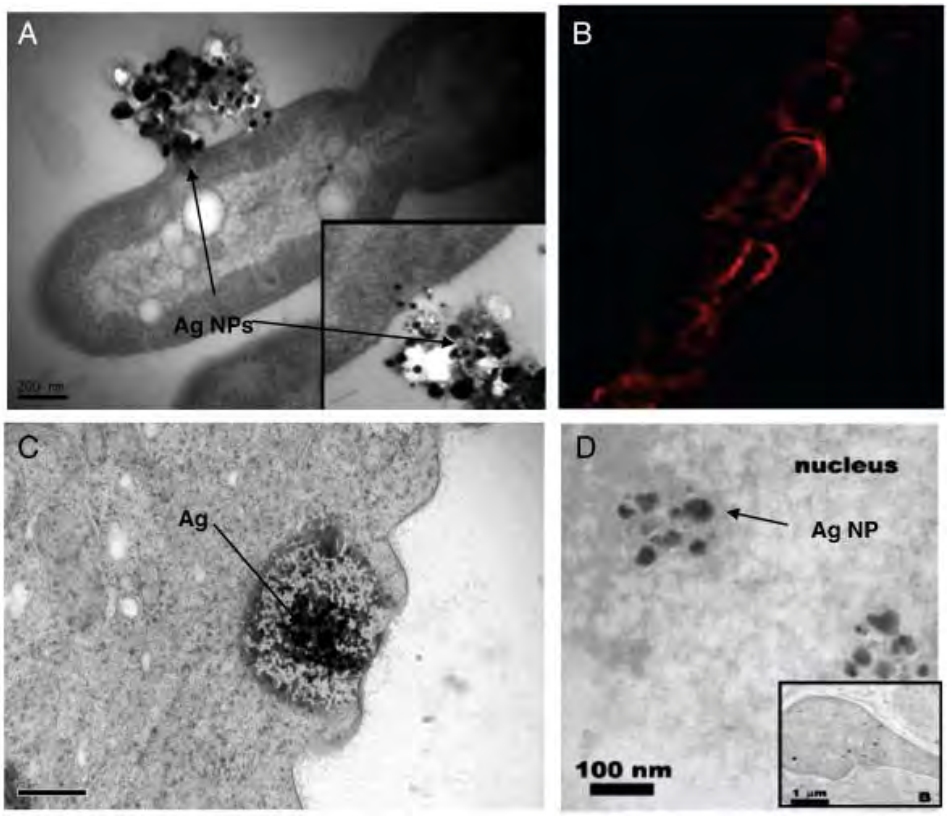

Figure 1.17 Image taken from: (Fabrega et al. 2011). Micrographs of in vivo uptake of Ag NPs by different organisms. A) TEM image of AgNPs being taken up by the prokaryote *Pseudomonas putida* (bacteria) after a 24 h exposure of 2 mg L^{-1} suspension of Ag NPs with 10 mg L^{-1} humic substances (Fabrega et al. 2009). B) Dark field image of AgNPs in the nematode *Caenorhabditis elegans* (roundworm) uterus after a 24 h exposure to 0.5 mg L^{-1} of AgNPs (Roh et al. 2009). C) TEM image of gill tissue dissected from rainbow trout after a 10 day waterborne exposure to 100 µg L^{-1} Ag NP suspension (Scown et al. 2010), and D) TEM images of BSA-AgNPs deposited in the cell and nucleus near the tail and trunk of zebrafish embryos treated with 25 µg L^{-1} BSA-Ag NPs (Asharani et al. 2008).

Table 1.2 Toxic effect of Ag NPs to different organisms. ND: not determined. Based on (Fabrega et al. 2011)

Organism	Size (nm)	Capping agent	Shape	Synthesis	Nominal conc. or LC50s	Dosing regime	Sample preparation	Major NP effects	Reference
vertebrates									
Zebrafish embryo	20–30	ND	Spherical	Electrolysis in tap water	10–20 ppt	72 h	Dilution with tap water	Penetration of Ag NP aggregates into skin and circulatory system	(Yeo et al. 2009)
Zebrafish	10–20	ND	Spherical	Electrolysis in tap water	0.4–4 ppm	2–36 days	Dilution with tap water	Alteration of p53 gene pathway. Defects in fin regeneration and penetration into organelles and cell nucleus	(Yeo et al. 2008b)
Zebrafish	20–30	Sodium citrate	Spherical	Gas phase condensation	LC50 7.07 mg L^{-1}	48 h	Sonication in UHP water	Differential toxicity of Ag NPs at different developmental stages overall Ag is more toxic than Ag NPs, except in fish fry stage	(Griffitt et al. 2008)
Zebrafish	26.6±8.8	Metal oxide	Spherical	Gas phase condensation	1000 mg L^{-1}	48 h	Sonication in UHP water	High binding of Ag NP with gills Distinct gene expression profile between Ag and Ag NP	(Griffitt et al. 2009)
Zebrafish embryo	5–20	BSA or potato starch	Spherical with borohydride	Chemical reduction	5–100 mg L^{-1}	72 h	ND	Deposition in cell nucleus, brain, nervous system and in blood	(Asharani et al. 2008)
Zebrafish embryo	11.6±3.5	ND	Spherical	Chemical reduction with borohydride	0.19 nM	0–2 h	Washed by centrifugation and incubated in egg water for 120 h	Transport of Ag NPs though chorion channels	(Lee et al. 2007)
Zebrafish	3, 10, 50, 100	No coating	Spherical	Citrate/ borohydride	LC50-3 nm 93 μM; LC50-10 nm 126 μM; LC50-50 nm 127 μM; LC50-100 nm 137 μM	120 h	Washed by centrifugation and resuspended in RO water without stabilisers	Size dependent Toxicity Morphological aberrations particle size dependent	(Bar-Ilan et al. 2009)

Organism	Size (nm)	Capping agent	Shape	Synthesis	Nominal conc. or LC50s	Dosing regime	Sample preparation	Major NP effects	Reference
Zebrafish	10 and 50	Citrate and PVP	ND	Commercially available and provided by other groups	1 mM Ag	days 0–5 post-fertilization	Dispersed in UHP water	Ag+ had a stronger effect on the fish, citrate NPs also showed toxicity	(Powers et al. 2011)
zebrafish	30-40	PVP	spherical	Commercially available with 0.2% PVP added	LC50 84 $\mu g\ L^{-1}$	48 h		Ag+ had a higher LC50	(Bilberg et al. 2012)
Perch	81	PVP	Elliptical/ multifaceted	ND	63–300 $\mu g\ L^{-1}$	2 days	Ag NPs were sonicated, centrifuged and filtered though a 0.22 µm pore filter	Ag NPs bound to gills and decrease tolerance to hypoxic conditions	(Bilberg et al. 2010)
Brown trout	10–35	Uncoated	Spherical	Purchased powder	10–100 $\mu g\ L^{-1}$	10 days	Sonication in ultrapure water for 30 min	Size dependent uptake AgNPs concentrated in gills and liver. Increase of oxidative stress in gills	(Scown et al. 2010)
Japanese medaka embryos	20 - 37	PVP	Spherical	Chemical reduction	100–1000 $\mu g\ L^{-1}$; LC50 1.03 mg L^{-1}	70 days	ND	100% embryo mortality was induced at 2 mg L^{-1}. They also observed a retarded development and pigmentation in embryos exposed to ≥ 400 $\mu g\ L^{-1}$ AgNPs	(Wu et al. 2010)
Japanese medaka	50	ND	cuboctahedral and decahedral	Commercially available	LC50 34.6 ±0.9	96 h	Sonication in UHP water	Expression of stress related genes indicated different modes of toxicity between Ag-NPs and Ag+.	(Chae et al. 2009)
Invertebrates									
Daphnia pulex	20–30	Sodium citrate	Spherical	Gas phase condensation	LC50 0.04 mg L^{-1}	48 h	Sonication in UHP water	Low toxicity of Ag NPs compared to Ag ions	(Griffitt et al. 2009)
Ceriodaphnia	20–30	Sodium citrate	Spherical	Gas phase condensation	LC50 0.067 mg L^{-1}	48 h	Sonication in UHP water	Higher toxicity of AgNPs compared to Ag ions	(Griffitt et al. 2009)
D. magna	36, 52, and 66 nm	Ag and Ag-Au, in citrate	ND	Citrate reduction	3 – 4 $\mu g\ L^{-1}$ for AgNPs and 15 $\mu g\ L^{-1}$ for Au-Ag	24 – 48 h	ND	Ag aggregated in Daphnia media but were much more toxic than Au-Ag. Ag-Au NPs showed toxicity values between that of Ag and Au but much closer to that of Ag.	(Li et al. 2010)

Organism	Size (nm)	Capping agent	Shape	Synthesis	Nominal conc. or LC50s	Dosing regime	Sample preparation	Major NP effects	Reference
D. magna	800, 100 and 6nm	Uncoated, citrate and coffee	Aggregates, spheres and triangles, spheres and rods	Commercially available, and reduction	LC50 1.4, 1.0 and 1.1 μg L^{-1}	48 h	Sonication in in reconstituted hard water	Differences in toxicity due to aggregation, but depends on Ag+ release	(Allen et al. 2010)
D. magna neonates	30nm and 0.6 - 1.6 μm	No coating	ND	Commercially available	0-1 and 10 mg L^{-1} for 96 h and 0 – 0.01 and 0.05 mg L^{-1} for 21 days	96 h and 21 days	Sonication in in reconstituted hard water	reduced moulting for AgNPs	(Gaiser et al. 2011)
D. magna	20nm	carbonate-coated	spherical	Commercially available	20, 50, 100, 200 and 500mg L^{-1}	24 h and 21 days	Sonication in UHP water	Higher toxicity of Ag ions compared to AgNPs	(Zhao et al. 2011)
D. magna		Lactate, PVP and sodium dodecylbenzene sulfonate	ND	Commercially available	1 – 100 μg L^{-1}	48 h	ND	Ag+ release was the cause of toxicity	(Zhao et al. 2012)
Caenorhabditis elegans	14–20	ND	ND	ND	0.05–0.5mg L^{-1}	24–72 h	Dispersed in UHP water and sonication for 13 h, stirring for 7 days and filtered 100 nm	Reduced reproductive success. Increase in oxidative stress Ag NPs accumulated around uterine area	(Roh et al. 2009)
Caenorhabditis elegans	7, 8, 38, 5, 22, 75, 21	Citrate, PVP and gum arabic	ND	Commercial NPs and chemical reduction	LC50 in EPA: 31; 3.5; 0.9; 2.7; 108; 40	3 days	Aqueous suspension	Lower ionic strength medium resulted in greater toxicity. AgNP toxicity depends on Ag+	(Yang et al. 2011)
Algae									
Pseudokirchneriella Subcapitata	20–30	Sodium citrate	Spherical	Gas phase condensation	LC50 0.19 mg L^{-1}	96 h	Sonication in UHP water	Low toxicity of Ag NPs compared to Ag ions	(Griffitt et al. 2009)
Chlamydomonas reinhardtii	25±13	Carbonate coated	Spherical	ND	EC501h: 3300 nM; EC50 5 h 829 nM	1 – 5 h	Aqueous suspension	Toxicity of Ag NPs mediated by Ag ions released from Ag NP in contact with cell	(Navarro et al. 2008)
Thalassiosira weissflogii	60–70	PVP	ND	ND	0.02 to 0.0002 nM	48 h	Filtered though a 0.22 μm pore size filter	Release of Ag+ from AgNPs reduced cell growth, photosynthesis and chlorophyll production	(Miao et al. 2009)
Ulva lactuca	> 100nm	ND	ND	Commercially available	2.5 -30 μg L^{-1}	48 h	Sonicated in UHP water	Ag+ more toxic than AgNPs	(Turner et al. 2012)

Organism	Size (nm)	Capping agent	Shape	Synthesis	Nominal conc. or LC50s	Dosing regime	Sample preparation	Major NP effects	Reference
Microbes									
Paramecium caudatum	30–40	Tween 80, PEG35000 or PVP 360	Spherical	Modified Tollens Process Chemical reduction of [Ag $(NH_3)_2$]+ with Dmaltose	LC50NP 39 mg L^{-1} LC 50 TweenNP 16 mg L^{-1}	1 h	Suspended in UHP water	Ag NP toxicity was enhanced when Tween 80 capped	(Kvitek et al. 2008)
Bacteria spp	26	PVPs, PEGs, Tween, non-ionic surfactants from Brij group	Spherical	Modified Tollens process. Chemical reduction of [Ag $(NH_3)_2]^+$ with Dmaltose	MIC range of 1.69 to 6.75 μg ml^{-1}	24 h	Aqueous dispersions	SDS, Tween 80 and PVP360 increased particle stabilisation as well as antibacterial activity of Ag NPs	(Kvitek et al. 2008)
Bacteria spp	16 ± 8	ND	Cuboctahedral, multiple twinned icosahedral and decahedral	Purchased NPs powder in a carbon matrix	0–100 μg ml^{-1}	30 min	Aqueous dispersion a and homogenate with ultrasonic cleaner	Ag NPs b10 nm attached to bacterial cells. NPs with a high reactivity facet [111] were the most toxic	(Morones et al. 2005)
E. coli	From 39	Citrate	Rod truncated, triangular and spherical	*Spherical:* chemical synthesis. by borohydride reduction; *Trunc. triang*: solution phase synthesis	0.1–10 μg ml^{-1}	0–26 h	Aqueous suspension	Truncated triangular NPs have a higher biocidal capacity than others	(Pal et al. 2007)
E. coli	9.3 ± 2.8	citrate	Spherical	Chemical synthesis by borohydride reduction	0.4–0.8 nM	30 min	Dilution in biological media (Hepes buffer and M9 medium)	Ag NPs are more toxic than Ag ions. Destabilisation of outer membrane, collapse of plasma memb. potential	(Lok et al. 2007)
E. coli	9.3 ± 2.8	citrate	Spherical	Chemical synthesis by borohydride reduction	0–100 μg ml^{-1}	24 h	Dilution in biological media (Hepes buffer and M9 medium)	Ag NP toxicity mediated by Ag+ from the NP. Smaller NPs are more toxic due to volume of oxidised surfaces and release of Ag+	(Lok et al. 2007)
E. coli	12	Daxad 19	ND	Chemical synthesis with ascorbic acid	0–100 μg ml^{-1}	10 h	Sonication in aqueous dispersion	Ag NP created 'pits' in the bacterial cell wall	(Sondi et al. 2004)

Organism	Size (nm)	Capping agent	Shape	Synthesis	Nominal conc. or LC50s	Dosing regime	Sample preparation	Major NP effects	Reference
E. coli	7, 29, 89	Gallic acid	Spherical and semi spherical	Chemical reduction	Minimum inhibition concentration: 6.25; 13.02 and 11.79 μg L^{-1}	24 h	Diluted with Mueller–Hinton broth inoculated	Antibacterial activity of the NPs varies when their size diminishes.	(Martinez-Castanon et al. 2008)
E. coli	35.4 ± 5.1	amorphous carbon	Spheres/ triangles	Commercially available	Anaerobic LC50: 0.10 ± 0.01 mg L^{-1}, aerobic: 0.87 ± 0.03 mg L^{-1}	24 h	Sonication in UHP water	AgNPs were 20 times less toxic than Ag+ in anaerobic conditions. They were more toxic after exposed to air.	(Xiu et al. 2011)
Nitrifying bacteria	21–21	PVA	ND	Chemical reduction with borohydride	0.05–1mg L^{-1}	180 days	Freshly synthesised suspensions	Growth inhibition correlated with Ag NPsb5 nm due to generation of intracellular ROS	(Choi et al. 2008)
Nitrifying bacteria	15 ± 9	PVA	Ellipsoidal and spherical	Chemical reduction with borohydride	1mg L^{-1}	18 h	From synthesis batch	The ligand sulfide forms AgxSy complexes or precipitates and reduced Ag NP toxicity by 80%	(Choi et al. 2009)
Pseudomonas fluorescens	65 ± 30	Citrate	Spherical/ triangular	Purchased powder	0–2000 ppb	24 h	Dispersion in 0.025 mM citrate solution, sonicated for 30 min for 4 days. Stirred in biological media for 24 h prior exposure	Toxicity of Ag NPs was pH dependent. However, the presence of organic matter mitigated Ag NP toxicity	(Fabrega et al. 2009)
Pseudomonas putida biofilm	65 ± 30	Citrate	Spherical/ triangular	Purchased powder	0–2000 ppb	24 h	Dispersion in 0.025 mM citrate solution, sonicated for 30 min for 4 days. Diluted in media and stirred for 24 h prior exposure	The presence of organic matter increased uptake of Ag NPs by biofilms. However, toxicity of Ag NP was mitigated with org. matter	(Fabrega et al. 2009)
S. aureus	7, 29, 89	Gallic acid	Spherical and semi spherical	Chemical reduction	Minimum inhibition concentration: 7.5; 16.67 and 33.71μg L^{-1}	24 h	Diluted with Mueller–Hinton broth inoculated	Antibacterial activity of the NPs varies when their size diminishes.	(Martinez-Castanon et al. 2008)

Organism	Size (nm)	Capping agent	Shape	Synthesis	Nominal conc. or LC50s	Dosing regime	Sample preparation	Major NP effects	Reference
bacillus	18, 10, 12, 10	Uncoated,citrate, PVP, branched polyethyleneimine	Spherical	Chemical synthesis	5 – 1000 mg L^{-1}	5 days	ND	Citrate-AgNPs were the least toxic, whereas the positively charged BPEI-AgNPs were the most toxic NPs.	(El Badawy et al. 2011)

Research has shown that toxicity depends on factors such as particle size, shape and surface properties, but even though AgNP toxicity has been studied there still is a high level of uncertainty with regards to their true toxicity (El Badawy et al. 2011). Some studies have suggested that AgNPs suspensions serve mostly as a source of Ag+, which has been said to be the responsible of NP toxicity (Xiu et al. 2011), while others suggest that toxicity will depend on AgNP uptake (Lubick 2008; Navarro et al. 2008). The effects of AgNP toxicity may be related to damages at cell membranes, to oxidative stress, or to interactions of Ag^{+} ions with proteins and enzymes (Navarro et al. 2008).

1.10.1 *Daphnia magna* for toxicological assays

Daphnia magna (shown in Figure 1.19), known as water flea, has been used for many toxicology tests due to the fact that these organisms are an important part of many aquatic food chains and a source of food for many fish species at the juvenile stage, including salmonids. Daphnia have a short life cycle and short life span; they are also easy to culture in the lab. Also, Daphnids are sensitive to a broad range of aquatic contaminants and are widely used as test organisms for evaluating toxicity of chemicals or effluents and the small size of daphnids requires only small volumes of test water, leading to ease of sampling and transporting waste water samples (Environment_Canada 1996).

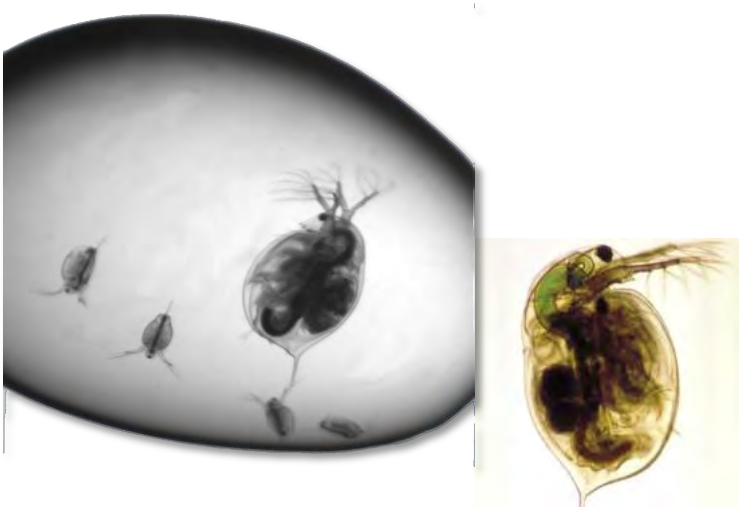

Figure 1.18 Daphnia magna pictures, the one on the left shows neonates as well as an adult (courtesy of Professor Mark Viant, University of Birmingham). The image on the right shows an adult D. magna in colour (Ebert 2005).

1.10.2 Toxicity to fish

As it has been mentioned before NMs can enter aquatic systems, aquatic organisms will be exposed to them and could be affected by dissolved or AgNPs. Fish have been used for toxicological assays, comparing the toxicity of AgNPs to Ag+ (Shaw et al. 2011).

Zebrafish is a common model organism in research related to pharmacology and genetics (Liu et al. 2012). It possesses a high degree of homology to human genomes, strong similarity to mammalian tissue structures and response to external threats (Langheinrich 2003; Powers et al. 2011). Other fish are also being used in toxicological studies of AgNPs. Juvenile zebrafish and Japanese medaka were more susceptible to AgNPs than to $AgNO_3$ in the same mass concentration (Fabrega et al. 2011). It has been said by some authors that the toxicity can't be attributed only to NP dissolution and the Ag+ formation (Griffitt et al. 2009; Yeo et al. 2009).

1.10.3 Toxicity to microbes

Due to the antibiotic properties of silver and AgNPs products, the toxicity of AgNPs to microbes has been more thoroughly investigated than invertebrate and vertebrate species (Fabrega et al. 2011). The mechanism of toxicity is not well understood, some studies suggest the size and shape has an effect on toxicity (Sondi et al. 2004; Pal et al. 2007; Kvitek et al. 2008) and others that the release of Ag+ is the responsible for the bactericidal effect (Navarro et al. 2008).

1.11 Research aims and objectives

The project aim is to synthesize AgNPs stabilized with different capping agents and of different sizes, characterise them and finally assess their stability in different media and environmentally relevant conditions. To achieve this goal the following steps will be performed:

Aim 1: To synthesize AgNPs using either citrate or PEG as the capping agent and of at least three different sizes. The NPs will be fully characterised by using a multi-method approach.

Aim 2: To assess the stability of AgNPs in *Daphnia magna* toxicity media, investigating the effect of media dilution on particle stability and *D. magna* viability.

Aim 3: To test the effects on AgNPs stability of different environmentally relevant conditions, such as synthetic waters, exposure to light and presence of organic matter (fulvic acid).

2

Methodology

2.1 Chapter Summary

Synthesis of AgNPs, sample and media preparation general details are provided in this chapter, as well as statistical methods, while the synthesis method development for the different particles is covered in chapter 3. Characterisation is a very important step after synthesis of nanoparticles (NPs) and after NP dispersion in media including in the environment. Particle size, charge, shape and specific surface area and other properties will have an influence on their environmental fate, behavior, mobility, aggregation and ecotoxicity. It is important to use a wide range of characterisation techniques in order to quantify the concentration and changes to the physico-chemical form of NPs (Ju-Nam et al. 2008; Baalousha et al. 2012a; Baalousha et al. 2012b). In this chapter we describe the different methods used to determine the characteristics of the silver nanoparticles (AgNPs) after synthesis (Chapter 3) and in different environmental and toxicological media (Chapters 4-5). Size was measured by dynamic light scattering (DLS), flow field flow fractionation (FIFFF), transmission electron microscopy (TEM), atomic force microscopy (AFM) and high resolution scanning transmission electron microscopy (HR-STEM); UV-vis was used to measure the surface plasmon band (SPB), energy dispersive X-ray *(*EDX) and electron energy loss spectroscopy (EELs) were used for elemental analysis of the particles; zeta potential was measured to assess particle stability; and inductively coupled plasma mass spectrometry (ICP-MS) was used to determine the concentration of Ag as well as for assessing ion concentration when coupled with ultrafiltration. At the end of the chapter Table 2.3 shows a summary of these methods.

2.2 Materials and methods

2.2.1 Chemicals

The chemicals and solvents used throughout were purchased from Sigma Aldrich and Fisher scientific. Ultra high purity water, UHP, (maximum resistivity of 18.2 MΩcm-1) was used for all experiments. All glass and plastic were washed before and after use with 10% nitric acid (HNO_3), to dissolve any particles, and rinsed with UHP water ensuring no traces of acid remained. Silver nitrate was stored in a dark container to prevent photo oxidation, and sodium borohydride ($NaBH_4$) was stored in a desiccator due to the fact that it is very hydroscopic.

Suwannee River fulvic acid (SRFA) was purchased from the International Humic Substances Society (IHSS) and aqueous solutions were prepared by dissolving the appropriate amount of solid in ultrapure water to make a stock solution of 400 mg L^{-1}, and left for 24 hours to hydrate. Dilutions of this stock solution were used to obtain the desired concentration within 2 days.

2.2.2 pH measurements

The pH measurements were conducted using a PHM 240 PH/ION meter lab probe. The probe was calibrated before use, using standard buffers of pH 4, pH 7 and pH 10, at room temperature. Solution pH values were adjusted, by the addition of dilute acid or base, usually HNO_3 or sodium hydroxide (NaOH).

2.2.3 Media and synthetic water preparation

Daphnia media preparation followed the OECD (Organisation for economic co-operation and development) guideline (OECD 1998) for the culturing and exposure to xenobiotics of Daphnia magna, with a minor modification as detailed previously (Taylor et al. 2009). Briefly, OECD recommended ISO media consisted of calcium chloride (294mg L^{-1}), magnesium sulphate (123.25mg L^{-1}), sodium carbonate (64.75mg L^{-1}) and potassium chloride (5.75mg L^{-1}) with additional sodium selenite (0.002mg L^{-1}) (Sigma Aldrich, UK). As dictated by the OECD guideline only media within pH range (6–9) was used. The media was used at full strength (ionic strength of 0.00884M) and after dilution by a factor of 2, 5 or 10 (labelled:

media1, media2, media5 and media10, respectively). All dilutions were made with UHP water and final pH was 7.5 in all cases (Römer et al. 2011).

Synthetic water (fresh very soft and soft, and seawater) were prepared based on the method recommended by the USEPA (United States Environmental Protection Agency) (USEPA 2002).

To prepare 1 L of standard, synthetic reconstituted water, the reagent grade chemicals in Table 2.1 were used as follows:

- Place 900ml of UHP water in a properly cleaned flask. .
- Add the $MgSO_4$, $NaHCO_3$, and KCl to the flask.
- Aerate overnight.
- Add the $CaSO_4 \cdot 2H_2O$ to 100ml of UHP water in a separate flask.

Stir on magnetic stirrer until calcium sulphate is dissolved, add to the 900ml solution above, and mix well.

- Aerate the combined solution vigorously for an additional 24 h to dissolve the added chemicals and stabilize the medium.

Table 2.1 Preparation of synthetic freshwater.

	Reagent added (mg L^{-1})					Approximate final water quality		
	$NaHCO_3$	$CaSO_4 \cdot 2H_2O$	$MgSO_4$	KCl	pH	Hardness[1]	Alkalinity[1]	Ionic Strength (M)
Very soft	12.0	7.5	7.5	0.5	7.1	10-13	10-13	0.000633
Soft	48.0	30.0	30.0	2.0	7.4	40-48	30-35	0.00253

[1] Expressed as mg $CaCO_3$/L.

To prepare 1 L of standard, synthetic, reconstituted seawater with a salinity of 31 % (Table 2.2), pH 7.4 and ionic strength 0.719M, the instructions below were followed. Other salinities can be prepared by making the appropriate dilutions.

- Place 1 L of UHP water in a properly cleaned flask.

- Weigh reagent grade salts listed in Table 2.2 and add, one at a time, to the UHP water. Stir well after adding each salt.

- Aerate the final solution at a rate of 1 L/h for 24 h.

Table 2.1 Preparation of synthetic seawater.

Compound	Concentration (g L^{-1})
NaCl	21.03
$NaSO_4$	3.52
KCl	0.61
KBr	0.088
$Na_2B_4O_7 \cdot 10H_2O$	0.034
$MgCl_2 \cdot 2H_2O$	9.50
$CaCl_2 \cdot 2H_2O$	1.32
$SrCl_2 \cdot 2H_2O$	0.02
$NaHCO_3$	0.17

2.2.4 Synthesis of citrate stabilized AgNPs

AgNPs stabilized with citrate were synthesized by varying previously reported methods (Henglein et al. 1999; Doty et al. 2005; Cumberland and Lead 2009). Three different sizes of AgNPs (labeled AgNP1, AgNP2 and AgNP3) were prepared from a standard reduction of the silver salt in sodium citrate. Solutions of 100ml sodium citrate (0.31mM), 100ml silver nitrate (0.25mM) and sodium borohydride (10mM for AgNP1 and AgNP3, and 0.25mM for AgNP2) were prepared in ultrapure water and kept at 4 ◦C in the dark for 30min. For AgNP1 and AgNP2, the silver nitrate and sodium citrate solutions were mixed together in a conical flask and vigorously stirred. Subsequently 6ml of the solution of the reducing agent, sodium borohydride ($NaBH_4$), was added in one batch. After 10 min of stirring, the solution was heated

slowly to boiling and heated for a further 90min, left overnight, filtered the next day at 0.1µm, and then cooled (4 ◦C, in the dark).

To obtain the smallest nanoparticles (labelled AgNP3), the heating process was performed without $NaBH_4$, and at the end 6ml of the 10mM reducing agent was added and the solution was heated for 10 extra minutes. More details on the synthesis are given in chapter 3.

AgNPs were cleaned to remove the excess reagents before use. Suspensions were cleaned by ultrafiltration (Amicon, 1 kDa regenerated cellulose membrane, Millipore) using a diafiltration method to prevent drying of the particles, explained in section 2.2.7. The particles were redispersed in citrate solution to avoid further growth, this process was repeated at least three times.

2.2.5 Synthesis of PEGylated AgNPs

Once the citrate NPs were produced and washed, aliquots were taken which were converted to PEG-SH coated NPs by adding enough thiolated PEG (Mw 5000, purchased from Sigma Aldrich) drop wise and under vigorous stirring into the citrate coated AgNPs to coat the particles with 4 molecules of PEG-SH per nm^2 (Fernandez-Lopez et al. 2009). The mixture was shaken for 30mins, left overnight and ultrafiltered. DLS, FI-FFF, AFM and TEM were used to confirm that the citrate coated AgNPs had been converted into PEGylated AgNPs with no further changes.

2.2.6 Sample preparation

The solution of AgNPs as prepared (12 mg L^{-1}) was added to the media (Römer et al. 2011) or synthetic water to obtain a solution of 2.2 mg L^{-1}. Controls with the same concentration as the particles in media or synthetic water were prepared as well, by adding citrate or UHP water. The particles were left in the different solutions for different periods of time to assess the changes in their properties. Some samples were also exposed to light. More detail is given in Chapter 4 and 5.

2.2.7 Filtration and ultrafiltration

Filtration was used to eliminate particles of large size after synthesis. A Millipore Sterifil filtration system with filters of cellulose nitrate membrane, pore size 0.1 μm and a diameter of 47 mm, were used. It is important to filter at least 50ml of UHP water before the sample is filtered in order to eliminate any impurities.

Ultrafiltration is an important step after the reactions to eliminate any unreacted reagents and also to assess dissolution of NPs over time. It was performed using an Amicon stirred cell (Millipore) under N_2 gas with a 1 kDa regenerated cellulose membrane. Dissolution of carbon dioxide due to the use of compressed air can cause large pH shifts, as well as oxidation in the case of sensitive solution, and it will potentially lead to other problems (Stirred_Ultrafiltration_Cells_User_Guide 2008). Membranes were left in a 2% HNO_3 solution for 24 hours, followed by adequate rinsing with water to remove acid traces and leachable metal ions. Initially, 50ml of UHP water was added and ultrafiltered, before the system was dry the NP suspension was added and after 70% of the solution was filtered it was replaced with the same volume of 0.15mM citrate solution water in the case of citrate capped NPs, or PEgylated solution in the case of PEG capped particles. This was repeated at least two times. Ultrafiltration is performed to prevent further growth of the particles and increase stability over time. Figure 2.1 shows both filtration devices.

Figure 2.1 Left: millipore sterifil filtration system. Right: Ultrafiltration equipment assembly.Sample is placed in chamber, N2 gas is passed over the sample from the top with the filtrate collected from the bottom. The sample is stirred to reduce aggregation as the sample concentrates. Images obtained from Fisher Scientific, UK.

2.3 Characterisation

2.3.1 Dynamic light scattering (DLS)

Dynamic light scattering (DLS) is a widely used technique to measure hydrodynamic diameter (d_H). It measures Brownian motion, which relates to particle size. d_H depends on different factors, like the size of the particle "core", the capping agent, and the concentration and type of ions in the medium.

In DLS a laser is shined onto a solution containing spherical particles and size can be obtained by analyzing the intensity fluctuations in the scattered light (Zetasizer - manual 2003-2004). Brownian motion causes a Doppler Shift when the light hits the moving particle, changing the wavelength of the incoming light. Small particles move quickly and large particles move more slowly in the case of Brownian motion for DLS. In polydisperse samples, reported mean diameters are weighted toward larger agglomerate sizes, because the amount of light scattered by larger nanoparticles is greater than that of smaller nanoparticles. This can overestimate particle size (Römer et al. 2011).

The relationship between the size of a particle and its speed is defined in the Stokes-Einstein equation (2.1), where k_B is the Boltzmann constant, T the absolute temperature, η is the viscosity of water and r is the hydrodynamic radius.

$$\boldsymbol{D}\mathrm{t} = \frac{\mathrm{kB}\,\boldsymbol{T}}{\boldsymbol{6\pi\eta r}} \tag{2.1}$$

The hydrodynamic diameter is reported as the intensity-weighted Z average, with the polydispersity index width (PdI) representing the standard deviation about the Z average assuming a monomodal distribution (Darlington et al. 2009). The Z average can be further converted to volume and number distribution.

In Figure 2.2 it can be seen the difference between intensity, volume and number distributions. A solution with spherical particles of diameter 5nm and 50nm present in equal numbers was measured (Zetasizer-manual 2003-2004). The number distribution of these two different particle sizes will show a plot

consisting of 2 peaks with a 1 to 1 ratio. Because the volume of a sphere is equal to $4/3\pi(d/2)^3$, if the number distribution was converted into volume then the 2 peaks would change to a 1:1000 ratio. If this was further converted into an intensity distribution, a 1:1000000 ratio between the 2 peaks would be obtained. This is because the intensity of scattering is proportional to d^6 (from Rayleighs approximation (2.2)). This explains the importance of the presence of a second peak.

$$I\alpha\, d^6 \qquad \text{and} \qquad I\alpha\, 1/\ ^4 \tag{2.2}$$

In general terms we can say that: d(intensity) > d(volume) > d(number)

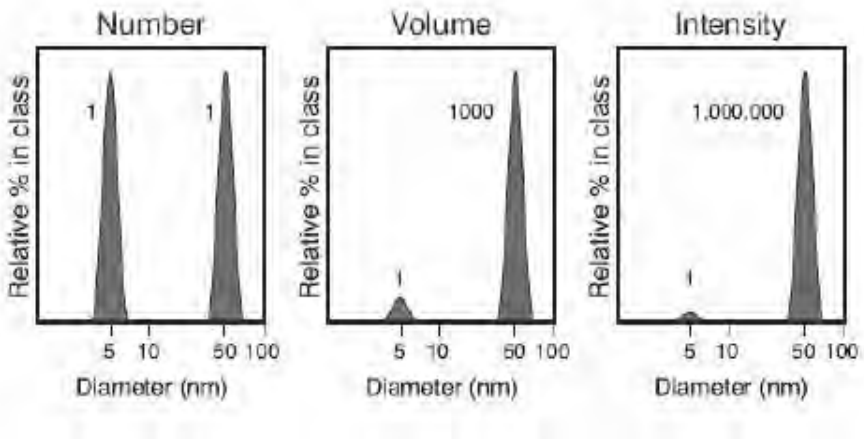

Figure 2.2. Influence of smaller particles on DLS measurements. An example of a sample containing equal amount of 5 nm and 50 nm particles showing: a) number distribution, b) volume distribution and the c) intensity distribution. Taken from (Zetasizer-manual 2003-2004).

Measurements were conducted with a Malvern Zetasizer 5000 (Figure 2.3) that combined particle sizing and electrophoresis (section 2.3.2) in low volume disposable cuvettes and at least five concordant measurements recorded to calculate a mean z average size and at 21^{o}C. The refractive index (0.54) and absorption (3) for silver samples were used to create the standard operating procedure (SOP).

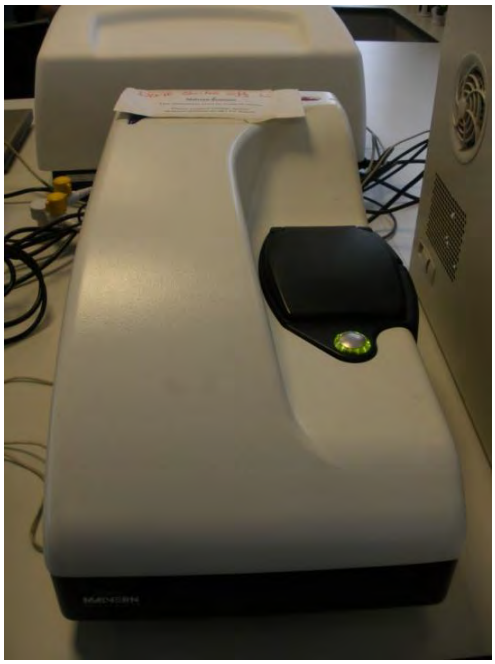

Figure 2.3. Malvern zetasizer 5000.

2.3.2 Electrophoretic mobility (EPM) and zeta potential

The zeta potential was measured with the Malvern Zetasizer 5000 and can be obtained by determining the electrophoretic mobility and then applying the Henry equation (2.3).

$$U_E = \frac{2\varepsilon\, z\, f(\kappa a)}{3\eta} \tag{2.3}$$

Where U_E is electrophoretic mobility, z is zeta potential, ε is the dielectric constant, η is viscosity and f(κa) is the Henry's function (which for particles in polar media is 1.5 and 1 for non-polar).

Particles in suspension will have an electrical double layer around them (Figure 2.4), which consists of two parts, the inner region called the stern layer, where the ions are strongly bound, and the outer, called the diffuse region, where they are less firmly attached. When a particle moves the ions within a boundary in the diffuse layer will move with it, but any ions beyond it do not travel with the particle. This is known as the slipping plane. The zeta potential is the potential that exists at this boundary.

Zeta potential depends on both the chemistry of the surface and the dispersant. It reflects the effective charge on the particles and is therefore related to the electrostatic repulsion (Borm et al. 2006). Zeta potential depends on the pH of the solution, the ionic strength (concentration or type of salt), changes in the concentration of a solution and capping agent (polymer, surfactant, etc). It can be reduced to zero at a specific pH referred to as the isoelectric point. Zeta potential is a very good index of the magnitude of the interaction between colloidal particles and these measurements are used to assess the stability of colloidal systems and hence the particles shelf life if they are charge stabilised. The higher the value of zeta potential, the more stable the dispersion is likely to be (Zetasizer-manual 2003-2004). Colloidal stability can be explained by DLVO theory, which has been previously explained in section 1.8.

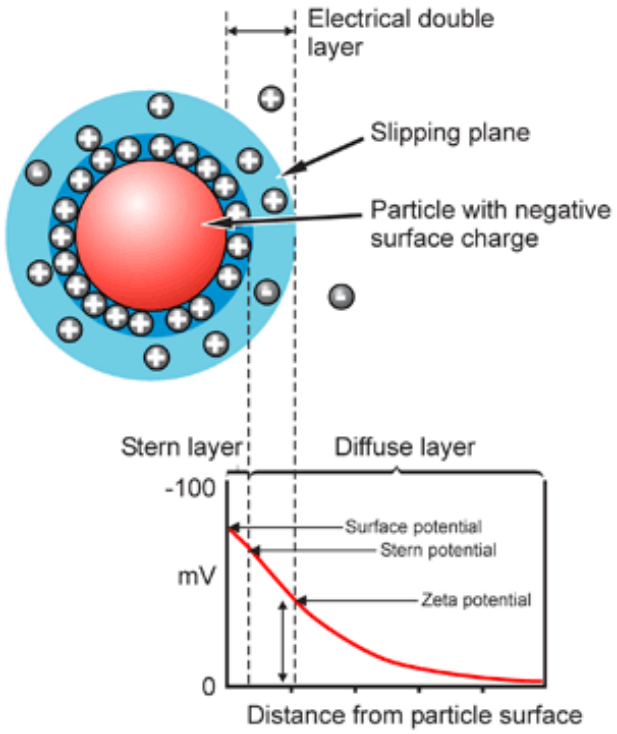

Figure 2.4. Schematic of the electrical double layer at the surface of solution-phase nanoparticles. Image from http://www.nanocomposix.com.

Electrophoresis happens when an electric field is applied across the dispersion and charged particles in the dispersion will move toward the electrode of opposite polarity (Jiang et al. 2009). The electrophoretic

mobility is obtained by performing an electrophoresis experiment on the sample and measuring the velocity of the particles using laser doppler velocimetry (LDV) (Zetasizer-manual 2003-2004). Measurements were performed at 21^{o}C and repeated at least 5 times per sample using a low volume zeta cell which was washed with UHP water in between each sample.

2.3.3 Flow field-flow fractionation (Fl-FFF)

Field-flow fractionation (FFF) is a family of separation techniques designed to separate particles based on diffusion coefficient (Popa et al. 2007). It has been used increasingly to separate and characterise particulate matter from solutions. Figure 2.5 shows how an FFF system works. In Flow FFF a second carrier fluid inlet provides the perpendicular field through a cross flow of solvent.

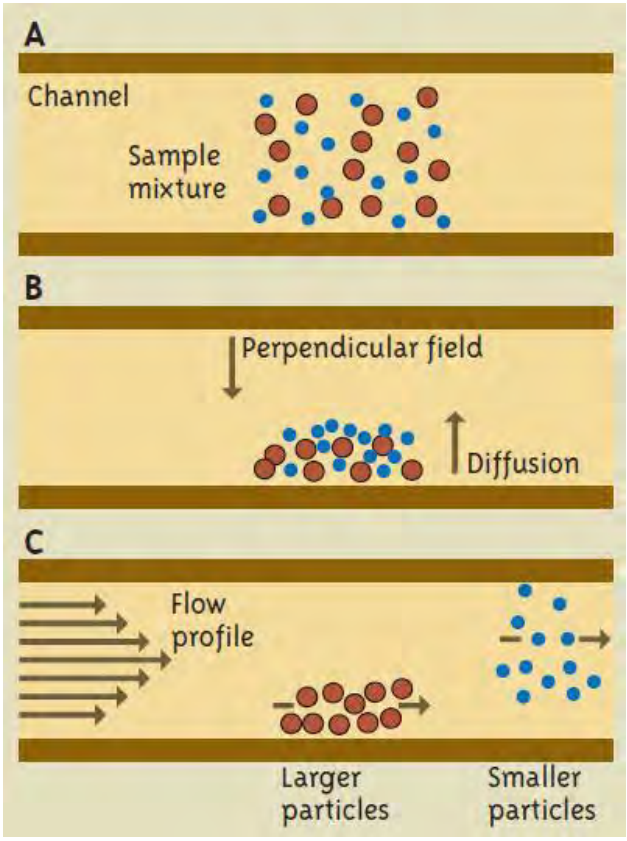

Figure 2.5. Field flow fractionation. (A) Sample is injected into the FFF unit as a diffuse mixture. (B) A perpendicular field is established, and the sample particulates distribute on the basis of diffusion rates versus field strength. (C) The external field is removed, the samples are flushed from the system, and particles farther from the chamber floor elute faster (Willis 2002).

This separation technique is based on hydrodynamic principles in which particles are separated because of their interaction with the crossflow field force (friction coefficient) and their translational diffusion (Baalousha et al. 2007). Smaller particles with higher diffusion constants find themselves at a greater distance from the accumulation wall whilst the larger particles are situated closer to the wall. This results in the elution of the smaller particles at a faster rate (Kanzer et al. 2010). For FIFFF, the separation mechanism is based on diffusion and not on chemical interaction as in chromatography (Hagendorfer et al. 2010). FIFFF has been coupled to several detectors for further analysis of the fractionated sample, such as UV-vis (Cumberland and Lead 2009), light scattering (Wyatt 1998), inductively coupled plasma-mass spectrometry (ICP-MS) (Baalousha et al. 2006; Krystek et al. 2011), transmission electronic microscopy (TEM) (Baalousha et al. 2006; Poda et al. 2011) or atomic force microscopy (AFM) (Baalousha et al. 2007).

Asymmetric flow field flow fractionation (A4F) is capable of separating particles between several µm down to 1 nm in hydrodynamic radius (Hagendorfer et al. 2010; Williams et al. 2010). Sample volumes from several µL up to 50ml can be introduced to the separation channel.

Separation takes place in a thin, ribbon-like channel in which a laminar flow with a parabolic flow velocity profile is subjected to a perpendicularly applied external field (Giddings 1993; Williams et al. 2010). The channel geometry and thickness is defined by the channel composition, which consists of two Perspex blocks separated by a spacer (Baalousha et al. 2011). The accumulation wall is made of a permeable ceramic frit and the upper wall is impermeable. Channel flow is perpendicular to a cross flow (Figure 2.6). The channel stream will drive the particles toward the outlet, as the cross flow pushes particles toward the accumulation wall.

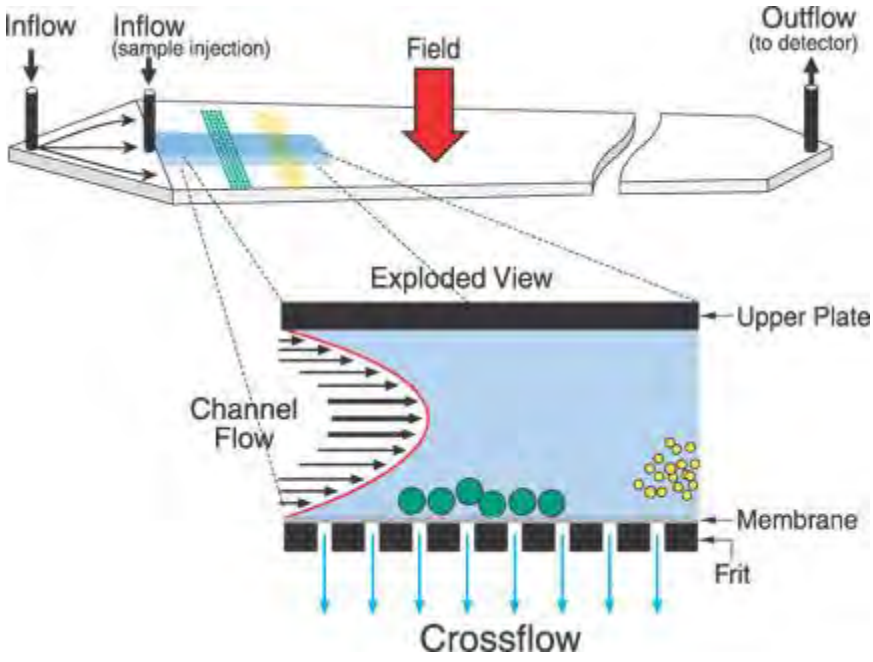

Figure 2.6. FFF separation: ribbon like FFF channel (top), sandwiched between channel walls this is usually 75–260 µm in thickness (image from http://www.wyatt.com). Different distributions of two particles within the channel (bottom).

There is an exact relationship between the retention time and the size of the particle based upon a Brownian mode of retention and full dilution within the carrier liquid (Schimpf, 2000). The retention time (*R*) is given by:

$$R = \frac{t^o}{t_r} \tag{2.4}$$

Based upon the analyte's retention time (t_r) and the void time within the channel (t^o). Where:

$$t^o = \frac{V^o}{F} \tag{2.5}$$

Where V^o is the channel void volume and *F* the volumetric flow rate. *R* is then related to the retention parameter (λ):

$$R = 6 \left[coth\left(\frac{1}{2}\right) - 2 \right] \tag{2.6}$$

In FFF theory, lambda (λ) can be expressed as ℓ (mean layer thickness) divided by the channel thickness, w, in non dimensional form:

$$= \frac{\ell}{w} \tag{2.7}$$

Where ℓ for each component is the ratio of diffusion coefficient D and field-induced velocity U (ℓ = D/ IUI). Small particles with large diffusion coefficients have higher ℓ values than larger particles with small diffusion coefficients. The force exerted on an analyte by the external field is related to λ by:

$$= \frac{kT}{F_w} \tag{2.8}$$

With *k* the Boltzmann constant, T the absolute temperature and F_w the force. This can then be related to the Stokes Diameter of the particle:

$$= \frac{kTV^o}{3\pi\ V_c w^2 d_{St}} \tag{2.9}$$

Where η is the viscosity, V_c the volumetric rate of cross flow and d_{St} the Stoke's diameter.

$$d_{St} = \frac{kTV^o}{3\pi\ V_c w^2} \tag{2.10}$$

As separation is based on D which is converted to size, the results are easily interpreted with residence time t_r would be approximately proportional to diameter. Size-based selectivity (eq. 2.11) for this technique is equal to 1, meaning very small changes can be detected.

$$S_d = \left|\frac{d(logt_r)}{d(logd)}\right| \tag{2.11}$$

The experiments were performed in an asymmetrical flow-field flow fractionator (FIFFF) (AF2000 Mid Temperature, Postnova Analytics, Germany), as seen in Figure 2.7. The accumulation wall consisted of a 1 kDa regenerated cellulose membrane. The eluent was delivered by separate cross-flow (PN1130 Isocratic pump) and channel flow pumps (PN4020 channel) and was degassed before delivery (PN7520 solvent degaser). The eluent was 10mM NaCl or $NaNO_3$, pH 7.5, as used in previous studies

(Cumberland and Lead 2009). Channel flow was set to 1 ml min^{-1} and the cross flow was set between 0.3 and 0.5 ml min^{-1} to obtain good separation of the void and sample peak. Particles eluted from the FlFFF channel were detected by a UV spectrometer, the detector was set at 400 nm wavelength for detection of the AgNPs. Data acquisition was via LC solution multi PDA (version 2.1, Postnova Analytics, Germany). The channel volume was calculated applying FlFFF theory (Schimpf et al. 2000) using standard polyacrylamide beads PAA of different sizes (Duke Scientific Corp.), 20, 30, 40 and/or 60nm, which were detected with the UV detector at 254 nm. Diffusion coefficients were calculated based on standard FlFFF theory and converted to size using the Stokes–Einstein relationship. Between 0.5 ml and 3 ml of the sample was injected, depending on the concentration of the analyte in solution, at least three independent replicates were analysed per sample and the data averaged. Excellent agreement (peak heights differing by <2%, in general) between replicates was observed (Römer et al. 2011).

The peak (dp), number (dn), and weight (dw) average hydrodynamic diameters and sample polydispersity were calculated for each sample in the different media applying Eqs. (2.12 – 2.14)

$$d_n = \frac{\sum_i C_i X_i}{\sum_i C_i} \tag{2.12}$$

$$d_w = \frac{\sum_i C_i {X_i}^2}{\sum_i C_i X_i} \tag{2.13}$$

$$\text{Polydispersity} = \frac{d_w}{d_n} \tag{2.14}$$

Where C_i is the concentration of the particles in each FlFFF slice and Xi is the measured property (i.e.,hydrodynamic diameter by FlFFF) (Baalousha et al. 2008).

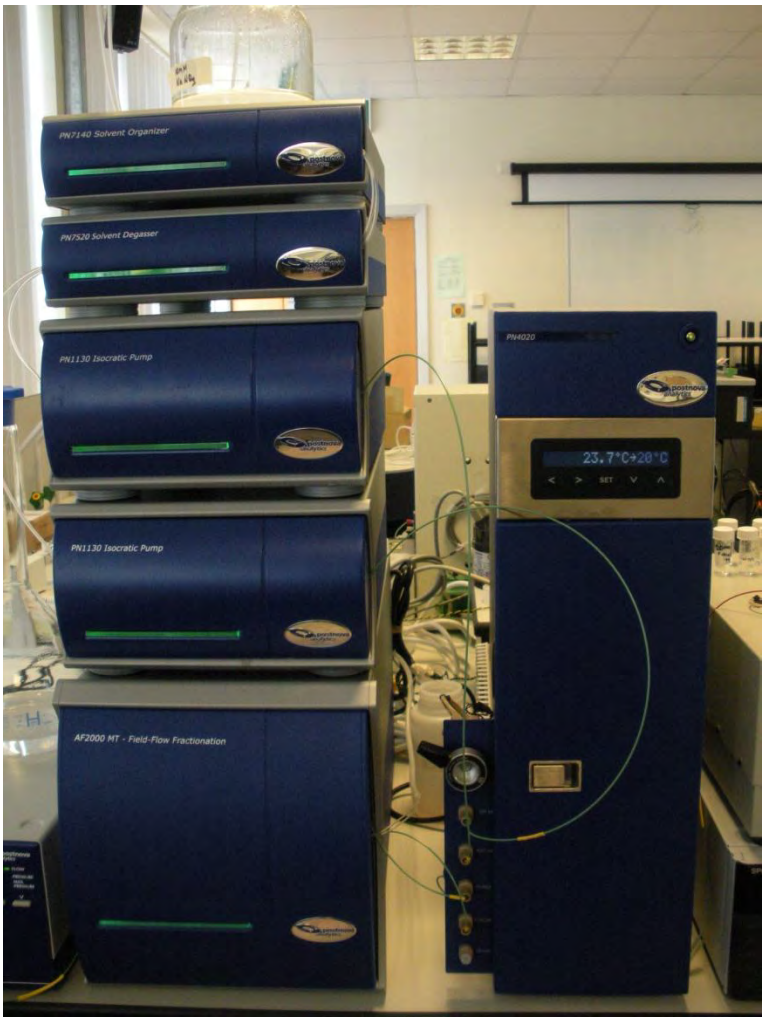

Figure 2.7. Asymmetrical flow-field flow fractionator (FIFFF) (AF2000 Mid Temperature, Postnova Analytics) used in the experiments.

2.3.4 Surface Plasmon Resonance (SPR)

The surface plasmon resonance is caused by the interaction with the incident light and the free electrons in the materials (Ju-Nam et al. 2008). The irradiation of light to a small spherical metallic nanoparticle will generate an oscillating electric field that causes the conduction electrons to oscillate coherently, as shown in Figure 2.8. The frequency of this oscillation is determined by different factors: electron density, effective electron mass, and the size and shape of the charge distribution. In the case of the bulk there is a mismatch between the plasmon dispersion relation and that of the photon, so they can't be excited by

plain light. In small particles there is no such mismatch, so they can be excited by plain light and thus, show colour. (Ghosh et al. 2007).

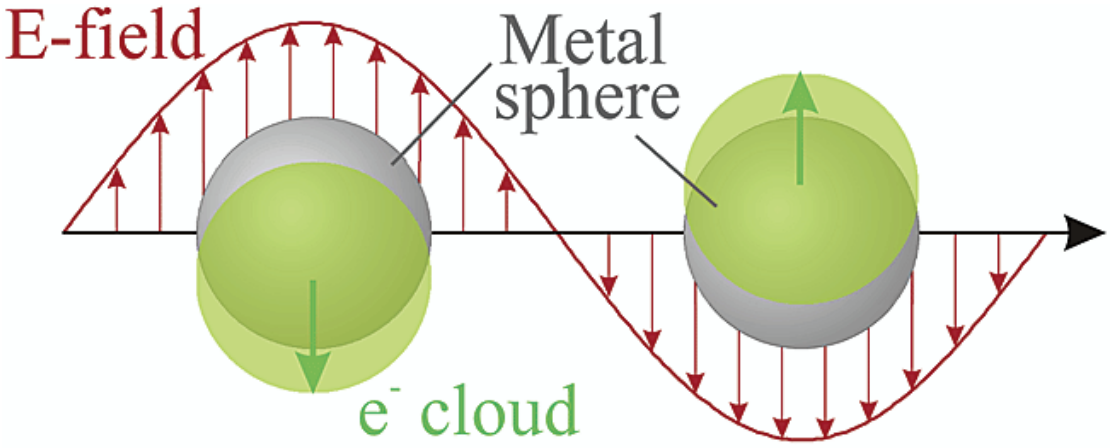

Figure 2.8. Schematic of plasmon oscillation for a sphere, showing the displacement of the conduction electron charge cloud relative to the nuclei (Kelly et al. 2003).

The dipole resonance occurs in the UV-Vis region for gold and silver nanoparticles, making them useful for optical applications (Eccles et al. 2010). AgNPs absorb light at around 400nm and show an intense yellow colour. Gold will absorb at 550 nm and will be red, in most cases.

The Mie scattering theory has been widely used to study the optical properties of isolated colloidal particles and their dependence on particle size effect (Ghosh et al. 2007). This theory is to this date the only simple and exact solution to Maxwell's equation relevant to spherical particles (Kelly et al. 2003).

Mie theory describes the absorption and scattering of spherical particles that have an arbitrary size. When a spherical particle that is much smaller than the wavelength of light (2R«), where R is the radius of the particle, interacts with light (Ghosh et al. 2007), we can relate the dipole plasmon frequency of a metal NP to the dielectric constant.

According to Mie theory we can derive the extinction and scattering coefficient to obtain (Ghosh et al. 2007):

$$\sigma_{sca} = \frac{2\pi}{K^2} \sum_{n=1}^{\infty} (2n+1) \{|a_n|^2 + |b_n|^2\} \quad (2.15)$$

$$\sigma_{ext} = \frac{2\pi}{K^2} Re(a_n + b_n) \quad (2.16)$$

Where Re represents the real part of the argument, in the mathematical sense, n is the complex refractive index of the particle, a_n and b_n are the Mie coefficients, and K is defined as:

$$K = \frac{2\pi n_{med}}{} \quad (2.17)$$

Where n_{med} is the real refractive index of the surrounding medium and is the wavelength of the incident light. Assuming 2R« :

$$\sigma_{sca} \approx \sigma_{ext}$$

$$\sigma_{ext} = 9\frac{w}{c} \epsilon_m^{3/2} V \frac{\epsilon_2(w)}{[\epsilon_1(w) + 2\epsilon_m]^2 + [\epsilon_2(w)]^2} \quad (2.18)$$

Where V is the volume of the spherical particle, *w* is the angular frequency of the exciting light, *c* is the velocity of light, and ϵ_m and $\epsilon(w) = \epsilon_1(w) + i\epsilon_2(w)$ are the dielectric functions of the surrounding medium and the material itself, respectively. Changes in the media can alter the plasmon behavior, as well as changes in the size of a shell for core-shell particles as well as changes in particle size. The peak will tend to shift to the red when size increases (Ghosh et al. 2007).

The SPR of the AgNPs suspensions was investigated using a Hewlett-Packard 8452A spectrometer in 1 cm pathway quartz cuvette and a 6800 Jenway double beam UV-Vis spectrophotometer, with a 1 cm path length plastic cuvette. The UV-Vis absorption spectra were collected over a wavelength range of 300-800nm, and sometimes starting from 200nm. Suitable blanks and controls were measured. AgNPs typically absorb around 400nm. A diagram of a UV-vis machine is shown in figure 2.9.

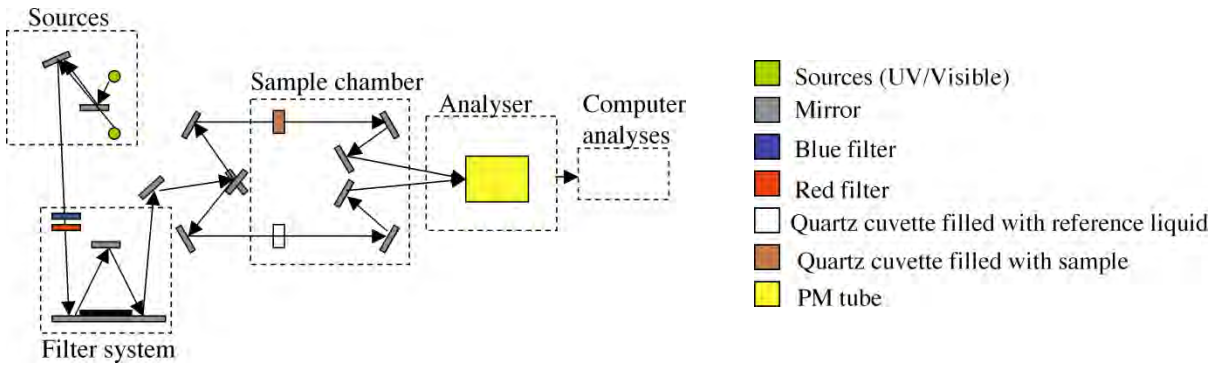

Figure 2.9. Diagram of a UV-vis. Courtesy of Ruth Merrifield.

The UV/Vis spectrophotometer uses two light sources: a deuterium arc lamp for the UV range, from 190 to 380 nm, and a tungsten- halogen lamp for the visible spectrum, from 380 to 800 nm or more. The light source is directed to a filter system that causes different wavelengths of light to be dispersed at different angles. They can be prisms or holographic gratings. After the light passes through the dispersion device and the sample of interest it reaches a detector. Photomultipliers are common, and photodiodes are being increasingly used. Path lengths for the sample and the reference cell need to be the same. The detector will take the difference between the signals passing through both cells to measure the absorption.

2.3.5 Inductively Coupled Plasma Mass Spectrometry (ICP-MS)

Because of its element-specific detection and high sensitivity, ICP-MS is ideal to study AgNPs and other inorganic nanoparticles (Mitrano et al. 2012). One advantage of this method is that the ICP-MS detector is very sensitive and selective, which allows the determination of silver nanoparticles at environmentally relevant concentrations (low ppb) (Poda et al. 2011). ICP spectrometry is commonly applied during the synthesis of nanoparticles, since it is perfectly suited to determine the total element concentration of the colloidal solutions (Scheffer et al. 2008). By using different separation methods, such as ultrafiltration (2.2.7), dialysis or ultracentrifugation (2.3.6), the concentration of both AgNPs and ionic silver (Ag+) can be determined.

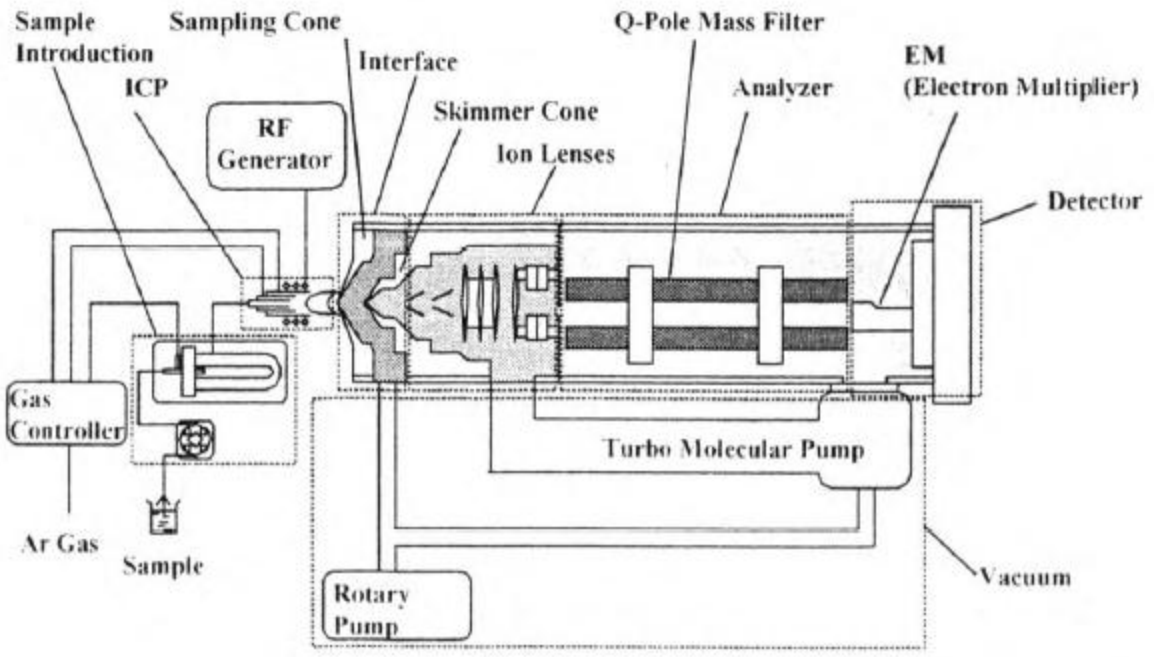

Figure 2.10. Schematic diagram of the Agilent 7500 ICP-MS.

The diagram of the ICP-MS system used is shown in Figure 2.10. There are five important parts in these technique: sample injection, ICP portion, interfacing, mass separation, and detection (Ha et al. 2011). The injector system has the ability to analyse liquid samples, it consists of a nebulizer and a sample chamber. ICP generates plasma from Ar gas and radio frequency power. The sample is converted into positive ion streams (1+) which are directed to the interface that connects the ICP part and the mass separation.

The analyses were conducted using an Agilent 7500ce with an Octopole Reaction System. The samples were filtered (section 2.3.1) and acidified to dissolve all silver in solution using nitric acid (HNO_3). For the AgNPs, HNO_3 was added to have a final concentration of 20%, the solution was shaken until it became colourless and later diluted 10 times to have a final concentration of 2% acid. For the filtrate (ionic silver, Ag+) the acid was added to have a final concentration of 2%. All samples were analysed by Dr. Steve Baker, University of Birmingham, UK.

2.3.6 Atomic Force Microscopy (AFM)

The AFM was invented and built in 1986 by Binnig, Quate and Gerber (Binnig et al. 1986). AFM was derived from scanning tunneling microscopy (STM), which measures the tunneling current between a conducting sharp tip and a conducting sample, which can be a limiting factor (PSIA 2002). AFM can image non-conductive samples and measure surface topography at nanometer vertical resolution. With minimal sample manipulation and low running costs AFM can work under a range of different conditions, including in air and liquid over a range of different temperatures (Tumer et al. 2007).

AFM uses a sharp tip attached to a micro-machined cantilever of a specific spring constant. Depending on the distance between the atoms at the tip of the cantilever and the ones at the sample‘s surface, there exists either an attractive or repulsive force/interaction that may be utilized to measure the sample surface (PSIA 2002).

When the distance between the tip and the surface atoms becomes very short, the interaction force is repulsive due to electrostatic repulsion, and when the distance gets relatively longer, the interatomic force becomes attractive due to the long-range van der Waals forces (PSIA 2002). This effect can be seen in Figure 2.11. This interatomic interaction can bend or deflect the cantilever.

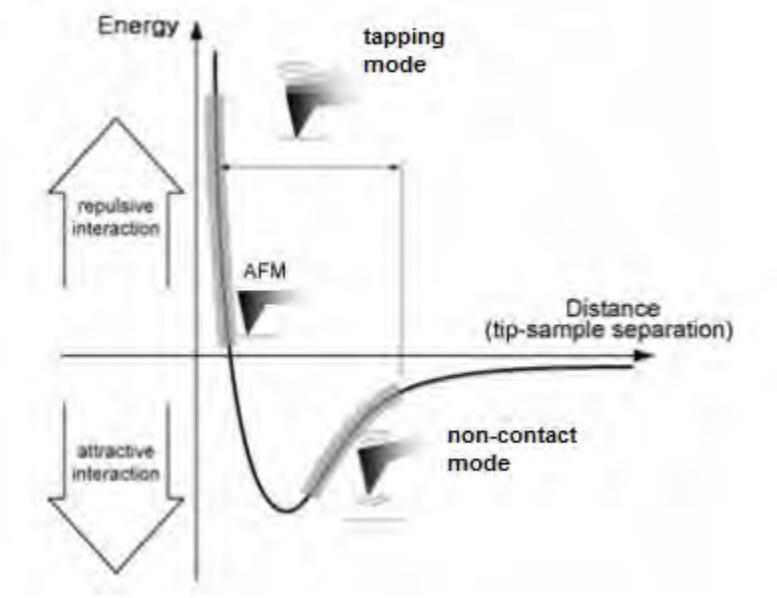

Figure 2.11. Relation between the force and the distance between atoms (PSIA 2002).

The cantilever will deflect in the z-direction when the tip scans the topography of sample surface. A photodiode, known as Position Sensitive Photo Detector (PSPD), detects the deflection of the cantilever through a laser beam focused on and reflected from the back of the cantilever (Ruozi et al. 2007), as seen in Figure 2.12. The tube-shaped scanner located under the sample will move it in the horizontal direction (X-Y) and in the vertical direction (Z) (see Figure 2.13), and the independent movement in the x, y, and z directions is impossible. The movement in the z-direction provides the topography of the sample surface.

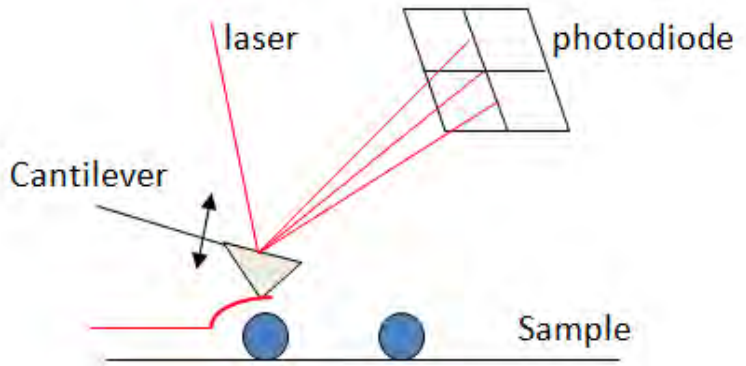

Figure 2.12. Diagram of AFM principle for imaging. Courtesy of Ruth Merrifield.

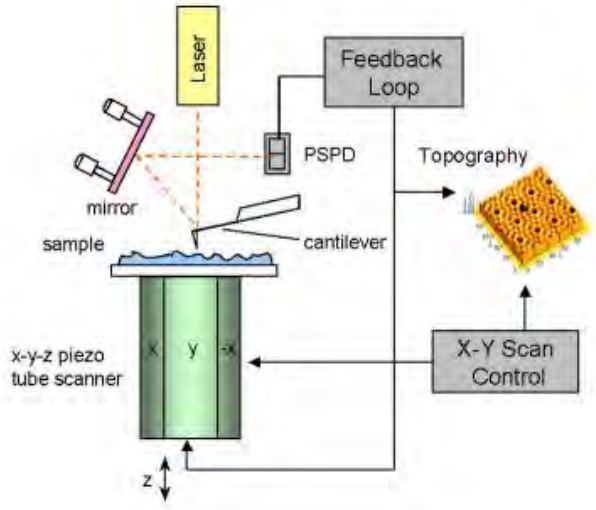

Figure 2.13. Diagram of conventional AFM's scanning (PSIA 2002).

Depending if the tip will approach or deflect from the surface, AFM can operate in different modalities, repulsive (contact) mode, attractive (non-contact) mode or tapping mode (Ruozi et al. 2007). These different modes can be seen in Figure 2.14. The mode used in this work to assess particle size and image topography was non-contact.

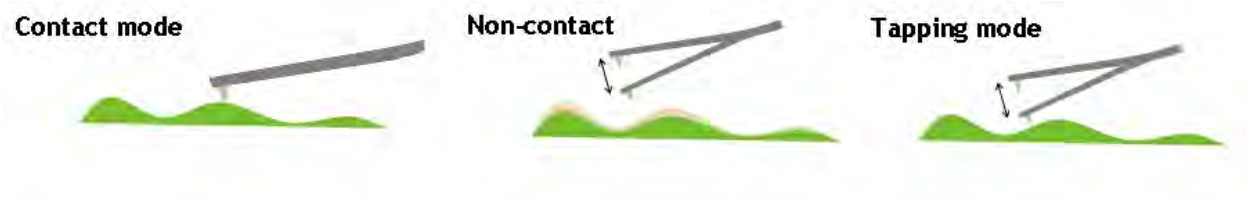

Figure 2.14. AFM Imaging modes. Image adapted from http://kristian.molhave.dk/.

- **Contact mode:** In this mode the study of the sample's topography is conducted by utilizing the vertical repulsive force between the sample and the probe tip. The probe will be in contact with the sample surface. The slightest amount of a cantilever's deflection can be detected as it moves across a sample surface. When the distance between the probe tip and the sample surface atoms is very small the system will have a sensitive response to the Repulsive Coulomb Interactions that exist between the ion cores, this will allow the user to measure the surface topography (PSIA 2002). This mode is used in liquid AFM and it's not a good method to scan nanoparticles on a dry surface due to the fact that the tip could drag the particles through the surface measured.

- **Non-contact mode:** In this mode there is a relatively larger distance between the tip and a sample surface. Surface topography can be measured by using the attractive atomic forces generated by this distance (PSIA 2002). Static electric attractive force (F_{el}) becomes dominant when this distance is relatively large, this force is very weak so there will be no change in the sample during the measurement. This is very convenient for nanoparticles on a dry surface, Non-contact mode can't measure the deflection of the cantilever directly, instead will detect the changes in the phase or the vibration amplitude of the cantilever.

- **Tapping mode:** is a hybrid between contact and non-contact mode. Like in non-contact mode, the cantilever vibrates in free-space in the vicinity of the resonant frequency. The cantilever gets very close to the sample surface while vibrating and will tap the surface repeatedly, and like in contact mode the tip will make contact with the sample surface (PSIA 2002). Tapping mode will damage the sample less than in contact mode since there is no drag force to pull the sample sideways, frictional or lateral force. It will also measure a sample with relatively rough surface and a large height difference over a large area better than non-contact mode.

Images were obtained from a XE 100 AFM (shown in Figure 2.15) in non-contact mode, recorded using XEP software and analised with XEI software. Non-contact mode silicon AFM Cantilevers PPP-NCHR were used, spring constant 42 N/m. X-Y scan sizes were 5 x 5 µm with resolution of 250 pixels per line. Scanning rates were optimised to acquire a stable and clear image without damaging the tip or detaching particles during scanning, usually 0.3 to 1 Hz.

Figure 2.15. AFM XE-100. Image obtained from Park systems product catalogue.

The samples for AFM measurements were prepared by ultracentrifugation method. To ensure optimal mica sheet (Agar Scientific) coverage the solutions were diluted 50 times. The diluted 10 ml samples were ultracentrifuged onto a freshly cleaved mica sheet. Beckman L7-65 Ultracentrifuge with SW40

swinging bucket rotor was used in the preparation. To provide a flat support for the mica, teflon caps were placed at the bottom of the tubes. A threaded slot to facilitate removal from centrifuge tubes was drilled. The ultracentrifugation parameters are similar to those reported by (Lienemann et al. 1998) and they are as follows: speed 30000 rpm, relative centrifugal field at rmax: 160000g, rav: 114000 g and rmin: 67200g, temperature 10^{o}C, run time 60min. After centrifugation the tubes were carefully emptied, the teflon caps removed and the mica sheets washed with UHP water and dried at ambient conditions prior to AFM analysis.

2.3.7 Transmission Electron microscopy (TEM)

Knoll and Ruska were the first to use the term “Electron Microscope” in 1932 (Knoll et al. 1932). They developed the idea of electron lenses into a practical reality and demonstrated electron images taken in the instrument (Williams et al. 1996). The main use of TEM is visualisation of material morphologies at a nanoscale, the atomic resolution real-space imaging of nanoparticles, by using the beam of unscattered electrons (Wang 2000). When equipped with energy dispersive X-ray spectrometer (EDX) qualitative chemical analysis can be performed by exploiting the interactions of the electrons with the atoms in the sample.

A schematic representation of the electron path in TEM is shown on Figure 2.16. At the top of the microscope column is a field emission gun (FEG), which produces the electrons extracted from a tip with a small range in kinetic energy. The gun will typically use a lanthanum hexaboride (LaB_6) or tungsten thermionic emission source (Wang 2000). The electrons are accelerated in the high tension unit to give them the energy required for imaging. A system of electromagnetic lenses focuses the electron beam on the sample (Kuntsche et al. 2011). Imaging lenses are used to focus and magnify the image formed as a result of the interaction of the electrons with the specimen. The electrons are projected onto a fluorescent screen, a visual image corresponding to the signal produced will form by the interaction between the beam spot and the specimen (Bozzola 2001; Goodwin 2004).

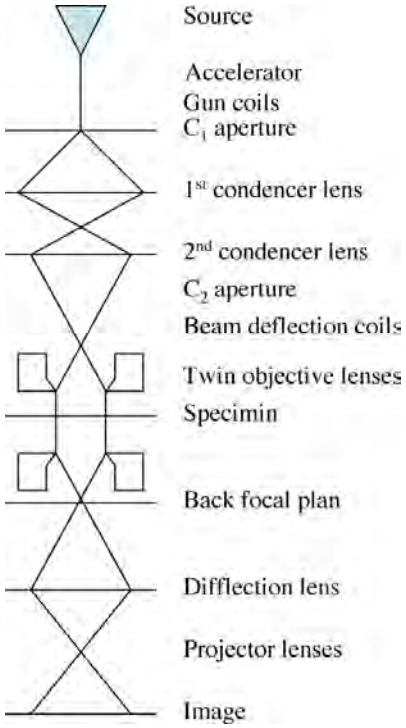

Figure 2.16. Schematic presentation of a transmission electron microscope and the electron path. Image courtesy of Ruth Merrifield, based on (Williams et al. 1996).

Transmission electron microscopy (TEM) images were obtained from a Phillips Tecnai F20 (accelerating voltage 200kv) with Oxford ISIS energy dispersive X-ray (EDX) and Gatan digi PEELS detectors, and recorded using Gatan Digital Micrograph software. Also, a JEOL 1200EX (accelerating voltage 80 kV) was used for imaging. TEM data was analyzed using Gatan Digital Micrograph (size distribution), Image J (circularity) and fractalyse (fractal dimension). EDX data was analyzed with INCAEnergy and AZtecEnergy software from Oxford Instruments. Both TEM machines are shown in Figure 2.17.

Samples were prepared by partially drying a drop of the particle solution on a cumesh400 holey carbon film (Agar scientific) at room temperature (Baalousha et al. 2008). The grid was washed thoroughly with UHP water and re-dried.

Figure 2.17. Tecnai F20 (left, image courtesy of http://www.fei.com) and JEOL 1200EX (right, image courtesy of http://www.caeonline.com).

2.3.8 Energy Dispersive X-ray spectrometer (EDX)

In a TEM sample, atoms can undergo inner-shell ionisation by the electron beam and be promoted to a higher energy excited state. They will relax back to the ground state by a process in which electrons from higher energy levels drop into the hole created in the vacant inner shell (Kirkland et al. 2007). The de-excitation process will emit X-rays, the X-ray emitted is characteristic of the atom involved and is used for elemental analysis when combined with TEM (Williams et al. 1996). A diagram is shown in Figure 2.18.

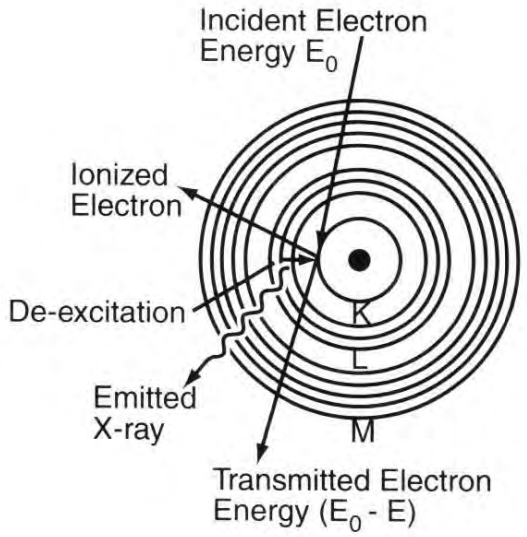

Figure 2.18. Diagram for the principle of EDX. De-excitation mechanisms for an atom that has undergone K-shell ionisation by primary electrons (Kirkland et al. 2007).

The X-rays produced are usually detected from the incident surface using a low take-off angle EDX detector. The detector tends to be in the same plane as the sample or 20^{o} to the horizontal. The detector is inserted within a few millimeters of the sample surface but only collects a small portion of the emitted X-ray signal, this is due to the limited solid collection angle of the detector (Kirkland et al. 2007). The sample is tilted to the detector (18^{o}) to provide a clear X-ray trajectory between the area that has been irradiated and the detector.

2.3.9 Scanning Transmission Electron microscopy (STEM)

The STEM concept was described by von Ardenne in 1938, he was the first to perform a STEM mode experiment by adding scan coils to a TEM (Bogner et al. 2007). The first visualization of single heavy atoms in the electron microscope was not until 1971 due to a lack of electronics and adequate electron sources at the time.

A STEM image may be considered as a collection of individual scattering experiments. The STEM, in comparison with TEM, is a low dose technique, and it is also possible to simultaneously capture both structural and chemical analysis by observing either the scattered angle and/or energy loss electrons. STEM looks very much like a TEM run backwards, which is the theory of reciprocity, it works on the principle of time reversal symmetry and when the electrons are elastically scattered. In Figure 2.19 we can interchange the source with a bright field detector and obtain a TEM (compare to Figure 2.16) (Kirkland et al. 2007).

In STEM a small diameter probe (a nanometre or less) is produced by the electron gun/lens system, a diagram is shown in Figure 2.19. The C1 lens will control the spot size of the beam by focusing the crossover point. The electron beam is focused to a small probe on the surface of the sample by the C2 lens and the upper part of the objective lens. The probe is serially scanned in a two dimensional raster across the specimen by the deflection coils, just above the objective lens. At each point some of the electrons undergo Rutherford scattering to high angles (50 mrads) and are collected by the high angle annular dark field detector (HAADF), the number of electrons scattered at each point on the sample is fed into a computer that builds up an incoherent Z (atomic number) contrast image pixel by pixel. The resolution is determined by the probe size on the specimen (Kirkland et al. 2007). The beam has to scan parallel to the optic axis at all times so that it mimics the parallel beam in a TEM even though it's scanning (Williams et al. 1996).

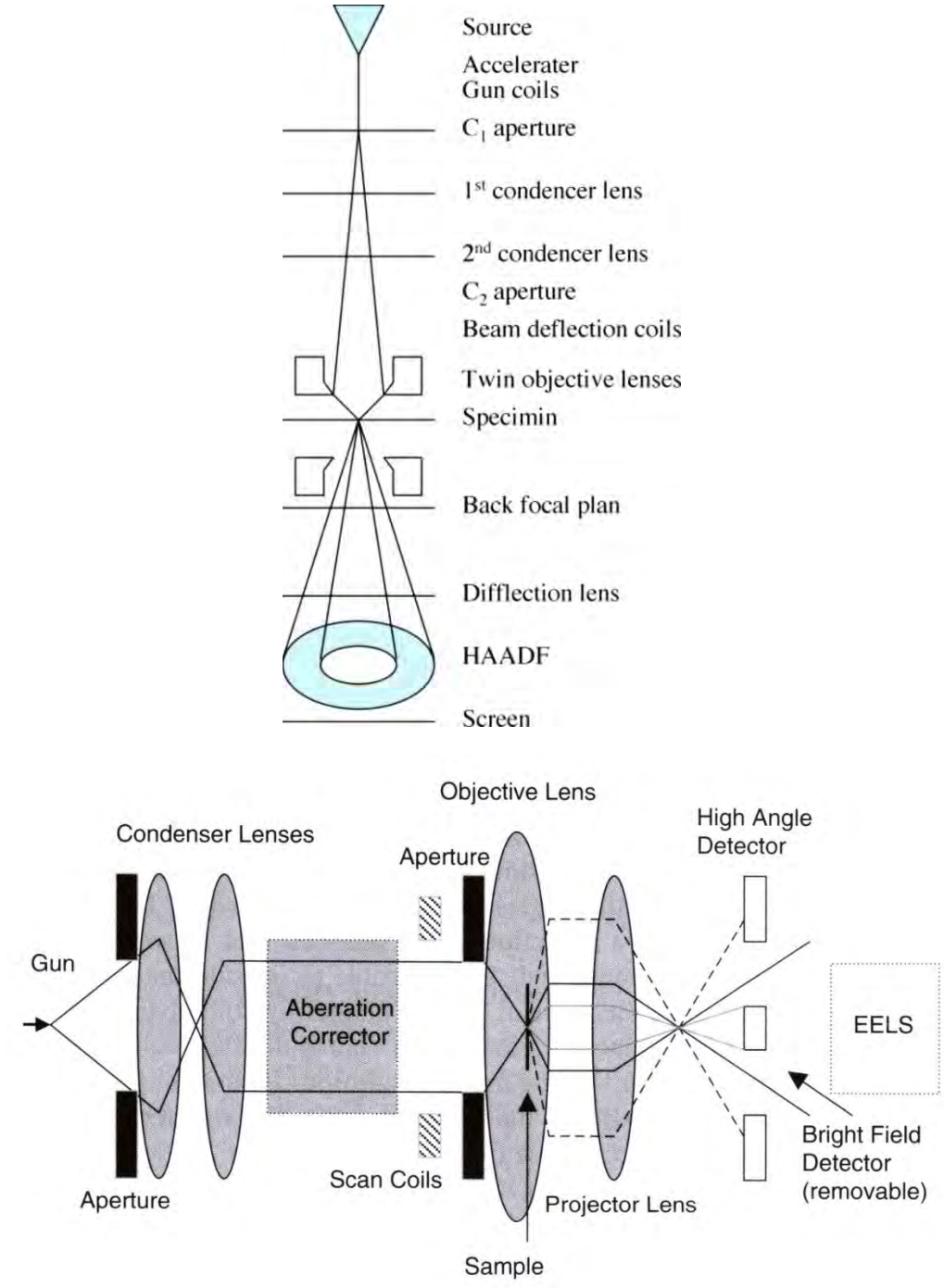

Figure 2.19. Top: Diagram of an STEM, courtesy of Ruth Merrifield. Bottom: Schematic of an aberration corrected STEM. Electron trajectories at the edge of the apertures are shown with solid lines. High angle scattering used to form Z-contrast images is indicated with dashed lines and low angle scattering used to form bright-field images is indicated with gray lines (Kirkland et al. 2007).

The HAADF detector collects transmitted electrons scattered to high angles (Kirkland et al. 2007). This detector provides an image with high Z-contrast, because the contrast depends upon the thickness and the square of the atomic number Z, this leads to direct interpretation of the signal. The differential cross section shown in equation 2.19 shows the amount of electrons that scatter into a small area proportional to Z, and it's known as Rutherford scattering.

$$\sigma(\theta) = \left(\frac{1}{4\pi\varepsilon_o}\frac{Ze^2}{mv^2}\right)\frac{1}{sin^4\left(\frac{\theta}{2}\right)} \quad (2.19)$$

Where, *e* is the charge on an electron, *m* is the mass of an electron, *v* is the velocity of the incoming electron, and θ is the angle to which the electrons are scattered. Electrons that are not Rutherford scattered, travel close to the optical axis, some are un-altered, some have energy loss through inelastic scattering, and others are scattered to low angles.

By using a STEM, images can be recorded at the same time as X-ray emission spectra. Retraction of the bright-field detector allows electrons to enter an electron energy-loss spectrometer (EELs) whilst still simultaneously recording the HAADF images (Kirkland et al. 2007). The analysis of these electrons is explained in section 2.3.10.

The STEM images were recorded by HAADF detectors in a JEOL JEM2100F coupled with a CEOS spherical-aberration probe corrector and a Gatan Enfina EELS. Spherical aberration causes electrons traveling at higher angles to the optical axis to be focus too strongly, which can be corrected by using a multipole lens. The correction effect is explained in Figure 2.20 and the multipole lens is shown in Figure 2.21.

Samples were prepared by partially drying a drop of the particle solution on a graphene enhanced lacey carbon tem copper grids (from Electron microscopy sciences) at room temperature. The grid was washed thoroughly with UHP water and re-dried.

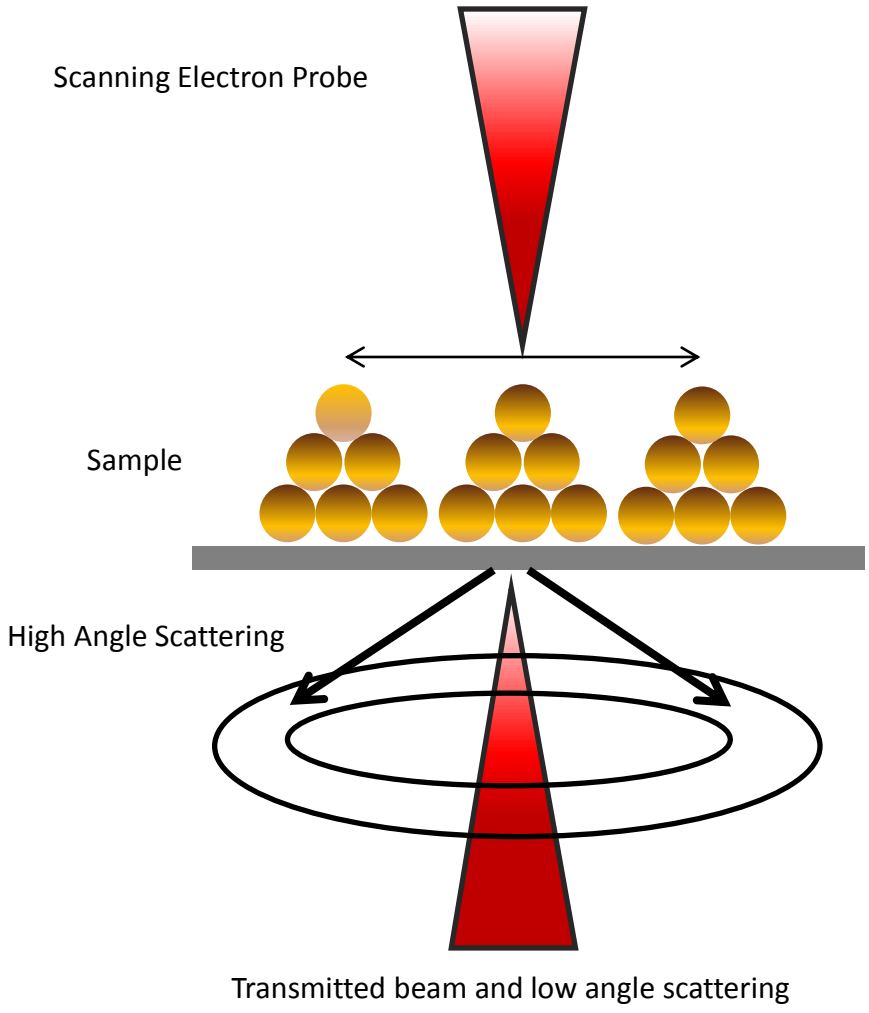

Figure 2.20. Diagram of a HAADF. In an Aberration corrected microscope, the probe size can be made small enough to obtain EELs spectrum of one/two atoms. With the right software the probe can be automatically scanned across the sample in a pre-defined grid allowing elemental mapping to be obtained.

2.3.10 Electron Energy-Loss Spectroscopy (EELs)

EELS involves analysis of the inelastic scattering suffered by the transmitted electron beam by measuring the electron-energy distribution. Inelastic scattering can be due to a range of processes: inter and intra band transitions, phonon excitations, inner shell ionisations, plasmon excitations and Cherenkov

radiation. The inner shell ionisations are the ones that are measured in EELs. After the electron beam, which originally has a narrow kinetic energy spread, has passed through the sample, the electrons are split into their relative energies, and collected by a detector. The amount of electrons collected for each energy will be recorded and plotted. The electrons are dispersed according to their energy loss using an electron spectrometer and recorded in parallel. This technique can provide high-resolution elemental analysis and mapping, as well as determination of the local electronic structure (Kirkland et al. 2007). Figure 2.21 shows a schematic diagram for a typical EELs.

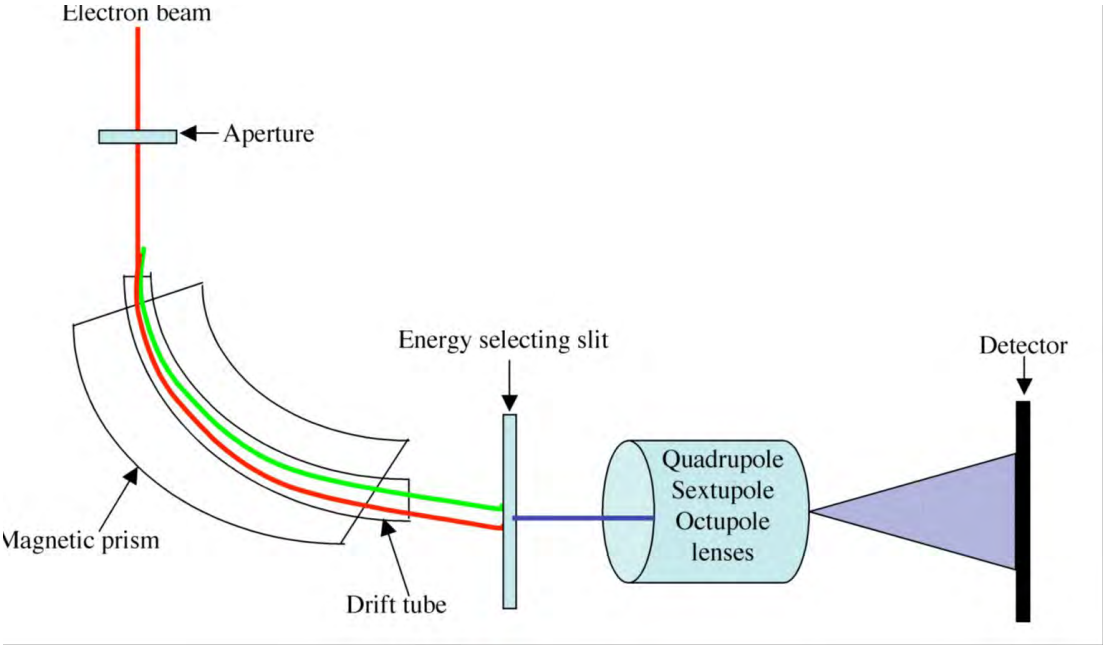

Figure 2.21. Schematic diagram of a typical EELS tube that can be fitted onto a TEM unit. The electrons enter through a slit that removes any that have been scattered to a high angle. They then pass through a magnetic prism and drift tube that split the electrons up into their relative energies and guide them. The energy to be analysed is then selected and detected. Courtesy of Ruth Merrifield.

There is a large amount of electrons that do not interact with the sample, these detected electrons that have the same energy as the original electron beam compose the zero loss peak. The electrons that have interacted with the inner shells of the atoms in the sample will have less energy. An example of an EELs

spectrum is shown in Figure 2.22. A common peak is the one for carbon, it is expected to be in the sample if there is a large number of electrons detected that have lost 285 eV from when they entered the sample, this is equal to the energy required to ionise the carbon K-edge. Two important peaks for the work performed are the silver M4,5 edges, which shows at 395 eV and the oxygen K which shows at 532 eV. These energy edges have structures to them as well as a main peak, which makes it easier to confirm what is present in EELS spectra.

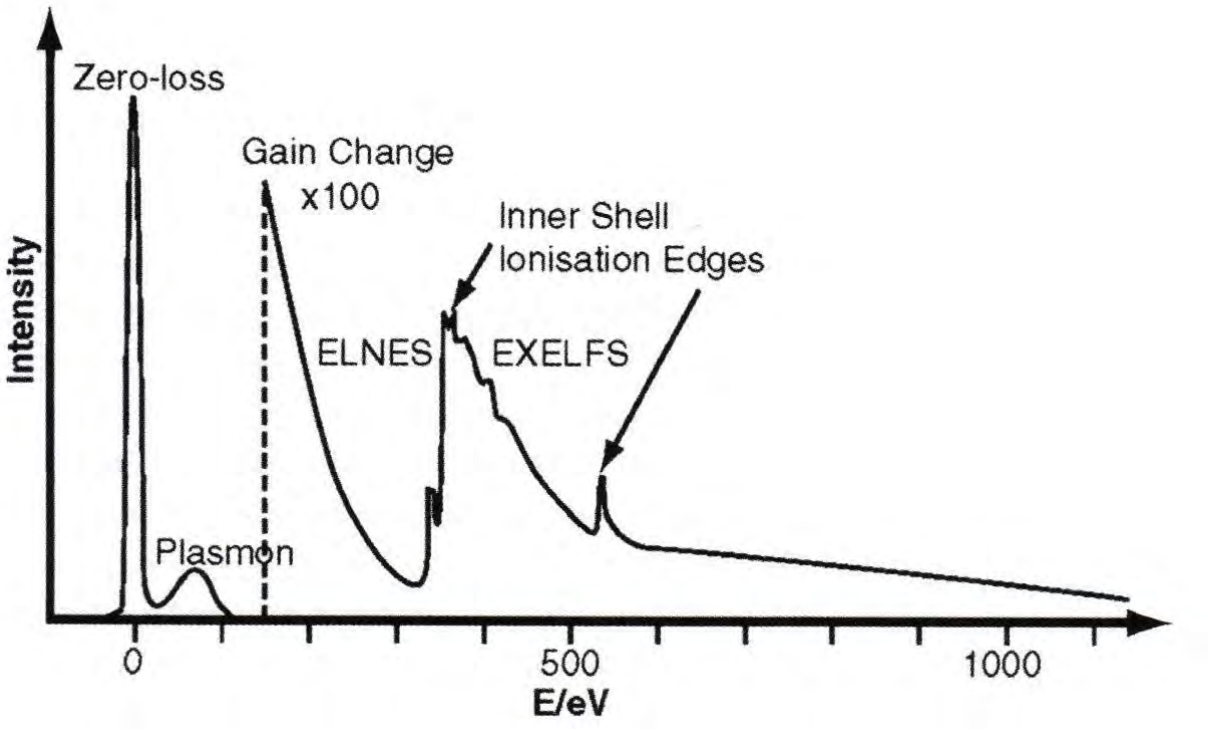

Figure 2.22. Schematic diagram of a general EELs spectrum (with a linear intensity scale and a gain change at a high energy loss) showing all of the general observable features.ELNEs stands for electron energy loss near edge structure, which modifies the basic atomic shape within the first 30-60 eV above the edge threshold. EXELFS stands for extended energy loss fine structure, which is a region of weaker and extended oscillations.

By using EELs we can obtain different types of spectra, we were interested in point, line and area spectra. A point spectra is just measured on one point, to obtain the peak we are interested on

determining. The background correction needs to be performed on the point spectrum just before the peak we are interested in and it can be done several times to obtain different peaks. In a line spectra the EELs will measure a certain number of point spectra along a line, and we can assess where the different elements can be located. An EELs map works similarly to a line spectrum, but it will measure a larger area. We can do an extraction of a signal to obtain a second signal, in the case of the AgNPs, we could extract the Ag to obtain an oxygen map. The main difference between EELS and EDX is that EELS measures absorption while EDX measures X-Rays due to ionization.

2.3.11 Statistical analysis

Particle size and number from TEM and AFM measurements were derived manually by using the TEM and AFM software and drawing calibrated lines across the particle's image. To obtain particle size average, mode, median and standard deviation, data were analysed in Excel. Standard deviation shows the variation from the average of the data, it is used to indicate the variation in repeat measured values, where there are at least three replicates.

$$\sigma = \sum \frac{(\times - \bar{\times})^2}{n-1} \tag{2.20}$$

Where Σ means we sum across the values, X represents each score, $\overline{X}$ is the mean or average value and n is the total number of values.

Excel data analysis add-in functions were used for the analysis of TEM and AFM data and displayed as histograms (where the data are grouped into bins, or small data ranges, and the bar charts plotted). The analysis of variance (ANOVA) was applied to compare more than one set of data at one time and is the overall test to determine whether groups means differ. A *p* value of < 0.05 indicates a significant difference at 95% confidence levels.

2.4 Summary of methods used

Table 2.3. Summary of the methods used.

Instrument	What it measures	Advantages	Disadvantages	Resolution
TEM	Phase contrast	Size distribution and shapes of the primary particle	Organic coatings are not visible. Thin samples 1/3 of extinction distance.	Sub nm
STEM	Z dependence	Idea of positions of material	Thin samples 1/3 of extinction distance. Can't identify materials	Sub nm
EELs	Energy loss of elements	Give detailed chemical information	Under vacuum, time consuming	nm (with STEM)
EDX	X-rays elemental mapping	Fast qualitative analysis	Results in peak overlaps	nm (with TEM)
DLS	Hydrodynamic diameter, zeta potential	Simple and fast size measurements	Poor sensitivity at low concentrations, nonselective to material, inability to distinguish mixtures or complex matrices, sensitive to large sizes.	1 – 2nm to 1-1.5 micrometers
UV-Vis	Absorption	Quick. Ensemble measurement of homogeneity	Difficult to interpret. Must know something about sample	~10nm wavelength range
AFM	Topography force	Can measure non-conductive samples.	Slow method, the piezoelectric tube and tip shape can lead to errors.	Height ~ 0.1nm Lateral ~ 20nm
FFF	Hydrodynamic size distribution calculated from UV, fluorescence or light scattering signal.	Element/particle specific detection and the ability to size particle mixture	Particles must be in a stable aqueous suspension.	Concentrations of μgL^{-1}, and sizes from 1nm to 100 µm

3

Synthesis and characterisation of silver nanoparticles with citrate and PEG as capping agent

---

Chapter Summary

We have synthesised monodisperse silver nanoparticles (AgNPs) using citrate and *thiol*- poly(ethylene glycol) (PEG-SH) as a capping agent. We have looked at how the particles can be varied by methodological adjustments, to produce stable and monodisperse AgNPs suspensions. Different experiments were performed to obtain citrate capped NPs, we are presenting in this chapter the different reactions that yielded stable and monodisperse nanoparticles. The properties of the NPs prepared changed due to the rate of reduction, changes in the concentration of the reducing agent and temperature. Monodisperse citrate-stabilised Ag NPs of three different sizes were synthesised in different conditions and fully characterised, the synthesis was based on a published method (Cumberland and Lead 2009) and was published in a subsequent paper (Römer et al. 2011). PEG-AgNPs were prepared from the citrate particles based on an already published method (Fernandez-Lopez et al. 2009). Stability of citrate-NPs was assessed in different dilutions of the media recommended by OECD for *Daphnia magna* toxicity testing, shown in chapter 4. The stability of citrate, PEG and PVP coated particles in OECD media prepared using different ions and of different concentrations was assessed by Mila Tejamaya (data not shown) and published (Tejamaya et al. 2012).

3.1 Introduction

The synthesis of citrate stabilized AgNPs is based on the method published by Turkevich to obtain gold nanoparticles (Turkevich et al. 1951). A silver nitrate salt ($AgNO_3$) in water is brought to boiling and a solution of sodium citrate was added. The solution was kept boiling for ca.1 h (Lee et al. 1982). Doty *et al.* improved this reaction by using sodium borohydride ($NaBH_4$) as a reducing agent (Doty et al. 2005).

A method to synthesize well defined nanoparticles was published by our group in 2009 (Cumberland and Lead 2009), which was a modified version of both methods mentioned before. The Ag NPs prepared were both small and monodisperse.

Poly(ethylene glycol) (PEG) is a widely studied polymer used as a capping agent for NPs, especially in biological applications, it is biocompatible, non-toxic, non-immunogenic, and hydrophilic (An et al. 2009). The PEGylated particles prepared in this work were based on a previously published method, in which citrate particles were coated with PEG-SH by adding enough thiolated PEG to coat the particles with 4 molecules of PEG-SH per nm^2 (Fernandez-Lopez et al. 2009).

3.1.1 Aims and objectives

The aim of this chapter is to produce stable monodisperse AgNPs deemed suitable for use in NP experiments of fate, behaviour, transport and eco-toxicology. The ability to produce NP suspensions of distinct particle size ranges and different capping agents is also important. To achieve these aims systematic investigation of reaction conditions can be done by: 1) changing the ratio of the reagents; 2) changing the temperature pre- and post-reaction 3) changing the presence and concentration of the reducing agent whilst checking for NP stability by measuring the particle size over time.

3.2 Synthesis of nanoparticles

3.2.1 Synthesis of citrate stabilized AgNPs

The synthesis of AgNPs has been explained in chapter 2, section 2.2.4. Three different sizes of AgNPs (labelled AgNP1 for 20nm, AgNP2 for 10nm and AgNP3 for 7nm) were prepared from a standard reduction of the silver salt in sodium citrate. The size of the particles was first assessed with a multi method approach (using DLS, FFF, TEM and AFM) and then followed over time with DLS to assess stability.

Figure 3.1 shows the reactions used to synthesize AgNP1, AgNP2 and AgNP3, and Table 3.1 shows a summary of all the reactions that yielded monodisperse and stable particles, the reactions used to prepare the particles used for further experiments are shown in bold. The reactions are labelled as AgNP1, AgNP2 or AgNP3 depending on the size of the particles obtained by the reactions, which we managed to obtained using different conditions. Sizes measured by DLS correspond to TEM (core size) as follows: AgNP1: 30- 35nm corresponds to 20nm, AgNP2: 20 – 25nm to 10nm, and 14- 16nm to 7nm. Reactions that yielded polydisperse particles are not discussed.

Figure 3.1. Reactions for AgNP2, AgNP1 and AgNP3 (from left to right) in the beginning of the reaction (left), NaBH4 hadn't been added to AgNP3, and at the end of the reaction (right).

3.2.1.1 Experiment to assess the rate of adding the reducing agent

The following experiment investigated the effect of altering the rate of addition of the reducing agent, sodium borohydride ($NaBH_4$), on AgNP size. Six ml of a solution containing $NaBH_4$ was dispensed into the magnetically stirred $AgNO_3$-citrate solution through four different methods:

a) Fast addition: by using 2 pipettes (5 ml and 1 ml in each hand) and quickly adding into the stirred $AgNO_3$-citrate solution (standard reaction, used for AgNP1 and for most of the reactions).
b) Fast addition (after heating): by using 2 pipettes as stated above, but after heating the $AgNO_3$-citrate solution for 90 minutes (Reactions where AgNP3 were obtained).
c) Medium speed addition: Six ml of $NaBH_4$ was placed into a small beaker and then poured into the stirred $AgNO_3$-citrate solution.
d) Slow addition: Six ml of 10mM $NaBH_4$ was added drop wise (1 drop every 5 seconds) into the stirred citrate and $AgNO_3$ solution by using a burette.

3.2.1.2 Experiment to assess the concentration of the reagents and reaction conditions

The following experiment investigated the effect of the concentration of the different reagents, $AgNO_3$, sodium citrate and sodium borohydride ($NaBH_4$), on AgNP size. Six ml of $NaBH_4$ was added into the magnetically stirred $AgNO_3$-citrate solution, as before.

a) Changing the ratio of $AgNO_3$ – citrate, the ratios were 1 to 1; 1 to 1.1 ; 1 to 2.2 and 1 to 5
b) Using different concentrations of the reducing agent: 0.125mM, 0.25mM, 0.5mM, 1mM, 5mM, 10mM and 20mM, and using aged 10mM $NaBH_4$.
c) Changing the reaction and heating time: 90 minutes for most reactions, 3 hours, and boiling boiling for 1 hour and for 90min before adding the reducing agent.

Table 3.1. Reactions done to synthesize citrated capped AgNPs.

Name of the sample	Temperature	Conditions changed	Initial Size by DLS (nm) and PDI	Core size (measured by TEM and AFM)
AgNP1	4°C to boil	Standard reaction, pipette used to add $NaBH_4$	35 ± 1 (0.186 ± 0.007)	20 nm
AgNP1	4°C to boil	Beaker used to add $NaBH_4$	32.2 ± 0.04 (0.133 ± 0.007)	
AgNP1	4°C to boil	3 hour heating	30 ± 1 (0.17 ± 0.01)	
AgNP1	4°C to boil	20mM $NaBH_4$	39 ± 2 (0.207 ± 0.005)	
AgNP1	4°C to boil	Aged 10mM $NaBH_4$ (1 day old) was used	33 ± 1 (0.243 ± 0.004)	
AgNP1	4°C to boil	0.25mM citrate	35.1 ± 0.8 (0.198 ± 0.006)	
AgNP1	4°C to boil	0.62mM citrate	35.3 ± 0.4 (0.206 ± 0.006)	
AgNP1	4°C to boil	50mM citrate	39 ± 5 (0.312 ± 0.07)	
AgNP2	4°C to boil	0.25mM $NaBH_4$	20 ± 1 (0.22 ± 0.01)	10 nm
AgNP2	4°C to boil	0.125mM NaBH4	17 ± 2 (0.20 ± 0.01)	
AgNP2	4°C to boil	0.50mM $NaBH_4$	19.03 ± 0.6 (0.21 ± 0.02)	
AgNP2	4°C to boil	1mM $NaBH_4$	21 ± 3 (0.262 ± 0.005)	
AgNP2	4°C to boil	5mM $NaBH_4$	27.0 ± 0.7 (0.107 ± 0.004)	
AgNP2	4°C to boil	burette (1drop / 5sec) used to add 10mM $NaBH_4$	23 ± 2 (0.20 ± 0.04)	
AgNP3	boiling $AgNO_3$ + cit (90min)	Solution boiled for 90min then 10mM $NaBH_4$ was added and heated 10 more mins	16 ± 1 (0.28 ± 0.07)	7 nm
AgNP3	boiling $AgNO_3$ + cit (1h)	Solution boiled for 1 hour then 10mM $NaBH_4$ was added and heated 10 more mins	15 ± 1 (0.401 ± 0.06)	
AgNP3	boiling $AgNO_3$ + cit (90min)	Solution boiled for 90min then 0.25mM $NaBH_4$ was added and heated 10 more mins	14.6 ± 0.5 (0.15 ± 0.01)	
AgNP3	boiling $AgNO_3$ + cit (90min)	Solution boiled for 90min then 1mM $NaBH_4$ was added and heated 10 more mins	18 ± 1 (0.21 ± 0.05)	

3.2.2 Synthesis of PEGylated AgNPs

The synthesis of AgNPs has been explained in chapter 2, section 2.2.5. Starting from the three different citrate capped AgNPs (labelled AgNP1 for 20nm, AgNP2 for 10nm and AgNP3 for 7nm) we obtained three sizes of PEGylated particles. The size of the particles was assessed by a multi method approach (using DLS, FFF, TEM and AFM) and then followed over time with DLS to assess stability, as it was done with the citrate capped NPs.

The particles were made with and without washing the citrate particles with ultrafiltration previous to the reaction with PEG-SH. This proved to be a crucial step to obtain monodisperse nanoparticles. The PEGylated particles also need to be washed with ultrafiltration using a PEG-SH containing solution.

3.3 Characterisation

The AgNPs were characterised using a multi-method approach. Sizing was performed by DLS, FI-FFF, TEM (including EDX) and AFM. SPR was measured with a UV-vis spectrometer. Zeta potential was measured using a DLS. The different instruments used and the sample preparation for each of the methods are discussed in chapter 2.

3.4 Results and discussion

3.4.1 Citrate stabilized AgNPs

Results for the different reaction that yielded monodisperse AgNPs are shown in Table 3.1. The reaction between $AgNO_3$ and citrate using $NaBH_4$ as a reducing agent in different conditions yielded monodisperse nanoparticles of three different sizes, labelled AgNP1, AgNP2 and AgNP3 (as seen in Table 3.1).

3.4.1.1 Rate of reactant addition, ratio of reagents and concentration

Fast addition by using pipettes was used to make 20nm particles (core size), around 30nm measured by DLS, labelled AgNP1, and for most of the reactions. Medium speed addition by using a small beaker also produced AgNP1. Slow addition using a burette to add the reducing agent drop wise into the stirred citrate and $AgNO_3$ resulted in 10nm particles, labelled AgNP2. Fast addition after heating the $AgNO_3$-citrate solution for 90 minutes or 1 hour yielded 7nm particles, labelled AgNP3.

The effect of the concentration of the different reagents was also assessed. Changing the ratio of $AgNO_3$ – citrate yielded NPs of 20nm in core size, labeled AgNP1, as shown in Table 3.1.

Using different concentrations of the reducing agent yielded two different particle sizes when added before heating, AgNP1 and AgNP2. AgNP2 were obtained when 0.125mM, 0.25mM, 0.5mM, 1mM, and 5mM of $NaBH_4$ was added; AgNP1 were obtained by adding higher concentrations of the reducing agent, 10mM and 20mM $NaBH_4$, and also by using aged $NaBH_4$, which had been in the fridge for 24 hours.

3.4.1.2 Heating time

Changing the heating time yielded different results when boiling 1 hour and 90 minutes before adding the reducing agent. The particles obtained were labeled AgNP3. The reactions were boiled for 90 minutes in most cases, and when the reaction was boiled for 3 hours AgNP1 were obtained.

3.4.1.3 Particles used for further studies

The key conditions in this type of reactions were:

1) the concentration of the $NaBH_4$ added
2) When $NaBH_4$ was added (before or after heating the $AgNO_3$ citrate solution).

A high concentration of reducing agent yielded larger nanoparticles (20nm in core size, AgNP1), lower concentrations and slow addition resulted in medium sized particles (10nm, AgNP2), and by adding

the reducing agent after heating yielded the smallest particles (7nm, AgNP3). The mechanism of formation of this type of NPs depends on the nucleation, which requires high activation energy, and a growth stage, that requires low activation energy. The size and the shape of the NPs will depend on the relative rates of these processes that can be controlled through the adjustment of the reaction parameters (García-Barrasa et al. 2011), as it has been discussed in Chapter 1.

The AgNPs used for further studies (shown in chapter 4 and 5) showed stability in a long period of time and were easy to make. Table 3.2 shows a summary of the results obtained for these particles by using different methods. The reduction method using $NaBH_4$ produces small-sized spherical AgNPs with sharp plasmon absorption in the 380−400-nm region, as it has been previously seen (Pillai et al. 2004; Cumberland and Lead 2009; Römer et al. 2011). Figure 3.2 shows the SPR data obtained for the different sizes of nanoparticles, which is very similar between the different particles, only showing a wider peak for the larger particles (which are the less monodisperse), which agrees with FFF results (Figure 3.4).

Silver seeds are produced by the reduction of metal ion precursors and the presence of a stabilizing agent, such as citrate, dictates the growth of these clusters. When $AgNO_3$ and citrate are heated without a reducing agent, small seeds are formed and the reaction remains colourless as seen in Figure 3.1. Particles of a very small size ($<$ 2nm) may be present, but SPR can detect NPs that are approximately between 2 and 50 nm (Link et al. 2000), so no signal was observed. Later, by the addition of the strong reducing agent they will grow to a larger size. The citrate complex slowly grows by further aggregation and it reaches an optimal size at which stage the strong repelling layer of citrate prevents further aggregation (Pillai et al. 2004). By adding the reducing agent before heating we are forming larger seeds that will yield larger and more polydisperse NPs. By reducing the concentration of the $NaBH_4$ we can also reduce the effect and obtain medium size particles that are more monodisperse. This effect was also observed when adding concentrated $NaBH_4$ dropwise to the solution. The seeds are formed at a slower rate than when added fast, resulting in smaller NPs. An important result was that SPR data showed no difference when the particles were the same size, even if they were produced by different methods, similar to the results shown in Figure 3.2.

Table 3.2. Size distributions for the monodisperse and stable citrate-AgNPs prepared, measured by DLS, TEM, AFM and FFF for the samples as prepared in nm.

Instrument	AgNP1	AgNP2	AgNP3
DLS (z average)	35 ± 1	20 ± 1	16 ± 1
DLS (PdI)	0.186 ± 0.007	0.22 ± 0.01	0.28 ± 0.07
Zeta potential in citrate (pH 7.5)	- 46	- 40	- 45
Zeta potential in water (pH 7.5)	−24.5	−20.5	−23
Fl-FFF	20.8 ± 0.4	9.6 ± 0.6	7.2 ± 0.2
TEM	17 ± 6 (*n* = 145)	10 ± 3 (*n* = 125)	7 ± 2 (*n* = 123)
Circularity (TEM)	0.91 ± 0.05	0.91 ± 0.04	0.91 ± 0.04
AFM	20 ± 9 (*n* = 100)	9 ± 3 (*n* = 124)	6 ± 3 (*n* = 109)

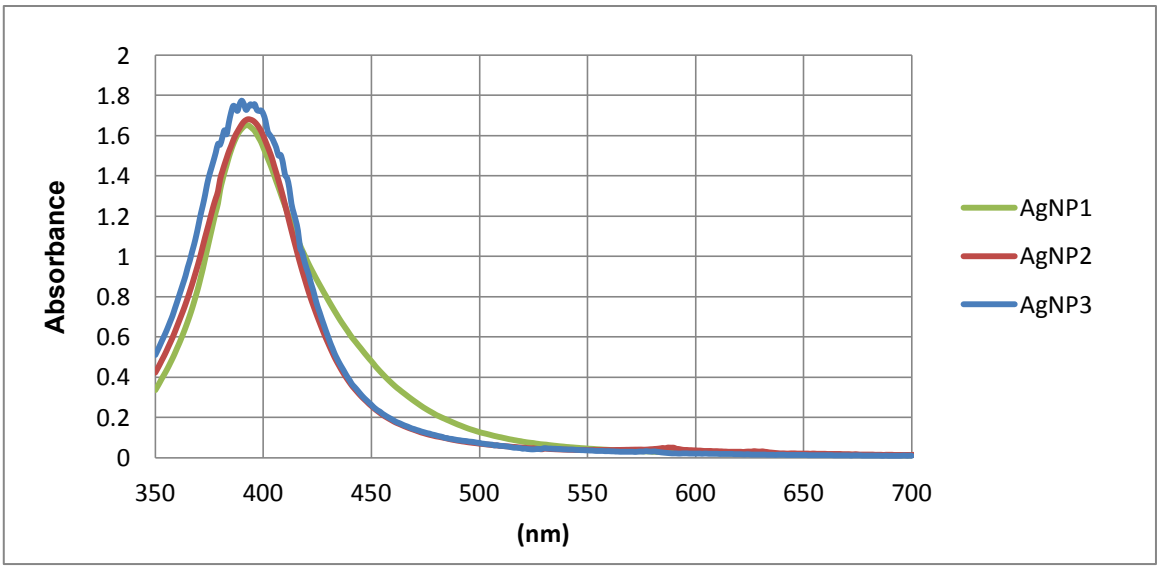

Figure 3.2. SPR data for AgNP1, AgNP2 and AgNP3.

Figure 3.3 shows the size distribution by intensity obtained with DLS for the different particles and Figure 3.4 shows the results obtained with FIFFF. Figure 3.5 and Figure 3.6 show the results obtained by TEM, Figure 3.5 shows the images obtained by TEM and Figure 3.6 the histogram. Figure 3.7 shows a typical silver signal obtained by EDX. Figure 3.8 shows images for the particles imaged by AFM and Figure 3.9 the histograms.

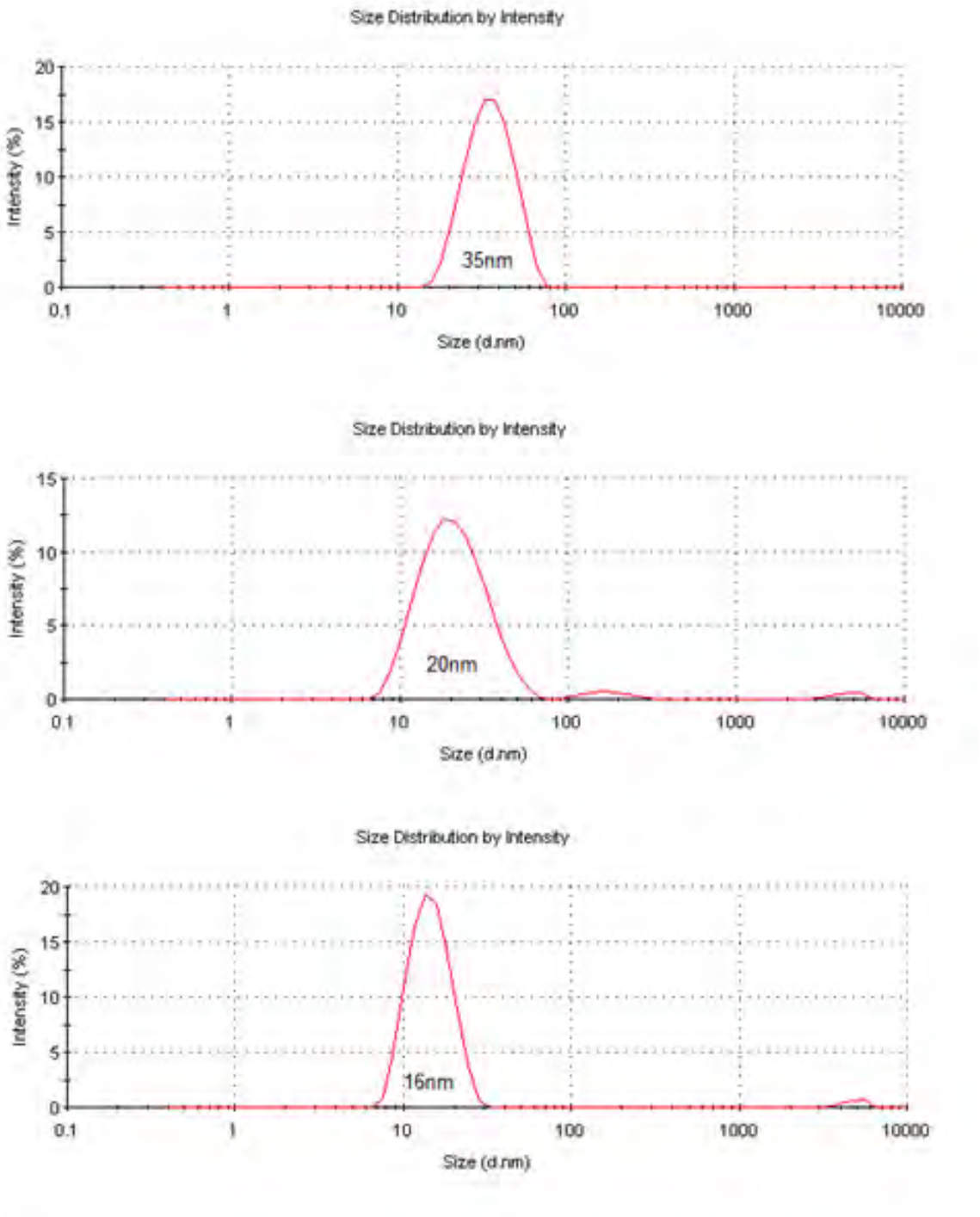

Figure 3.3. Size distribution by intensity obtained with DLS for AgNP1, AgNP2 and AgNP3.

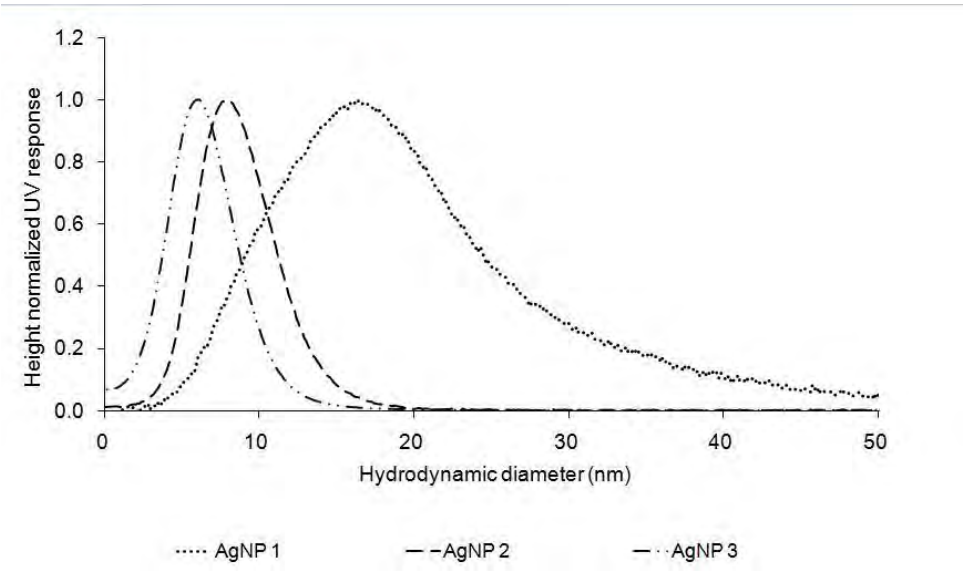

Figure 3.4. Size distribution results obtained with FFF for the nanoparticles in citrate.

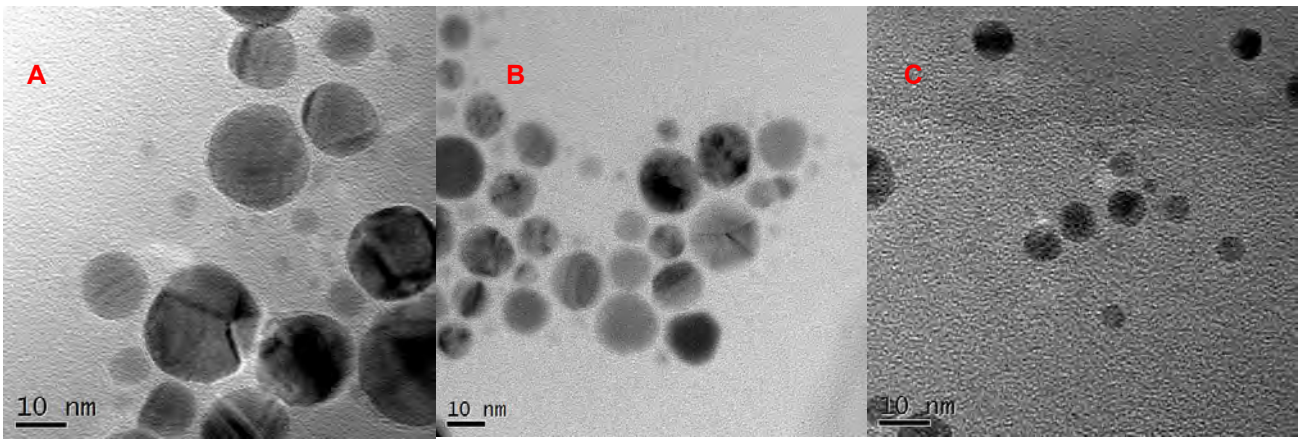

Figure 3.5. Transmission electron microscope images of a) AgNP1, b) AgNP2 and c) AgNP3. Images obtained by Tecnai.

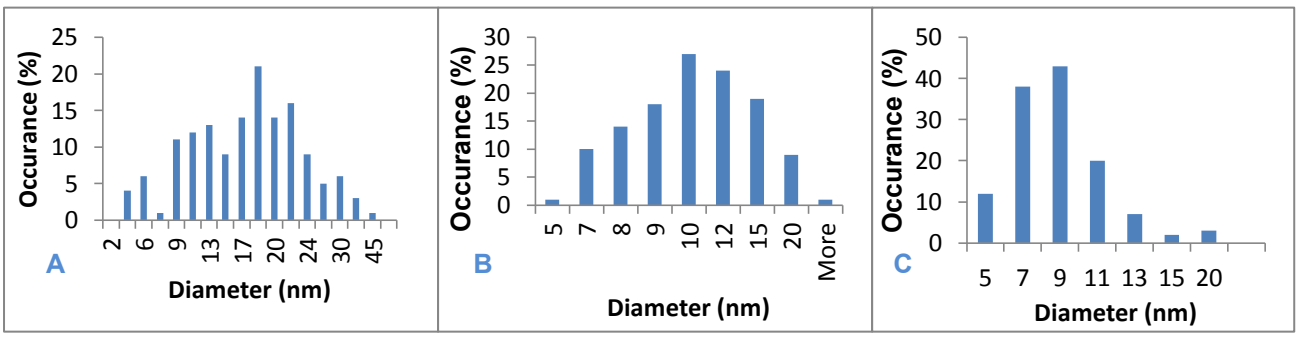

Figure 3.6. Histograms shown particle size distribution of the different samples measured by TEM, a) AgNP1, b) AgNP2 and c) AgNP3.

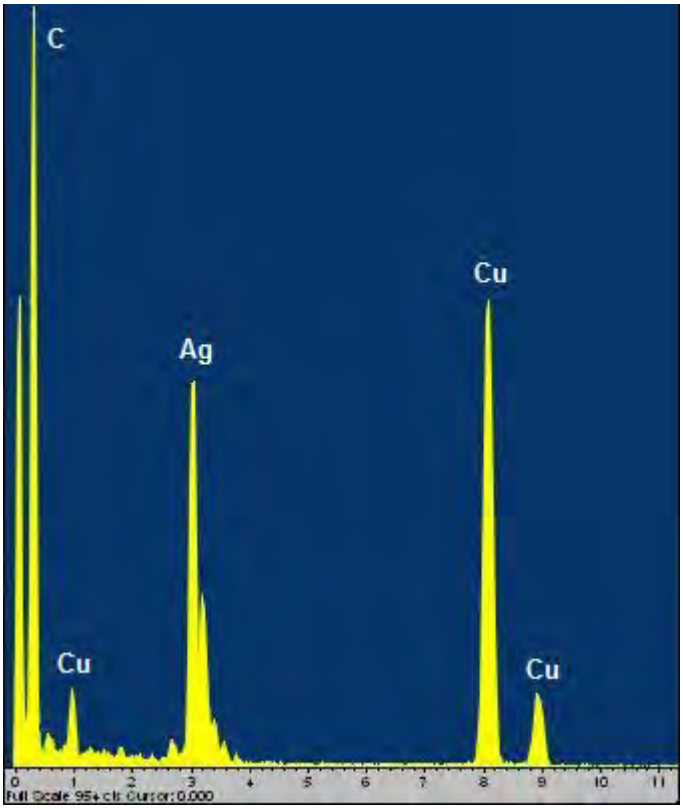

Figure 3.7. Example of an EDX spectrum taken for AgNP1. Typical peaks are shown, the copper and carbon signal come from the grid used, we are interested in the silver peak. Results were similar for the rest of the samples. Data analysed with INCAEnergy (oxford instruments).

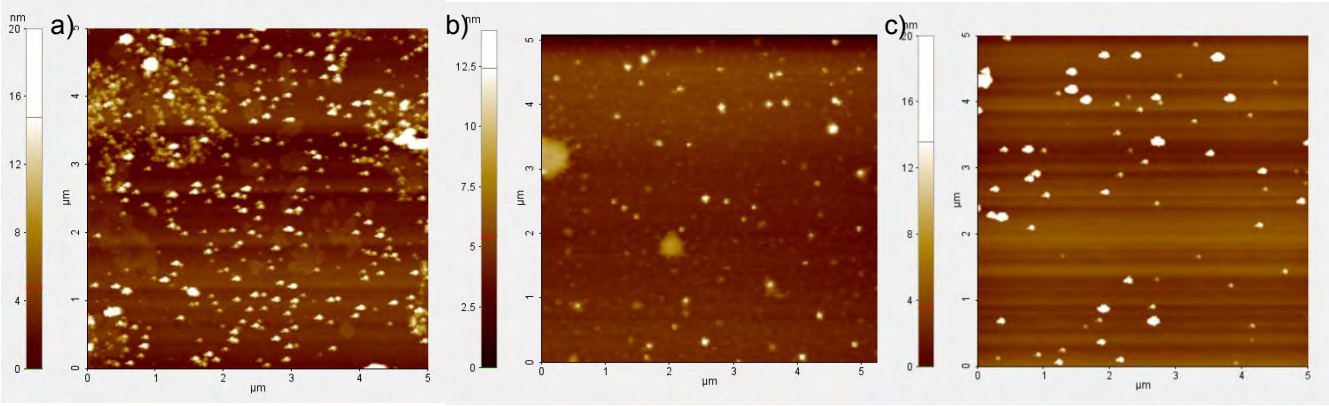

Figure 3.8. Atomic force microscopy images of a) AgNP1, b) AgNP2 and c) AgNP3.

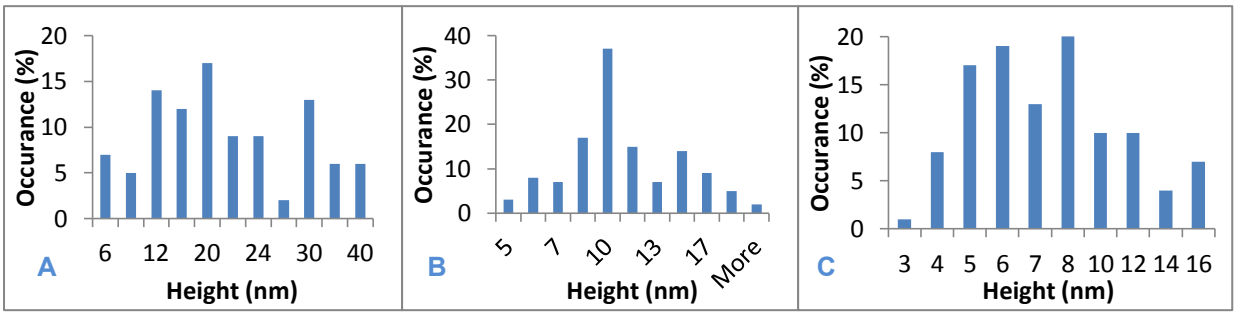

Figure 3.9. Histograms shown particle size distribution of the different samples measured by AFM, a) AgNP1, b) AgNP2 and c) AgNP3.

A multi-method approach is used to reduce bias and increase information content. TEM and AFM measure the number average diameter of particles (d_n), Fl-FFF measures the weight average diameter of particles (d_w) and DLS measures a z-averaged translational diffusion coefficient (d_z) and intensity weighted size (Tejamaya et al. 2012). In general for monodisperse particles: $d_z = d_w = d_n$, but for more polydisperse samples: $d_z > d_w > d_n$ (Domingos et al. 2009). In the case of citrate coated particles, the size obtained by DLS is considerably larger than the size obtained by FIFFF, TEM and AFM, as shown in table 3.2, and this result was consistent and agrees with the results we have previously obtained (Baalousha et al. 2008; Cumberland and Lead 2009; Römer et al. 2011). We note that the FFF size is mass based and when converted to particle number based value is expected to be somewhat smaller (Baalousha et al. 2008), and DLS overestimates particle size, as it measures intensity weighted size. The good agreement between the TEM, AFM, and FIFFF data indicates that these are monodisperse hard spheres (Baalousha et al. 2008).

By using EDX we can see the different elements present in a sample, as shown in Figure 3.7 for AgNP1. Elements present in a sample under the electron probe can be identified by the X-rays generated, which are characteristic for each element. A spectrum of the X-rays can be constructed with the collected data from a particular spot on the specimen surface. The X-ray energy scale corresponds to the x-axis of the spectrum and various elements are registered along this axis. A series of peaks along the x-axis are generated, each peak will correspond to a particular element.

Zeta potential was determined for the different particles in citrate, also in water with changing pH values (from 2 to 12) to find the point of zero charge. All particles had a zeta potential of around −40

when in citrate (Table 3.2), which was less negative in water alone at relevant pH values. The lower zeta potential after dilution by water alone compared to dilution using a citrate solution is likely due to the desorption of weakly bound citrate after dilution in water as the system re-equilibrates. The point of zero charge is at a pH value lower than 2, as full protonation of the citrate stabiliser occurs at this low pH value. These results show that the particles prepared are stable in a range of pH values in water (Römer et al. 2011) as long as the citrate solution concentration is maintained.

The washing step by using ultrafiltration proved to be crucial for particle synthesis. In the case of AgNP3, and less so for AgNP2 and AgNP1, if this step wasn't performed a couple of days after synthesizing the particles they would continue growing and would become polydisperse. This agrees with the results obtained by ICP-MS, shown in Table 3.3. We believe that there are residual reagents in solution that could induce further growth of the particles over time. In the case of AgNP1 and AgNP2 if this step was skipped a lot of very small particles would be formed and the solution became polydisperse, as shown in Figure 3.10. These small particles were silver (as obtained with EDX, Figure 3.11) and with size $<$ 2nm.

Table 3.3. Concentration of Ag in the different nanoparticles made, in the nanoparticle solution and in the supernatant after ultrafiltration, measured by ICP-MS.

Sample name	Concentration of Ag in the solution (ppm)	Concentration of Ag in the supernatant (after ultrafiltration) (ppb)	Yield of the reaction (%)	% of silver in supernatant
AgNP1	12.05	211.0	93	1.6
AgNP2	10.44	465.7	78.8	3.6
AgNP3	11.46	541.1	88.5	4.1

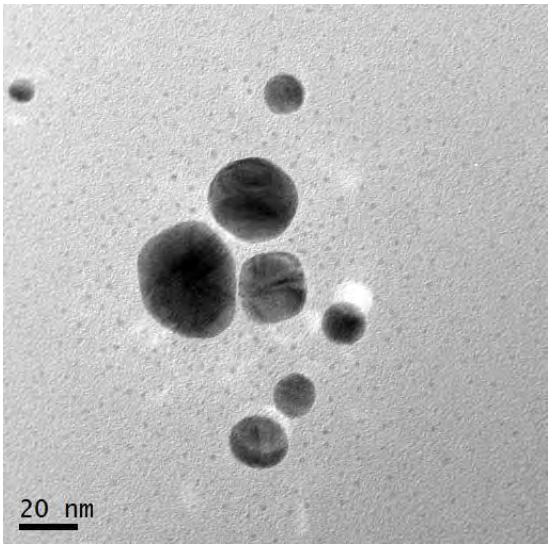

Figure 3.10. TEM image for unwashed AgNP1 particles. Image obtained by Tecnai F20.

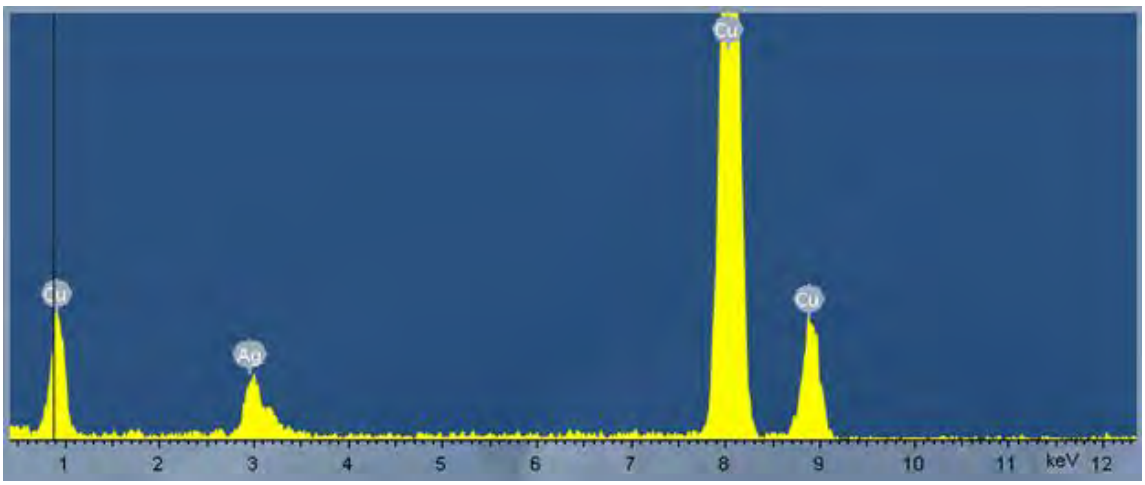

Figure 3.11. Example of an EDX spectrum taken for a small particle in the sample of Figure 3.10. Typical peaks are shown, the copper signal comes from the grid used. We are interested in the silver peak, which is small because the particle is very small. Analysed with INCAEnergy (Oxford instruments).

Particle size was measured over time by DLS to assess their stability. The results are shown in Table 3.4. The particles were kept at 4°C and in the dark. AgNP1 are stable even after almost 3 years, the SPR of the fresh and aged particles is shown in Figure 3.12, which shows there is not a significant loss of the intensity of the peak after 3 years. AgNP2 and AgNP3 were stable for 7 months, after that the solutions became polydisperse when measured by DLS.

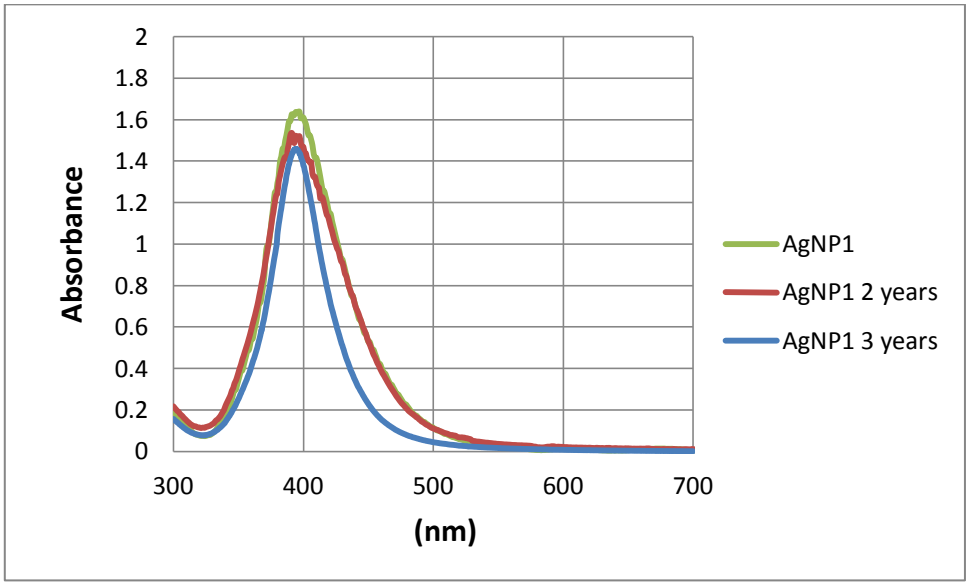

Figure 3.12. SPR spectra for AgNP1 followed for 3 years. The NPs were stored in the dark at 4°C.

Table 3.4. Size of nanoparticles measured by DLS over time.

Time / size(nm) (PDI)	AgNP1	AgNP2	AgNP3
fresh	35 ± 1 (0.186 ± 0.007)	20 ± 1 (0.22 ± 0.01)	16.0 ± 0.5 (0.15 ± 0.01)
1 week	35.6 ± 0.7 (0.156 ± 0.007)	20 ± 1 (0.21 ± 0.02)	16 ± 0.6 (0.28 ± 0.04)
1 month	38 ± 2 (0.219 ± 0.008)	20 ± 1 (0.22 ± 0.01)	17 ± 1 (0.21 ± 0.05)
7 months	-	22 ± 1 (0.20 ± 0.01)	17 (0.30 ± 0.01)
1 year	39 ± 1 (0.24 ± 0.02)	polydisperse	polydisperse

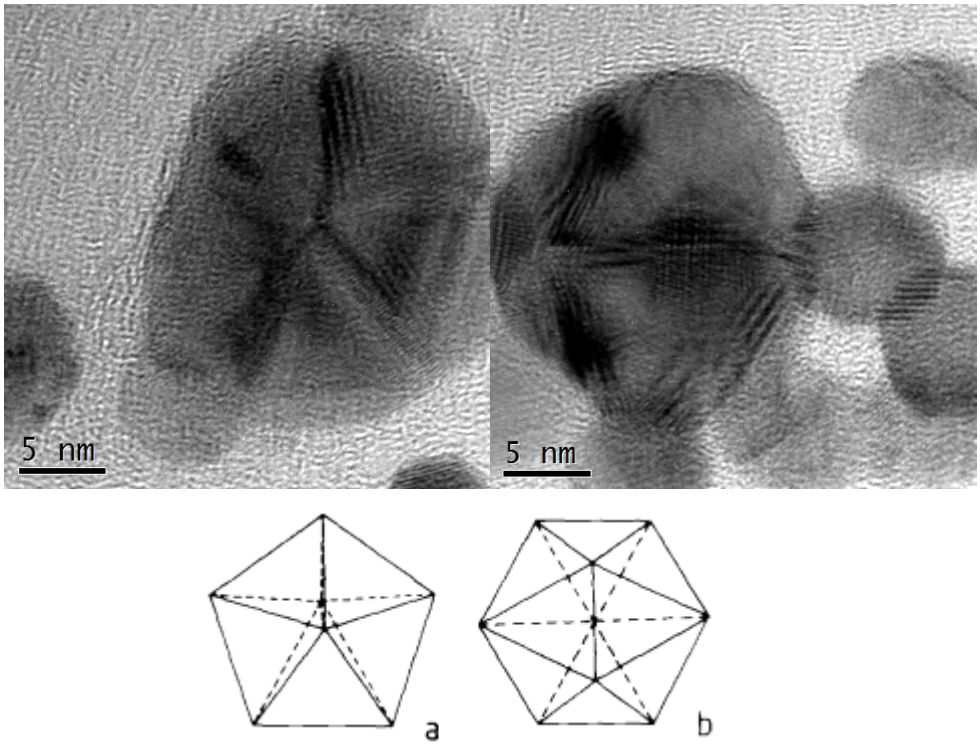

Figure 3.13. Top: High-resolution TEM of a colloidal silver particle observed along the [111] direction and its schematic model, as seen in (Silvert et al. 1997), bottom: Schematic models of the multiply-twinned particle: (a) decahedron; (b) icosahedrons (Marks et al. 1981).

Figure 3.13 shows an example of two images of particles from AgNP2. The shape of the particles, explained on chapter 1, section 1.6, is polyhedral and it is possible to observe that the particles are multiply twinned and can be represented schematically as a decahedron (top, left) and an icosahedron (top, right) (Silvert et al. 1997). These observations are in agreement with those reported in the literature (Marks et al. 1981; Gai et al. 1986) and show that the particles prepared are monocrystalline and polyhedral. Small metal particles often exist in the form of decahedral and icosahedral multiply twinned particles consisting of five and twenty tetrahedra respectively, as drawn schematically in Figure 3.13 (bottom), with twinning on their [111] planes (Marks et al. 1981).

3.4.2 PEGylated AgNPs

Starting from the three different citrated capped AgNPs we obtained three sizes of PEGylated particles, labeled AgNP1-PEG, AgNP2-PEG and AgNP3-PEG. The suspensions of synthesized particles were yellow in colour with an absorption peak at $_{max}$ 393-394nm, same as for citrate particles. Figure 3.14 shows the SPR data for the different particles after being prepared with PEG. It can be seen that there is no significant change on the peak before and after coating, and between different particles sizes, as seen in the case of the citrate particles. The loss in the SPR peak after adding PEG can be due to changes in concentration of the solution or the washing process.

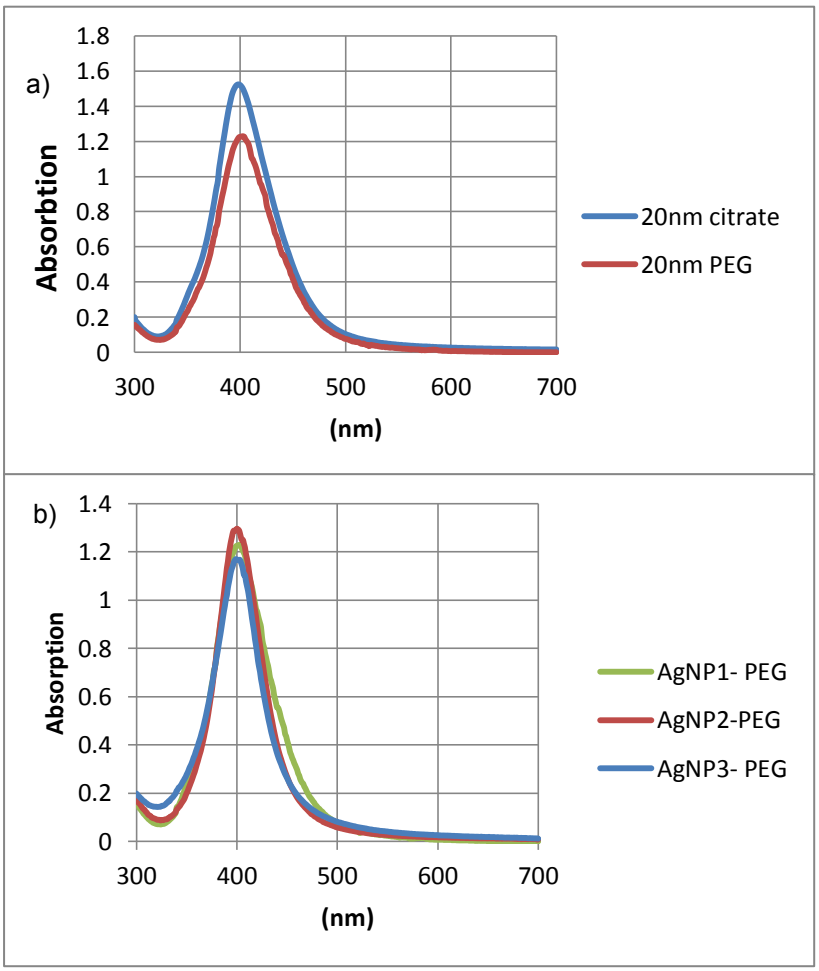

Figure 3.14. a) SPR spectra for AgNP1, before and after adding PEG, b) for the three different sizes obtained.

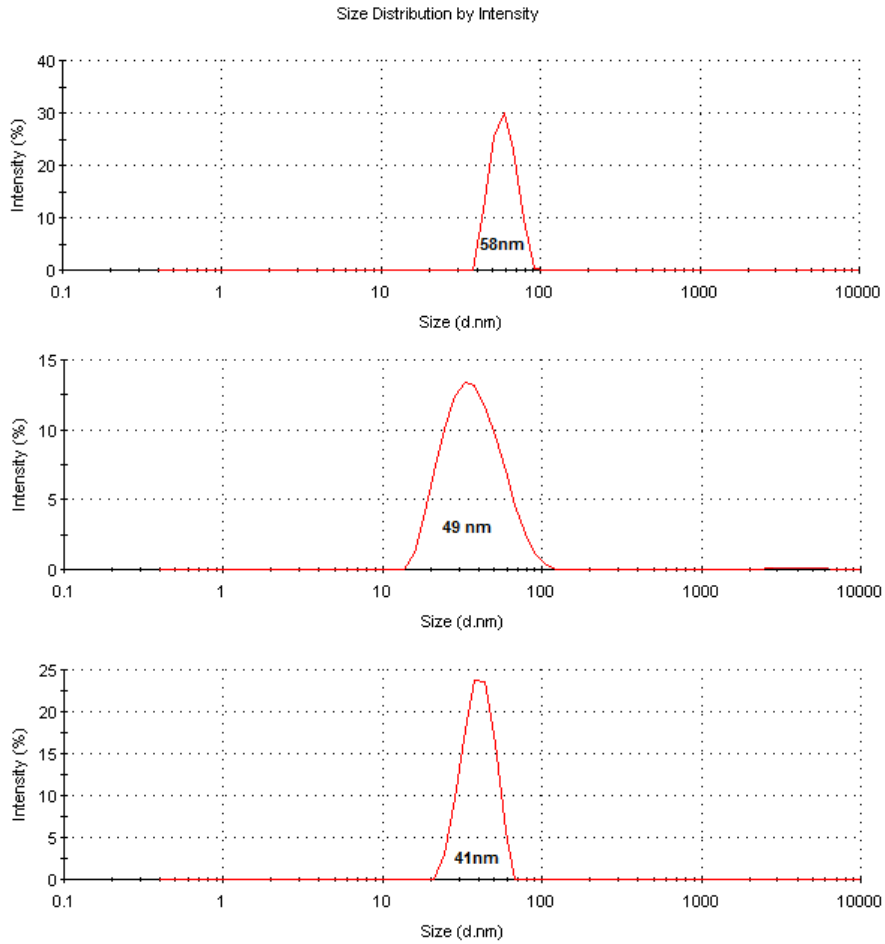

Figure 3.15. Size distribution by intensity obtained with DLS for AgNP1-PEG, AgNP2-PEG and AgNP3-PEG.

Table 3.5. Size distributions for the monodisperse and stable PEG-AgNPs prepared, measured by DLS, TEM, AFM and FFF for the samples as prepared.

Instrument	PEG-AgNP1	PEG-AgNP2	PEG-AgNP3
DLS (z average)	59.9 ± 0.8	49 ± 1	41 ± 1
DLS (PdI)	0.21 ± 0.03	0.218 ± 0.003	0.27 ± 0.05
Zeta potential unwashed (pH 6)	-16 ± 1	-25 ± 1	-18 ± 2
Zeta potential washed (pH 7.5)	-4.0 ± 0.6	-5.1 ± 0.4	-4.5 ± 0.5
FI-FFF	53.7 ± 0.8	54 ± 1	33 ± 1
TEM	22.1 ± 6.2 (*n* = 100)	10.3 ± 3.2 (*n* = 100)	7.4 ± 2.4 (*n* = 110)
AFM	48 ± 10	45 ± 8	33 ± 7

As it can be seen in Table 3.5 and Figure 3.15, the size of nanoparticles measured by DLS increased to around double the size of the particles capped with citrate (Table 3.2 and Figure 3.3). When the particles were measured by TEM we obtained the core size (Figure 3.16 and 3.17). For particles coated with a polymer, TEM will yield a smaller size than the one measured by DLS and FI-FFF.

The zeta potential result is high when the particles haven't been washed because of the presence of citrate still in solution. When the particles are washed the zeta potential decreased significantly. The value was measured in a range of pH values and the point of zero charge was not obtained (data not shown), we believe it should be at a pH lower than 2, as obtained for the citrate particles.

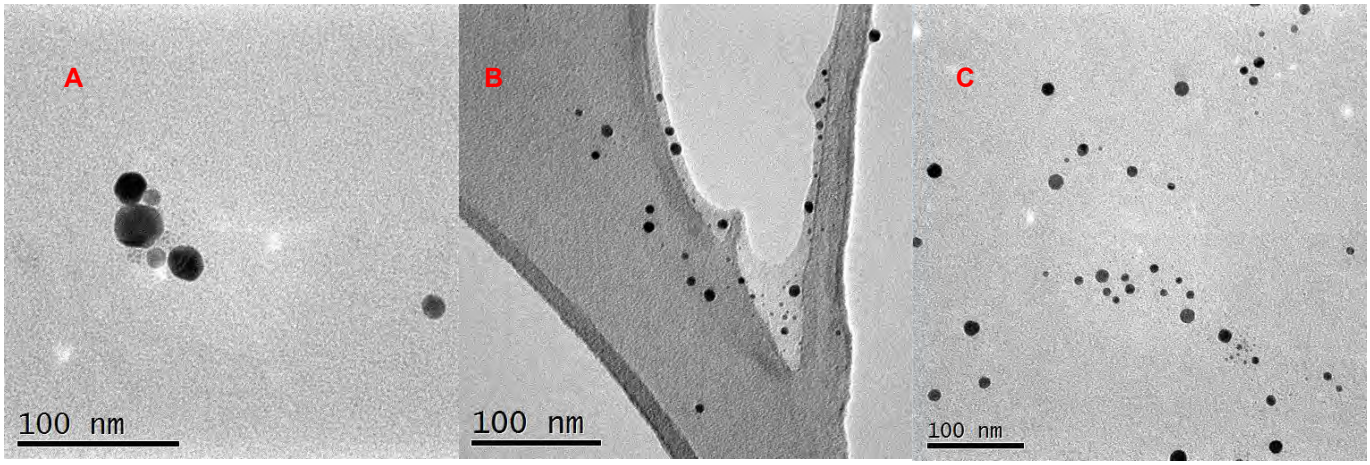

Figure 3.16. Transmission electron microscope images of a) AgNP1- PEG, b) AgNP2- PEG and c) AgNP3-PEG. Images were obtained with JEOL 1200EX.

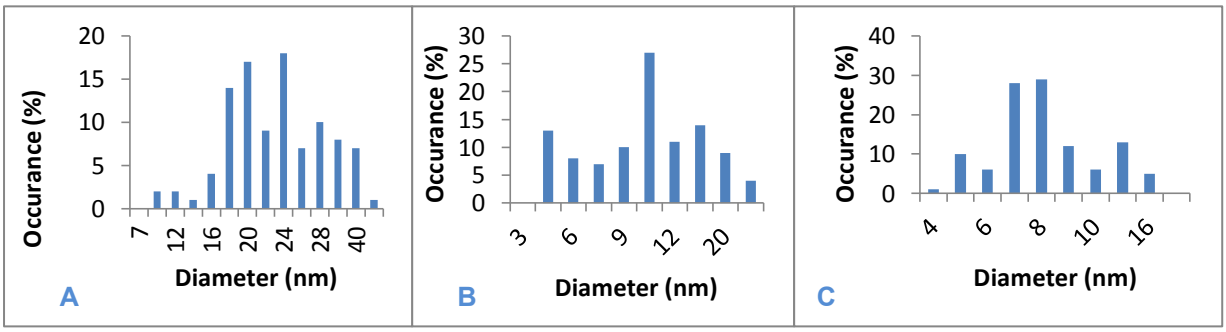

Figure 3.17. Histograms shown particle size distribution of the different samples measured by TEM, a) AgNP1-PEG, b) AgNP2-PEG and c) AgNP3-PEG.Data was compared to the values obtained for the citrate particles and results show no significant statistical difference between the values (AgNP1 *p* = 0.48, AgNP2 *p* = 0.94, AgNP3 *p* = 0.71).

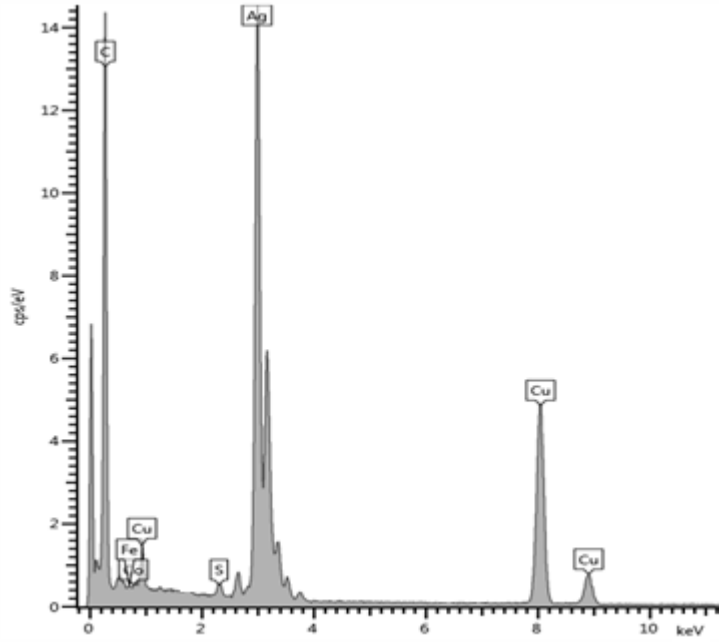

Figure 3.18. EDX obtained for AgNP1- PEG using AZtecEnergy from Oxford Instruments.

In the EDX spectrum for the PEG particles (Figure 3.18) we find the expected peaks for AgNPs in copper-carbon grids. We also find a sulphur peak, which we believe corresponds to the thiol group present in the PEG used to prepare the particles (Figure 3.19). The other peaks (Co, Fe) we believe are contamination from the TEM machine used.

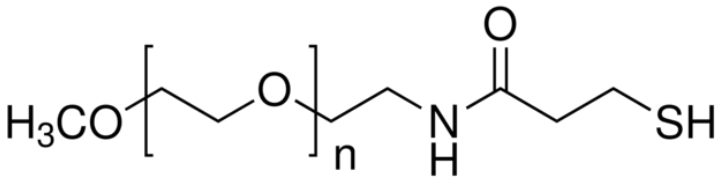

Figure 3.19. The formula for PEG-SH used in the preparation of the particles. Courtesy of sigma Aldrich, Mercaptopolyethylene glycol monomethyl ether (PEG-thiol).

We found the sulphur signal in every EDX measurement performed, in different samples and different times. A map of the different elements obtained with EDX can be seen in Figure 3.20. This was taken on a different sample than the one used in Figure 3.17. We can see a sulphur signal in areas where there is silver signal, which tells us that there is PEG-SH present around the particles.

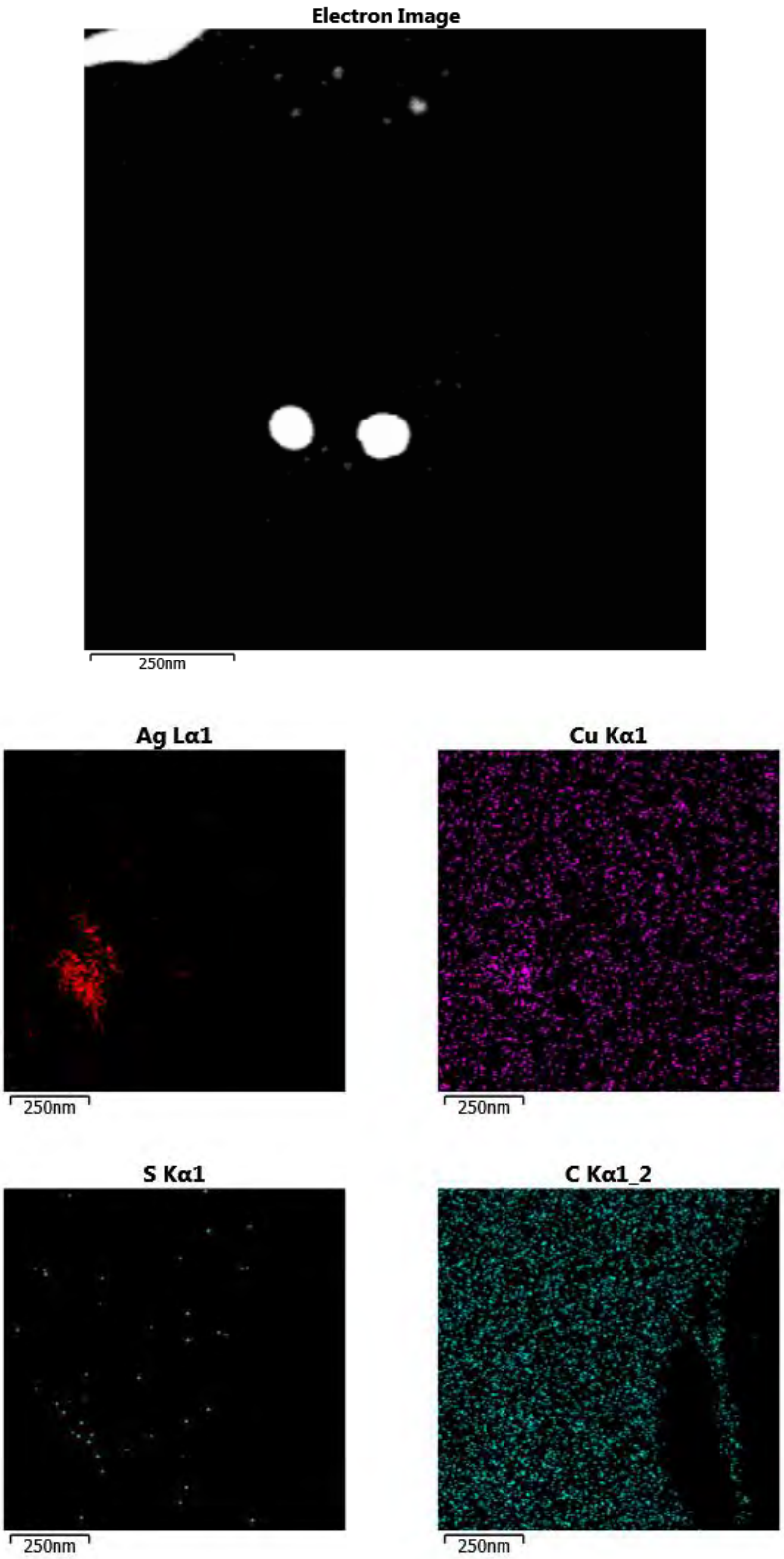

Figure 3.20. EDX map performed with tecnai F20 and analyzed with AZtecEnergy (oxford instruments).

.

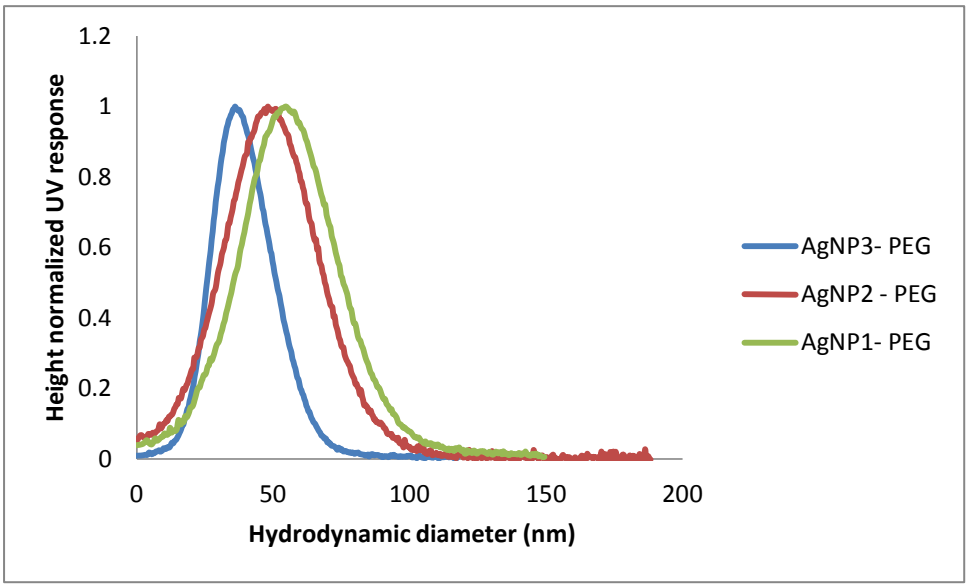

Figure 3.21. Size distribution results obtained with FFF for the nanoparticles in citrate.

Table 3.6. Size distribution measured by FFF for the different AgNPs- PEG.

Sample	AgNP1	AgNP2	AgNP3
d_p	53.7	49.5	32.9
*d*n	56.2	55.4	38.6
*d*w	63.7	62.6	43.1
*d*w /*d*n	1.13	1.12	1.10
Recovery (%)	80	82	77

d_p = hydrodynamic diameter (nm) corresponding to the peak maximum; *d*n = number average hydrodynamic diameter (nm); *d*w = weight average hydrodynamic diameter (nm); *d*w /*d*n = sample polydispersity.

Table 3.6 shows that all the AgNPs- PEG have a narrow hydrodynamic diameter distribution as measured by FlFFF (Fig. 3.21), which seems to be similar to the weight and number average diameter, and polydispersity values are low. The sizes obtained were larger than the ones for citrate, which confirms the presence of the capping agent. Recovery values are around 80% for all samples. The sizes obtained by FI-FFF agree with DLS and AFM (see Table 3.2 for citrate and Table 3.5 for PEG).

The size measured by AFM seems to be slightly smaller than DLS and FI-FFF, but is larger than TEM, which shows that the capping agent remains on the particles even after the mica sheet were left

to dry in a closed vial overnight (samples were prepared by ultracentrifugation and measured in dry, using non-contact AFM). Results are shown in Table 3.5 and Figures 3.22 and 3.23. It has been previously shown that drying the sample for AFM measurements does not substantially affect size (Balnois et al. 2002; Baalousha et al. 2012).

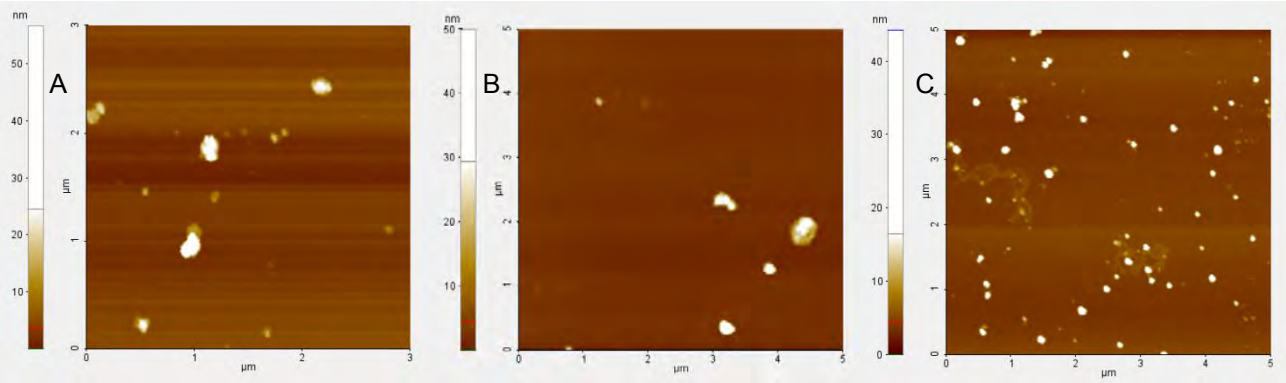

Figure 3.22. AFM images of a) AgNP1-PEG, b) AgNP2-PEG and c) AgNP3-PEG.

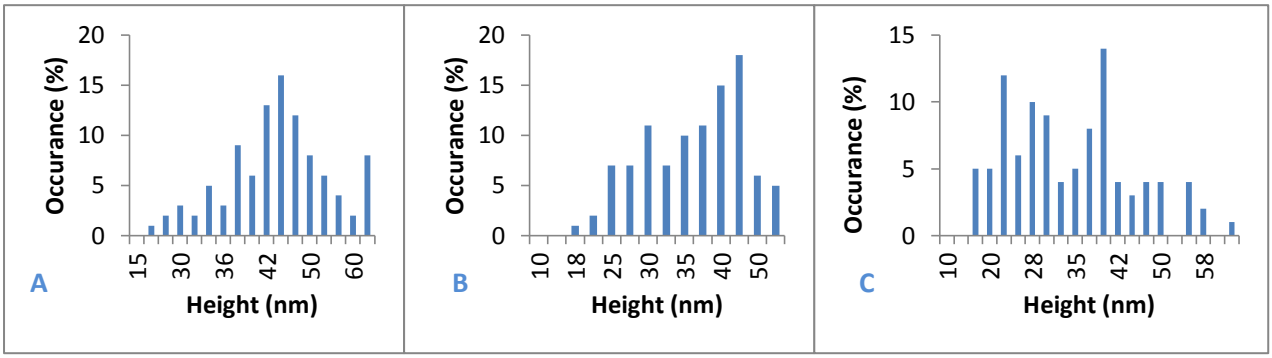

Figure 3.23. Histograms shown particle size distribution of the different samples measured by AFM a) AgNP1-PEG, b) AgNP2-PEG and c) AgNP3-PEG.

The washing step was also crucial for the PEG stabilized AgNPs. If the washing step was skipped after making the particles we found very small particles would be formed and the solution became polydisperse, the same effect observed for citrate particles shown in Figure 3.10.

As well as in the case of citrate capped AgNPs, particle size was measured over time by DLS to assess their stability. The results are shown in Table 3.7. The particles were kept in a fridge and in the dark. The particles have remained stable for a year in all cases, with no change in UV signal.

Table 3.7. Size of nanoparticles stabilized by PEG measured by DLS over time.

Time / size(nm) (PDI)	AgNP1	AgNP2	AgNP3
fresh	59.9 ± 0.8 (0.21 ± 0.03)	49 ± 1 (0.218 ± 0.003)	41 ± 1 (0.27 ± 0.05)
2 weeks	58 ± 1 (0.35 ± 0.05)	48.6 ± 0.8 (0.36 ± 0.04)	40.8 ± 0.8 (0.22 ± 0.03)
1 month	60 ± 1 (0.30 ± 0.06)	50 ± 1 (0.22 ± 0.01)	41 ± 1 (0.23 ± 0.03)
6 month	60 ± 1 (0.32 ± 0.06)	50 ± 1 (0.288 ± 0.003)	43.0 ± 0.6 (0.220 ± 0.008)
1 year	61 ± 1 (0.302 ± 0.003)	51.6 ± 0.9 (0.199 ± 0.008)	42 ± 2 (0.27 ± 0.01)

3.5 Conclusions

We have been able to synthesize and fully characterise three different sizes of AgNPs with two different capping agents, citrate and PEG, that have remained stable for a long period of time.

The factors determining NP size in a standard borohydride reduction with silver nitrate in the presence of citrate seems to be concentration of the reducing agent and when it is added. By controlling one or more of these factors, monodisperse nanoparticles were obtained. From these citrate capped particles, PEG coated nanoparticles were obtained by the addition of a PEG solution.

In the next chapter, chapter 4, the stability of citrate particles from these experiments in *Daphnia magna* media was assessed. PEG particles were used in a paper produced by Mila Tejamaya (Tejamaya et al. 2012), in which the stability of both PEG and citrate particles was assessed in *Daphnia* media and the media without chloride (having used instead nitrate or sulphate salts to

prepare the media). Chapter 5 shows a study of the behaviour of AgNP1 (citrate stabilized) under realistic environmental conditions.

Further work can be performed on both citrate and PEG stabilized particles. The difference in the behavior of the different sizes of citrate and PEG stabilized AgNPs in environmentally relevant conditions can be assessed. The influence of light and different conditions wasn't performed on the PEG particles.

4

Aggregation and dispersion of silver nanoparticles in exposure media for aquatic toxicity tests

---

Chapter Summary

Silver nanoparticles (AgNPs) are currently being very widely used in industry, mainly because of their anti-bacterial properties, with applications in many areas. Once released into the environment, the mobility, bioavailability, and toxicity of AgNPs in any ecosystem are dominated by colloidal stability. There have been studies on the stability or the aggregation of various nanoparticles (NPs) under a range of environmental conditions, but there is little information on fully characterised AgNPs in media used in (eco) toxicity studies. In this study, the citrate-stabilised Ag NPs synthesized and discussed in Chapter 3, were characterised in different dilutions of the media recommended by OECD for *Daphnia magna* (water flea) toxicity testing by using a multi-method approach. Stability of NPs was assessed over 24 hours, and less so over 21 days, similar time periods to the OECD acute and chronic toxicity tests for *D. magna*. All particles aggregated quickly in the media with high ionic strength (media1), resulting in a loss of colour from the solution. The size of particles could be measured by DLS, TEM ad AFM in most cases after 24 hrs, although a fractogram by FFF could not be obtained due to aggregation and polydispersity of the sample. After diluting the media by a factor of 2, 5 or 10,

aggregation was reduced, although the smallest NPs were unstable under all media conditions. Media diluted up to 10-fold in the absence of AgNPs did not induce any loss of mobility or fecundity in *D. magna*. These results confirm that standard OECD media causes aggregation of AgNPs, which result in changes in organism exposure levels and the nature of the exposed particles compared to exposure to fully dispersed particles. A brief range finding experiment in a 10-fold dilution of the media indicated the concentration at which 7nm particles caused 50% immobilisation (LC_{50}) of *D. magna* neonates (<24hrs) to be 5.36 $\mu g\ L^{-1}$, LC_{50} couldn't be calculated in media1. For $AgNO_3$ LC_{50} values for media1 and media10 were 1.43 and 0.87 $\mu g\ L^{-1}$, respectively. AgNPs aggregate in high ionic strength media and aggregated forms are much less toxic. Lower toxicity can be due to reduced uptake, reduced availability, reduced surface area, amongst other things. Nanoparticles are likely to have far greater biological effects than suggested thus far by poorly controlled exposures. We recommend that the standard OECD media is diluted by a factor of ca 10 for use with these NPs and this test media, which reduces AgNP aggregation without affecting the viability of the text organism. This chapter is based on two papers, one in Journal of Chromatography a (Römer et al. 2011) and one being prepared for Environmental Science and Technology.

4.1 Introduction

Silver nanoparticles (AgNPs) are the most commonly used currently in industry; according to the Woodrow Wilson database (2011), the most common material mentioned in nanotechnology consumer product descriptions is now silver (313 products). It is the relatively low cost of manufacturing and bactericide properties of AgNPs that has made them very popular in recent years. They are used in a wide range of consumer products and materials increasing their market value, such as plastics, pastes, soaps, textiles and metals (Fabrega et al. 2011). This increasing popularity means that these particles are currently being released to the environment (Mueller et al. 2008; Gottschalk et al. 2010) and their toxicity must be assessed. They have been shown to be toxic to microbes and invertebrates although somewhat less so to fish and humans (Klaine et al. 2008). AgNPs through their use in consumer products doesn't seem to adversely affect humans, but can result in AgNPs releases into the environment and dissolved silver, which are likely to persist and bioaccumulate (Fabrega et al. 2011).

Once released into the environment, the mobility, bioavailability, and toxicity of AgNPs are dominated by their colloidal stability (El Badawy et al. 2010). Many factors can affect colloidal stability, including the type of capping agent, the local environmental conditions, such as pH, ionic strength, and the background electrolyte composition (Cosgrove 2005; Chen et al. 2006; Tielemans et al. 2006; Petosa et al. 2010). There have been a number of studies on the stability or the aggregation of various NPs under a range of environmental conditions (Cumberland and Lead 2009; El Badawy et al. 2010), but there is little information on AgNPs (Chen et al. 2006; Jiang et al. 2009; El Badawy et al. 2010; Chinnapongse et al. 2011; Delay et al. 2011; Huynh et al. 2011; MacCuspie 2011; MacCuspie et al. 2011; MacCuspie et al. 2011) and almost none investigating the impacts of ecotoxicological exposure media on stability (Poda et al. 2011; Römer et al. 2011; Tejamaya et al. 2012).

The lack of appropriate data is of concern as the dispersion and stability of tested nanoparticles for *in vitro* or *in vivo* exposures will alter both the effective nanoparticle dose and the nature of the toxicant (dispersed and aggregated form) (Jiang et al. 2009). Such changes may lead to altered absorption, distribution, metabolism, excretion (ADME) and mechanisms of toxicity, affecting interpretation of toxicity data (Renwick et al. 2001; Borm et al. 2006; Choi et al. 2007). Due to these effects, it is essential for an ecotoxicology test to fully characterise the particles in the media that will be used.

The freshwater invertebrate species *Daphnia magna* is a well established test organism in ecotoxicology, and recognized by the OECD, United States Environmental Protection Agency (USEPA) and the European Union (Registration, Evaluation, and Authorization of Chemicals, REACH) due to ease of culture, short life span and ecological importance. Specifically, the OECD has outlined two aquatic toxicity tests employing *D. magna* assessing both acute (24 hrs) immobilization and chronic reproductive (21 days) perturbation (OECD 1998; OECD 2004). The acute and chronic OECD tests comprise half of the core USEPA environmental toxicity assessment, required for all new chemical substances expected to have substantial environmental release (≥1000 kg/yr released to surface water after wastewater treatment) (Nabholz et al. 1997) and thus have a clear importance as a regulatory tool for controlling discharges of potentially toxic materials. The EU regulation REACH requires performance of the acute test on *D. magna* only for substances manufactured or imported in

quantities of > 10 metric tons/year; for substances produced or imported at >100 metric tons chronic data on daphnids may be required (decided on a case-by-case basis) (Ruden et al. 2010).

Whilst OECD exposure media for aquatic organisms are appropriate for traditional chemical toxicity testing, the propensity of nanomaterials to agglomerate in complex solutions (Jiang et al. 2009) can lead to unexpected results. In this study, monodisperse citrate-stabilized AgNPs of well defined sizes were characterised in media used for OECD *D. magna* toxicity testing (labeled media1), and in dilutions of this media (labeled media2, media5 and media10 for a 2, 5 and 10-fold dilution of the media), as well as in just UHP water. Detailed information of aggregation was collected by dynamic light scattering (DLS), flow field flow fractionation (FIFFF) and by zeta potential measurement in all media dilutions and in water. We used transmission electron microscopy (TEM) and atomic force microscopy (AFM) to assess the aggregation and stability of the particles in media1, media2 and media10. Parallel measurements of *D. magna* viability in media and identical dilutions, and the range finding experiment in concentrated and 10-fold dilution of the media indicated the concentration at which 7nm AgNPs and silver nitrate ($AgNO_3$) caused 50% immobilisation (LC_{50}) of *D. magna* neonates. These results allow recommendation of optimised test methods for the investigation of *D. magna* toxicity.

4.2 Experimental

4.2.1 Synthesis of citrate stabilized AgNPs

The synthesis of AgNPs has been explained in chapter 2, section 2.2.4, and chapter 3. Three different sizes of AgNPs (labeled AgNP1 for 20nm, AgNP2 for 10nm and AgNP3 for 7nm) were prepared and fully characterised.

4.2.2 Preparation of the media for culture of *Daphnia magna*

Preparation of the media was explain in chapter 2, section 2.2.3. The media was used at full strength (ionic strength of 0.00884M) and after dilution by a factor of 2, 5 or 10 (labelled: media1, media2, media5 and media10, respectively).

4.2.3 Stability test

Preparation of the AgNPs in the media was explain in chapter 2, section 2.2.6. The particles were left in the different solutions for 24 hours and 21 days. The final pH of the solutions was adjusted to 7.5.

To test if the particles in media1 could be stabilized without any media dilution, 1ml of 0.31mM sodium citrate was added to the media (total volume was 5ml) before the addition of the different particles, and also by adding fulvic acid (FA) to obtain a final concentration of 8mg L^{-1} of FA. Preparation of FA is shown in chapter 2, section 2.2.1.

4.2.4 Particle characterisation

4.2.4.1 Flow–field flow fractionation (FIFFF)

Separation was performed in an asymmetrical FIFF (AF2000 Mid Temperature, *Postnova Analytics*, Germany), explained in chapter 2, section 2.3.3. The eluent was 0.01M NaCl, pH 7.5, as used in previous studies (Cumberland and Lead 2009). Channel flow was set to 1mLmin^{-1} and the cross flow was set between 0.3 and 0.5 mL min^{-1} to obtain good separation of the void and sample peak. The channel volume was calculated applying FIFFF theory, as previously described, using 33 and 60nm

polyacrylamide beads (Dondi et al. 2000), which were detected with the UV detector at 254nm. Diffusion coefficients were calculated based on standard FIFFF theory and converted to size using the Stokes-Einstein relationship (Dondi et al. 2000). Between 1ml and 2ml of the sample was injected, 1ml for the samples as prepared and in water (controls), and 2ml for the samples in media, at least three independent replicates were analysed per sample and the data averaged. Excellent agreement (peak heights differing by <2%, in general) between replicates was observed. The particles in the media and in water were measured by FIFFF after 24 hours.

4.2.4.2 DLS and zeta potential

Both methods were explained in chapter 2, sections 2.3.1 and 2.3.2 respectively. Measurements were made on all samples after 24 hrs. DLS was measured for all samples over a 5 hour period. Samples were also measured after 24 hrs and 21 days.

4.2.4.3 Surface plasmon resonance

Spectral scans were obtained from an ultraviolet–visible spectrometer (Lightwave) through a 1cm pathway quartz cuvette (VWR). The instrument was referenced with a sealed water cell and wavelengths were collected from 200 to 800nm from at least three measurements and were blank corrected. SPR was explained in chapter 2, section 2.3.4.

4.2.4.4 Transmission electron microscopy (TEM) and EDX

Transmission electron microscopy (TEM) samples were prepared by drop method at room temperature, as explained previously in chapter 2, section 2.3.7. Images were obtained from a Phillips Tecnai F20, with Oxford ISIS energy dispersive X-ray (EDX) and Gatan digi PEELS detectors, and recorded using Gatan Digital Micrograph software. Data was analyzed using Gatan Digital Micrograph (size distribution), Image J (circularity) and Fractalyse (fractal dimension). Image processing for fractal analyses were performed as described in chapter 1, section 1.9. EDX data was analyzed with AZtecEnergy from Oxford Instruments.

4.2.4.5 Atomic Force Microscopy (AFM)

Samples for AFM measurements were prepared by ultracentrifugation method, as described in chapter 2, section 2.3.6. Images were obtained from a XE 100 AFM in non-contact mode, recorded using XEP software and analyzed with XEI software.

4.2.4.6 Calculations

Using the sizes measured by TEM, AFM and the viscosity (measured by James Bowen, University of Birmingham) of the different media dilutions, we calculated the time for all the particles in the solution to migrate to the bottom of the fluid under gravity, T. Calculation were performed with equation 4.1:

$$T = \frac{9l}{2r^2(\rho_p - \rho_s)g} \quad (4.1)$$

l = Depth of solution (0.08 metres)

= Viscosity of the solution (0.001048 for media1 and 0.00105 Pa.s for media10)

r = radius of the particle (Units m)

$_p$ = Density of the particle (10490 kg.m^{-3})

$_s$ = Density of the displaced fluid (1000 kg.m^{-3})

g = The acceleration due to gravity (approximately 9.81 m.s^{-2})

The analysis of variance (ANOVA) was applied to compare more than one set of data at one time and is the overall test to determine whether groups means differ. A p value of < 0.05 indicates a significant difference at 95% confidence levels.

4.2.5 *Daphnia magna* tests

D. magna work was performed by Tom White and Alex Gavin in the Biosciences (University of Birmingham).

4.2.5.1 *D. magna* acute toxicity testing

Acute *D. magna* toxicity tests following OECD guidelines (OECD 1998) were performed using media dilutions in parallel with the NP agglomeration tests. Groups of 10 *D. magna* neonates (<24 hrs old) were rinsed using UHP water and immediately transferred to 250ml beakers containing media1, media2, media5, media10, media20 (media1 diluted by factor of 20) and UHP water (100ml, n=4 beakers per media concentration). Rinsing avoids contamination of the exposure media by the culture media, which is particularly important for the highly dilute exposure media studies. Immobilisation of neonates was visually assessed after 24 and 48 hrs and noted alongside any other irregularities (e.g. organism becoming trapped at the liquid surface). According to OECD guidelines (OECD 1998) any neonate unable to swim within 15 seconds of gentle test vessel agitation is defined as immobilised regardless of antennae movement. As defined in these guidelines, no food or supplements were provided during the test period, and pH was recorded at 0 and 48 hrs.

4.2.5.2 *D. magna* chronic reproductive toxicity testing

Chronic *D. magna* reproductive toxicity tests following OECD guidelines (OECD 1998) were performed using media dilutions suggested by the apparent no observed effect level (NOEL) in the acute toxicity tests. Single *D. magna* neonates (<24 hrs old) were rinsed and immediately transferred to 250ml beakers containing media1, media10, media20 and UHP water (100ml, n=5 per media concentration). Animals were maintained in these beakers for 21 days, with twice weekly media replacement and daily algal feeding (*Chlorella vulgaris*, 100µl on days 1-2, 150µl on days 3-7, 200µl on days 8-21) but with no additional supplements. To assess reproductive capability, the number of offspring were counted and removed from the test vessel daily. Again any other irregularities were recorded.

4.2.5.3 Acute Exposures to AgNP3 and $AgNO_3$

Nominal exposure concentrations of 0.1, 0.5, 1, 2.5, 5, 7.5 and 10 $\mu g\ L^{-1}$ were selected for a targeted acute toxicity exposure in both media1 and media10. Capping agent (Citrate) and negative controls

were used. Groups of 10 *D. magna* neonates (<24hrs old) were added to exposure vessels containing 250 ml of media10 or media1 and exposed for 48 hours to one of the concentrations listed above (n=3 exposure vessels per concentration, per media type) in accordance to OECD exposure guidelines (OECD 2004). No food or supplements were added during the exposure period. The pH of the exposure media was measured at 0 and 48 h. Neonate immobilisation was visually assessed at 48 hours and noted alongside any behavioural abnormalities such as trapping at liquid surface. The 48 hour LC_{50} was calculated via the trimmed Spearman-Karber method (Hamilton et al. 1977).

Analogously, neonates were exposed to 0.1, 0.25, 0.5, 0.75, 1, 5 and 10 µg L^{-1} of silver nitrate ($AgNO_3$) in both media types. Additional exposures at 1.78, 2.37, 3.16 and 4.22 µg L^{-1} of $AgNO_3$ were required to induce partial immobilisation in media1; a necessity for LC_{50} calculation.

4.3 Results

4.3.1 The effect of *D. magna* toxicity testing media on AgNP properties

4.3.1.1 DLS, zeta potential, UV-vis and FI-FFF measurements

The stability of particles AgNP1, AgNP2 and AgNP3 in daphnia media was assessed by measuring the size of the particles in different dilutions of the media by DLS, FIFFF, TEM and AFM, while zeta potential and SPR were also measured. The dilutions of the media were made by adding water, which we have previously shown (Luoma 2008; Cumberland and Lead 2009) reduces stability by desorption of citrate of the particles due to re-equilibration between solution phase and surface-bound citrate.

After dilution, DLS was measured every hour for up to 5 h and then after 24 h and 21 days, all samples showed aggregation immediately after being added to the media, increasing with time until they reached stability at about 5 h. Size distribution by intensity measured by DLS for media1 and media10 are shown in Figure 4.1. In media1 we can see aggregates of AgNPs of between 100 and 200 nm in size after 24 h, depending on the particles used initially. Visual observation showed that the

solution went from yellow to colourless almost immediately; a similar loss of the 400 nm peak as measured by UV–vis spectroscopy was also observed due to loss of material from suspension by aggregation and settling. Similar results were obtained for media2, although there was some extra stability associated with AgNP2, where aggregates of about 60 nm in size were measured and remain stable, even after 21 days (data not shown). However, for samples AgNP1 and AgNP3 the solution also went colourless after an hour, showing a high level of aggregation. The media was further diluted to obtain media5 and media10. The particles of sample AgNP1 were largely stable in both dilutions but some aggregation was observed after 24 h, which increased over the next 21 days. In the case of AgNP2 there was a slight increase in size in both dilutions (increasing from 20 nm without media to 35 nm after 24 h in media10), and some larger aggregates were also observed by DLS. For AgNP3, the DLS data showed quite extensive aggregation with both of the dilutions and high polydispersity of the particles. Aggregation in media10 is less pronounced for all samples, as we can see in Figure 4.1.

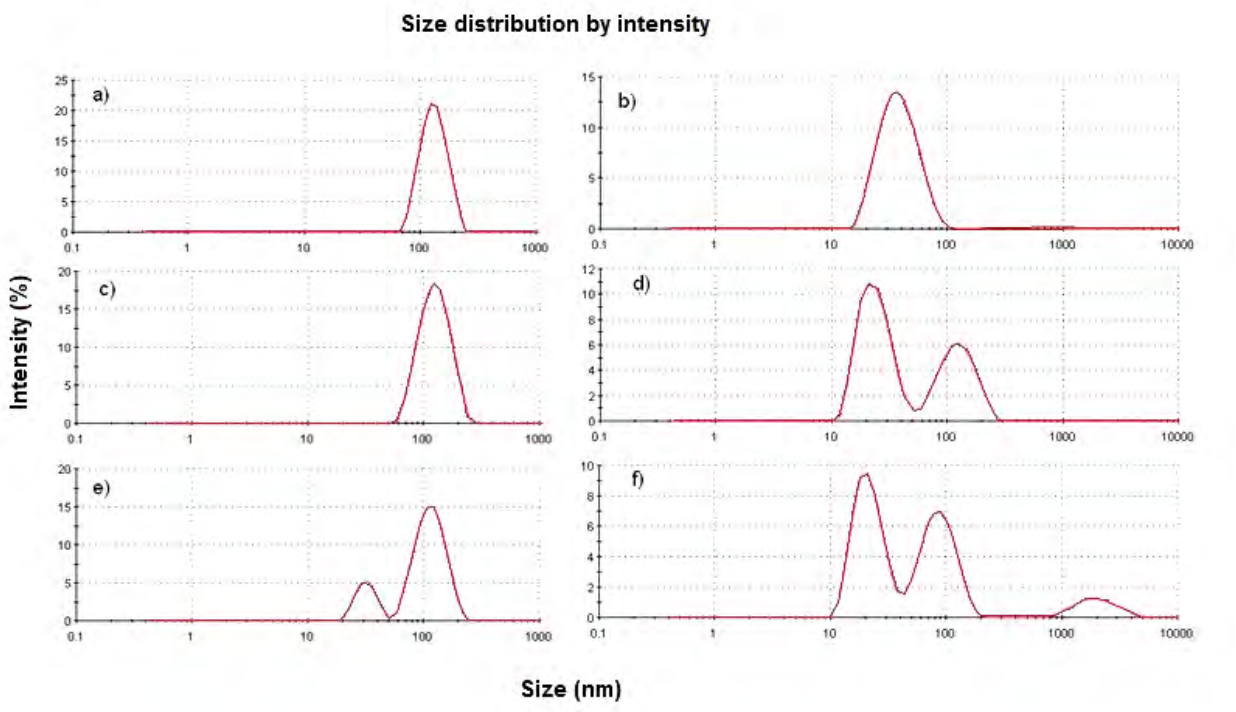

Figure 4.1. Size distribution by intensity obtained with DLS after 24 hours in media1 and media10 (left and right, respectively) for AgNP1 (a, b), AgNP2 (c, d) and AgNP3 (e, f).

Zeta potential data from the same samples are shown in Table 4.1. Clearly these values become less negative in all media dilutions compared to the particles in water, which qualitatively agrees with the

results obtained by DLS that show aggregation, although the zeta potential measurements were insufficiently sensitive to discriminate between media dilutions. Figure 4.2 shows the FFF results obtained for the three particles with the *D. magna* exposure media and in media dilutions and water. The peak (dp), number (dn), and weight (dw) average hydrodynamic diameters and sample polydispersity were calculated for each AgNP sample in the different media applying Eqs. (2.12) – (2.14), as explained in chapter 2, section 2.2, and results are summarized in Table 4.2.

Table 4.1. Electrophoretic mobility for the particles at different dilutions of the media. pH of the solutions was 7.5 (the same as media1).

Sample name	Zeta potential in water	Zeta potential in media1	Zeta potential in media2	Zeta potential in media5	Zeta potential in media10
AgNP1	- 24.5	-16	-10.5	- 10.1	- 11.9
AgNP2	- 20.5	-8.6	-7.9	-7.7	- 11.0
AgNP3	- 23	-8.5	-9.7	-10.0	- 10.0

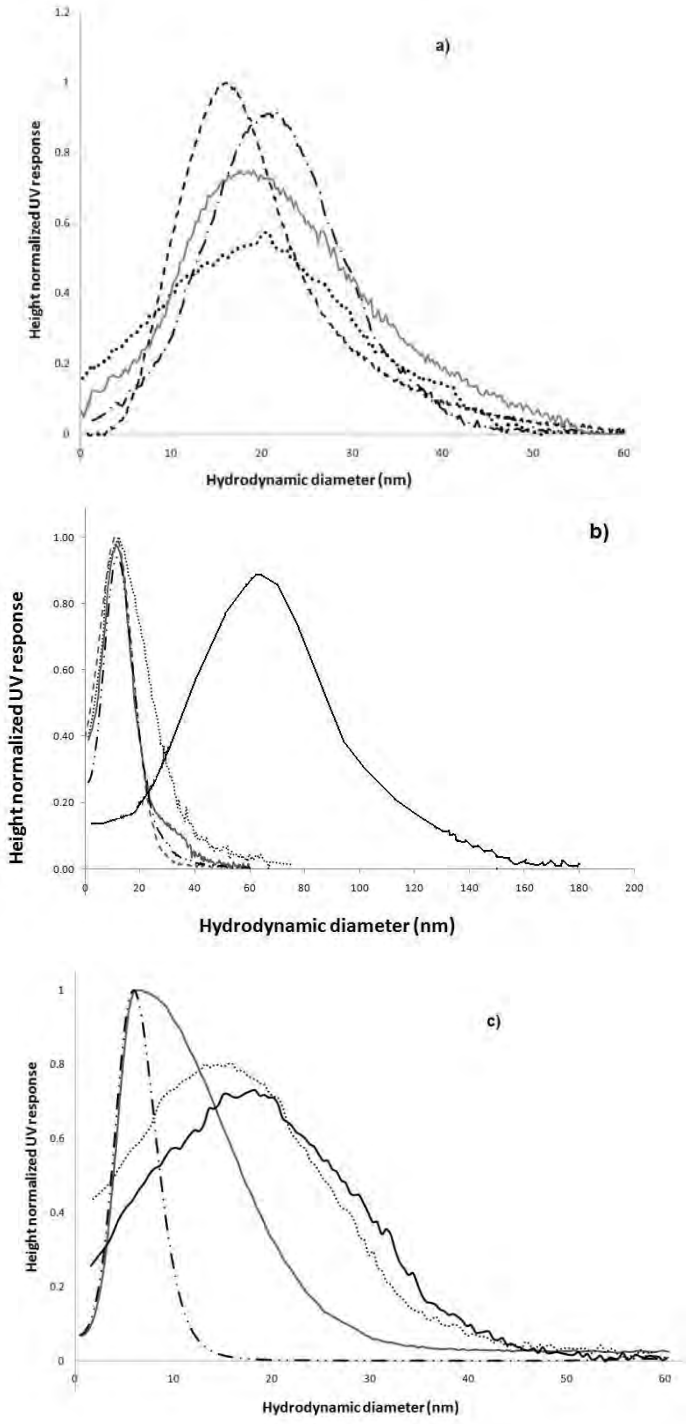

Figure 4.2. Size distribution results obtained with FFF for the AgNPs in different dilutions of Daphnia media.Results for AgNP1 are shown in a) where - - - shows the particles as prepared, ….. shows the particles in water, _ . _ . shows the particles in media5 and the gray line shows the particles in media10. AgNP2 is shown in b) where - - - shows the particles as prepared, ….. shows the particles in water, the black line shows the particles in media2, the gray line in media5 and _ . _ . shows the particles in media10. AgNP3 is shown in c) where _ . _ . shows the

particles as prepared, the gray line shows the particles in water, the black line shows the particles in media5 and , ….. shows the particles in media10.

Table 4.2. Size distribution measured by FFF for the different Ag NPs in different dilutions of Daphnia media.

Media	Sample	AgNP1	AgNP2	AgNP3
As prepared	d_p	20.8	9.6	7.2
	*d*n	20.07	9.2	7
	*d*w	20.9	11.9	11.6
	*d*w /*d*n	1.19	1.3	1.6
	Recovery (%)	64	67	64
UHP water	d_p	20.4	11.7	8.4
	*d*n	55.2	16.9	22.7
	*d*w	86.6	24	39.6
	*d*w /*d*n	1.6	1.4	1.7
	Recovery (%)	62	66	64
Media2	d_p		64	
	*d*n		77.6	
	*d*w	n.m	206.5	n.m
	*d*w /*d*n		3.14	
	Recovery (%)		64	
Media5	d_p	20.5	12.6	8.7
	*d*n	37.1	14	35.7
	*d*w	59	18.9	45.6
	*d*w /*d*n	1.6	1.4	1.7
	Recovery (%)	64	64	61
Media10	d_p	21.5	10.7	9.9
	*d*n	38.7	18.8	25.7
	*d*w	59.1	26.3	34.1
	*d*w /*d*n	1.5	1.4	1.3
	Recovery (%)	64	65	62.5

d_p = hydrodynamic diameter (nm) corresponding to the peak maximum; *d*n = number average hydrodynamic diameter (nm); *d*w = weight average hydrodynamic diameter (nm); *d*w */d*n = sample polydispersity. Particles in media1 were not measurable by FIFFF.

In media1 the samples were highly polydisperse and no fractogram was observed, possibly due to particle aggregation and sedimentation. In media2 a fractogram for AgNP2 only was observed, showing a stable peak at ca. 60 nm (Figure 4.2b), i.e., only small aggregates were present; data could not be collected for the other NPs due to aggregation. Media5 and media10, showed peaks of similar size to the particles as prepared, with some broadening and tailing. We can see that in general peaks have right shifted, and were broader and flatter than when in a citrate solution or water (Figure 4.2 a–c), this show an increase in particle size. However, there are no obvious reductions of peak area, as we have seen elsewhere (Baalousha et al. 2008) in the presence of substantial aggregation. Recovery values are around 65% for all samples, but it decreases in the case of the samples which show some aggregation (data from DLS), i.e., AgNP3 in media5 and media10. Taken together, the data indicate that aggregation is occurring but is relatively minor in the media5 and media10. We can see in Table 4.2 that polydispersity values are lower for media10 than for media5, as well as dn and dw values.

4.3.1.2 AFM, TEM and EDX measurements

TEM images obtained for all particles in the different media dilutions (media1, media2 and media10) are shown in Figure 4.3 and EDX results are in Figure 4.4. The images obtained by AFM are shown in Figure 4.5. For media1 and media2, as expected, large aggregates can be seen by both methods.

AFM and TEM samples were prepared differently due to the fact that large aggregates would not stick to the mica sheet used for AFM with drop deposition method, which proved to be a good method for TEM grid preparation. AFM can measure large aggregates that will be missed by DLS after sedimentation, and is able to measure sample height, which can't be seen with TEM because it can only image in 2D. Even though AFM is a very useful method to assess the height of the aggregates, it was difficult to obtain many images, as it had to be performed at very slow speed (0.3 Hz) and many

times the tip would lose contact with the surface. We managed to obtain more images with TEM, and Table 4.3 shows the size of the largest and smallest aggregate found for all particles added. It was difficult to obtain an aggregate size distribution because of the polydispersity of the sample. We also found single particles that were very polydisperse.

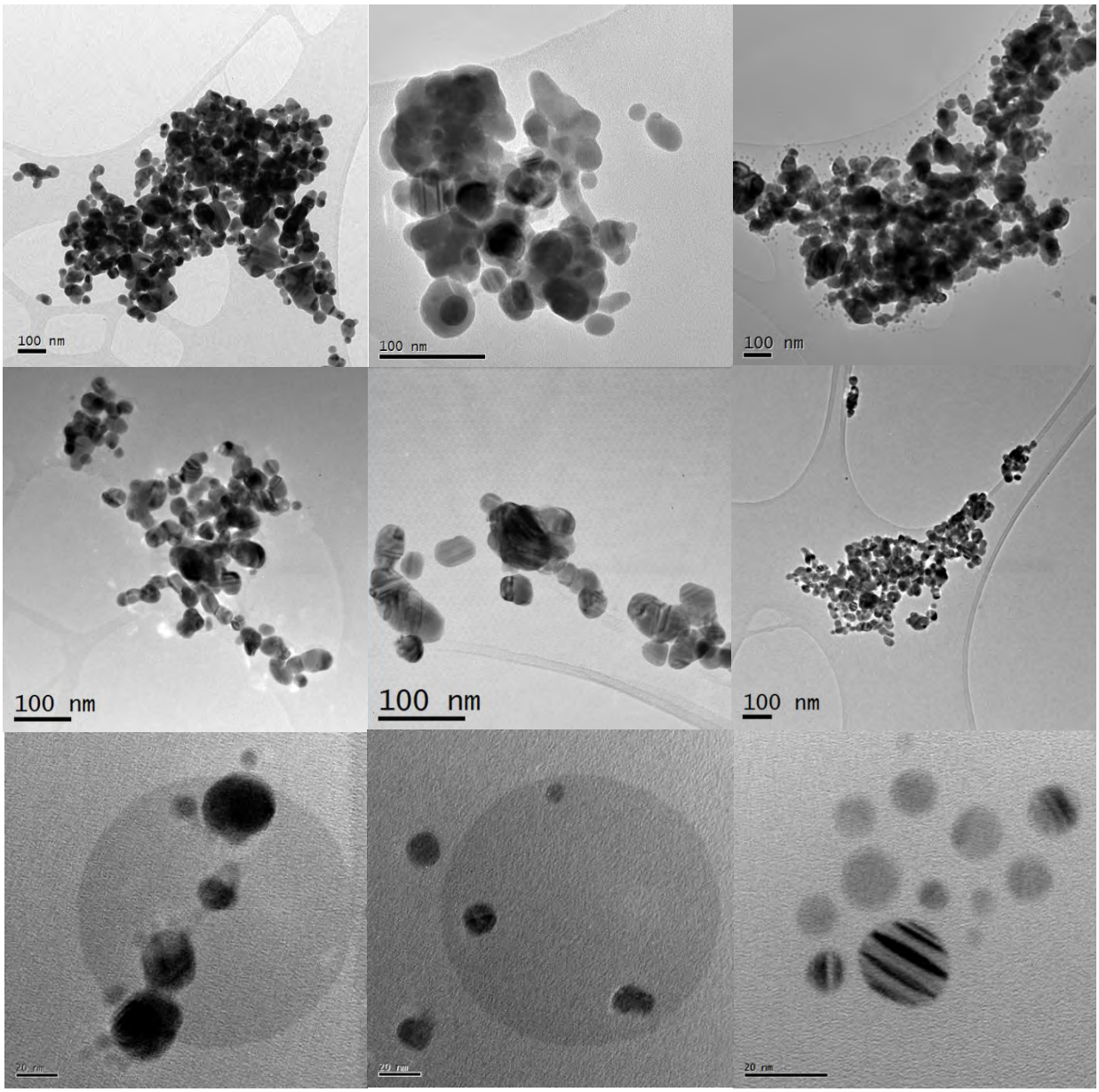

Figure 4.3. TEM images for AgNP1 (first row from left to right), AgNP2 (middle) and AgNP3 (right row) in media 1 (top row), media2 (middle row) and media10 (bottom row), after 24 hours. The scale bar for media1 and media2 is 100nm and 20nm for media10.

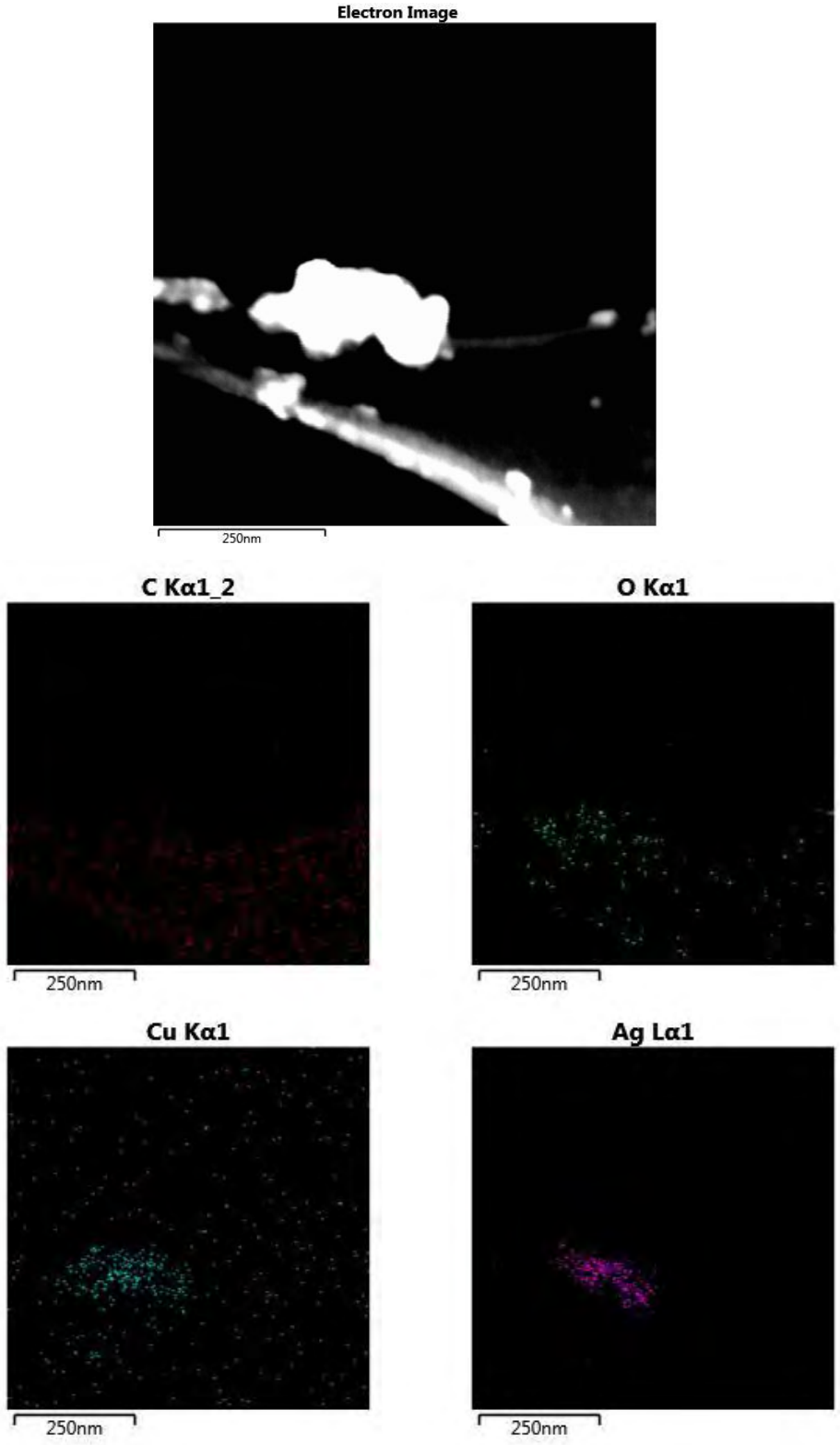

Figure 4.4. EDX map for AgNP1 aggregates in media2 performed with Tecnai F20 and analyzed with AZtecEnergy (oxford instruments).

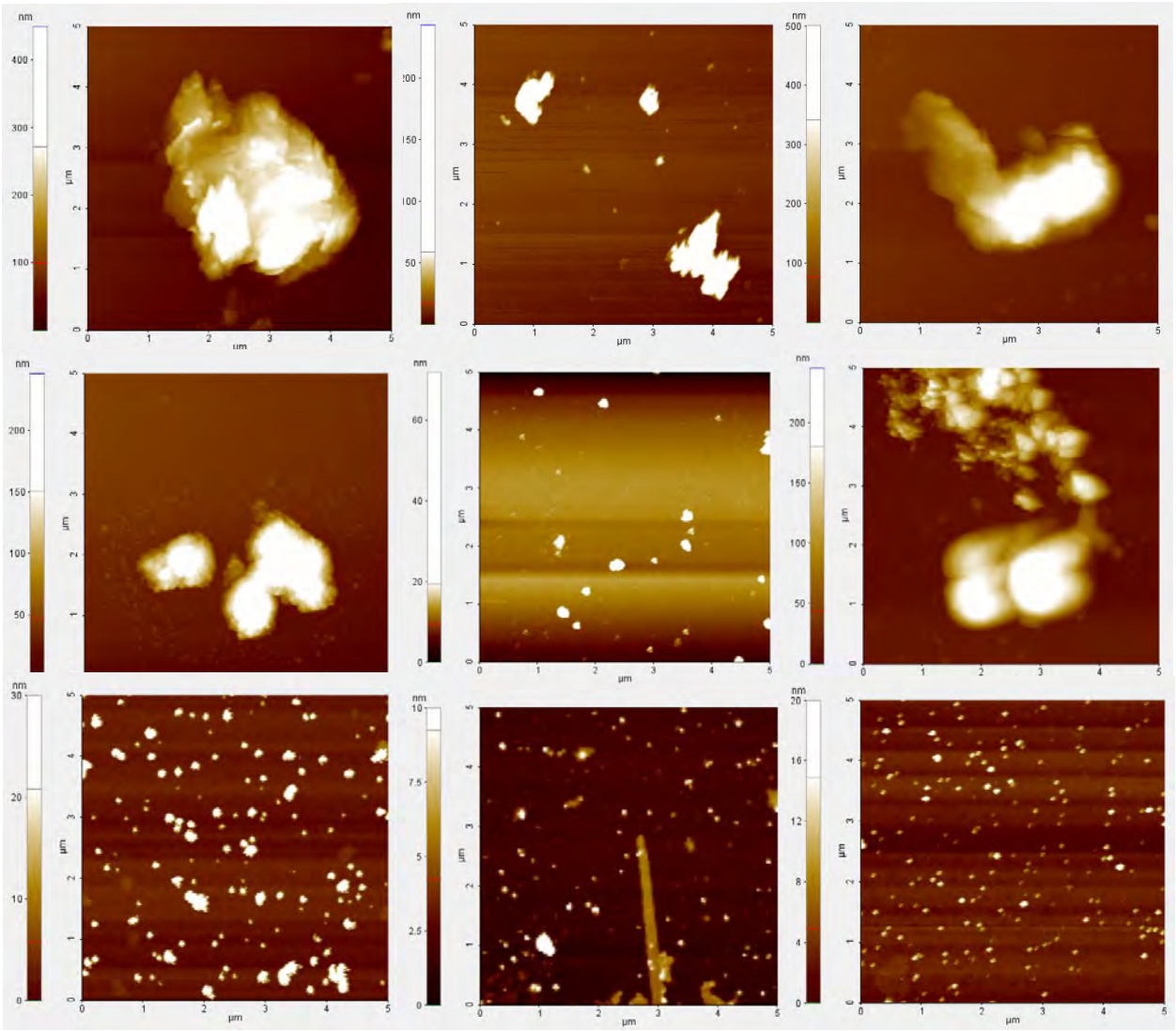

Figure 4.5. AFM images for AgNP1 (first row from left to right), AgNP2 (middle) and AgNP3 (right row) in media 1 (top row), media2 (middles row) and media10 (bottom row), after 24 hours.The AFM images are 5 x 5 µm and the samples were prepared by centrifugation method.

Table 4.3. Properties of the AgNPs prepared in media1 and media2, measured by TEM.

measurement	Media1			Media2		
	AgNP1	AgNP2	AgNP3	AgNP1	AgNP2	AgNP3
Circularity	0.17 ± 0.06	0.25 ± 0.11	0.28 ± 0.13	0.31 ± 0.16	0.32 ± 0.13	0.25 ± 0.12
Fractal dimension (D)	1.91 ± 0.11	1.94 ± 0.08	1.88 ± 0.13	1.87 ± 0.10	2.05 ± 0.36	1.91 ± 0.16
Aggregate size (nm)	117 - 1774	100 - 400	50 - 3300	80 -1200	40 - 510	60 - 1100
Single particle size (nm)	1.7 - 41	4 - 60	2 - 40	5 - 55	3 - 80	3 - 60

The results for media10 are shown in Table 4.4 and Figures 4.3 and 4.5. We can observe that the particles seem to be stable in this media dilution. The values calculated for rate of sedimentation are shown in Table 4.5.

Table 4.4. Size distributions for the different AgNPs in media10, measured by TEM and AFM.

Instrument	AgNP1	AgNP2	AgNP3
TEM	19 ± 9 (n=109)	13 ± 7 (n=103)	10 ± 5 (n=200)
AFM	22 ± 9 (n=113)	10 ± 3 (n=100)	7 ± 3 (n=146)
circularity	0.91 ± 0.04	0.93 ± 0.05	0.95 ± 0.06

Table 4.5. Rate of sedimentation in media1 and media10, calculated from Stokes' Law, eq. (4.1).

measurement	Media1						Media10		
	AgNP1		AgNP2		AgNP3		AgNP1	AgNP2	AgNP3
Sedimentation time (days)	30	0.13 (3.2 h)	19	1.2 (23 h)	76	0.017 (25 min)	470	1879	3836
Size of particle (nm)	117	1774	100	400	50	3300	20	10	7

4.3.2 Acute effect of media dilution on *D. magna*

D. magna neonates (<24 h) did not become immobilised when cultured in any of the diluted media for 24 or 48 h. However, in UHP water there was significant ($p < 0.001$) immobilisation of 25 ± 6% of the neonates after 24 h, which increased to 35 ± 4% after 48 h (Table 4.6). Some neonates become trapped at the surface in media2 and media5 groups, although this was not observed in the highest dilution (media10) and there was no consistent trend.

Table 4.6. Acute effect of media dilution on *D. magna*.

Media	Starting pH	Ending pH	24 hr Immobilisation (%) [a]	48 hr Immobilisation (%) [a]	Comments
Media1	7.33 ± 0.02	7.28 ± 0.02	3 ± 2	3 ± 2	-
Media2	7.01 ± 0.03	6.98 ± 0.04	0	0	Some surface trapping
Media5	6.72 ± 0.04	6.65 ± 0.03	0	0	Some surface trapping, one example of irregular swimming
Media10	6.37 ± 0.03	6.37 ± 0.03	0	0	-
UHP water	6.05 ± 0.04	6.09 ± 0.03	25 ± 6 ***	35 ± 4 ***	-

[a] Significance determined from ANOVA across all 5 media concentrations (*** $p<0.001$)

4.3.3 Chronic effect of media dilution on *D. magna* reproduction

When maintained in UHP water, all the organisms became immobilised (see Table 4.7) within 96 h, considerably earlier than the production of the first brood of neonates; therefore the number of offspring produced was zero. In the other media dilutions there was a complete lack of immobilisation across the 21-day period. In media20 neonate output was significantly ($p < 0.01$) lower than that of media10 and media1, however, there was no significant difference between the latter two dilutions. In addition to low fecundity in media20 there was also evidence of surface trapping and production of immobilised neonates.

Table 4.7. Chronic effects of media dilution on *D. magna* reproduction (over 21-day study).

Media	Immobilisation (%) [a]	No. of offspring produced [a]	Comments
Media1	0	61.8 ± 4.0	-
Media10	0	56.8 ± 12.3	-
Media20	0	10.6 ± 5.1 **	Dead neonates some surface trapping.
UHP water	100 ***	0 ***	-

[a] Significance determined from ANOVA across all 4 media concentrations (** p<0.01, *** p<0.001)

4.3.4 Acute Exposures to AgNP3 and $AgNO_3$, calculation of LC_{50}

In media10, increasing concentrations of AgNP3 resulted in increased immobilisation of *D. magna* neonates (Table 4.8). Using the Spearman-Karber method, the LC_{50} was calculated to be 5.36 $\mu g\ L^{-1}$, with lower and upper confidence intervals of 4.69 $\mu g\ L^{-1}$ and 6.12 $\mu g\ L^{-1}$ respectively (Table 4.9). There was no immobilisation in either the control or the citrate control and although some surface trapping (an indication of stress in *D. magna* (OECD 1998; OECD 2004), was observed in the 0.5, 1, 2.5, 5 and 7.5 $\mu g\ L^{-1}$ exposure groups, it was not in a dose dependent manner (Table 4.8).

In contrast, the same concentrations in media1 failed to induce any immobilisation in all but the highest dose group, where only 3.33% was observed (Table 4.8). Again, no immobilisation was observed in any of the control groups (Table 4.8). A value for the LC_{50} could not be calculated from these results.

Table 4.8. Percentage immobilisation observed 48 h after exposure of *D. magna* neonates to AgNP3 in media1 and media10.The LC_{50} of these particles in media10 along with 95% confidence intervals was calculated by the Trimmed Spearman-Karber method.

Dose Group (μg L^{-1})	Media1 Mortality (%)	Media10 Mortality (%)
Control	0.00	0.00
Citrate	0.00	0.00
0.1	0.00	0.00
0.5	0.00	0.00
1.0	0.00	0.00
2.5	0.00	6.67
5.0	0.00	33.33
7.5	0.00	70.00
10.0	3.33	100.00

Table 4.9. The LC50 values as well as upper and lower 95% confidence intervals of AgNP3 and AgNO3 in media1 and media10.The values were calculated using the Trimmed Spearman-Karber method. The LC_{50} of AgNPs in Media1 was incalculable.

	Media 1		Media 10	
Toxicant	**$AgNO_3$**	**AgNP3**	**$AgNO_3$**	**AgNP3**
95% LCI	1.35	-	0.71	4.69
LC_{50}	**1.43**	**-**	**0.87**	**5.36**
95% UCI	1.52	-	1.07	6.12

The dose response of *D. magna* to $AgNO_3$ in both media1 and media10 is similar, results are shown in Table 4.10 with calculated LC_{50} values of 1.43 and 0.87 respectively (Table 4.9). There was one incident of a possible anomalous result in the media10 acute toxicity exposure, where 6 members of one 10-neonate repeat died, with the remaining 4 showing signs of stress (surface trapping) whereas

the remaining two 10-neonate repeats showed no fatalities, with no apparent signs of stress. This occurred in a low concentration exposure (0.25 µg L^{-1}), causing overall mortality to be 20% in that group, which is a much greater rate than that recorded in the next two higher exposure groups. These results were included in further calculations.

Table 4.10. Percentage immobilisation observed 48 h after exposure of *D. magna* neonates to silver nitrate ($AgNO_3$) in media1 and media10. Originally, concentrations of 0.1, 0.25, 0.5, 0.75, 1, 5 and 10 µg L^{-1} of $AgNO_3$ were used in both types of media, however in media1 no partial death was observed at these concentrations, so further exposures at 1.78, 2.37, 3.16 and 4.22 µg L^{-1} $AgNO_3$ were done in media1 only in an attempt to characterise the dose-response curve further.

Dose Group (µg/L)	Media 1 Mortality (%)	Media 10 Mortality (%)
Control	0.00	0.00
0.1	0.00	3.33
0.25	0.00	20.00
0.5	0.00	3.33
0.75	0.00	16.67
1	0.00	76.67
1.78	83.33	-
2.37	100.00	-
3.16	100.00	-
4.22	100.00	-
5	100.00	100.00
10	100.00	100.00

4.4 Discussion

Clearly, the standard OECD test media caused substantial aggregation of AgNPs and media dilution reduced this effect. This increased stability with reduced ionic strength is, in accordance with expectations, based on DLVO theory (Lead et al. 2009), where increased ionic strength shields charges, reduces the diffuse layer thickness and allows NPs to come into contact sufficiently closely to aggregate. Zeta potential changes between the different dilutions of the media were not observed, possibly due to addition of Cl^- via the media (El Badawy et al. 2010). Silver halides, such as AgCl, are well known to form insoluble precipitates in solution with net negative charge (Cosgrove 2005). Thus, the measured zeta potential values, and potentially some of the DLS data, are a combination of the information on the AgNPs and the AgCl particles, making interpretation more difficult. Indeed, the effect of the conditions on AgNP aggregation has been previously studied (El Badawy et al. 2010) using environmentally relevant conditions. Aggregation in solutions with high ionic strength, in particular those containing divalent cations (Ca^{2+}), was found, although elevated levels of Cl^- also increase stability of citrate stabilized AgNPs at low ionic strength conditions. Other research (Cumberland and Lead 2009) used FFF and DLS to test the stability of citrate stabilized AgNPs in solutions with added sodium, calcium and humic substances (HS). Addition of sodium and calcium caused aggregation of the AgNPs, even at low concentrations, but the addition of low and environmentally relevant concentrations of HS stabilized the NPs and reduced losses by aggregation.

If media is diluted with water, in addition to reducing salt concentration, the surface citrate which is weakly bound to the NPs, desorbs due to re-equilibration between surface and solution, and this reduces NP stability (table 4.2). It has been shown previously (Cumberland and Lead 2009) that dilution with citrate maintains stability and minimizes aggregation.

Stability of the particles in the *D. Magna* exposure media could be potentially improved by adding citrate, but possibly with the addition of extra complexity in interpreting subsequent toxicity data. Sodium citrate and FA were added to media1 before the addition of the different particles to improve stabilization of the particles. It was found that the extra capping agents added did not hinder or stop aggregation in media1, we could see an immediate change in colour of the solution (from yellow to

colourless), UV-vis could not be measured, and DLS showed aggregation. Aggregation can't be avoided by adding extra reagents to the Daphnia media, thus, dilution of media1 is still necessary to assess the toxicity of monodisperse AgNPs.

According to FIFFF measurements, sample AgNP1 remains stable in the diluted media (as seen in Table 4.1) but there is broadening and tailing of the peaks (Figure 4.2a). A peak maximum of 20 nm is observed by FIFFF for the NPs as prepared, and it remains constant in water, media5 and media10. This peak maximum is not identical to the weight or number average diameter (Table 4.2). AgNP1 have a larger size distribution than the other AgNPs, as seen in chapter 3, Figure 3.4, in part due to greater tailing observed at larger size as size control is more difficult during synthesis. It can also because the conditions were optimised for the elution of the smaller NPs. Sample AgNP2 shows stable peaks indicative of dispersed NPs in the diluted exposure media (media5 and media10), with a small amount of peak broadening and tailing. The fact that we obtain a fractogram for AgNP2 in media2 is not fully understood and requires further work to ascertain. Presumably, the stability is related to the relative strength of the citrate-NP interactions which are stronger in the case of AgNP2 giving greater stability. The hydrodynamic diameter, the weight and number average diameter obtained for the particles in media2 have very different values, and polydispersity is quite high (Table 4.2).

Although FFF fractograms were available for the AgNP3 in the diluted media, a clear right shift (larger sizes) in maximum peak heights was observed, along with tailing and broadening of the peaks, and also a decrease in the recovery (from 64% as prepared to 61% in media5 and 62.5% in media10). A broadening of the hydrodynamic diameter can be observed, but no significant change in the polydispersity. Aggregation and stability of the particles is size dependent, with smaller particles being less stable than larger ones. Small particles are more mobile, interact more quickly and have a greater surface energy, so will be more prone to adhere on contact, assuming the same citrate coverage and stabilisation effect. In such cases, extra stability might be provided by further dilutions and maintaining stable citrate concentrations after dilutions.

Table 4.2 shows that all the AgNPs as prepared have a narrow hydrodynamic diameter distribution as measured by FlFFF (Figure 4.2), which seems to be similar to the weight and number average diameter, and polydispersity values are low. When the particles are dispersed in UHP water we see a change in this, the weight and number average diameter increase in value, and we can see a change in the fractogram (Figure 4.2), polydispersity still has low values, increasing slightly; recovery values seem to be slightly lower than the value obtained for the particles in citrate. When the particles in media5 and media10 were measured we observe that the weight and number average diameter are very different from the hydrodynamic diameter, and recovery remains relatively stable, except for AgNP3. Polydispersity values do not change substantially in the media compared to the particles in UHP water. We use the hydrodynamic diameter corresponding to the peak maximum, because the number and weight average are affected by the overall aggregation (i.e., by values at large sizes or the tailing in the FlFFF fractograms) (Baalousha et al. 2008). The broadening of the hydrodynamic diameter distribution fractogram indicates the increase in aggregation and formation of large aggregates. Recovery agrees with this effect, especially for AgNP3, in which we expect a higher aggregation, based on DLS data.

Comparison of the DLS and FFF data was informative. DLS could detect large aggregates (when the z average size was calculated) that FFF was not able to measure; these aggregates remained in the FFF channel, which turned black over time, due to the formation of oxides and sulfides, in suspensions containing large aggregates. With FFF, small unaggregated particles were measured that were not visible with DLS. Analysis of FFF (Table 4.2) and DLS (Figure 4.1) data indicate that, where FFF fractograms were observed, loss by aggregation was not extensive.

TEM (Figure 4.3) and AFM images (Figure 4.5) show large aggregates for the particles in media1 and media2. Figure 4.4 shows the EDX map obtained for AgNP1 in media2, showing a silver signal in the place of the aggregate. Similar results were obtained for different aggregates and different samples.

Circularity values for the aggregates in both media1 and media2 were consistently small (Table 4.3 and Table 3.2), which is expected due to the change in size and shape. The values between aggregates in media1 and 2 were not statistically different (having a $p = 0.053$). Fractal dimension (D) was also calculated and results show no significant statistical difference between the values (p =

0.20). Fractal dimension can be calculated by using a geometric power law scaling the relationship between each dimensional geometry, which in this case was the projected area for two dimensions and characteristic length scales of the aggregate (Lee et al. 2004; Baalousha et al. 2008). Fractal dimensions calculations are explained in chapter 1, section 1.5.3. In all cases the particles form compact aggregates with a fractal dimension indicative of a rate-limited aggregation (Buffle et al. 1998). We believe that citrate somewhat improved particle stability by restricting contact between particles, the reaction rate of two particles in the limiting regime is much slower than the collision rate, a large number of collisions will be required before two particles can stick together (Lin et al. 1990b). This type of agglomeration mechanism most likely results in slower sedimentation, thus keeping the NP aggregates in suspension for longer periods of time. It can be observed that large aggregates in media1 have a short sedimentation time (Table 4.5), and will sediment much faster than the particles in media10. In the case of AgNP3, used to calculate LC_{50}, larger aggregates will sediment after less than an hour.

The results for AgNP2 in media1 and media2 were consistent between FFF, DLS, AFM and TEM, showing smaller aggregates than the rest of the particles, although some larger aggregates were also observed with TEM and AFM and not with FIFFF or DLS. This effect is not really understood, we hypothesize that it has to do with structural differences in the AgNP2, they might have more citrate per surface area than AgNP1 and AgNP3, and thus will be more stable and aggregation will be more difficult.

In the case of media10 we can observe single particles, shown in Figures 4.3 and 4.5 and Table 4.4, which corresponds with the data obtained with DLS and FIFFF. The sizes in media10 measured by AFM and TEM compared to the size of the particles measured as prepared were statistically different ($p < 0.05$) for all particle sizes. Circularity values were also statistically different from the values of the particles as prepared (Table 3.2 and Table 4.4), which can be due to an increase in size of the single particles. Even though we obtained these values, we found well dispersed single particles in this media, which will allow us to obtain clear results for single particles in toxicological tests.

The response of $AgNO_3$ toxicity to increasing media salinity is similar to that observed with AgNP3. Both toxicants appear to exhibit reduced toxicity in response to increasing media ionic strength.

Nanoparticle exposures in media1 show an absence of lethal response from the neonates compared to the full dose response curve observed when exposures take place in media10. This suggests that the toxicity of these particles is significantly reduced in response to increasing ionic strength of the media, which might be due to the formation of silver chloride (AgCl) species (El Badaway et al. 2010). For $AgNO_3$, the calculated LC_{50} values for suspended Ag in media1 and media10 are much closer than the values calculated from nanoparticle exposures, but are still significantly different when comparing 95% confidence intervals as the regions do not overlap. The minimisation and quantification of aggregation is clearly important in certain nanotoxicology testing. Aggregation will affect NP properties and toxicity by (a) reducing the nominal (added) dose to which the organisms are exposed and (b) altering the nature of the toxicant to which the organisms are exposed.

In this case, dose doesn't change based on sedimentation rates, especially in the case of smaller aggregates, hence aggregation is the reason for lower toxicity at higher ionic strength. Lower toxicity can be due to reduced uptake, reduced availability, reduced surface area, amongst other things.

Changes in the nature of the toxicant, the formation of aggregates, have separate but related and important effects which require consideration. Ideally, the quantification of effects on pelagic species requires the use of dispersed materials and we suggest that this is the case with *D. magna*; aggregation alters the nature of toxicant complicating interpretation. For instance, nano-aggregates may be more efficiently ingested by *D. magna* (Rosenkranz et al. 2009), as the aggregates sizes that sediment are likely to be of a similar size to their natural prey (algae) and their feeding efficiency may be expected to be higher for aggregates, while bioavailability of the dispersed material is likely to be more efficient. However, it is clear that aggregates are less toxic, their uptake and/or cell interaction must be lower and the aggregates are not internalised into cells as easily. We could also expect other effects, such as potential disaggregation, and the effects may vary on organism by organism basis. We can assume that the change in aggregate size is the issue, as well as the change in the toxicant, not changes in the mass dose. In addition, the specific surface area available to interact with biota will be larger in the dispersed form, as well as the number of particles, and there may be greater effects of the dispersed material. It is therefore important to ensure dispersion for pelagic species, while also providing a full characterisation of dispersed NPs and their aggregates prior to exposures. In addition,

it is essential to measure dose and toxicant nature more exactly over the time of the exposure, in order that interpretation of data be controlled far more precisely.

Our results suggest that media10, i.e., a dilution of standard OECD media conditions by a factor of 10, provides optimal conditions for these NPs, minimising aggregation while avoiding immobilisation and maintaining fecundity of *D. magna*. Clearly such media changes must be performed on a case by case based on understanding requirements for both NP and test organism.

4. Conclusions

We have synthesised and characterised citrate-stabilised, monodisperse silver nanoparticles at three different sizes. The effect of adding the particles to Daphnia exposure media at standard OECD conditions was aggregation of the particles, however, relatively small reductions of ionic strength allowed the larger particles in particular to remain stable for the period of time needed for Daphnia exposures, and the smallest particles, AgNP3, showed reduced aggregation. Under acute conditions, Daphnia immobilisation was evident in UHP water only, in contrast to all tested media dilutions in which neonates showed only slight signs of distress. However, the more sensitive chronic reproductive toxicity test revealed absolute immobilisation in UHP water and a highly significant reduction in fecundity in media20. It has also been observed that AgNP3 and $AgNO_3$ appear to exhibit reduced toxicity in response to increasing media salinity. Our results therefore suggest that media10, i.e., a 10-fold dilution of standard OECD media, provides optimal conditions for these NPs, minimising aggregation while avoiding *D. magna* immobilisation and maintaining normal reproductive output.

5

A STEM- EELS study of AgNPs behaviour under realistic environmental conditions

---

Chapter Summary

This chapter focuses on the effects of environmentally relevant conditions on citrate-capped 20 nm AgNPs by assessing their stability in synthetic aquatic media, the influence of the presence of fulvic acid (FA) and the effect of light. UV–vis absorbance, dynamic light scattering, and STEM-EELs were used to evaluate the colloidal stability, to study crystal structure and surface chemistry, of AgNPs in different conditions. The particles were added to different environmentally relevant solution and exposed to sunlight or kept in the dark for different periods of time. Other conditions were assessed, like the particles as prepared exposed to light, suspended in ultra high purity (UHP) water or with an excess of FA. Some particles were measured by STEM-EELS, in all cases no oxidation was found, and oxygen was measured only when an FA shell was observed on the particles. EELS studies were also performed on the particles as prepared and on particles left on a TEM grid for 4 weeks, which showed oxidation.

Samples that maintained colloidal stability in various degrees during time studies had lower salinity. The addition of FA helped, in most cases, maintain colloidal stability in the presence of light. Some AgNPs will be stable in freshwater long enough to enter estuarine or marine systems successfully.

Particles in seawater aggregated almost immediately, even in the presence of FA. The work in this chapter was performed with the help of Dr. Zhi Wei Wang, from Nanoscale Physics Research Laboratory at the University of Birmingham, School of Physics and Astronomy. It was also presented in a poster Environmental Effects of Nanoparticles and Nanomaterials Conference in London, UK, September 2011 and earned 3rd prize. A paper is being prepared.

5.1 Introduction

Silver nanoparticles (AgNPs) are currently being very widely used in industry, mainly because of their anti-bacterial properties, with applications in many areas (Ju-Nam et al. 2008). Once released into the environment, the mobility, bioavailability, and toxicity of AgNPs in any ecosystem are dominated by colloidal stability (El Badawy et al. 2010). AgNPs released in wastewater may be converted into Ag+ ions, complexed with ligands, agglomerated or still be present as nanoparticles (Choi et al. 2009).

It is important to understand what happens with NPs in environmentally relevant conditions, especially on their surface. It is not well understood what happens to AgNPs in the environment, but Ag has been studied extensively. The most abundant form of Ag in the open ocean is silver chloride ($AgCl_2$) and Ag-thiolate complexes have been found in highly polluted waters (Wijnhoven et al. 2009). Silver can be found as chlorides, bromides and iodides in fresh water and soils under oxidizing conditions. Also, silver can exist as a free metal and silver sulphide under reducing conditions. It has been shown that NOM helps particle stability in media with low ionic strength (Cumberland and Lead 2009). Fulvic acid (FA) or humic acid (HA) enhance NP stability either electrostatically or sterically after being adsorbed to the surface (Li et al. 2012).

Any changes in the nanoparticle size, morphology or chemistry under environmental conditions potentially affects their toxicity (Cheng et al. 2011). Several papers have been published on the influence of environmentally relevant conditions on nanoparticles, but to date there is no work done with STEM-EELs, which can look at different parameters, such as crystal structure and surface chemistry, with near atomic resolution. Choi *et al.* (2009) assessed the effect on polyvinyl-alcohol (PVA) capped AgNP toxicity after being exposed to ligands (SO_4^{2-}, S^{2-}, Cl^-, PO_4^{3-}, and $EDTA^-$)

commonly present in wastewater. They found that the addition of sulphide at a final concentration of 10 mM reduced the toxicity of the particles by 80%, The Ag-S NPs were measured with SEM coupled with EDX. Chinnapongse *et al.* (2011) studied the stability of citrate-capped 20 nm AgNPs by measuring their colloidal stability in natural freshwaters and synthetic aquatic media, using DLS, UV-vis and AFM. Cheng *et al.* (2011) examined the effect of sunlight on the stability and toxicity of 6 and 25 nm Ag nanoparticles coated with gum arabic (GA) and (PVP), using UV-vis and TEM to assess the changes on the particles. Toxicity to a wetland plant, Lolium multiflorum, indicated that the toxicity of the NPs is greatly reduced after sunlight irradiation. Li *et al.* (2012) found morphological changes on citrate capped AgNPs exposed to sunlight, but found no impact on Ag+ solubility. The particles were suspended in river water and studied over a period of 15 days in the presence and absence of light.

It is believed that oxidation of AgNPs will influence their toxicity and stability. Djokic *et al.* (1998) showed that only Ag films containing silver oxides showed antimicrobial activities. Fan *et al.* (2001) studied the solubility of oxidized silver films, which could generate Ag(I) and Ag(0) species. Lok *et al.* (2007) found that only partially oxidized AgNPs exhibit antibacterial properties, they believe the Ag-oxide may carry chemisorbed Ag+ in quantities that are sufficient to mediate antibacterial activities.

In this work we have studied the influence of environmentally relevant conditions, such as light, natural organic matter (NOM), and salt concentration, on particle stability and surface changes.

5.2 Experimental

5.2.1 Synthesis of citrate stabilized AgNPs

The synthesis of AgNPs has been explained in chapter 2, section 2.2.4, and chapter 3. AgNP1 (20nm) were used for this experiments. AgNP3 (7nm) were also measured with STEM-EELS as prepared.

5.2.2 Preparation of synthetic water and fulvic acid

Preparation of the different synthetic waters used was explain in chapter 2, section 2.2.3. Synthetic freshwater (very soft and soft) and synthetic seawater were used. The preparation of FA is also explained in chapter 2, section 2.2.1.

5.2.3 Preparation of the AgNPs samples in the media

Preparation of the AgNPs in the media was explain in chapter 2, section 2.2.6. FA was added to some samples from a stock solution (section 2.2.1), when added to the NPs as prepared it had a final concentration of 20mg L^{-1} and when added to the synthetic water it had a concentration of 8mg L^{-1}. It was always added to the water before adding the particles. The particles were left in the different solutions for different periods of time, ranging from 24 hours, 4 weeks, to 6 months, depending on particle stability. Some solutions were exposed to natural sunlight and some were kept in the dark. The samples prepared are shown in table 5.1.

Table 5.1. Samples used to assess the stability and changes of AgNPs in different conditions.

Name	Media used	Presence of FA	Presence of natural sunlight	STEM- EELs measurement	Time of exposure
AgNP1	Citrate solution	✘	NE	Freshly prepared	NE
AgNP1-oxi	Exposed to air when dry on grid	✘	NE	Left on TEM grid for 4 weeks	4 weeks
AgNP3	Citrate solution	✘	NE	Freshly prepared	NE
AgNP1-light	Citrate solution	✘	✔	After 24 h and 25 days exposed to light in citrate solution	4 weeks
AgNP1-H_2O	UHP water	✘	✔	NM	6 weeks
AgNP1-FA light	20 mg L^{-1} FA	✔	✔	After 24 h and 10 weeks	6 months
AgNP1- FA dark	20 mg L^{-1} FA	✔	✘		
AgNP1-VS light	Very soft synthetic freshwater (IS: 0.633 mM)	✘	✔	After 4 weeks	4 weeks
AgNP1- VS FA light		✔	✔		
AgNP1-VS dark		✘	✘	NM	
AgNP1-VS FA dark		✔	✘		
AgNP1-S light		✘	✔	After 24 h	6 weeks
AgNP1-S FA light	Soft synthetic freshwater (IS: 2.53 mM)	✔	✔		
AgNP1-S dark		✘	✘	NM	4 weeks
AgNP1-S FA dark		✔	✘		
AgNP1-Sea light	Synthetic seawater (IS: 0.719M)	✘	✔	NM	24 h
AgNP1-Sea FA light		✔	✔		

NM – not measured, NE – not exposed to light

✘ - No, ✔ - Yes

5.2.4 Particle characterisation

The particles in different conditions were characterised with different methods during a certain period of time (depending on particle stability).

5.2.4.1 DLS

DLS was explained in chapter 2, section 2.3.1. Measurements were made on all samples after addition of the particles to the solution, after 24 hrs, and then on a weekly basis until measurements were not possible anymore.

5.2.4.2 Surface plasmon resonance (UV-vis)

Spectral scans were obtained from a 6800 Jenway double beam UV-Vis spectrophotometer, with a 1 cm path length plastic cuvette. The instrument was referenced with a water cell and wavelengths were collected from 300 or 350 to 700nm from at least three measurements and were blank corrected. SPR was explained in chapter 2, section 2.3.4.

5.2.4.3 Scanning Transmission Electron microscopy (STEM) and Electron Energy-Loss Spectroscopy (EELs)

STEM samples were prepared by drop method at room temperature, as explained previously in chapter 2, section 2.3.7. Sections 2.3.9 and 2.3.10 explain how STEM and EELs work. STEM-EELs measurements were performed by Dr. Zhi Wei Wang, from Nanoscale Physics Research Laboratory at the University of Birmingham, School of Physics and Astronomy, with my help. STEM images were recorded by HAADF detectors in a JEOL JEM2100F coupled with a CEOS spherical-aberration probe corrector and a Gatan Enfina EELS. The zero loss peak was calibrated roughly at 0ev but was not re-calibrated throughout the measurements as we were only quantitatively searching for the presence of Ag and had no need to measure the exact position, drifts on EELS graphs are explained as pre-

calibration features. Images were analysed by me, with the help of Zhi Wei Wang and Ruth Merrifield. The samples measured are reported in Table 5.1.

5.3 Results

5.3.1 Samples as prepared

5.3.1.1 STEM-EELS measurements on AgNP1 and AgNP3

AgNP1 and AgNP3, discussed in detail on chapter 3, were measured with STEM-EELs to assess particle shape and surface structure as prepared; a typical image obtained with STEM for the different particles is shown in Figure 5.1. Graphene grids were used for the measurements in most cases. These grids are not as uniform as the carbon films used for TEM, but they are better for EELS analysis because a strong spectral signal can be collected from the NPs located on a small region of one or just a few atomic graphene layers. In figure 5.1 lattice fringes are visible and marked with an arrow on particle B. Particle C is shown from a [110] plane, showing an FCC like structure (Explained in chapter 1, section 1.5.2) with some defects visible in the region marked with an arrow. Particle D has a quasi-crystal structure, which appears to consist of multiple twin sections.

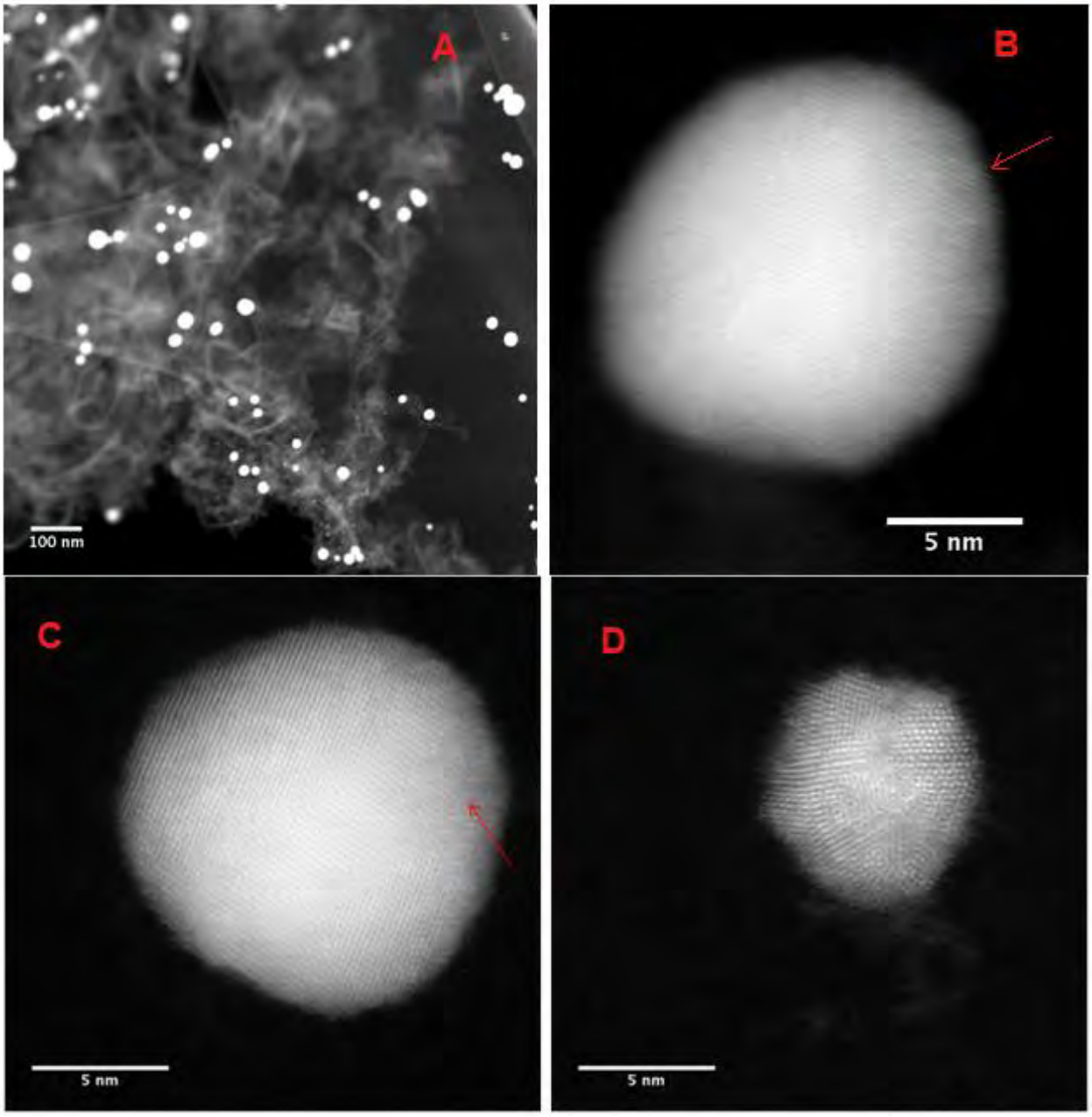

Figure 5.1. Typical image for AgNP1 (A, B) and AgNP3 (C, D) measured with STEM. Image A shows typical HAADF images of AgNP1 on the commercial graphene supports.

By using STEM-EELs changes on the surface of the particles can be assessed, such as oxidation. The EELs point spectra analysis for the AgNP1 that show the presence of Ag is shown in Figure 5.2. The silver M4,5 edges, which shows at 395 eV, can be observed in spectrum A, and there is no

oxygen K peak, which should be observed at 532 eV. Spectrum B shows that there is no oxygen K peak on the carbon grid, no AgO layers were observed.

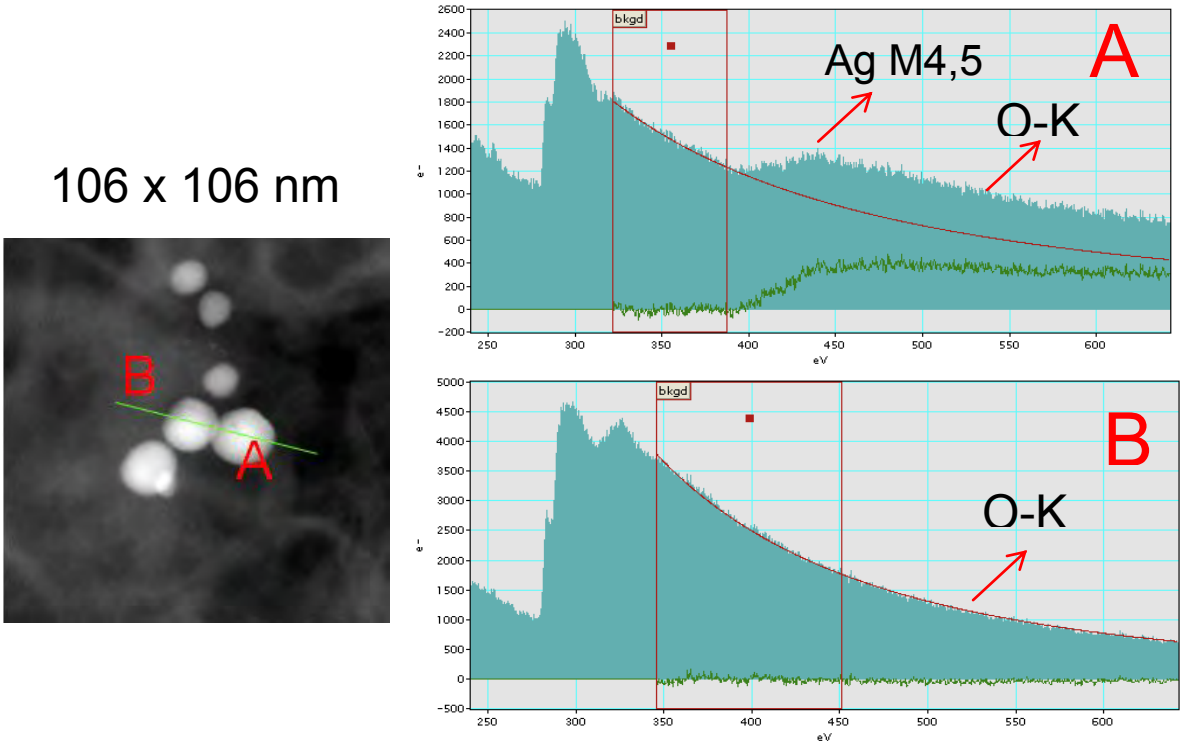

Figure 5.2. EELs point spectra for AgNP1. No clear oxygen core-loss edge are observed in any of the following cases, (i) when the beam goes through the NPs marked as A and (ii) when the beam goes only through the carbon substrate (marked B). O-K (no) marks the absence of an oxygen peak.

Figure 5.3 shows a line spectrum, and Figure 5.4 shows a map spectrum for the particles as prepared. Similar results were obtained for AgNP3 (data not shown). These different type of measurements are explained in chapter 2, section 2.3.10. A line spectrum obtained by EELs measures a certain number of point spectra along a line, which will give information on where the different elements can be located. A map measured with EELs will be similar to a line spectrum, but it will measure a larger area. Measurement of a line spectrum is faster than a map spectrum, it can be a quick way to obtain information about the sample in a large area, and map spectrum is slower but gives more detailed information from a larger area. No oxygen signal was observed in line or area spectrum measurements. Figure 5.4 shows a coherent intensity distribution between HAADF image and the Ag-EELS mapping image.

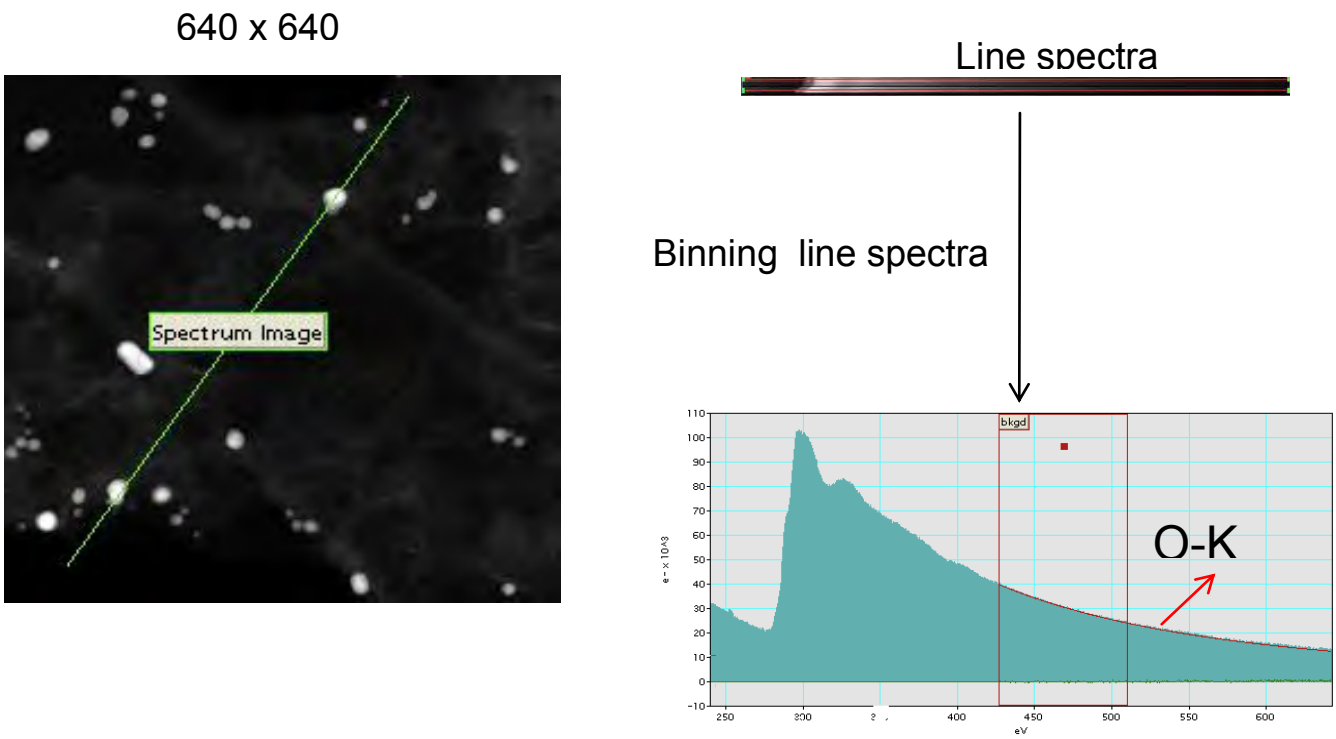

Figure 0.1 Figure 5.3. EELs line spectra for AgNP1.

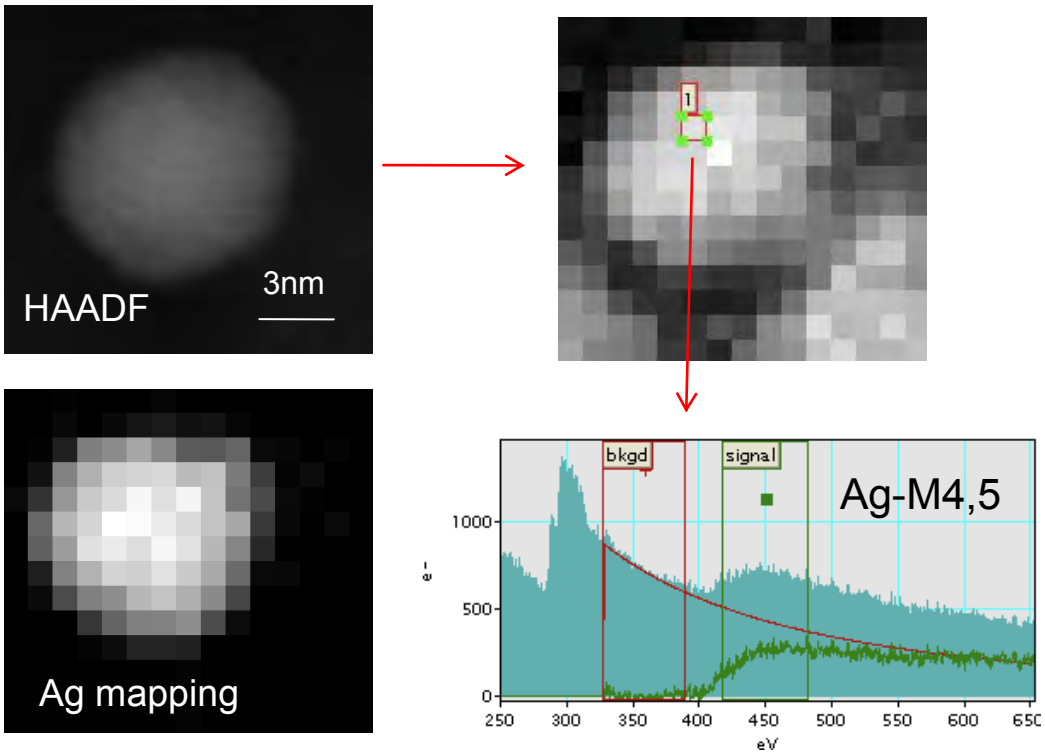

Figure 5.4. EELs map spectra for AgNP1.

When AgNP1 was left on a TEM grid for 4 weeks and measured by EELs oxidation was clearly observed (AgNP1-oxi). Figure 5.5 shows an HAADF-STEM image of these oxidized AgNP1. The particles have a core-shell structure; the shell shows an amorphous state that indicates oxidization. Silver oxide (AgO) is imaged with weaker intensity than Ag because of the presence of oxygen, which is a lighter element.

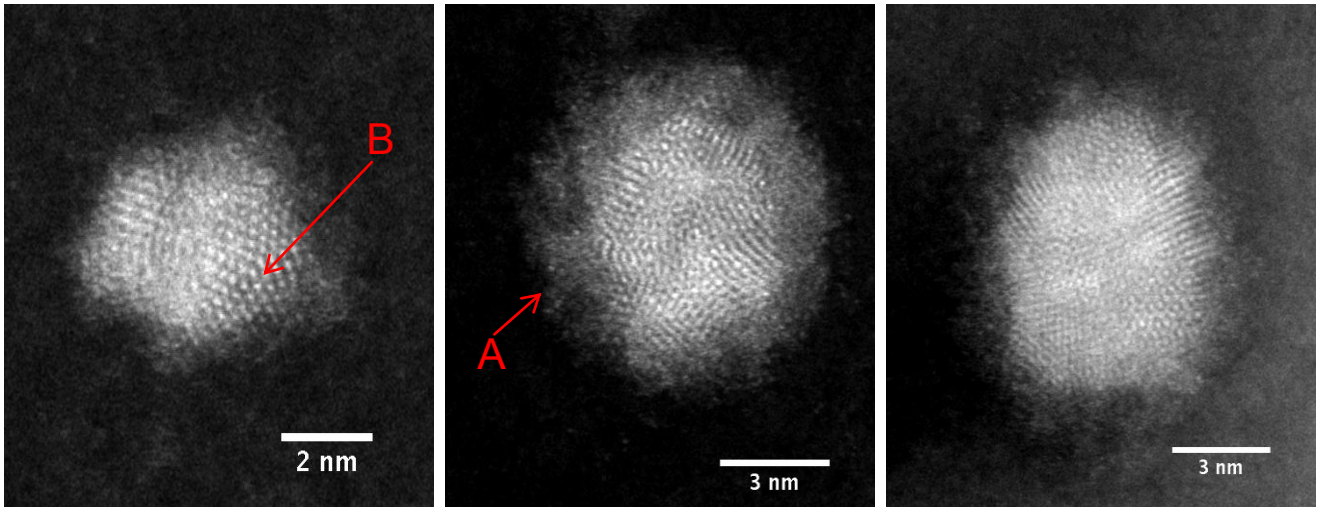

Figure 5.5. HAADF-STEM images of AgNP1 left on a TEM grid for 4 weeks showing clear core-shell structures. The amorphous shell is marked by the arrow A, and indicates oxidation.

Figure 5.6 shows a line spectrum where a clear oxidation of the outer shell is observed, shown in point spectrum marked as A. Point spectrum B shows some oxidation on the carbon grid. These results show that oxidized particles can be measured with STEM-EELs and that oxidation occurs in air. It has been observed that the particles as prepared are spherical and show no oxidation, whilst if the particles are left dry on a TEM grid and exposed to air they will oxidize and form amorphous core-shell structures. These results, which were initially an artifact due to waiting time for the STEM-EELS, are useful a) because they show the ability of the STEM-EELS instrument to detect Ag-oxide and b) as the results can be interpreted meaningfully in terms of environmental relevance, due to the fact that soils and atmospheric particles are likely major sinks for NPs, where particles are subject to wetting and drying cycles.

Figure 5.6. EELs line spectra for AgNP1 left on a TEM grid for 4 weeks. The oxygen EELS signal can be observed when the beam is incident on the Ag particles (marked A).The signal can also be observed when the beam is only on the carbon substrate (marked B).

5.3.2 Measurements on AgNP1 exposed to sunlight

Two different solutions of AgNP1 were exposed to natural sunlight, concentrated AgNP1 (12 mg L^{-1} in citrate solution) and diluted with UHP water (final concentration of 2.2 mg L^{-1}). The samples were left exposed to sunlight for a month (as prepared) and 6 weeks (in UHP water).

5.3.2.1 Concentrated AgNP1 exposed to sunlight (AgNP1-light)

When concentrated particles are exposed to light there is an obvious colour change of the solution, as seen in Figure 5.7. After 15 days the solution starts to become green, and the UV signal changes (see Figure 5.8) showing a second peak at 600nm, which gets sharper and more clear with time. There seems to be no significant change in the UV signal until this point. After 25 days the solution turns completely green and there is a third peak in the UV spectrum at 465 nm. After 30 days it becomes black and then precipitates.

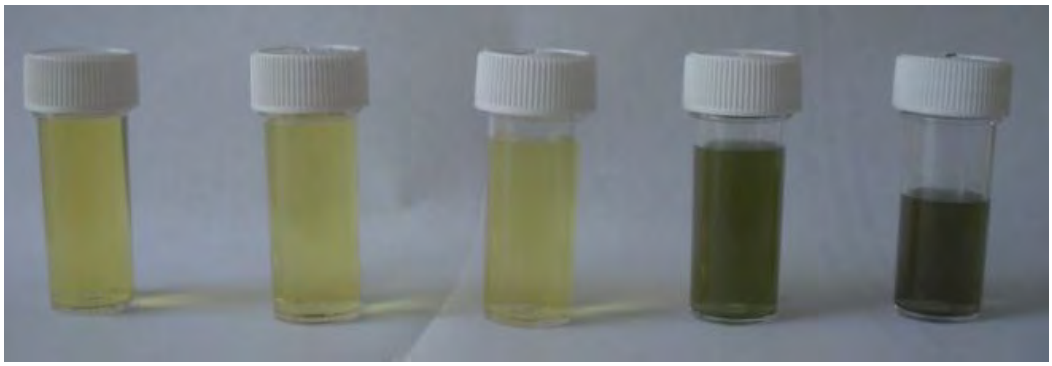

Figure 5.7. Concentrated AgNP1 (12 mg L-1) exposed to sunlight over time. From left to right, as prepared, after 5 days, 2 weeks, 25 days and 1 month.

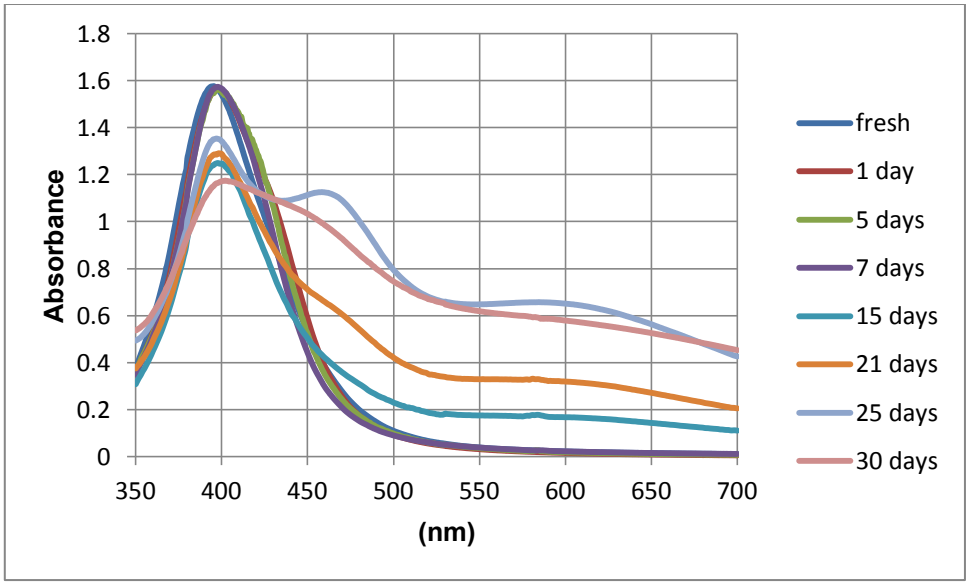

Figure 5.8. UV data for AgNP1 exposed to sunlight over time.

As it can be seen in Figure 5.9, the particles grow in size only after day 21 and the sample becomes polydisperse, they seem to become more polydisperse on day 25 and grow even more in size at day 30. Figure 5.10 show the UV-vis spectra for the particles as prepared and after 25 days, where a clear change in the signal can be observed, showing different peaks after the exposure to sunlight. DLS results are shown in Figure 5.11, where a size increase and a more polydisperse sample can be observed after 25 days.

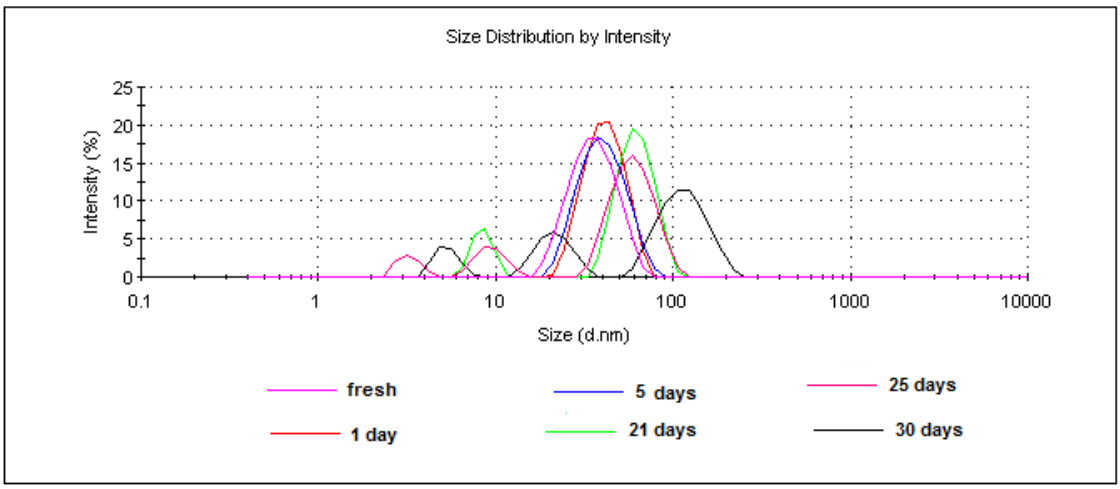

Figure 5.9. DLS data for AgNP1 exposed to sunlight over time.

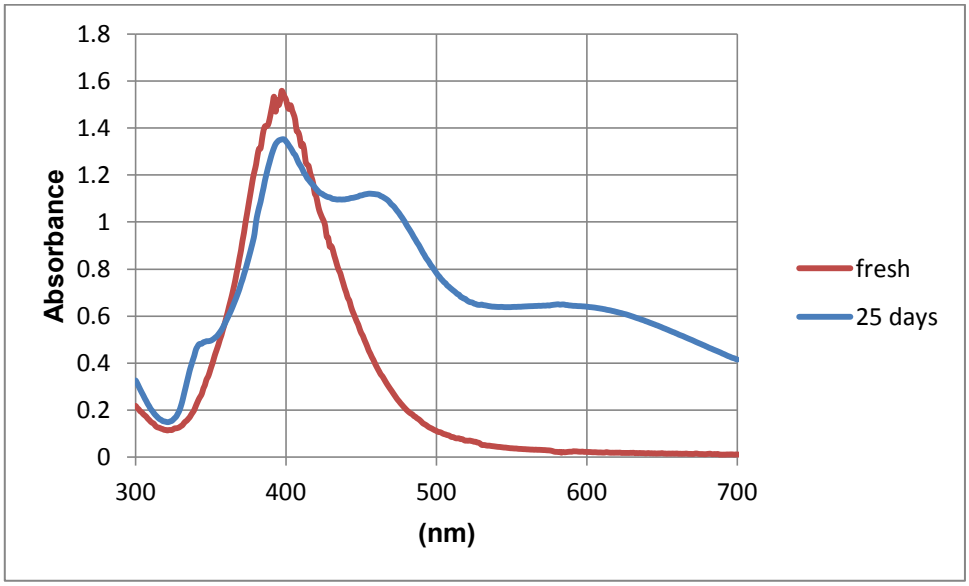

Figure 5.10. UV data for AgNP1 as prepared and exposed to sunlight for 25 days.

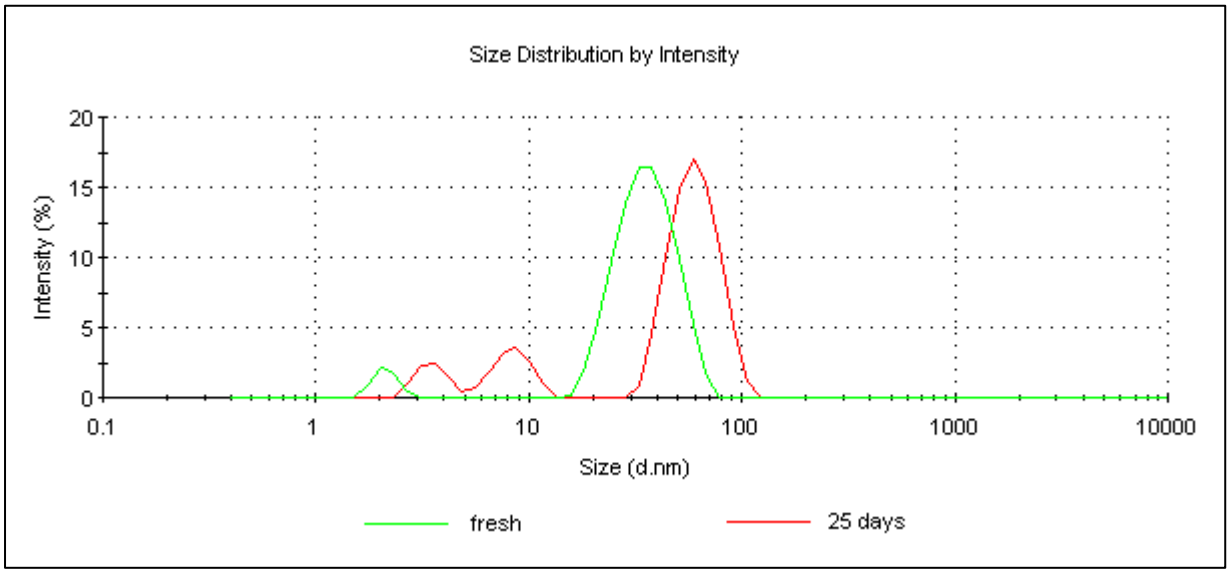

Figure 5.11. DLS data for AgNP1 as prepared and after being exposed to sunlight for 25 days.

When the particles were measured by EELS no changes were observed after 24 hours, as seen in Figure 5.12, particle size distribution remains stable. In this case, the Ag peak is not strong (since the beam does not cover many Ag atoms and was taken at the edge of the particle), but the peak

corresponding to the Ag-M4,5 edges is clearly visible. There is no O-K signal arising in the spectrum position, which indicates that there is no oxidation on this particle. These results were consistent on all particles measured, showing no oxidation.

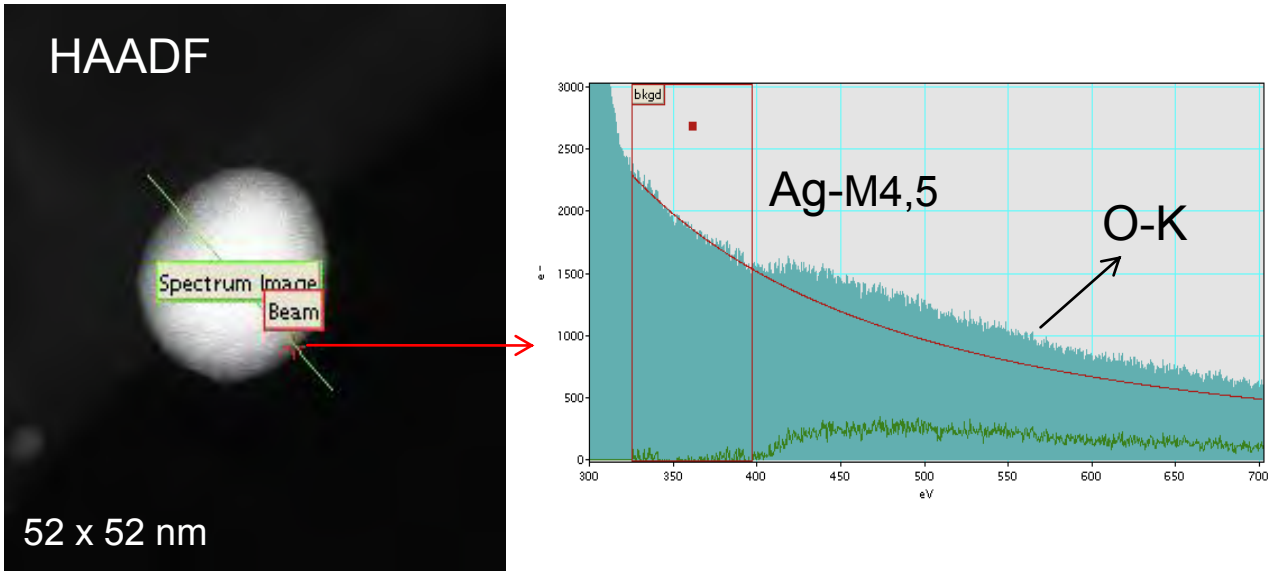

Figure 5.12. EELs line spectra for AgNP1 exposed to sunlight for 24 hours. The spectrum as shown above was taken from the edge of the particle (marked by a red crossing).

After 25 days the particles had changed in shape and size, we found rods, triangles, hexagones, large and very small particles, as seen in Figure 5.13. The original sample had spherical particles of more or less 20nm in core size, and no small particles were observed as seen in Figure 5.1-A. The presence of sunlight may cause etching and dissolution of the spherical NPs followed by recrystallization (Henglein 1993; Yang et al. 2007) and has induced morphological changes on citrate coated AgNPs (Li et al. 2012). Shape changes can explain the size increase measured by DLS, as well as the changes in the UV-vis spectrum obtain after 25 days. Some particles remain unchanged, which might be due to the fact that the solution is concentrated, therefore some particles dissolve in the solution, others change in shape or aggregate and others remain stable.

Photoreduction of Ag+ by the photoactivity of citrate has been widely used for the synthesis of AgNPs, or to achieve morphological changes on existing AgNPs (Ahern et al. 1987; Maillard et al. 2003) When this process occurs on AgNP systems, more heterogeneous structures (e.g., individual particles connected by secondary solid phases) can be formed, particularly when aggregation occurs

(Li et al. 2012). Particles may not oxidise and reprecipitate after reduction of Ag+ but could act as nucleating centres for new particles from a reduction. Shape changes could also occur due to reduction of existing Ag+ from the reactant.

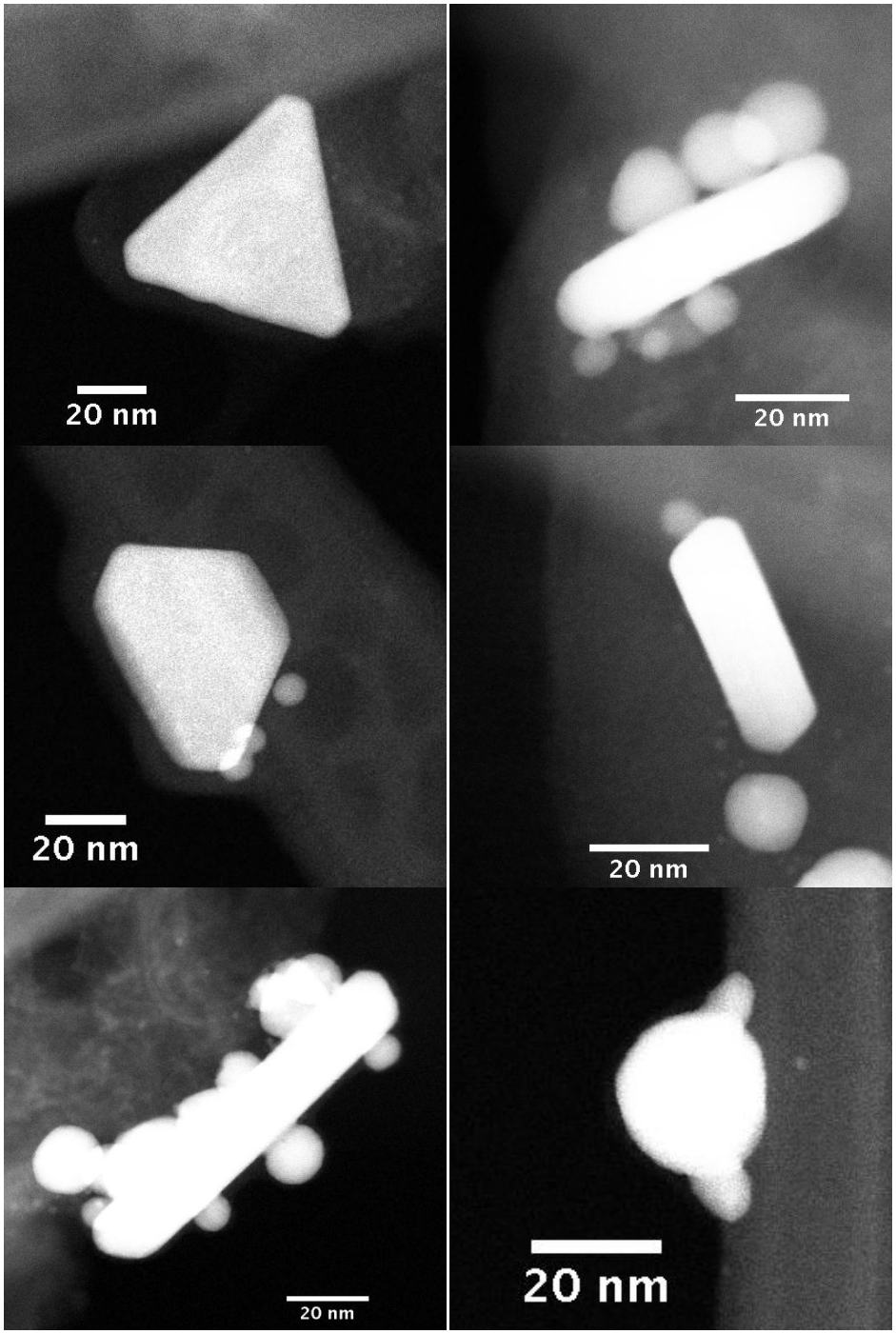

Figure 5.13. HAADF-STEM images of AgNP1 exposed to sunlight for 25 days. Some particles were found to have non-spherical shapes. We could also find spherical particles, as seen at the bottom right image.

Even though particles show size and shape change induced by the presence of sunlight, they showed no surface change (e.g. oxidation), as seen in Figure 5.14, when measured by EELs. The spectrum taken is from the edge of the particle. The systematic investigation performed does not show any obvious AgO layers existing in the particles.

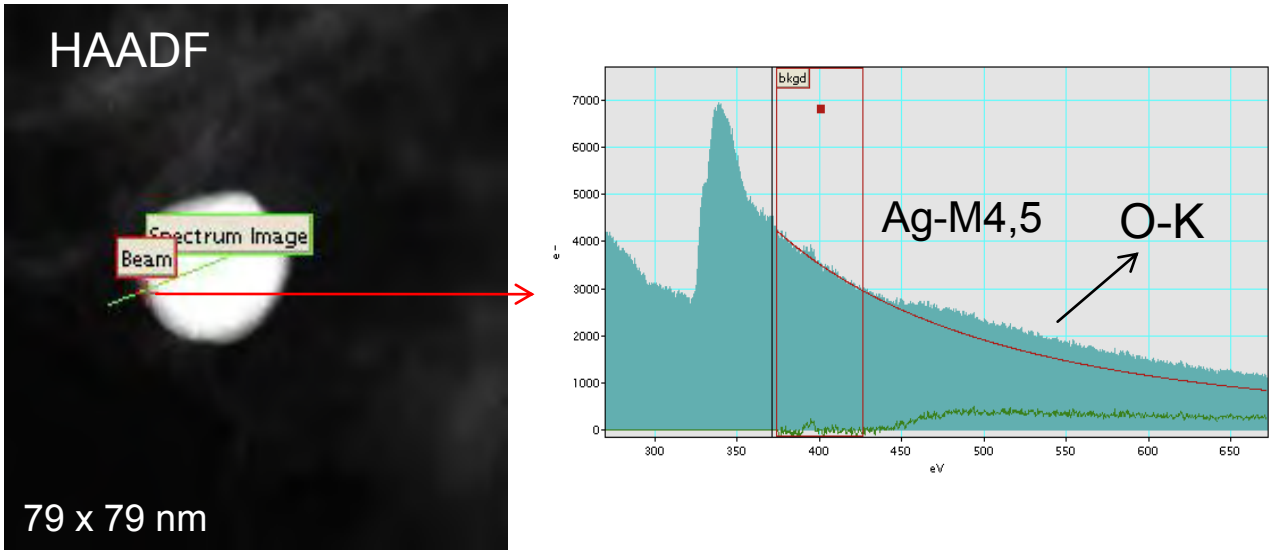

Figure 5.14. EELs line spectra for AgNP1 exposed to sunlight for 25 days. The point spectrum shown was taken from the edge of the particle (marked by a red crossing).

Figure 5.15 shows images for spherical particles imaged by STEM after 24 hours and 25 days exposed to light. The images of the two particles show uniform lattices, and no oxidation observed.

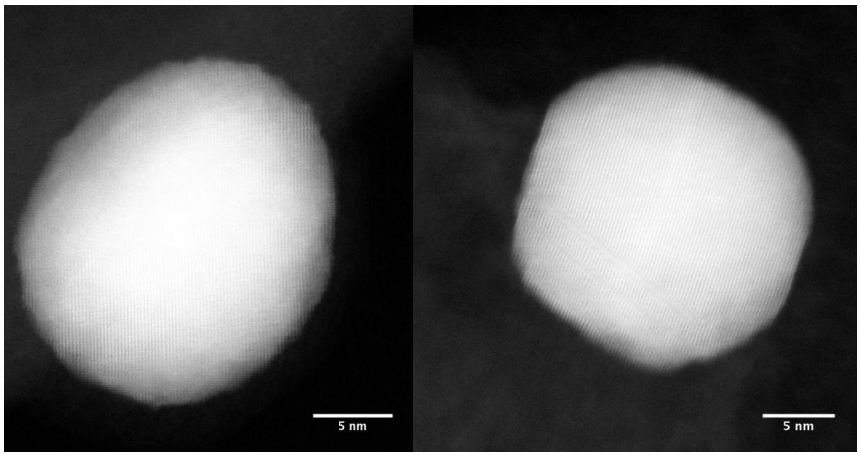

Figure 5.15. HAADF-STEM images of AgNP1 exposed to sunlight for 24 hours (left) and 25 days (right).

5.3.2.2 AgNP1 in UHP water exposed to sunlight (AgNP1- H_2O)

A solution of AgNP1 was diluted 5 times using UHP water and exposed to sunlight. A change in the UV-vis signal and size measured by DLS was observed in a period of 5 weeks. There was no colour change, as seen in the case of the concentrated particles, just a loss of colouration over time as seen in Figure 5.16 and a decrease on the UV-vis signal (70% after 5 weeks, and 53% after 1 month), as seen in Figure 5.17, the peak also red-shifted. Because of the fact that the sample is more dilute (now being 2.2 mg L^{-1}) it is believed that the recrystallization effect is not observed in these particles, but only disolution of the AgNPs may be occuring. It is also important to take into account that UHP water is very reactive and corrosive, thus NPs will be less stable dispersed in it.

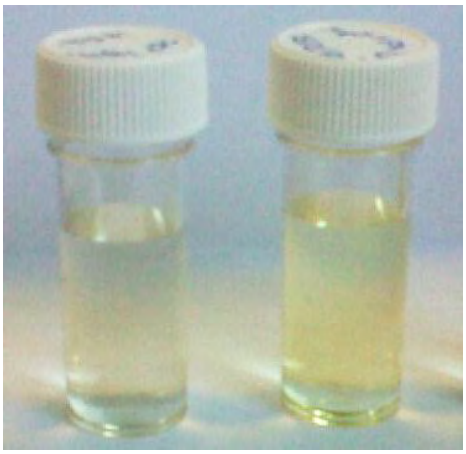

Figure 5.16. AgNP1 in UHP water exposed to sunlight after a month (left) and fresh (right).

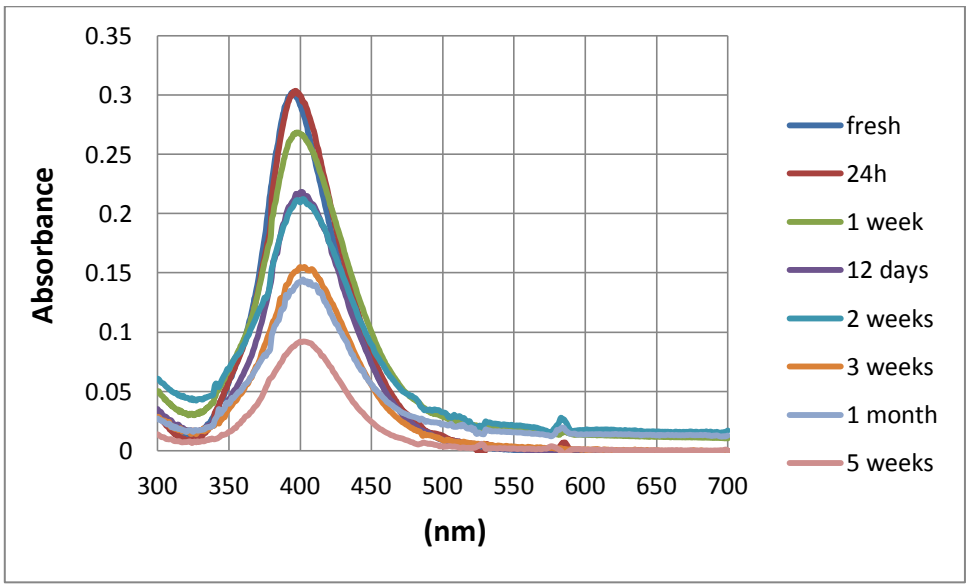

Figure 5.17. UV data for AgNP1 in UHP water exposed to sunlight over time.

It can be seen in Figure 5.18 that the particles don't change in size until after 4 weeks. DLS or UV-vis could not be measured for the particles after six weeks because there was a total loss of colour in the sample (due to aggregation or dissolution). STEM-EELs data was not collected for this set of samples.

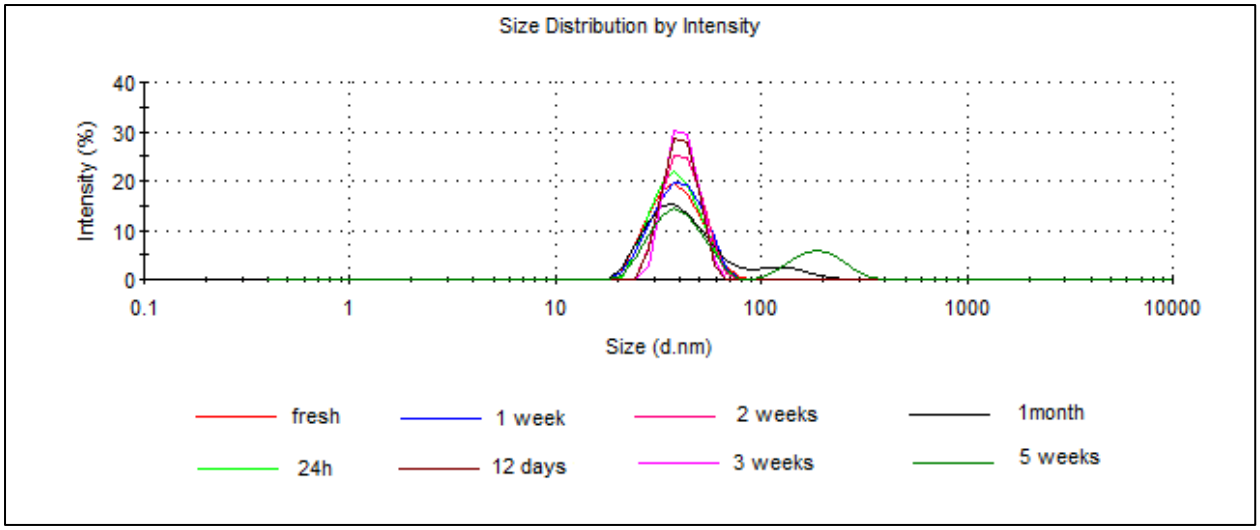

Figure 5.18. DLS data for AgNP1 in UHP water after being exposed to sunlight over time.

5.3.3 Measurements on AgNP1 under environmentally relevant conditions

5.3.3.1 AgNP1 with Fulvic acid (exposed to sunlight and kept in the dark)

AgNP1 with 20 mg L^{-1} FA exposed to sunlight and in the dark showed similar results to each other. It has been found that the particles show no changes (when measured with UV-vis, DLS or STEM-EELs) after being exposed to sunlight or kept in the dark. The UV-vis spectra for the particles in FA after 6 months is shown in Figure 5.19 compared to the particles as prepared. DLS size showed no change over time (data not shown). Natural organic matter (NOM), like FA, has been shown to enhance NP stability both electrostatically and sterically after being adsorbed to the surface (Chen et al. 2006; Chen et al. 2007; Cumberland and Lead 2009).

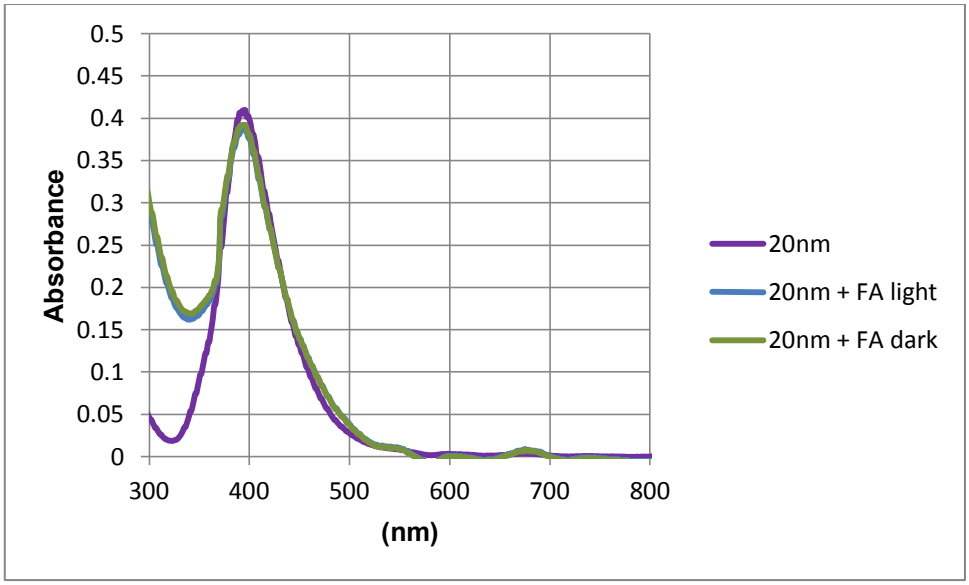

Figure 5.19. UV-vis spectrum for AgNP1 as prepared compared to the spectrum for AgNP1 in 20 mg L-1 FA exposed to sunlight after 6 months and the dark for the same period of time.

The particles, both exposed to light and kept in the dark, were measured with STEM- EELs after 24 hours and after 10 weeks. Figure 5.20 shows examples of the different spectra taken for this set of particles. The particles show a clear silver peak (Figure 5.20, A), and when EELs measurements were performed on the edge of the particle an oxygen signal was observed (Figure 5.20, D). We believe the oxygen signal corresponds to a FA shell, which has shown improved stability of NPs in the past (Baalousha et al. 2008; Diegoli et al. 2008; Cumberland and Lead 2009). A typical FA molecule, shown in Figure 5.20 (C), contains a lot of oxygen that can be detected on the particles by STEM-EELs. Figure 5.21 shows HAADF-STEM images of two particles were a shell can be observed. This oxygen signal does not come from the grid, as it has been demonstrated before (Figure 5.2 and 5.3). Similar results were obtained for the particles in the dark, and after being kept in the light and in the dark for 10 weeks (data not shown). The particles show shell, but the oxygen signal does not correspond to the one from AgO.

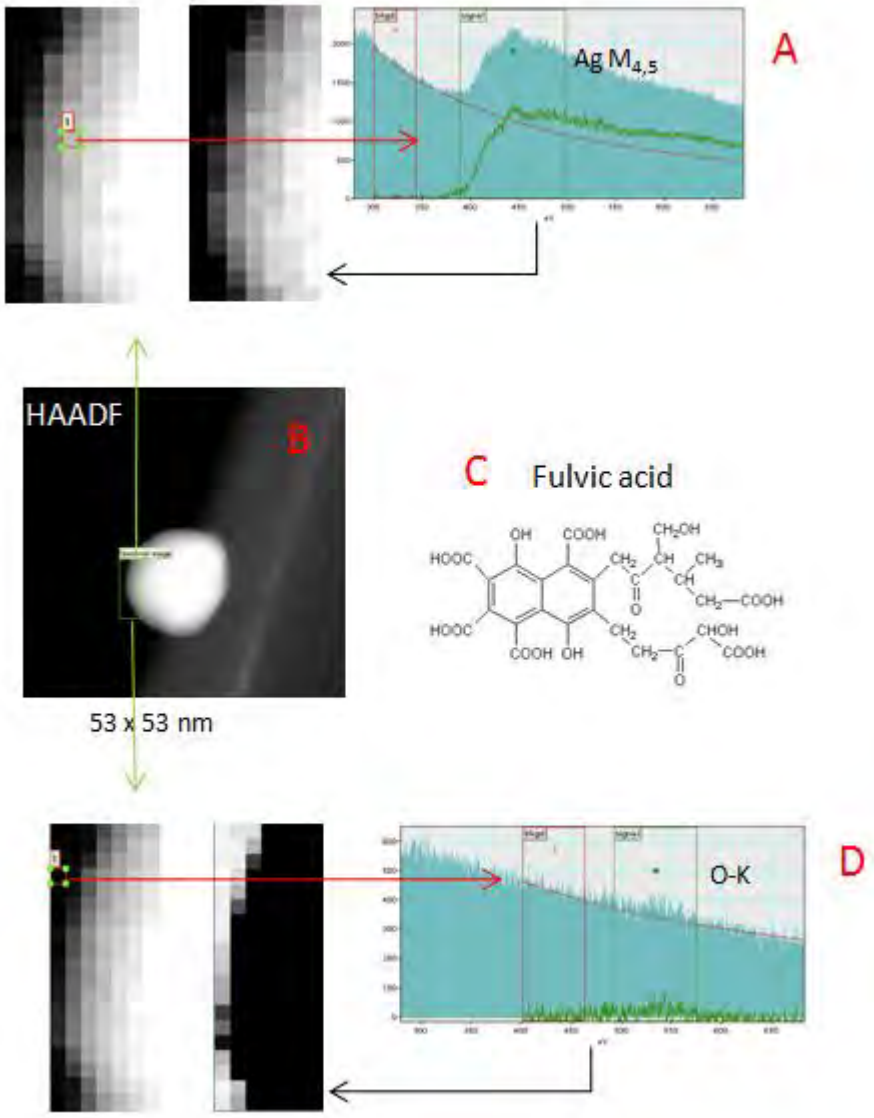

Figure 5.20. EELs area map spectra for AgNP1 with FA exposed to light for 24 hours. A: Map spectrum for Ag, inside the particle; B: HAADF image for the particle; C: typical fulvic acid molecule; and D: Spectrum showing the oxygen signal coming from the outside of the particle. Results show a coherent intensity distribution between the HAADF and the Ag EELs mapping image and the oxygen EELs image.

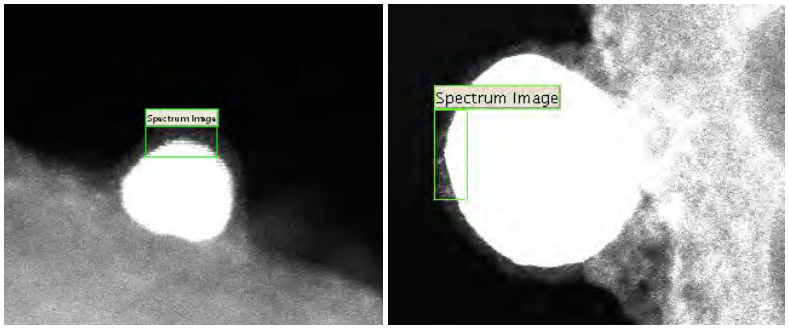

Figure 5.21. HAADF-STEM images of AgNP1 + FA exposed to sunlight for 24 hours (left), and left in the dark (right). Contrast was adjusted to see the shell on the particles.

5.3.3.2 AgNP1 in very soft water, with and without fulvic acid (exposed to sunlight and kept in the dark)

When AgNP1 were in very soft fresh synthetic water (explained in chapter 2, section 2.2.3) a reduction of 36% in the UV signal was observed after 4 weeks (Figure 5.22), the red-shift in maximum wavelength of the peak (from 396 nm to 407 nm after 4 weeks) suggests agglomerates were forming and increasing in size (Chinnapongse et al. 2011). No aggregation was observed when the size was measured with DLS (Figure 5.23). There was no significant loss of the colour of the solution throughout the experiment.

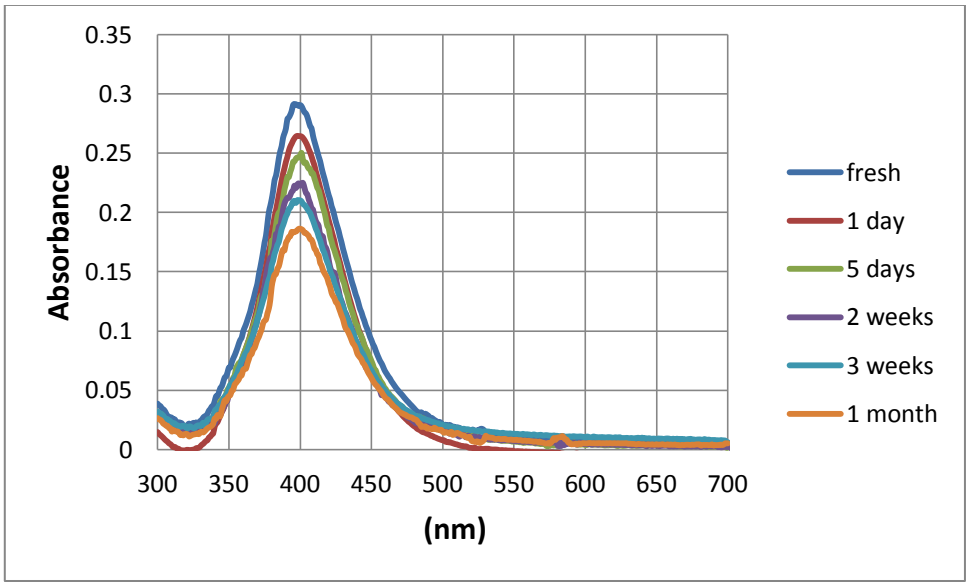

Figure 5.22. UV data for AgNP1 in very soft water exposed to sunlight over time.

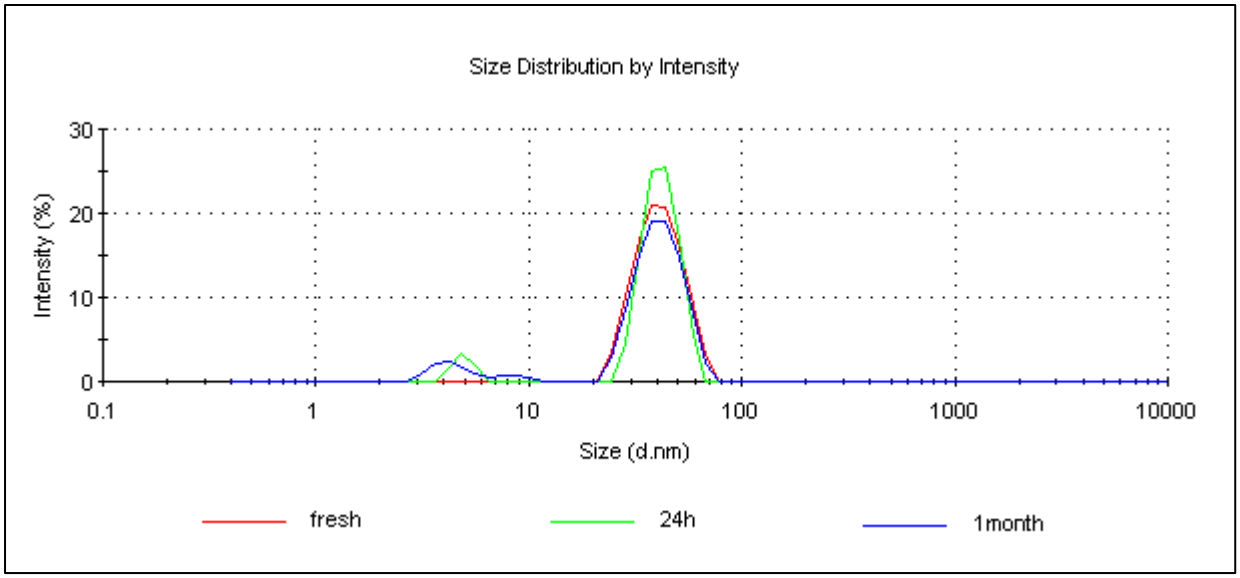

Figure 5.23. DLS data for AgNP1 in very soft water, measured when freshly added, after 24 hours and after 4 weeks exposed to sunlight.

When FA was added to the in very soft fresh synthetic water the particles were more stable. A reduction in the UV signal of 27% was observed after 4 weeks (Figure 5.24), less so than for the particles with no FA, and no shift was observed. Aggregation was also not observed when the size was measured with DLS (Figure 5.25) and there was no significant loss in the colour of the solution throughout the experiment.

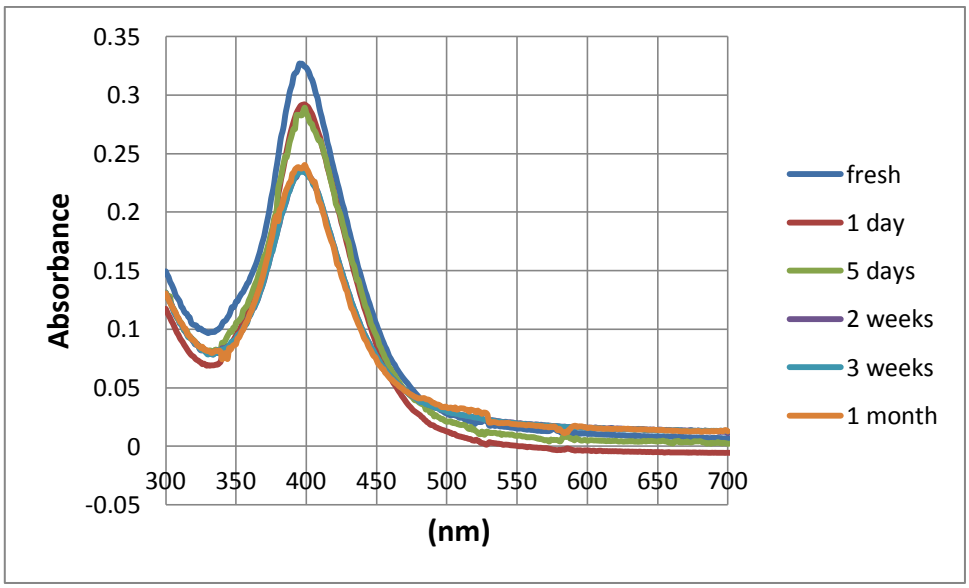

Figure 5.24. UV data for AgNP1 + FA in very soft water exposed to sunlight over time.

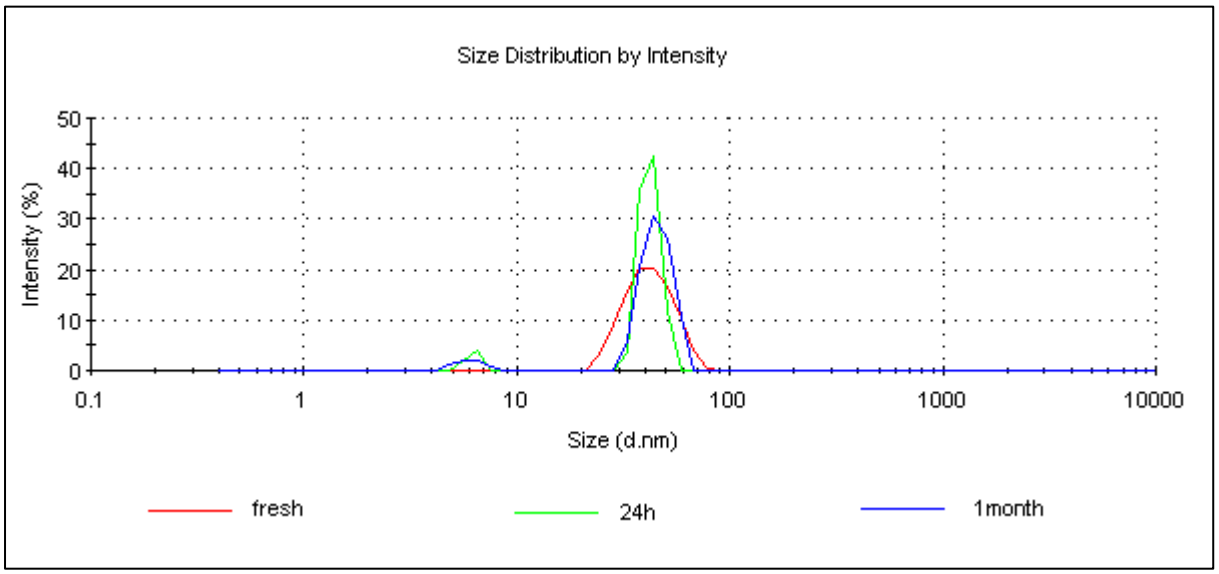

Figure 5.25. DLS data for AgNP1 + FA in very soft water, measured when freshly added, after 24 hours and after 4 weeks exposed to sunlight.

When the particles were kept in the dark (with and without FA) in very soft water the particles were stable even after 8 weeks. There was no loss in the UV-vis spectra and no change in size after 8 weeks (data not shown).

The results for STEM-EELs on the particles in soft water with and without FA exposed to light for 4 weeks are shown in Figures 5.26 to 5.28. No oxygen was found in all cases, even though an FA shell could be seen in the case of the AgNP1 + FA. No changes in size or shape were observed in this period of time.

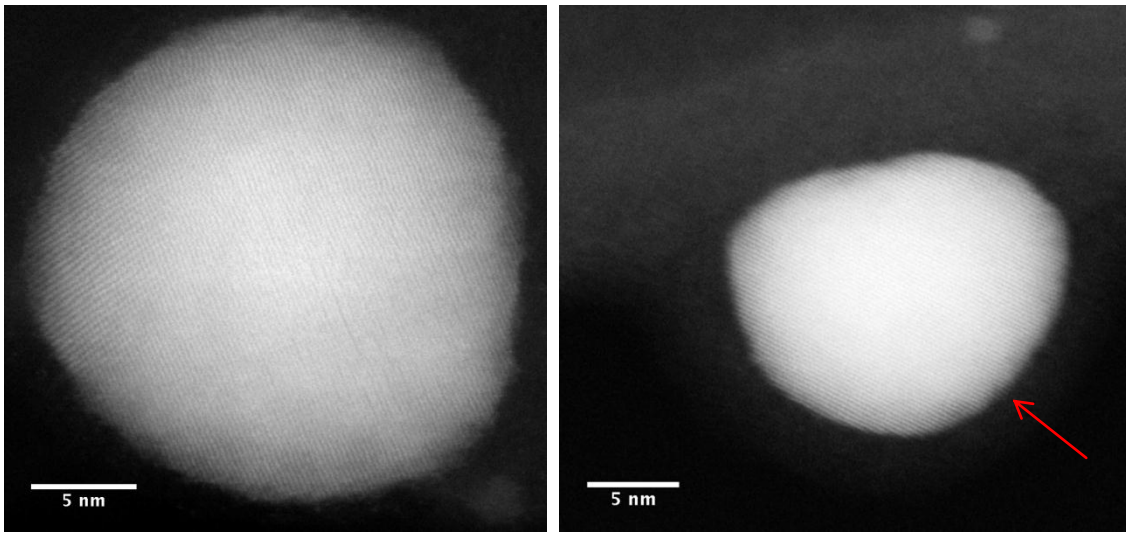

Figure 5.26. HAADF-STEM images of AgNP1 in very soft synthetic freshwater exposed to sunlight for 4 weeks, without FA (left), and with FA (right).No oxygen signal was measured. A FA shell can be seen on the particle on the right (as marked with the red arrow), but the oxygen was not measurable.

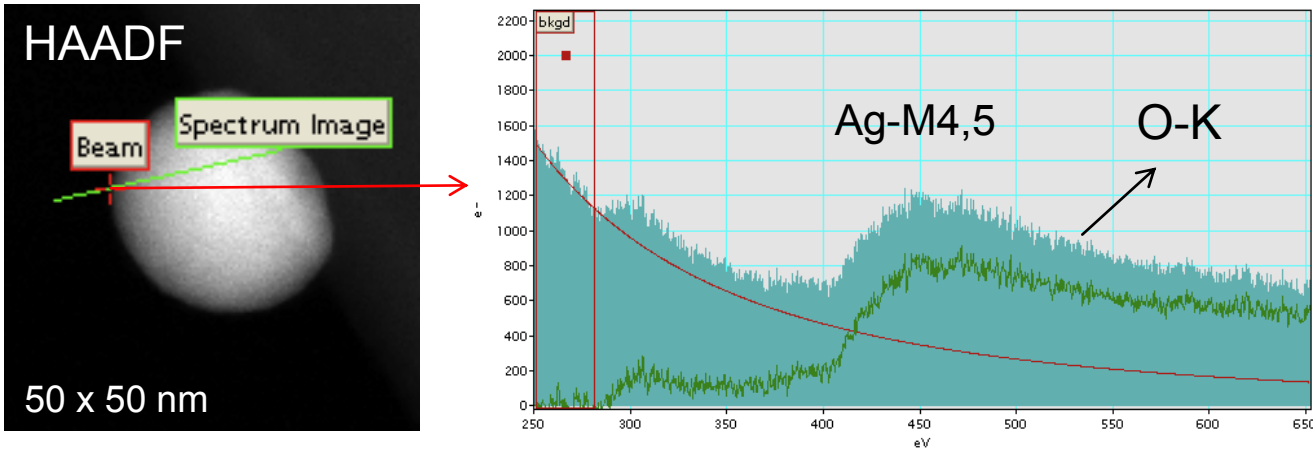

Figure 5.27. EELs line spectra for AgNP1 in very soft synthetic freshwater exposed to sunlight for 4 weeks.The spectrum shown corresponds to the edge of the particle (marked by a red crossing). The systematic investigation performed does not show any oxygen signal.

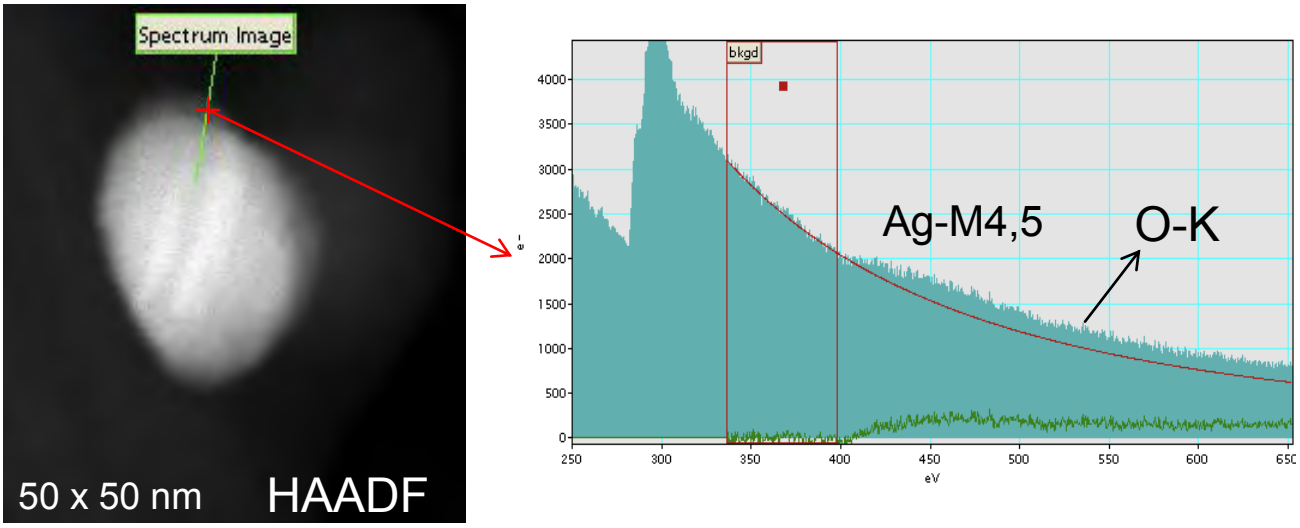

Figure 5.28. EELs line spectra for AgNP1 + FA in very soft synthetic freshwater exposed to sunlight for 4 weeks.The spectrum shown corresponds to the edge of the particle (marked by a red crossing). No obvious oxygen signal could be observed.

5.3.3.3 AgNP1 in soft water, with and without fulvic acid (exposed to light and kept in the dark)

Synthetic fresh soft water has a much higher ionic strength (2.53mM) than the very soft water (0.633mM) previously used (Data shown in chapter 2, section 2.2.3). When the particles were in soft water exposed to light a reduction of 78% in the UV signal was observed after 5 weeks (Figure 5.29). The observed red-shift and broadening of the absorption band relative to the original AgNPs suggest aggregation had occurred, as it has been mention before. After 24h the peak maximum red shifted from 403nm to 407nm, and to 410nm after 4 weeks. Aggregation was observed after 12 days by DLS (Figure 5.30). The colour of the solution changed over time until the solution became colourless (6 weeks).

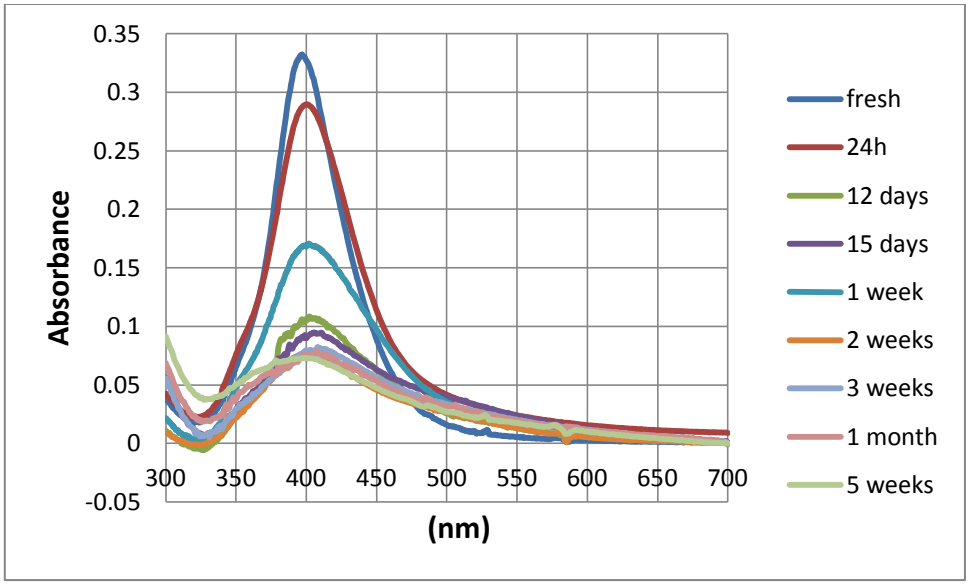

Figure 5.29. UV data for AgNP1 in soft water exposed to sunlight over time.

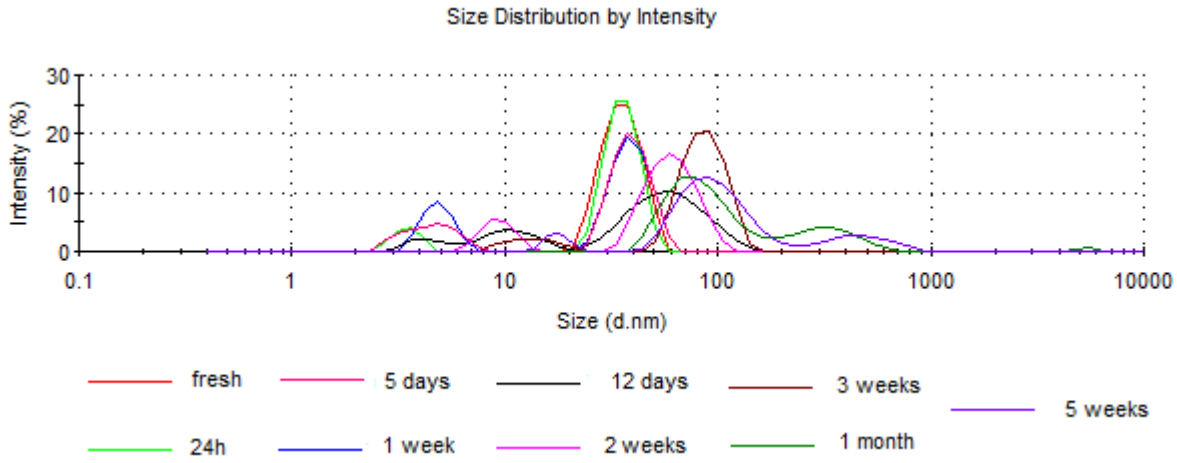

Figure 5.30. DLS data for AgNP1 in soft water exposed to sunlight over time.

When the particles in soft water were kept in the dark a reduction of 78% in the UV signal was observed after 4 weeks (Figure 5.31), which was the same for the particles exposed to sunlight (Figure 5.32). A red shift was also observed, from 402 nm to 414 nm. Aggregation was measured with DLS (Figure 5.33). These results show that ions in solution might play an important role in particle stability. The presence of ions have improved stability in the case of the particles in very soft water, compared to the particles with only UHP water, but when the ionic strength increases it makes the particles unstable, even without the influence of sunlight.

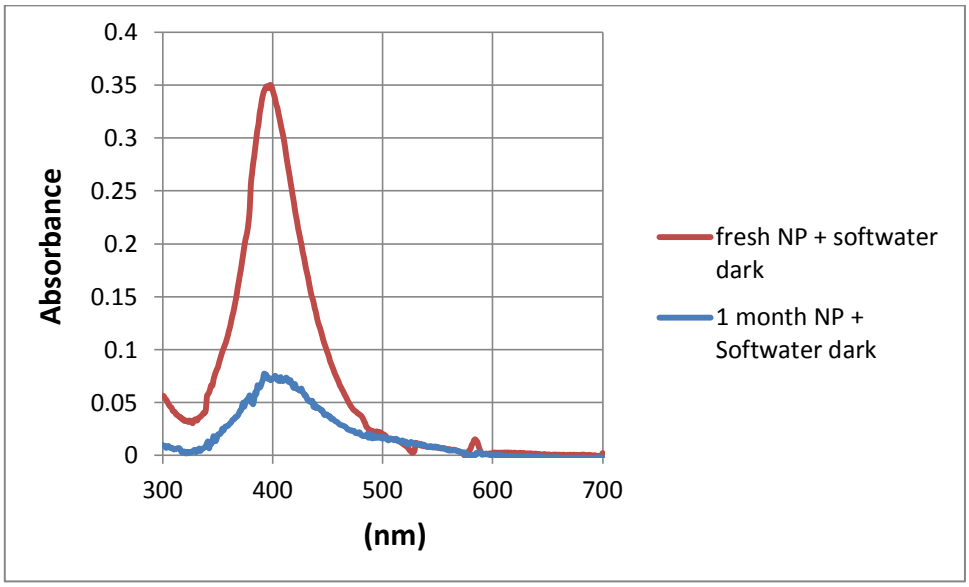

Figure 5.31. UV data for AgNP1 in soft water kept in the dark for 4 weeks.

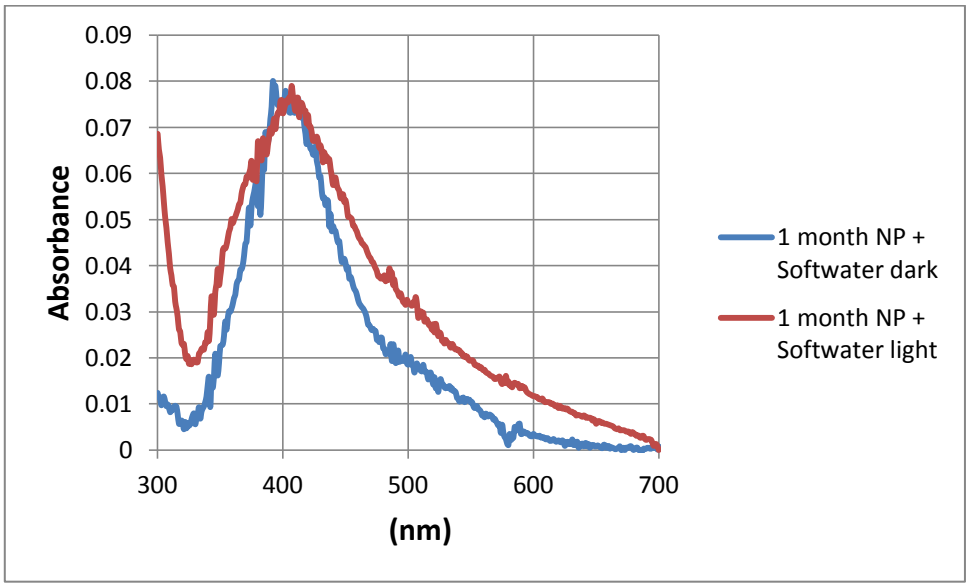

Figure 5.32. UV data for AgNP1 in soft water kept in the dark and exposed to sunlight for 4 weeks.

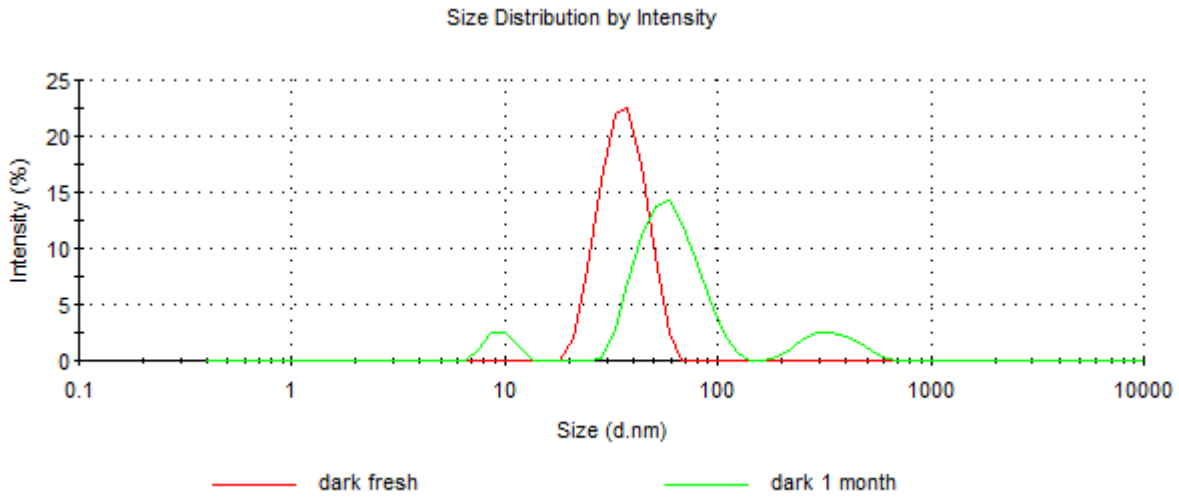

Figure 5.33. DLS data for AgNP1 in soft water kept in the dark for 4 weeks.

When FA was added to the soft synthetic water particle stability was improved, as seen before. A reduction in the UV signal of 51% was observed after 4 weeks (Figure 5.34), much less than for the particles without FA. A red shift was also observed, from 404 nm to 407 nm after 4 weeks. Aggregation was measured with DLS (Figure 5.35) after 12 days. After 6 weeks there was a total loss of colour.

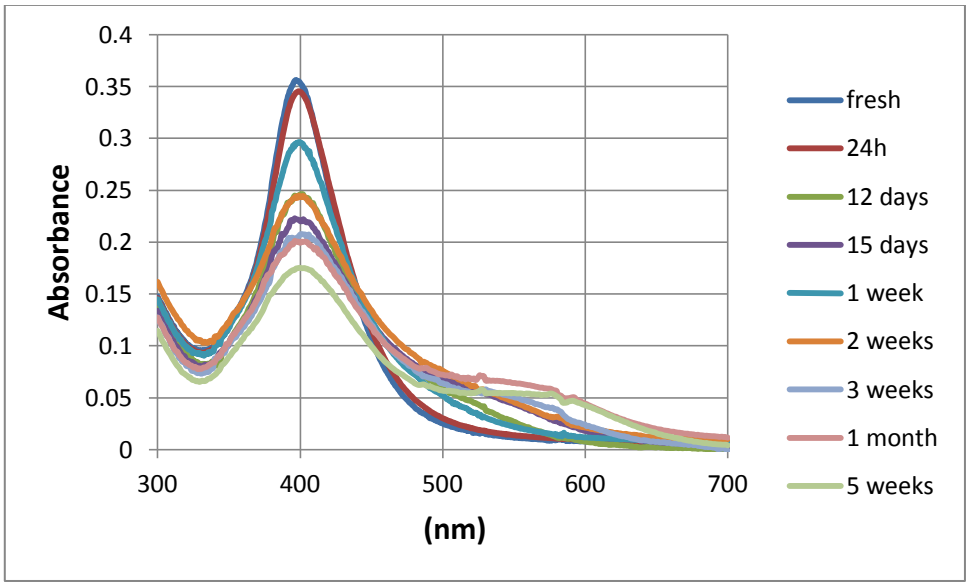

Figure 5.34. UV data for AgNP1 + FA in soft water exposed to sunlight over time.

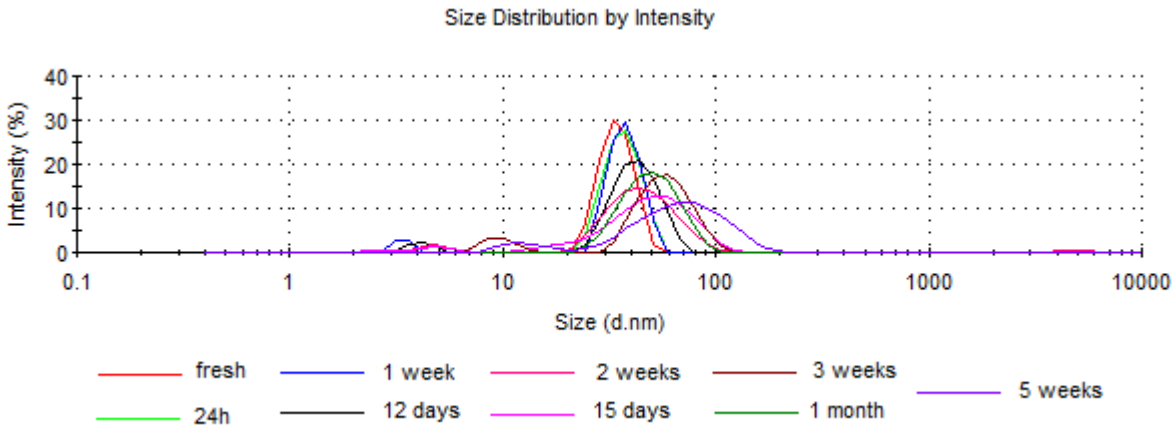

Figure 5.35. DLS data for AgNP1 + FA in soft water exposed to sunlight over time.

When the particles in soft water with FA were kept in the dark for 4 weeks a larger loss in the UV signal was observed than for the particles exposed to sunlight (58%), as seen both in Figure 5.36 and 5.37. It was found that when the particles were exposed to sunlight a second small peak appeared at around 600nm, which it is not found when the particles were kept in the dark (Figure 5.37), which can be due to the fact that sunlight is affecting particle shape. Aggregation was observed by DLS after 4 weeks (Figure 5.38).

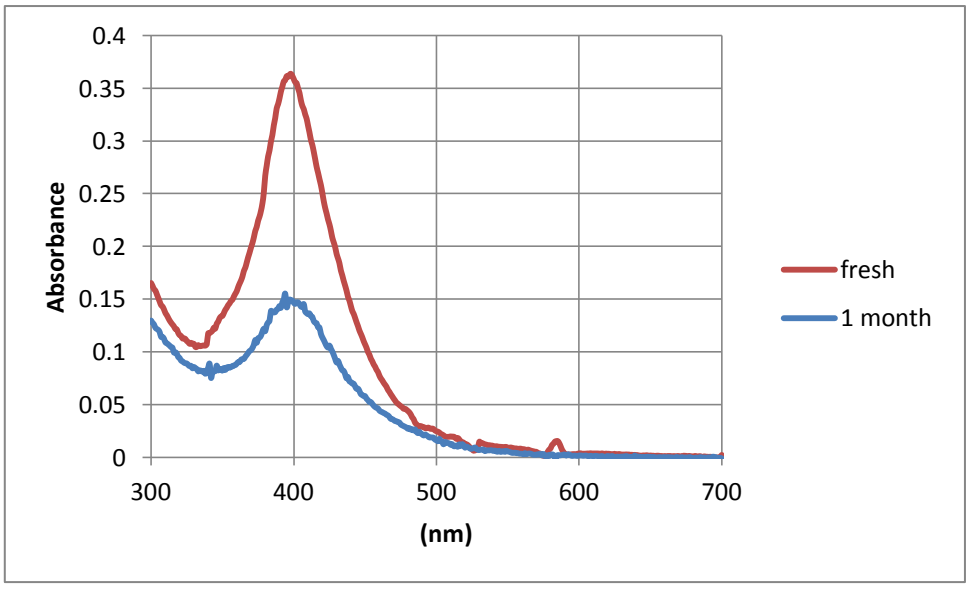

Figure 5.36. UV data for AgNP1 + FA in soft water kept in the dark for 4 weeks.

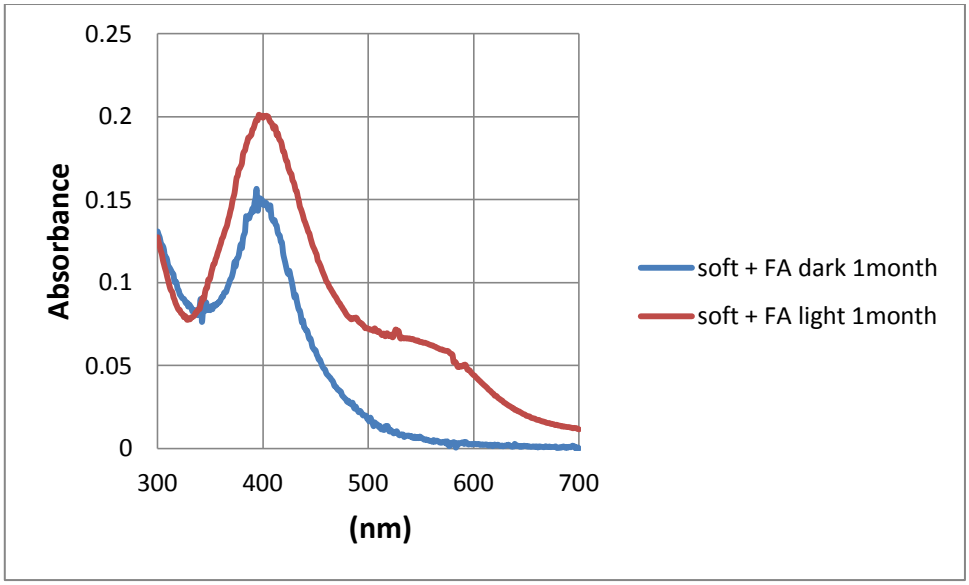

Figure 5.37. UV data for AgNP1 + FA in soft water kept in the dark and exposed to sunlight for 4 weeks.

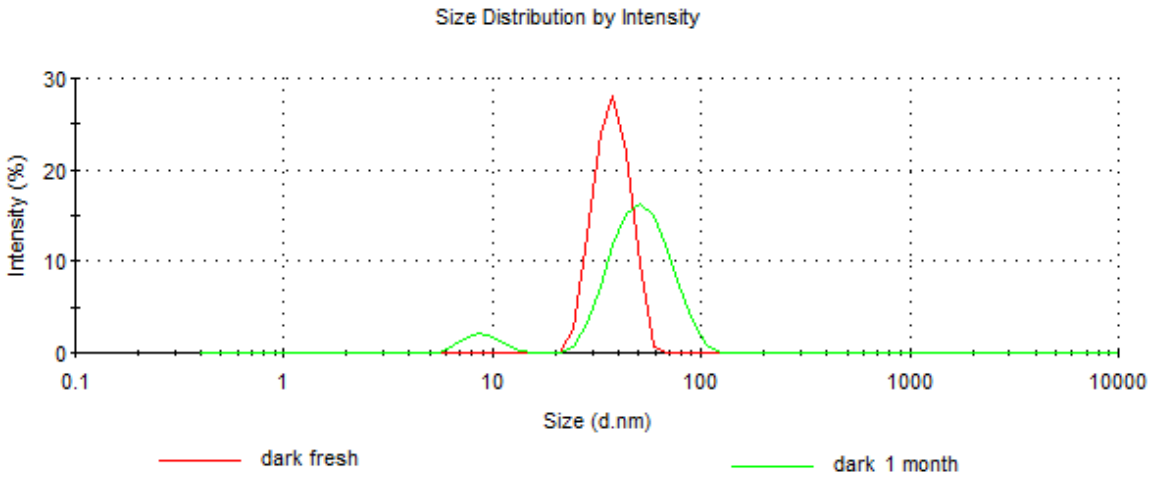

Figure 5.38. DLS data for AgNP1 + FA in soft water kept in the dark for 1 month.

Sunlight seems to have an effect on FA and making it more reactive towards the AgNPs. An increased ionic strenght will influence the fast dilution of the AgNPs, but less so if the FA is tightly bound to the NP core.

Figure 5.39 shows the colour change of the particles in soft water with and without FA exposed to sunlight after 12 days (when a change in size of the particles is measured for the first time) compared to the particles exposed to sunlight for 5 days.

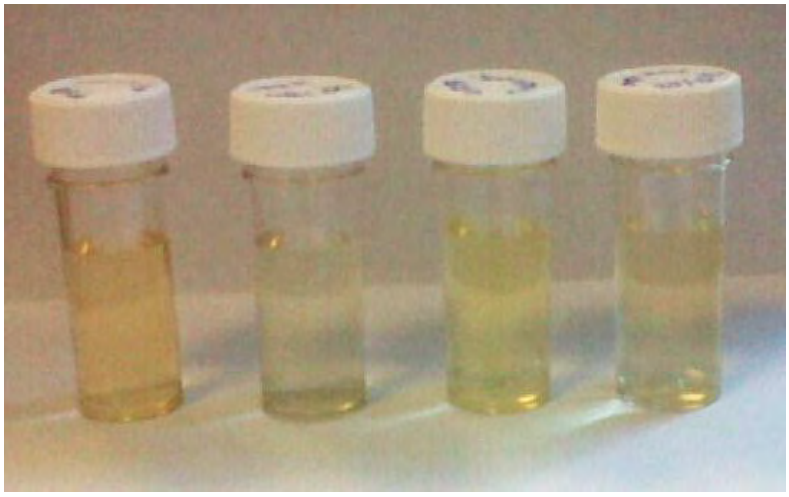

Figure 5.39. AgNP1 in soft water exposed to sunlight. From left ot right: AgNP1 + FA for 12 days, without FA for 12 days, without FA for 5 days and with FA for 5 days.

The results obtained with STEM-EELs for the particles in soft water after 24 hours, with and without FA, are shown in Figures 5.40 to 5.43. No oxidation was observed. In the case of the particles without FA exposed to sunlight for 24 hours formation of very small particles is observed (Figure 5.40) which was not observed in the particles with FA (Figure 5.42). Anionic ligands (such as chloride and sulfate) in the presence of oxygen may cause etching and dissolution of the spherical NPs (Yang et al. 2007; Tejamaya et al. 2012).

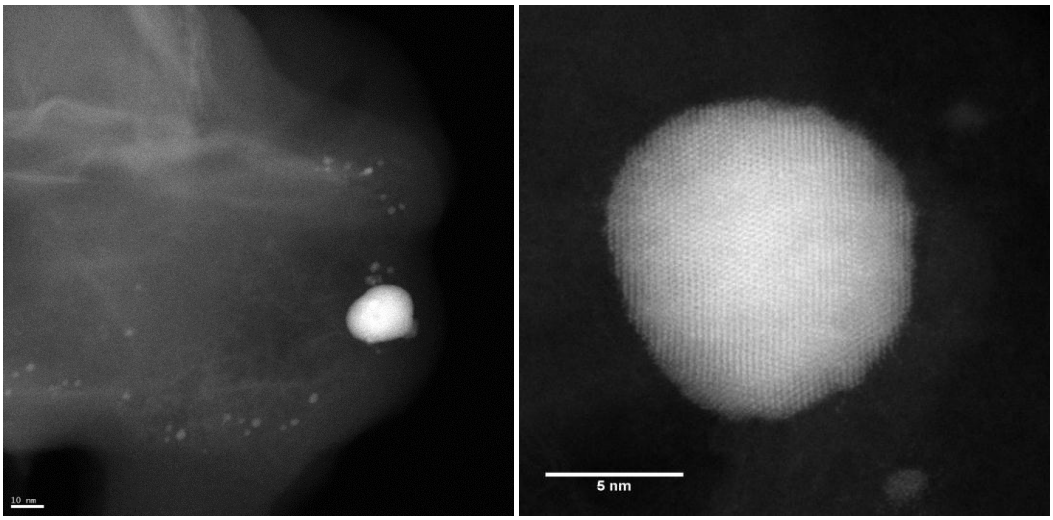

Figure 5.40. HAADF-STEM images of AgNP1 in soft synthetic freshwater exposed to sunlight for 24 hours without FA.

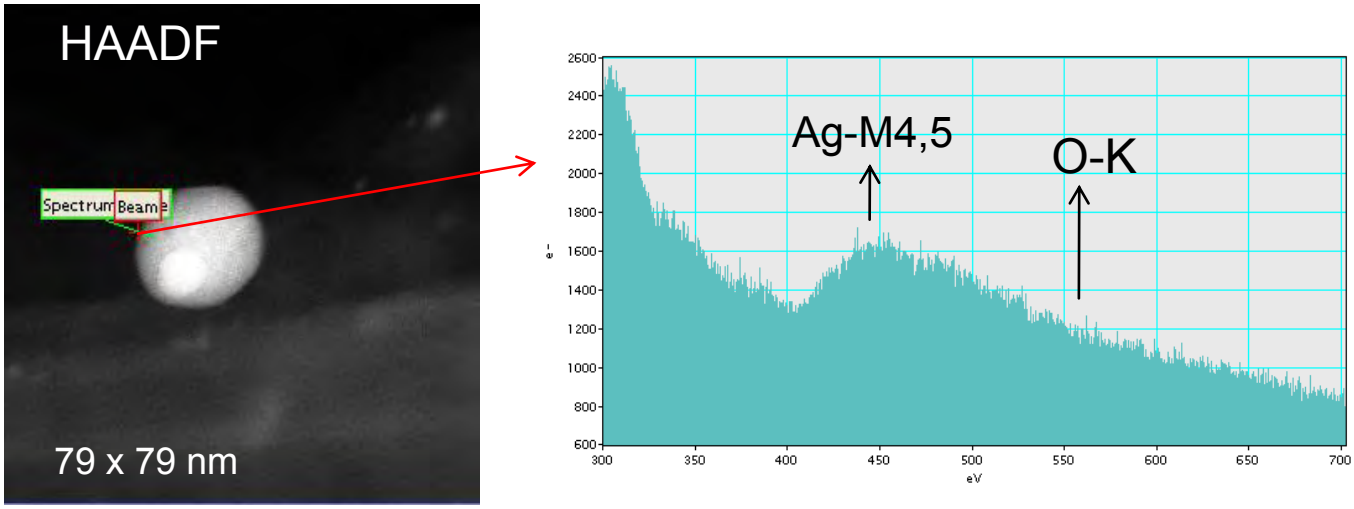

Figure 5.41. EELs line spectra for AgNP1 in soft synthetic freshwater exposed to light for 24 hours. The spectrum shown corresponds to the edge of the particle (marked by a red crossing). No obvious oxygen signal could be observed.

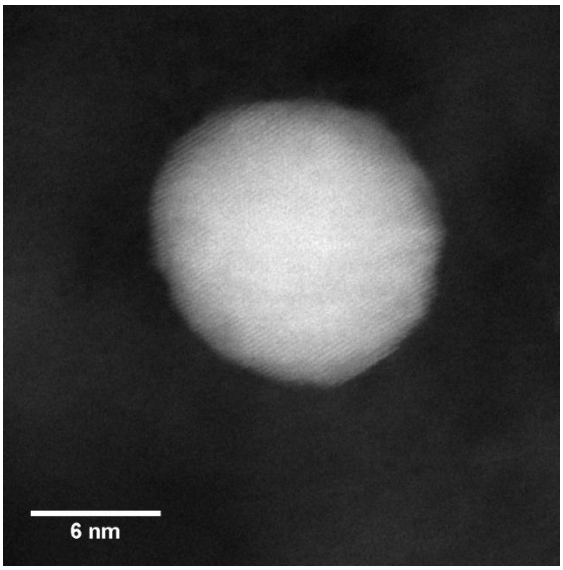

Figure 5.42. HAADF-STEM images of AgNP1 in soft synthetic freshwater exposed to sunlight for 24 hours with FA.

When the particles were exposed to sunlight with FA a shell was observed which can be due to the presence of FA on the particle surface (Figure 5.43), as it has been seen before, and a strong oxygen signal coming from the shell could be measured as well as a silver signal coming from the particle.

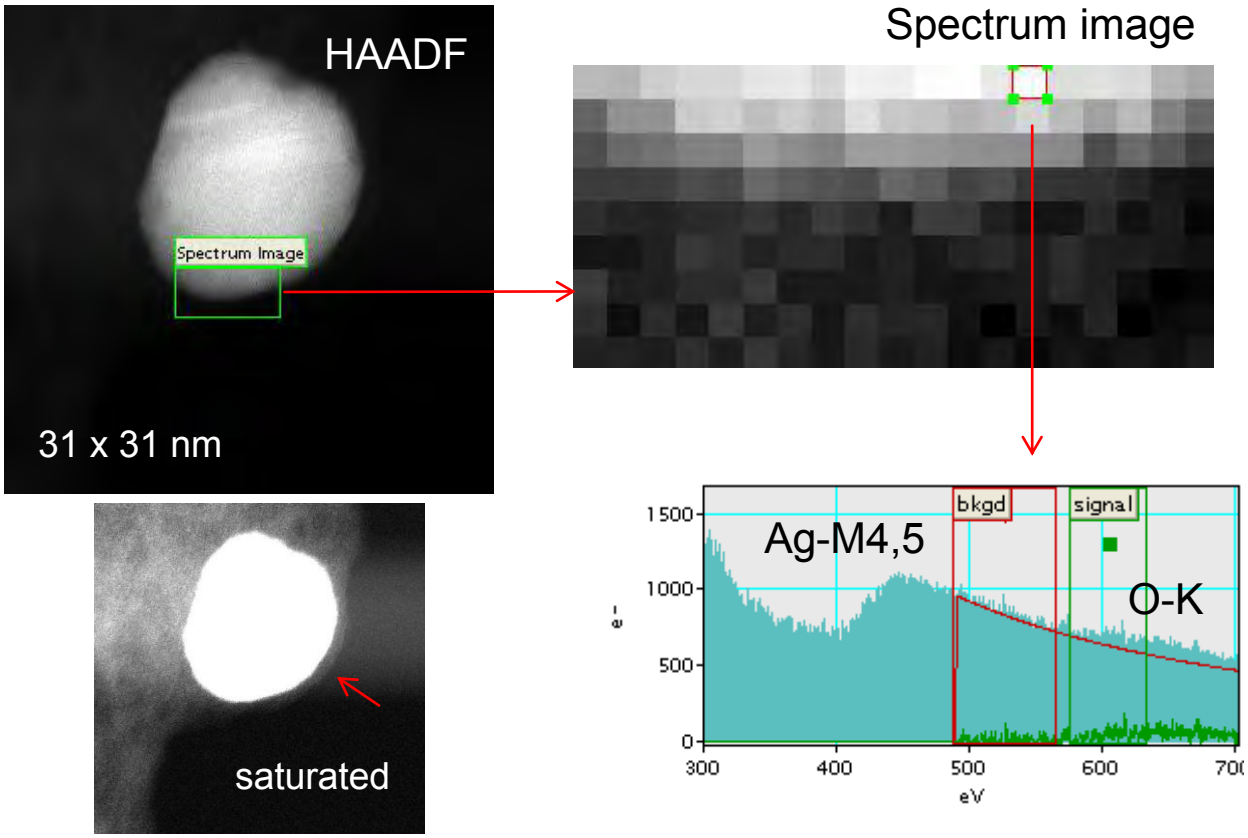

Figure 5.43. EELs area oxygen map spectrum for AgNP1 + FA in soft synthetic freshwater exposed to light for 24 hours. We can clearly see an oxygen peak corresponding to the FA shell and a Ag signal coming from the edge of the particle.

5.3.3.4 AgNP1 in sea water, with a without fulvic acid exposed to light

The particles in seawater (with or without FA) aggregated almost immediately after being added. UV-vis signal was not measurable and a large size was measured by DLS. After 24 hours exposed to sunlight size was not measurable by DLS (probably because of precipitation), as well as a UV-vis signal.

5.4 Discussion

The work performed in this chapter showed different results on the effect of environmentally relevant conditions on AgNPs. The NPs as prepared showed changes in size and shape when exposed to light, but when they were diluted in UHP water this effect was not observed, just a loss of the UV signal over time. When the particles were kept in 20 mg L^{-1} of FA they were stable for 6 months, being exposed to sunlight or kept in the dark, which shows the stabilising effect of FA on AgNPs. It has been observed that when humic substances (HS) are added the stability of NPs is much enhanced over a wide pH range despite the dilution effect (Diegoli et al. 2008), as it can be seen in Figure 5.44. Enhanced aggregation through charge neutralization and bridging mechanisms caused by fibrillar attachment (Buffle et al. 1998; Baalousha et al. 2008) might also occur in natural water.

In the absence of HS as seen in Figure 5.44 (a), when the pH of the dispersion is decreased, protonation of the citrate anions occurs; the NPs will come into close proximity and aggregate. This type of effect can also happen because of high ionic strength solutions. Aggregation will cause the appearance of a longitudinal plasmon band. When the HS are added to the citrate-stabilised NPs dispersion (Figure 5.44 (b)), partial substitution of the small citrate anions by the polyanionic HS is likely to occur. When the pH of the solution is decreased protonation of the HS will occur and the NPs will lose their electrostatic stabilisation. Aggregation is retarded by the steric stabilisation offered by the HS and the longitudinal plasmon band is absent from the UV–visible spectra of aggregating dispersion containing HS (Diegoli et al. 2008).

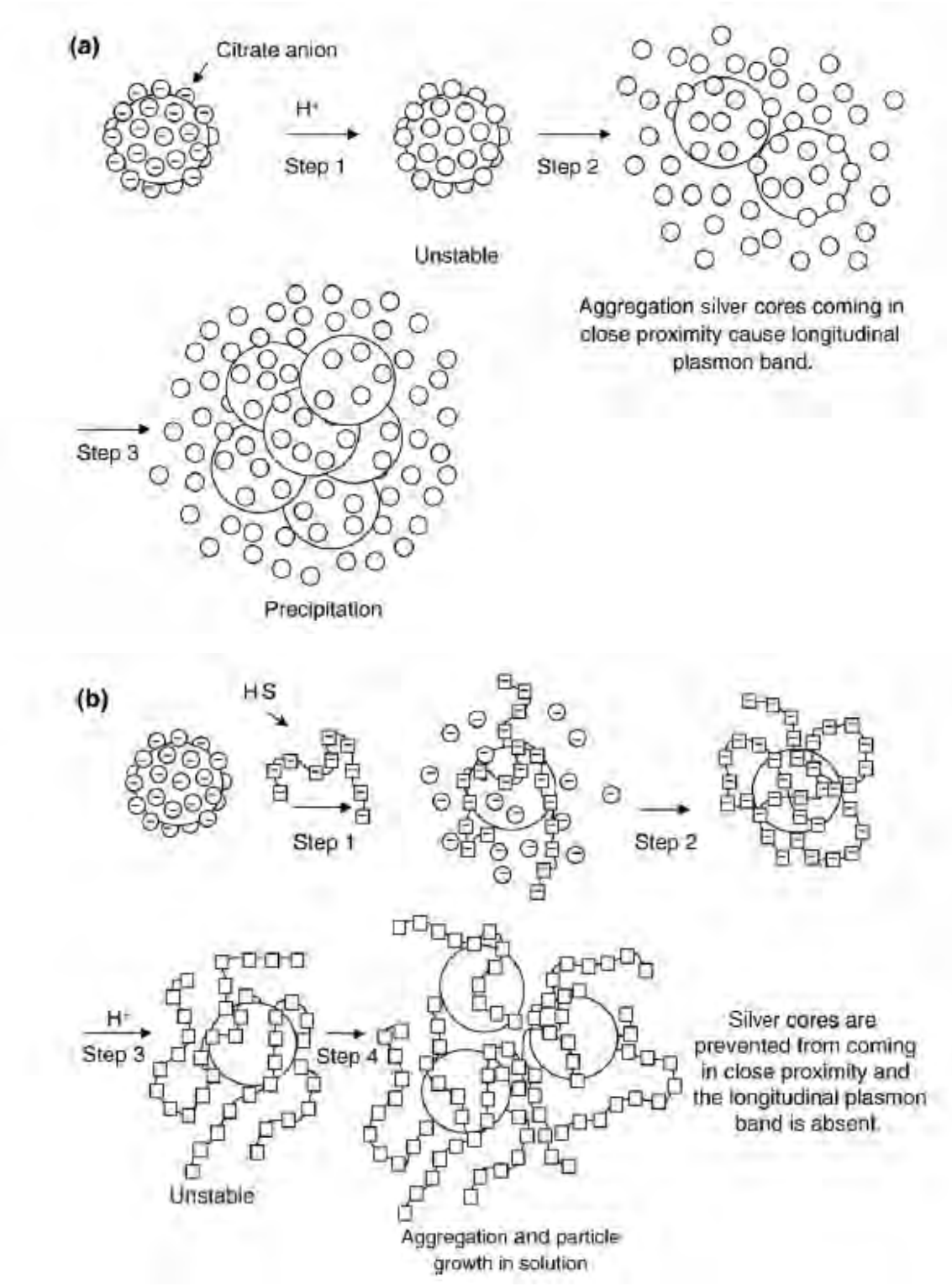

Figure 5.44. Schematic representation of the aggregation process for (a) citrate stabilised NPs and (b) NP + HS dispersions (Diegoli et al. 2008).

When adding AgNPs to very soft water we found an improved stability of the AgNPs compared to the particles in just UHP water, the particles were even more stable when FA was added and were completely stable (for 4 weeks) when kept in the dark. We believe that the ions present in solution

helped particle stability in this case, which could be due to chloride surface film or to increased charge stability. Increasing the ionic strength of the solution, using soft water, yielded the opposite effect, resulting in a total loss of the UV signal after 6 weeks, by adding FA stability was improved, but when the solution with FA was kept in the dark the particles were less stable than the ones exposed to sunlight. We believe that the polyanionic FA will increase its interaction with the AgNPs when the solution is exposed to sunlight, when they are kept in the dark the AgNPs will not interact as strongly with the FA and will be more unstable.

Humic substances have the ability to change their size in suspension, i.e. aggregate and disaggregate; this will depend on ionic strength and pH (Diegoli et al. 2008). The total charge on the humic acid is neutralized or screened at high ionic strength or low pH values. The potential total charge on the humic acid surface can be increased when the concentration of protons and cations in solution is reduced. This change will influence the HS conformation and aggregation status (Baalousha et al. 2006). In hard waters and estuarine systems, waters with high ionic strength, aggregation will be rapid and extensive, increased stability will be likely in other soft freshwaters with lower ionic strength (Diegoli et al. 2008). Addition of low and environmentally relevant concentrations of HS has stabilised citrate capped AgNPs and reduced losses by aggregation/sedimentation and permit FlFFF analysis (Cumberland and Lead 2009).

In most cases where the AgNPs were exposed to sunlight a red-shift was observed. It is believed that the red-shift and broadening of the absorption band relative to metallic AgNPs of the same size suggest the presence of an oxidized layer on the particle surface (Chen et al. 2006; Li et al. 2011). It is believed, as shown in Figure 5.45, that oxidation of the surface of a particle will be the first step in particle dissolution when they are in an oxygenated solution and in the presence of electrolytes (Li et al. 2011). We believe that after this process occurs, the water present removes this shell quickly, so when the particles were measured by STEM-EELs no oxidation was observed. Dissolution seems to be the primary effect of sunlight on AgNPs in freshwater, which needs to be studied next. We are able to measure the presence of AgO, as it was observed on the AgNPs left on a TEM grid for 4 weeks, using STEM-EELs, this was the product of an oxygenated and ion free media, without any water present, so there is no effect of water as transporting agent of oxidised surface layer.

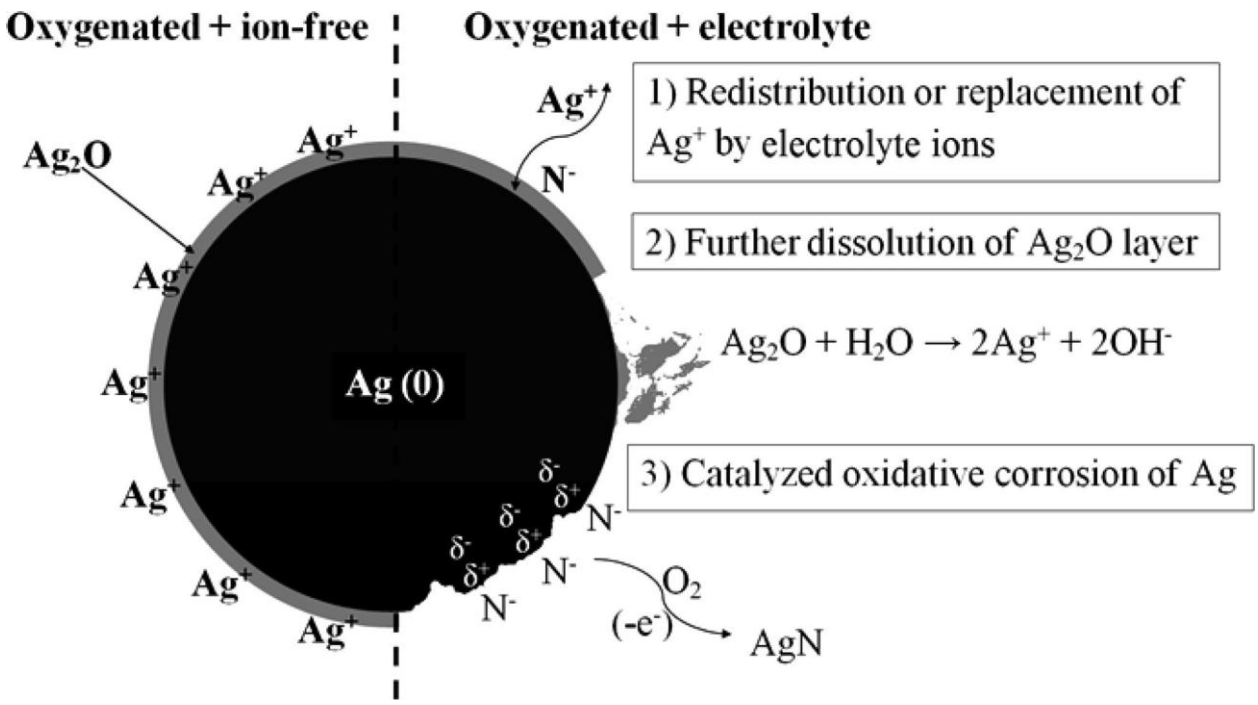

Figure 5.45. Schematic illustration of surface oxidation and dissolution of the oxide layer coated AgNPs (Li et al. 2011).

Charge stabilised AgNPs (citrate) have shown to be less stable than steric stabilised NPs, having PVP or PEG as capping agent (Tejamaya et al. 2012). The anions present in solution also seem to have an effect on AgNPs stability, especially influencing shape changes and dissolution. In a paper published by our group, when chloride was replaced in Daphnia media, to remove chloride-silver interactions, with either nitrate or sulphate it resulted in increased shape and dissolution changes (Tejamaya et al. 2012). TEM images showed substantial shape changes for citrate capped AgNPs, with triangular and hexagonal shapes along with aggregates and very small particles in both nitrate and sulphate media, as seen in Figure 5.46. PEG and PVP capped AgNPs underwent little observable changes, but some plate-like particles were also observed in sulphate media. PVP capped AgNPs were the most stable of the three in every type of Daphnia media.

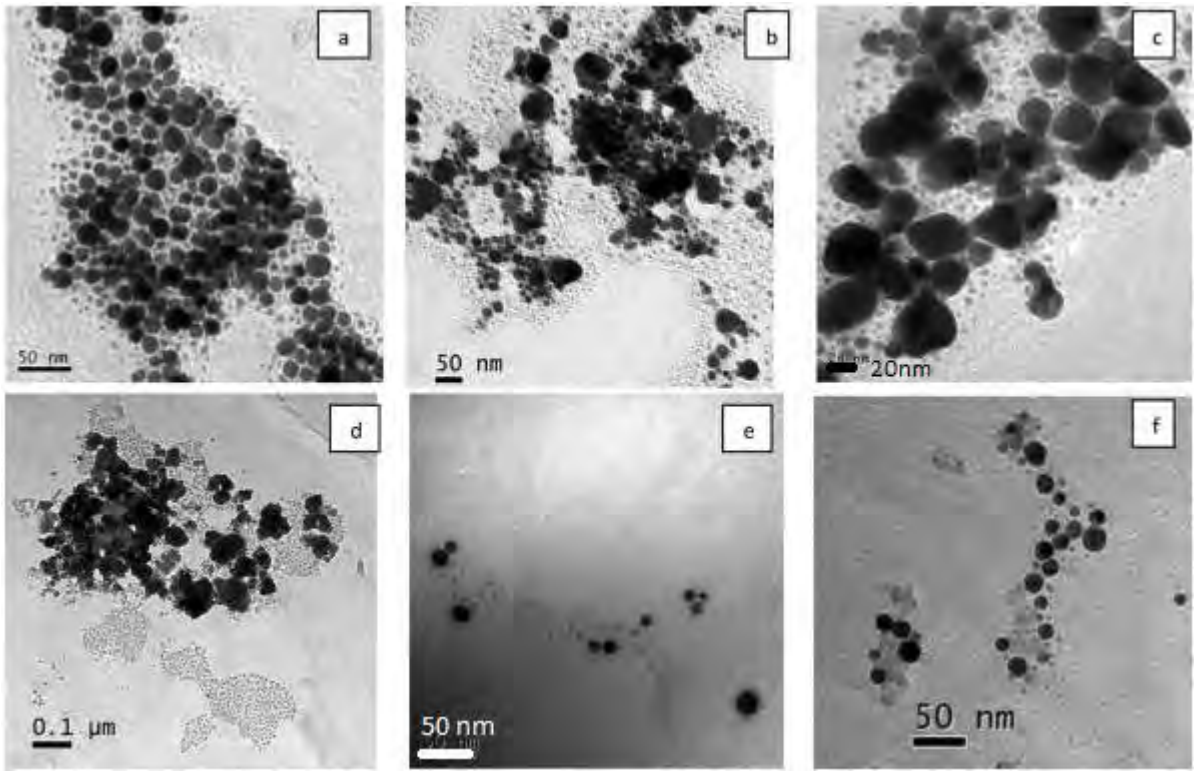

Figure 5.46. TEM images of AgNPs after 21 days incubation in different media: a) citrate capped AgNPs in media10 (chloride media), b) citrate capped AgNPs in nitrate media dilute 10 times, c) citrate capped AgNPs in sulphate media diluted 10 times, d) citrate capped AgNPs in nitrate media, e) PVP capped AgNPs in chloride media (media1), and f) PEG capped AgNPs in chloride media (media1) (Tejamaya et al. 2012).

Another study performed in our group showed that gold NPs sterically stabilised with PVP were stable in very different conditions, such as ionic strength, pH and the presence of NOM. The structure, shape, surface charge and chemistry of the gold NPs remained unchanged (Hitchman 2011). The behaviour of these gold NPs was then studied when influenced by flow between the stream flow and stream bed, and then within the bed itself. The fate and behaviour of these NPs was analysed with a recirculating flume. The gold NPs seem to freely exchange between the bed and the free flow and appear to follow flow paths within the bed after entry before being recirculated. This reduced deposition within the bed could result in long range transportation of the NPs under similar conditions. It also seems from this study that NPs move in clumps of higher concentration areas throughout both the stream free flow and the gravel river bed.

Stable NPs in freshwater will have the ability to enter marine systems. To date there are not many studies investigating the changes in NPs using conditions similar to those in marine environment. Seawater compared to freshwater has a much higher ionic strength, and thus will cause aggregation, as it has been seen. It has been observed that small increases in salinity above that of freshwater (~2.5%) can cause aggregation and precipitation processes, which will reduce NP concentration dramatically (Stolpe et al. 2007). The toxicity and behaviour of NPs in seawater will be very different from that in freshwater. NPs will have a tendency to aggregate, agglomerate, and settle, which suggests that benthic estuarine organisms (Figure 5.47) may be at higher risk.

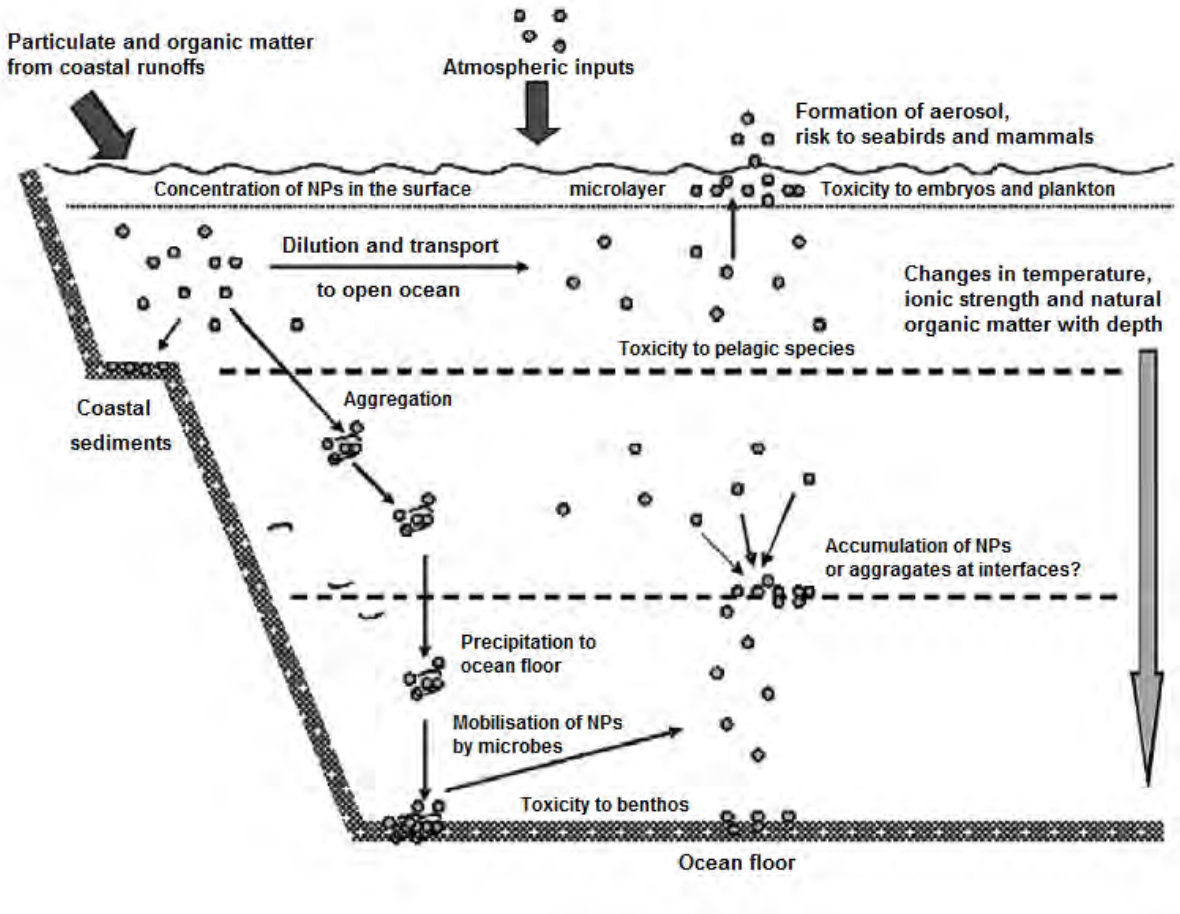

Figure 5.47. Schematic diagram outlining the possible fate of NPs in the marine environment and the organisms at risk of exposure. From (Klaine et al. 2008).

The marine environment has high ionic strength, is more alkaline, and has a wide variety of NOM and different colloids (Klaine et al. 2008). Different sources of NPs can act as contaminants of the marine environment, as seen in Figure 5.47. Due to the fact that NPs have shown stability on soft freshwater,

they could end up in the sea as a final sink. Aggregates of NPs may sink very slowly, as in freshwater systems, to the ocean floor, but it is not clear if NPs will have the tendency to accumulate between cold and warm currents. Pelagic species that feed at these zones may be at risk, while deposition in the sediment causes a risk of exposure to benthic species.

Particles can also accumulate in the surface microlayers of the ocean's surface, where they can get trapped by viscous and surface tension properties (Simkiss 1990; Wurl et al. 2004). In this surface microlayer NPs could be exposed and be a risk to marine birds and mammals as well as other organisms that live in it.

5.5 Conclusions

After investigating the stability of particles under different conditions by using different methods, especially with the use of STEM-EELs, it has been concluded:

- AgNP1 and AgNP3 as prepared are spherical FCC particles with some defects, as measured with STEM-EELs. In some cases we could observe quasi-crystal structures, which may consist of multiple twin sections.
- When particles are left on a TEM grid for 4 weeks oxidation was observed using STEM-EELs.
- AgNP1 as prepared exposed to sunlight changed in shape. Small particles may be fragmented from larger spherical particles due to a partial dissolution and recrystallization, and this effect is observed for the concentrated particles and not for the particles in UHP water.
- AgNP1 in UHP water exposed to light possibly dissolved completely after 6 weeks. UHP water is very corrosive and reaction, which will decrease stability of the NPs suspended in it.
- AgNP1 with 20mg L^{-1} FA were very stable and remained unchanged in the dark or exposed to light even after 6 months.
- AgNP1 in synthetic very soft freshwater exposed to sunlight were more stable than the particles in UHP water, the presence of ions in solution might have helped stability. When FA was added the particles became more stable. When the solutions were kept in the dark we

found no change after 4 weeks, which shows that light had an important role on the stability of these particles.

- AgNP1 in synthetic soft freshwater exposed to light and in the dark were very unstable. Anionic ligands in the presence of oxygen may cause etching and dissolution of the spherical NPs, which is an effect that was reduced by the presence of FA. When the particles were kept in the dark, the particles without FA behaved the same, but when FA was added a higher loss of the UV signal was observed, and no second peak was found, as seen in the case of the NPs exposed to sunlight with FA.
- AgNP1 in synthetic seawater aggregated or precipitated inmediately after added to solution.

The results shown in this chapter indicate that some AgNPs will be stable long enough in freshwater to successfully enter estuarine or marine systems. It has been found that salinity, the presence of sunlight and NOM play an important role on particle stability. NPs reaching land could possibly migrate into surface and groundwaters, contaminate soil, and interact with biota. NPs in direct discharges, solid wastes, wastewater effluents, or accidental spillages can be transported to aquatic systems by wind or rainwater runoff (Klaine et al. 2008). Residence time in surface waters and their transport in ground water ((Kretzschmar et al. 2005) will be influenced by the aggregation status of colloids (Lead et al. 2006).

6

Conclusions and Future work

6.1 Conclusions

The worked performed in this dissertation aimed to investigate different areas that are important for environmental effects on nanoparticle stability. The research is outlined below.

6.1.1 Aim 1: Synthesis and characterisation of AgNPs using citrate and PEG.

We obtained AgNPs of three different sizes and two different capping agents, citrate and PEG, that are easy to synthesize and have been fully characterised by a multi-method approach. The NPs have remained stable for a long period of time.

The concentration of the reducing agent and when it is added showed to be the determining factor in the synthesis of citrate NPs. From these citrate capped particles, we managed to obtain PEG NPs.

These particles were used for stability work in our lab, which has yielded two publications so far, and have been sent to other groups to be used in toxicological work.

6.1.2 <u>Aim 2:</u> Assess the stability of AgNPs in *Daphnia magna* toxicity media, investigating the effect of media dilution on particle stability and *D. magna* viability.

The effect of adding the particles to Daphnia exposure media at standard OECD conditions was aggregation of the particles, however, relatively small reductions of ionic strength allowed the larger particles in particular to remain stable for the period of time needed for Daphnia exposures, and the smallest particles, AgNP3, showed reduced aggregation. Under acute conditions, Daphnia immobilisation was evident in UHP water only, in contrast to all tested media dilutions in which neonates showed only slight signs of distress. However, the more sensitive chronic reproductive toxicity test revealed absolute immobilisation in UHP water and a highly significant reduction in fecundity in media20. LC50 could be calculated for AgNP3 in media10 (5.36 $\mu g\ L^{-1}$) but not for media1. It has also been observed that AgNP3 and $AgNO_3$ appear to exhibit reduced toxicity in response to increasing media salinity. Our results therefore suggest that media10, i.e., a 10-fold dilution of standard OECD media, provides optimal conditions for these NPs, minimising aggregation while avoiding *D. magna* immobilisation and maintaining normal reproductive output.

6.1.3 <u>Aim 3:</u> Test the effects on AgNPs stability of different environmentally relevant conditions, such as synthetic waters, exposure to light and presence of organic matter (fulvic acid).

We found that particles AgNP1 and AgNP3 as prepared are spherical FCC particles with some defects, as measured with STEM-EELs. In some cases we could observe quasi-crystal structures, which may consist of multiple twin sections. We found oxidized particles using STEM-EELs when they were left on a TEM grid for 1 month. When AgNP1 as prepared were exposed to light we found a change in shape and size. Small particles may dissolve and nucleate from larger spherical particles due to a partial dissolution and recrystallization, and this effect is observed for the concentrated particles and not for the particles in UHP water. When the particles in UHP water were exposed to

light we think that they dissolved completely after 6 weeks, as seen in the results obtained by DLS and UV-vis. When adding FA (20mg L^{-1}) particle stability was improved substantially, even when exposed to light or kept in the dark, and remained stable after 6 months. When particles in synthetic very soft freshwater were exposed to light they were more stable than the particles in UHP water, leading us to believe that the presence of ions in solution might have helped stability. When FA was added the particles became more stable. When particles in very soft water were kept in the dark we found no change after 1 month, which leads us to believe that sunlight had an important role on these particles. When ionic strength was increased by using synthetic soft freshwater particles were very unstable, in the sunlight or in the dark. When the particles were kept in the dark, the particles without FA behaved the same, but when FA was added we found a higher loss of the UV signal, and no second peak, as seen in particles exposed to sunlight with FA, which leads us to believe that sunlight my promote the binding of FA to the AgNPs, thus improving stability. Anionic ligands in the presence of oxygen may cause etching and dissolution of the spherical NPs, which is an effect that was reduced by the presence of FA. In synthetic seawater particles aggregated or precipitated inmediately after added to solution.

Ionic strength, sunlight and the presence of FA play an important role on particle stability. We believe that ions in solution can help particle stability until a certain degree, but when this strength is increased it can reduce stability. Sunlight seems to promote dissolution of the particles. The addition of FA clearly improves stability.

6.2 Future work

Further work can be performed on both citrate and PEG stabilized particles. The difference in the behavior of the different sizes of citrate and PEG stabilized AgNPs in environmentally relevant conditions can be assessed. The influence of light and different environmentally relevant conditions was not performed on the PEG particles and should be studied.

The synthesis of AgNPs with other capping agents, such as PVP or FA, starting from citrate capped nanoparticles should be investigated. Having a series of particles with the same core size and a different capping agent could be used as reference materials.

Stability studies in Daphnia media were performed to use the citrate capped nanoparticles for *D. magna* toxicity studies, which will be performed by other groups. The stability of PEG particles was assessed by Mila Tejamaya and published. PEG and citrate particles were sent out to other groups for toxicity studies in the project Bioavailability and Effects in the Environment of manufactured nanomaterials (nanoBEE).

Dissolution studies should be performed, especially for the particles in soft water exposed to light and in the dark (with and without FA), to confirm the results obtained using DLS and UV-vis.

References

Ahern, A. M. and R. L. Garrell (1987). "Insitu photoreduced silver-nitrate as a substrate for surface-enhanced raman-spectroscopy." Analytical Chemistry **59**(23): 2813-2816.

Allen, H. J., C. A. Impellitteri, D. A. Macke, J. L. Heckman, H. C. Poynton, J. M. Lazorchak, S. Govindaswamy, D. L. Roose and M. N. Nadagouda (2010). "Effects from filtration, capping agents, and presence/absence of food on the toxicity of silver nanoparticles to Daphnia magna " Environmental Toxicology and Chemistry **29**(12): 2742-2750.

Alvarez, P. J. J., V. Colvin, J. Lead and V. Stone (2009). "Research Priorities to Advance Eco-Responsible Nanotechnology." Acs Nano **3**(7): 1616-1619.

AmericanElements. (2011). "AmericanElements. Silver Nanoparticles. ." from http://www.americanelements.com/agnp.html.

An, S. Y., M. P. N. Bui, Y. J. Nam, K. N. Han, C. A. Li, J. Choo, E. K. Lee, S. Katoh, Y. Kumada and G. H. Seong (2009). "Preparation of monodisperse and size-controlled poly(ethylene glycol) hydrogel nanoparticles using liposome templates." Journal of Colloid and Interface Science **331**(1): 98-103.

Asharani, P. V., Y. L. Wu, Z. Y. Gong and S. Valiyaveettil (2008). "Toxicity of silver nanoparticles in zebrafish models." Nanotechnology **19**(25).

Auffan, M., J. Rose, J. Y. Bottero, G. V. Lowry, J. P. Jolivet and M. R. Wiesner (2009). "Towards a definition of inorganic nanoparticles from an environmental, health and safety perspective." Nature Nanotechnology **4**(10): 634-641.

Baalousha, M., Y. Ju-Nam, P. A. Cole, B. Gaiser, T. F. Fernandes, J. A. Hriljac, M. A. Jepson, V. Stone, C. R. Tyler and J. R. Lead (2012a). "Characterization of cerium oxide nanoparticles—Part 1: Size measurements." Environmental Toxicology and Chemistry **31**(5): 983-993.

Baalousha, M., Y. Ju-Nam, P. A. Cole, J. A. Hriljac, I. P. Jones, C. R. Tyler, V. Stone, T. F. Fernandes, M. A. Jepson and J. R. Lead (2012b). "Characterization of cerium oxide nanoparticles—Part 2: Nonsize measurements." Environmental Toxicology and Chemistry **31**(5): 994-1003.

Baalousha, M., F. V. D. Kammer, M. Motelica-Heino, M. Baborowski, C. Hofmeister and P. Le Coustumer (2006). "Size-based speciation of natural colloidal particles by flow field flow

fractionation, inductively coupled plasma-mass spectroscopy, and transmission electron microscopy/X-ray energy dispersive spectroscopy: Colloids-trace element interaction." Environmental Science & Technology **40**(7): 2156-2162.

Baalousha, M. and J. R. Lead (2007). "Characterization of natural aquatic colloids (< 5 nm) by flow-field flow fractionation and atomic force microscopy." Environmental Science & Technology **41**(4): 1111-1117.

Baalousha, M. and J. R. Lead (2012). "Rationalizing Nanomaterial Sizes Measured by Atomic Force Microscopy, Flow Field-Flow Fractionation, and Dynamic Light Scattering: Sample Preparation, Polydispersity, and Particle Structure." Environmental Science & Technology.

Baalousha, M., A. Manciulea, S. Cumberland, K. Kendall and J. R. Lead (2008). "Aggregation and surface properties of iron oxide nanoparticles: Influence of pH and natural organic matter." Environmental Toxicology and Chemistry **27**(9): 1875-1882.

Baalousha, M., M. Motelica-Heino and P. Le Coustumer (2006). "Conformation and size of humic substances: Effects of major cation concentration and type, pH, salinity, and residence time." Colloids and Surfaces a-Physicochemical and Engineering Aspects **272**(1-2): 48-55.

Baalousha, M., B. Stolpe and J. R. Lead (2011). "Flow field-flow fractionation for the analysis and characterization of natural colloids and manufactured nanoparticles in environmental systems: A critical review." Journal of Chromatography A **1218**(27): 4078-4103.

Balnois, E. and K. J. Wilkinson (2002). "Sample preparation techniques for the observation of environmental biopolymers by atomic force microscopy." Colloids and Surfaces A: Physicochemical and Engineering Aspects **207**(1–3): 229-242.

Bar-Ilan, O., R. M. Albrecht, V. E. Fako and D. Y. Furgeson (2009). "Toxicity Assessments of Multisized Gold and Silver Nanoparticles in Zebrafish Embryos." Small **5**(16): 1897-1910.

Belloni, J., M. Mostafavi, H. Remita, J. L. Marignier and M. O. Delcourt (1998). "Radiation-induced synthesis of mono- and multi-metallic clusters and nanocolloids." New Journal of Chemistry **22**(11): 1239-1255.

Benn, T. M. and P. Westerhoff (2008). "Nanoparticle silver released into water from commercially available sock fabrics." Environmental Science & Technology **42**(11): 4133-4139.

Berry, C. and D. Skillman (1963). "Ideal size-distribution and growth rate in microcrystalline precipitates." J Physic. Chem. **67**(9): 1827–1830.

Bhattacharjee, S., J. Y. Chen and M. Elimelech (2000). "DLVO interaction energy between spheroidal particles and a flat surface." Colloids and Surfaces A: Physicochemical and Engineering Aspects **165**(1–3): 143-156.

Bilberg, K., M. B. Hovgaard, F. Besenbacher and E. Baatrup (2012). "In Vivo Toxicity of Silver Nanoparticles and Silver Ions in Zebrafish (Danio rerio)." Journal of Toxicology **2012**.

Bilberg, K., H. Malte, T. Wang and E. Baatrup (2010). "Silver nanoparticles and silver nitrate cause respiratory stress in Eurasian perch (Perca fluviatilis)." Aquatic Toxicology **96**(2): 159-165.

Binnig, G., C. F. Quate and C. Gerber (1986). "Atomic Force Microscope." Physical Review Letters **56**(9): 930-933.

Blaser, S. A., M. Scheringer, M. MacLeod and K. Hungerbuhler (2008). "Estimation of cumulative aquatic exposure and risk due to silver: Contribution of nano-functionalized plastics and textiles." Science of the Total Environment **390**(2-3): 396-409.

Bogner, A., P. H. Jouneau, G. Thollet, D. Basset and C. Gauthier (2007). "A history of scanning electron microscopy developments: Towards “wet-STEM” imaging." Micron **38**(4): 390-401.

Boistelle, R. and J. P. Astier (1988). "Crystallization mechanisms in solution." Journal of Crystal Growth **90**(1–3): 14-30.

Borm, P., F. C. Klaessig, T. D. Landry, B. Moudgil, J. Pauluhn, K. Thomas, R. Trottier and S. Wood (2006). "Research Strategies for Safety Evaluation of Nanomaterials, Part V: Role of Dissolution in Biological Fate and Effects of Nanoscale Particles." Toxicological Sciences **90**(1): 23-32.

Borm, P. J. A., D. Robbins, S. Haubold, T. Kuhlbusch, H. Fissan, K. Donaldson, R. Schins, V. Stone, W. Kreyling, J. Lademann, J. Krutmann, D. Warheit and E. Oberdorster (2006). "The potential risks of nanomaterials: a review carried out for ECETOC." Particle and Fibre Toxicology **3**: 11.

Bozzola, J. J. (2001). Electron Microscopy. eLS, John Wiley & Sons, Ltd.

BSI (2007). Terminology for nanomaterials.

Buffle, J., K. J. Wilkinson, S. Stoll, M. Filella and J. Zhang (1998). "A Generalized Description of Aquatic Colloidal Interactions: The Three-colloidal Component Approach." Environmental Science & Technology **32**(19): 2887-2899.

Chae, Y. J., C. H. Pham, J. Lee, E. Bae, J. Yi and M. B. Gu (2009). "Evaluation of the toxic impact of silver nanoparticles on Japanese medaka (Oryzias latipes)." Aquatic Toxicology **94**(4): 320-327.

Chen, K. L. and M. Elimelech (2006). "Aggregation and deposition kinetics of fullerene (C-60) nanoparticles." Langmuir **22**(26): 10994-11001.

Chen, K. L. and M. Elimelech (2007). "Influence of humic acid on the aggregation kinetics of fullerene (C-60) nanoparticles in monovalent and divalent electrolyte solutions." Journal of Colloid and Interface Science **309**(1): 126-134.

Chen, M., L. Y. Wang, J. T. Han, J. Y. Zhang, Z. Y. Li and D. J. Qian (2006). "Preparation and study of polyacryamide-stabilized silver nanoparticles through a one-pot process." Journal of Physical Chemistry B **110**(23): 11224-11231.

Cheng, Y., L. Yin, S. Lin, M. Wiesner, E. Bernhardt and J. Liu (2011). "Toxicity Reduction of Polymer-Stabilized Silver Nanoparticles by Sunlight." The Journal of Physical Chemistry C **115**(11): 4425-4432.

Chinnapongse, S. L., R. I. MacCuspie and V. A. Hackley (2011). "Persistence of singly dispersed silver nanoparticles in natural freshwaters, synthetic seawater, and simulated estuarine waters." Science of the Total Environment **409**(12): 2443-2450.

Choi, H. S., W. Liu, P. Misra, E. Tanaka, J. P. Zimmer, B. Itty Ipe, M. G. Bawendi and J. V. Frangioni (2007). "Renal clearance of quantum dots." Nature biotechnology **25**: 1165-1170.

Choi, O., T. E. Cleuenger, B. L. Deng, R. Y. Surampalli, L. Ross and Z. Q. Hu (2009). "Role of sulfide and ligand strength in controlling nanosilver toxicity." Water Research **43**(7): 1879-1886.

Choi, O. and Z. Q. Hu (2008). "Size dependent and reactive oxygen species related nanosilver toxicity to nitrifying bacteria." Environmental Science & Technology **42**(12): 4583-4588.

Chopra, I. (2007). "The increasing use of silver-based products as antimicrobial agents: a useful development or a cause for concern? - Author's response." Journal of Antimicrobial Chemotherapy **60**(2): 447-448.

Christian, P. and M. Bromfield (2010). "Preparation of small silver, gold and copper nanoparticles which disperse in both polar and non-polar solvents." Journal of Materials Chemistry **20**(6): 1135-1139.

Christian, P., F. Von der Kammer, M. Baalousha and T. Hofmann (2008). "Nanoparticles: structure, properties, preparation and behaviour in environmental media." Ecotoxicology **17**(5): 326-343.

Colvin, V. L. (2003). "The potential environmental impact of engineered nanomaterials." Nat Biotech **21**(10): 1166-1170.

Cosgrove, T. (2005). Colloid science: Principles, methods and applications. , Blackwell Publishing: UK.

Cumberland, S. A. and J. R. Lead (2009). "Particle size distributions of silver nanoparticles at environmentally relevant conditions." Journal of Chromatography A **1216**(52): 9099-9105.

Dair, B. J., D. M. Saylor, T. E. Cargal, G. R. French, K. M. Kennedy, R. S. Casas, J. E. Guyer, J. A. Warren, C. S. Kim and S. K. Pollack (2010). "The Effect of Substrate Material on Silver Nanoparticle Antimicrobial Efficacy." Journal of Nanoscience and Nanotechnology **10**(12): 8456-8462.

Darlington, T. K., A. M. Neigh, M. T. Spencer, O. T. Nguyen and S. J. Oldenburg (2009). "NANOPARTICLE CHARACTERISTICS AFFECTING ENVIRONMENTAL FATE AND TRANSPORT THROUGH SOIL." Environmental Toxicology and Chemistry **28**(6): 1191-1199.

Delay, M., T. Dolt, A. Woellhaf, R. Sembritzki and F. H. Frimmel (2011). "Interactions and stability of silver nanoparticles in the aqueous phase: Influence of natural organic matter (NOM) and ionic strength." Journal of Chromatography A **1218**(27): 4206-4212.

Demling, R. H. and L. DeSanti (2001). "Effects of silver on wound management. ." Wounds **13**(Suppl A): 4-15.

Dhawan, A. and V. Sharma (2010). "Toxicity assessment of nanomaterials: methods and challenges." Analytical and Bioanalytical Chemistry **398**(2): 589-605.

Diegoli, S., A. L. Manciulea, S. Begum, I. P. Jones, J. R. Lead and J. A. Preece (2008). "Interaction between manufactured gold nanoparticles and naturally occurring organic macromolecules." Science of the Total Environment **402**(1): 51-61.

Djokić, S. S. and R. E. Burrell (1998). "Visual detection of protein adsorption onto electrochemically oxidized aluminum surfaces." Biosensors and Bioelectronics **13**(3–4): 271-278.

Domingos, R. F., M. A. Baalousha, Y. Ju-Nam, M. M. Reid, N. Tufenkji, J. R. Lead, G. G. Leppard and K. J. Wilkinson (2009). "Characterizing Manufactured Nanoparticles in the Environment:

Multimethod Determination of Particle Sizes." Environmental Science & Technology **43**(19): 7277-7284.

Domínguez-Vera, J., N. Gálvez, P. Sánchez, A. Mota, S. Trasobares, J. Hernández and J. Calvino (2007). "Size-Controlled Water-Soluble Ag Nanoparticles." Eur. J. Inorg. Chem. : 4823–4826.

Dondi, F. and M. Martin (2000). Physicochemical measurements and distributions from field-flow fractionation. Field-Flow Fractionation Handbook. M. Schimpf, K. Caldwell and J. C. Giddings. New York, Wiley-Interscience**:** 103.

Doty, R. C., T. R. Tshikhudo, M. Brust and D. G. Fernig (2005). "Extremely stable water-soluble Ag nanoparticles." Chemistry of Materials **17**(18): 4630-4635.

Eccles, J. W. L., U. Bangert, M. Bromfield, P. Christian, A. J. Harvey and P. Thomas (2010). UV-Vis plasmon studies of metal nanoparticles. Electron Microscopy and Analysis Group Conference 2009. R. T. Baker. Bristol, Iop Publishing Ltd. **241**.

Eckelman, M. J. and T. E. Graedel (2007). "Silver emissions and their environmental impacts: A multilevel assessment." Environmental Science & Technology **41**(17): 6283-6289.

El Badawy, A. M., T. P. Luxton, R. G. Silva, K. G. Scheckel, M. T. Suidan and T. M. Tolaymat (2010). "Impact of Environmental Conditions (pH, Ionic Strength, and Electrolyte Type) on the Surface Charge and Aggregation of Silver Nanoparticles Suspensions." Environmental Science & Technology **44**(4): 1260-1266.

El Badawy, A. M., R. G. Silva, B. Morris, K. G. Scheckel, M. T. Suidan and T. M. Tolaymat (2011). "Surface Charge-Dependent Toxicity of Silver Nanoparticles." Environmental Science & Technology **45**(1): 283-287.

Environment_Canada (1996). Biological test method: Acute lethality test using Daphnia spp. Ottawa, Canada, Environment Canada.

EuropeanComission (2011). "Commission recommendation of 18 October 2011 on the definition of nanomaterial." Official Journal of the European Union: 38-40.

Fabrega, J., S. R. Fawcett, J. C. Renshaw and J. R. Lead (2009). "Silver Nanoparticle Impact on Bacterial Growth: Effect of pH, Concentration, and Organic Matter." Environmental Science & Technology **43**(19): 7285-7290.

Fabrega, J., S. N. Luoma, C. R. Tyler, T. S. Galloway and J. R. Lead (2011). "Silver nanoparticles: Behaviour and effects in the aquatic environment." Environment International **37**(2): 517-531.

Fan, F.-R. F. and A. J. Bard (2001). "Chemical, Electrochemical, Gravimetric, and Microscopic Studies on Antimicrobial Silver Films." The Journal of Physical Chemistry B **106**(2): 279-287.

Faraday, M. (1857). "The Bakerian Lecture: Experimental Relations of Gold (and Other Metals) to Light." Philosophical Transactions of the Royal Society of London **147**: 145-181.

Fernandez-Lopez, C., C. Mateo-Mateo, R. A. Alvarez-Puebla, J. Perez-Juste, I. Pastoriza-Santos and L. M. Liz-Marzan (2009). "Highly Controlled Silica Coating of PEG-Capped Metal Nanoparticles and Preparation of SERS-Encoded Particles." Langmuir **25**(24): 13894-13899.

Frens, G. (1973). "Controlled nucleation for the regulation of the particle size in monodispersed gold suspensions." Nat Phys Sci. (241): 20-22.

Fujita, H., M. Izawa and H. Yamazaki (1962). "Gamma-Ray-induced Formation of Gold Sol from Chloroauric Acid Solution." Nature **196**(4855): 666 - 667.

Gai, P. L., M. J. Goringe and J. C. Barry (1986). "HREM Image-contrast from supported small metal particles." Journal of Microscopy-Oxford **142**: 9-24.

Gaiser, B. K., A. Biswas, P. Rosenkranz, M. A. Jepson, J. R. Lead, V. Stone, C. R. Tyler and T. F. Fernandes (2011). "Effects of silver and cerium dioxide micro- and nano-sized particles on Daphnia magna." Journal of Environmental Monitoring **13**(5): 1227-1235.

Gao, J., S. Youn, A. Hovsepyan, V. L. Llaneza, Y. Wang, G. Bitton and J. C. J. Bonzongo (2009). "Dispersion and Toxicity of Selected Manufactured Nanomaterials in Natural River Water Samples: Effects of Water Chemical Composition." Environmental Science & Technology **43**(9): 3322-3328.

García-Barrasa, J., J. López-de-Luzuriaga and M. Monge (2011). "Silver nanoparticles: synthesis through chemical methods in solution and biomedical applications." Central European Journal of Chemistry **9**(1): 7-19.

Ghosh, S. K. and T. Pal (2007). "Interparticle coupling effect on the surface plasmon resonance of gold nanoparticles: From theory to applications." Chemical Reviews **107**(11): 4797-4862.

Giddings, J. C. (1993). "Field-Flow Fractionation: Analysis of Macromolecular, Colloidal, and Particulate Materials." Science **260**(5113): 1456-1465.

Glavee, G. N., K. J. Klabunde, C. M. Sorensen and G. C. Hadjapanayis (1992). "Borohydride Reductions of Metal Ions. A New Understanding of the Chemistry Leading to Nanoscale Particles of Metals, Borides, and Metal Borates." Langmuir **8**(3): 771-773.

Goodwin, J. (2004). Colloids and interfaces with surfactants and polymers; an introduction., John Wiley and Sons Ltd.

Gottschalk, F., T. Sonderer, R. W. Scholz and B. Nowack (2009). "Modeled Environmental Concentrations of Engineered Nanomaterials (TiO2, ZnO, Ag, CNT, Fullerenes) for Different Regions." Environmental Science & Technology **43**(24): 9216-9222.

Gottschalk, F., T. Sonderer, R. W. Scholz and B. Nowack (2010). " Possibilities and limitations of modeling environmental exposure to engineered nanomaterials by probabilistic material flow analysis " Environmental Toxicology and Chemistry **29**(5): 1036-1048.

Griffitt, R. J., K. Hyndman, N. D. Denslow and D. S. Barber (2009). "Comparison of Molecular and Histological Changes in Zebrafish Gills Exposed to Metallic Nanoparticles." Toxicological Sciences **107**(2): 404-415.

Griffitt, R. J., J. Luo, J. Gao, J. C. Bonzongo and D. S. Barber (2008). "Effects of particle composition and species on toxicity of metallic nanomaterials in aquatic organisms." Environmental Toxicology and Chemistry **27**(9): 1972-1978.

Ha, Y., O. G. Tsay and D. G. Churchill (2011). "A tutorial and mini-review of the ICP-MS technique for determinations of transition metal ion and main group element concentration in the neurodegenerative and brain sciences." Monatshefte Fur Chemie **142**(4): 385-398.

Hagendorfer, H., C. Lorenz, R. Kaegi, B. Sinnet, R. Gehrig, N. V. Goetz, M. Scheringer, C. Ludwig and A. Ulrich (2010). "Size-fractionated characterization and quantification of nanoparticle release rates from a consumer spray product containing engineered nanoparticles." Journal of Nanoparticle Research **12**(7): 2481-2494.

Haick, H. (2007). "Chemical sensors based on molecularly modified metallic nanoparticles." Journal of Physics D-Applied Physics **40**(23): 7173-7186.

Hamilton, M. A., R. C. Russo and R. V. Thurston (1977). "Trimmed Spearman-Karber method for estimating median lethal concentrations in toxicity bioassays." Environmental Science & Technology **11**(7): 714-719.

Handy, R. D., F. von der Kammer, J. R. Lead, M. Hassellov, R. Owen and M. Crane (2008). "The ecotoxicology and chemistry of manufactured nanoparticles." Ecotoxicology **17**(4): 287-314.

Hannink, R. H. J. and A. J. Hill (2006). Nanostructure control of materials. Cambridge, England, Woodhead publishing limited.

Hassellöv, M. and R. Kaegi (2009). Analysis and Characterization of Manufactured Nanoparticles in Aquatic Environments. Environmental and Human Health Impacts of Nanotechnology, John Wiley & Sons, Ltd**:** 211-266.

Helland, Å. (2004). Nanoparticles: A Closer Look at the Risks to Human Health and the Environment. Lund, Sweden Lund University. **Master of Science in Environmental Management and Policy:** 105.

Henglein, A. (1993). "Physicochemical properties of small metal particles in solution: "microelectrode" reactions, chemisorption, composite metal particles, and the atom-to-metal transition." The Journal of Physical Chemistry **97**(21): 5457-5471.

Henglein, A. and M. Giersig (1999). "Formation of colloidal silver nanoparticles: Capping action of citrate." Journal of Physical Chemistry B **103**(44): 9533-9539.

Henglein, A. and D. Meisel (1998). "Radiolytic control of the size of colloidal gold nanoparticles." Langmuir **14**(26): 7392-7396.

Henry, T. B., F. M. Menn, J. T. Fleming, J. Wilgus, R. N. Compton and G. S. Sayler (2007). "Attributing effects of aqueous C-60 nano-aggregates to tetrahydrofuran decomposition products in larval zebrafish by assessment of gene expression." Environmental Health Perspectives **115**(7): 1059-1065.

Hitchman, A. (2011). The transport of manufactured nanoparticles within the hyporheic zone. Birmingham, University of Birmingham. **PhD:** 203.

Hoppe, C. E., M. Lazzari, I. Pardinas-Blanco and M. A. Lopez-Quintela (2006). "One-step synthesis of gold and silver hydrosols using poly(N-vinyl-2-pyrrolidone) as a reducing agent." Langmuir **22**(16): 7027-7034.

Hosokawa, M. (2007). Nanoparticle Technology Handbook, Elsevier.

Huang, H. H., X. P. Ni, G. L. Loy, C. H. Chew, K. L. Tan, F. C. Loh, J. F. Deng and G. Q. Xu (1996). "Photochemical formation of silver nanoparticles in poly(N-vinylpyrrolidone)." Langmuir **12**(4): 909-912.

Huang, T. and X. H. N. Xu (2010). "Synthesis and characterization of tunable rainbow colored colloidal silver nanoparticles using single-nanoparticle plasmonic microscopy and spectroscopy." Journal of Materials Chemistry **20**(44): 9867-9876.

Hugo, W. B. and A. D. Russell (1982). Types of antimicrobial agents. . Principles and Practice of Disinfection, Preservation and Sterilisation. . A. D. Russell, W. B. Hugo and G. A. J. Ayliffe. Oxford, UK, Blackwell Scientific

Hussain, I., M. Brust, A. J. Papworth and A. I. Cooper (2003). "Preparation of acrylate-stabilized gold and silver hydrosols and gold-polymer composite films." Langmuir **19**(11): 4831-4835.

Huynh, K. A. and K. L. Chen (2011). "Aggregation Kinetics of Citrate and Polyvinylpyrrolidone Coated Silver Nanoparticles in Monovalent and Divalent Electrolyte Solutions." Environmental Science & Technology **45**(13): 5564-5571.

Jana, N. R., L. Gearheart and C. J. Murphy (2001). "Wet chemical synthesis of silver nanorods and nanowires of controllable aspect ratio." Chemical Communications(7): 617-618.

Jarvie, H. P., H. Al-Obaidi, S. M. King, M. J. Bowes, M. J. Lawrence, A. F. Drake, M. A. Green and P. J. Dobson (2009). "Fate of Silica Nanoparticles in Simulated Primary Wastewater Treatment." Environmental Science & Technology **43**(22): 8622-8628.

Jarvie, H. P. and S. M. King (2010). "Just scratching the surface? New techniques show how surface functionality of nanoparticles influences their environmental fate." Nano Today **5**(4): 248-250.

Jiang, J. K., G. Oberdorster and P. Biswas (2009). "Characterization of size, surface charge, and agglomeration state of nanoparticle dispersions for toxicological studies." Journal of Nanoparticle Research **11**(1): 77-89.

Johnson, A. C., M. J. Bowes, A. Crossley, H. P. Jarvie, K. Jurkschat, M. D. Jurgens, A. J. Lawlor, B. Park, P. Rowland, D. Spurgeon, C. Svendsen, I. P. Thompson, R. J. Barnes, R. J. Williams and N. Xu (2011). "An assessment of the fate, behaviour and environmental risk associated with sunscreen TiO(2) nanoparticles in UK field scenarios." Science of the Total Environment **409**(13): 2503-2510.

Ju-Nam, Y. and J. Lead (2008). "Manufactured nanoparticles: An overview of their chemistry, interactions and potential environmental implications. ." Sci. Total Environ. **400**: 396-414.

Kaegi, R., B. Sinnet, S. Zuleeg, H. Hagendorfer, E. Mueller, R. Vonbank, M. Boller and M. Burkhardt (2010). "Release of silver nanoparticles from outdoor facades." Environmental Pollution **158**(9): 2900-2905.

Kaegi, R., A. Ulrich, B. Sinnet, R. Vonbank, A. Wichser, S. Zuleeg, H. Simmler, S. Brunner, H. Vonmont, M. Burkhardt and M. Boller (2008). "Synthetic TiO2 nanoparticle emission from exterior facades into the aquatic environment." Environmental Pollution **156**(2): 233-239.

Kanzer, J., S. Hupfeld, T. Vasskog, I. Tho, P. Holig, M. Magerlein, G. Fricker and M. Brandl (2010). "In situ formation of nanoparticles upon dispersion of melt extrudate formulations in aqueous medium assessed by asymmetrical flow field-flow fractionation." Journal of Pharmaceutical and Biomedical Analysis **53**(3): 359-365.

Kelly, K. L., E. Coronado, L. L. Zhao and G. C. Schatz (2003). "The optical properties of metal nanoparticles: The influence of size, shape, and dielectric environment." Journal of Physical Chemistry B **107**(3): 668-677.

Kennedy, A. J., J. C. Gunter, M. A. Chappell, J. D. Goss, M. S. Hull, R. A. Kirgan and J. A. Steevens (2009). "Influence of nanotube preparation in aquatic bioassays." Environmental Toxicology and Chemistry **28**(9): 1930-1938.

Kim, B., C. S. Park, M. Murayama and M. F. Hochella (2010). "Discovery and Characterization of Silver Sulfide Nanoparticles in Final Sewage Sludge Products." Environmental Science & Technology **44**(19): 7509-7514.

Kim, J. S., E. Kuk, K. N. Yu, J. H. Kim, S. J. Park, H. J. Lee, S. H. Kim, Y. K. Park, Y. H. Park, C. Y. Hwang, Y. K. Kim, Y. S. Lee, D. H. Jeong and M. H. Cho (2007). "Antimicrobial effects of silver nanoparticles." Nanomedicine-Nanotechnology Biology and Medicine **3**(1): 95-101.

Kirkland, A. I. and J. L. Hutchison, Eds. (2007). Nanocharacterisation. Cambridge, UK, The Royal Society of Chemistry.

Kittler, S., C. Greulich, J. Diendorf, M. Koller and M. Epple (2010). "Toxicity of Silver Nanoparticles Increases during Storage Because of Slow Dissolution under Release of Silver Ions." Chemistry of Materials **22**(16): 4548-4554.

Klabunde, K. J. and R. M. Richards, Eds. (2009). Nanoscale materials in chemistry. Hoboken, New Jersey, John Wiley & Sons, Inc.,.

Klaine, S. J., P. J. J. Alvarez, G. E. Batley, T. F. Fernandes, R. D. Handy, D. Y. Lyon, S. Mahendra, M. J. McLaughlin and J. R. Lead (2008). "Nanomaterials in the environment: Behavior, fate, bioavailability, and effects." Environmental Toxicology and Chemistry **27**(9): 1825-1851.

Klasen, H. J. (2000). "A historical review of the use of silver in the treatment of burns. II. Renewed interest for silver." Burns **26**(2): 131-138.

Knoll, M. and E. Ruska (1932). "The Electron Microscope." Zeitschrift Fur Physik **78**(5-6): 318-339.

Kretzschmar, R. and T. Schafer (2005). "Metal retention and transport on colloidal particles in the environment." Elements **1**(4): 205-210.

Krystek, P., A. Ulrich, C. C. Garcia, S. Manohar and R. Ritsema (2011). "Application of plasma spectrometry for the analysis of engineered nanoparticles in suspensions and products." Journal of Analytical Atomic Spectrometry **26**(9): 1701-1721.

Kumar, C. S. S. R. (2009). Metallic nanomaterials, Wiley-VCH.

Kumar, R., S. Howdle and H. Munstedt (2005). "Polyamide/silver antimicrobials: Effect of filler types on the silver ion release." Journal of Biomedical Materials Research Part B-Applied Biomaterials **75B**(2): 311-319.

Kuntsche, J., J. C. Horst and H. Bunjes (2011). "Cryogenic transmission electron microscopy (cryo-TEM) for studying the morphology of colloidal drug delivery systems." International Journal of Pharmaceutics **417**(1–2): 120-137.

Kvitek, L., A. Panacek, J. Soukupova, M. Kolar, R. Vecerova, R. Prucek, M. Holecova and R. Zboril (2008). "Effect of surfactants and polymers on stability and antibacterial activity of silver nanoparticles (NPs)." Journal of Physical Chemistry C **112**(15): 5825-5834.

Langheinrich, U. (2003). "Zebrafish: A new model on the pharmaceutical catwalk." BioEssays **25**(9): 904-912.

Lead, J. and E. Smith (2009). Environmental and human health impacts of nanotechnology., Blackwell Publishing: UK.

Lead, J. R. and K. J. Wilkinson (2006). "Aquatic colloids and nanoparticles: Current knowledge and future trends." Environmental Chemistry **3**(3): 159-171.

Lee, C. and T. A. Kramer (2004). "Prediction of three-dimensional fractal dimensions using the two-dimensional properties of fractal aggregates." Advances in Colloid and Interface Science **112**(1-3): 49-57.

Lee, H. Y., H. K. Park, Y. M. Lee, K. Kim and S. B. Park (2007). "A practical procedure for producing silver nanocoated fabric and its antibacterial evaluation for biomedical applications." Chemical Communications(28): 2959-2961.

Lee, P. C. and D. Meisel (1982). "Adsorption and Surface-Enhanced Raman of Dyes on Silver and Gold Sols." Journal of Physical Chemistry **86**(17): 3391-3395.

Levard, C., E. M. Hotze, G. V. Lowry and G. E. Brown (2012). "Environmental Transformations of Silver Nanoparticles: Impact on Stability and Toxicity." Environmental Science & Technology.

Li, T., B. Albee, M. Alemayehu, R. Diaz, L. Ingham, S. Kamal, M. Rodriguez and S. Whaley Bishnoi (2010). "Comparative toxicity study of Ag, Au, and Ag–Au bimetallic nanoparticles on Daphnia magna." Analytical and Bioanalytical Chemistry **398**(2): 689-700.

Li, W. G., Q. X. Jia and H. L. Wang (2006). "Facile synthesis of metal nanoparticles using conducting polymer colloids." Polymer **47**(1): 23-26.

Li, X. and J. J. Lenhart (2012). "Aggregation and Dissolution of Silver Nanoparticles in Natural Surface Water." Environmental Science & Technology **46**(10): 5378-5386.

Li, X., J. J. Lenhart and H. W. Walker (2011). "Aggregation Kinetics and Dissolution of Coated Silver Nanoparticles." Langmuir **28**(2): 1095-1104.

Lienemann, C.-P., A. Heissenberger, G. G. Leppard and D. Perret (1998). "Optimal preparation of water samples for the examination of colloidal material by transmission electron microscopy." Aquatic Microbial Ecology **14**(2): 205-213.

Lin, M. Y., H. M. Lindsay, D. A. Weitz, R. C. Ball, R. Klein and P. Meakin (1990b). "Universal reaction-limited colloid aggregation " Physical Review A **41**(4): 2005-2020.

Lin, M. Y., H. M. Lindsay, D. A. Weitz, R. Klein, R. C. Ball and P. Meakin (1990a). "Universal diffusion-limited colloid aggregation." Journal of Physics-Condensed Matter **2**(13): 3093-3113.

Link, S. and M. A. El-Sayed (2000). "Shape and size dependence of radiative, non-radiative and photothermal properties of gold nanocrystals." International Reviews in Physical Chemistry **19**(3): 409-453.

Liu, Y., B. Liu, D. F. Feng, C. Y. Gao, M. Wu, N. N. He, X. L. Yang, L. Li and X. Z. Feng (2012). "A progressive approach on zebrafish toward sensitive evaluation of nanoparticles' toxicity." Integrative Biology **4**(3): 285-291.

Lok, C.-N., C.-M. Ho, R. Chen, Q.-Y. He, W.-Y. Yu, H. Sun, P. Tam, J.-F. Chiu and C.-M. Che (2007). "Silver nanoparticles: partial oxidation and antibacterial activities." Journal of Biological Inorganic Chemistry **12**(4): 527-534.

Longenberger, L. and G. Mills (1995). "Formation of metal particles in aqueous solutions of polymers and in basic alcohols." Journal of Physical Chemistry **99**(2): 475-478.

Lovern, S. B. and R. Klaper (2006). "Daphnia magna mortality when exposed to titanium dioxide and fullerene (C-60) nanoparticles." Environmental Toxicology and Chemistry **25**(4): 1132-1137.

Lubick, N. (2008). "Nanosilver toxicity: ions, nanoparticies-or both?" Environmental Science & Technology **42**(23): 8617-8617.

Luoma, S. L. (2008). PEN Report. Washington, DC, US, Woodrow Wilson International Center for Scholars and The Pew Charitable Trusts.

MacCuspie, R. I. (2011). "Colloidal stability of silver nanoparticles in biologically relevant conditions." Journal of Nanoparticle Research **13**(7): 2893-2908.

MacCuspie, R. I., A. J. Allen and V. A. Hackley (2011). "Dispersion stabilization of silver nanoparticles in synthetic lung fluid studied under in situ conditions." Nanotoxicology **5**(2): 140-156.

MacCuspie, R. I., K. Rogers, M. Patra, Z. Suo, A. J. Allen, M. N. Martin and V. A. Hackley (2011). "Challenges for physical characterization of silver nanoparticles under pristine and environmentally relevant conditions." Journal of Environmental Monitoring **13**(5): 1212-1226.

Maillard, M., P. R. Huang and L. Brus (2003). "Silver nanodisk growth by surface plasmon enhanced photoreduction of adsorbed Ag+." Nano Letters **3**(11): 1611-1615.

Marks, L. D. and D. J. Smith (1981). "High resolution studies of small particles of gold and silver: I. Multiply-twinned particles." Journal of Crystal Growth **54**(3): 425-432.

Martinez-Castanon, G. A., N. Nino-Martinez, F. Martinez-Gutierrez, J. R. Martinez-Mendoza and F. Ruiz (2008). "Synthesis and antibacterial activity of silver nanoparticles with different sizes." Journal of Nanoparticle Research **10**(8): 1343-1348.

Miao, A. J., K. A. Schwehr, C. Xu, S. J. Zhang, Z. P. Luo, A. Quigg and P. H. Santschi (2009). "The algal toxicity of silver engineered nanoparticles and detoxification by exopolymeric substances." Environmental Pollution **157**(11): 3034-3041.

Mitrano, D. M., E. K. Lesher, A. Bednar, J. Monserud, C. P. Higgins and J. F. Ranville (2012). "Detecting nanoparticulate silver using single-particle inductively coupled plasma-mass spectrometry." Environmental Toxicology and Chemistry **31**(1): 115-121.

Monge, M (2008). "Nanomateriales de plata: propiedades bactericidas." Universidad de Rioja.

Morones, J. R., J. L. Elechiguerra, A. Camacho, K. Holt, J. B. Kouri, J. T. Ramirez and M. J. Yacaman (2005). "The bactericidal effect of silver nanoparticles." Nanotechnology **16**(10): 2346-2353.

Moyer, C. A., L. Brentano, D. L. Gravens, H. W. Margraf and W. W. Monafo (1965). "Treatment of large human burns with 0.5 per cent silver nitrate solution. ." Archives of Surgery **90**(6): 812-&.

Mueller, N. C. and B. Nowack (2008). "Exposure modeling of engineered nanoparticles in the environment." Environmental Science & Technology **42**(12): 4447-4453.

Mukherjee, B. and J. W. Weaver (2010). "Aggregation and Charge Behavior of Metallic and Nonmetallic Nanoparticles in the Presence of Competing Similarly-Charged Inorganic Ions." Environmental Science & Technology **44**(9): 3332-3338.

Nabholz, J. V., R. G. Clements and M. G. Zeeman (1997). "Information needs for risk assessment in EPA's office of pollution prevention and toxics." Ecological Applications **7**(4): 1094-1098.

NanoScale. (2011). "NanoScale. NanoActive Titanium Dioxide. ." from http://www.nanoscalecorp.com/resources/Literature/NanoActive_Titanium_Dioxide.pdf.

Navarro, E., F. Piccapietra, B. Wagner, F. Marconi, R. Kaegi, N. Odzak, L. Sigg and R. Behra (2008). "Toxicity of Silver Nanoparticles to Chlamydomonas reinhardtii." Environmental Science & Technology **42**(23): 8959-8964.

Nowack, B., H. F. Krug and M. Height (2011). "120 Years of Nanosilver History: Implications for Policy Makers." Environmental Science & Technology **45**(4): 1177-1183.

OECD (1998). GuidelinesforTestingofChemicals, No.211 — Daphnia magna Reproduction Test. Paris, Organisation for Economic Cooperation and Development.

OECD (2004). GuidelinesforTestingofChemicals, No.202 — Daphnia magna Reproduction Test. Paris, Organisation for Economic Cooperation and Development.

OECD (2009). Preliminary review of OECD test guidelines for their applicability to manufactured nanomaterials. ENV/JM/MONO. Paris, Organisation for Economic Cooperation and Development. **21:** 1-71.

OECD (2010a). Guidance manual for the testing of manufactured nanomaterials: OECD's sponsorship programme (first revision). . ENV/JM/MONO(2009)20/Rev. Paris, Organisation for Economic Cooperation and Development**:** 1-92.

Pal, S., Y. K. Tak and J. M. Song (2007). "Does the antibacterial activity of silver nanoparticles depend on the shape of the nanoparticle? A study of the gram-negative bacterium Escherichia coli." Applied and Environmental Microbiology **73**(6): 1712-1720.

Perelshtein, I., G. Applerot, N. Perkas, G. Guibert, S. Mikhailov and A. Gedanken (2008). "Sonochemical coating of silver nanoparticles on textile fabrics (nylon, polyester and cotton) and their antibacterial activity." Nanotechnology **19**(24).

Petosa, A. R., D. P. Jaisi, I. R. Quevedo, M. Elimelech and N. Tufenkji (2010). "Aggregation and Deposition of Engineered Nanomaterials in Aquatic Environments: Role of Physicochemical Interactions." Environmental Science & Technology **44**(17): 6532-6549.

Pillai, Z. S. and P. V. Kamat (2004). "What factors control the size and shape of silver nanoparticles in the citrate ion reduction method?" Journal of Physical Chemistry B **108**(3): 945-951.

Poda, A. R., A. J. Bednar, A. J. Kennedy, A. Harmon, M. Hull, D. M. Mitrano, J. F. Ranville and J. Steevens (2011). "Characterization of silver nanoparticles using flow-field flow fractionation interfaced to inductively coupled plasma mass spectrometry." Journal of Chromatography A **1218**(27): 4219-4225.

Poole, C. and F. Owens (2003). Introduction to Nanotechnology. Hoboken, Wiley-Interscience.

Popa, M., T. Pradell, D. Crespo and J. M. Calderon-Moreno (2007). "Stable silver colloidal dispersions using short chain polyethylene glycol." Colloids and Surfaces a-Physicochemical and Engineering Aspects **303**(3): 184-190.

Powers, C. M., T. A. Slotkin, F. J. Seidler, A. R. Badireddy and S. Padilla (2011). "Silver nanoparticles alter zebrafish development and larval behavior: Distinct roles for particle size, coating and composition." Neurotoxicology and Teratology **33**(6): 708-714.

PROSPECT. (2010). "Interim Report for Ecotoxicology testing of Manufactured ZnO and CeO2 Nanoparticles. ." 2012, from http://www.nanotechia-prospect.org/publications/basic.

PSIA (2002). XE-100 user manual.

Reinfelder, J. R. and S. I. Chang (1999). "Speciation and microalgal bioavailability of inorganic silver." Environmental Science & Technology **33**(11): 1860-1863.

Renwick, L. C., K. Donaldson and A. Clouter (2001). "Impairment of alveolar macrophage phagocytosis by ultrafine particles." Toxicology and Applied Pharmacology **172**(2): 119-127.

Rizzi, F. R., S. Stoll, N. Senesi and J. Buffle (2004). "A transmission electron microscopy study of the fractal properties and aggregation processes of humic acids." Soil Science **169**(11): 765-775.

Roh, J.-y., S. J. Sim, J. Yi, K. Park, K. H. Chung, D.-y. Ryu and J. Choi (2009). "Ecotoxicity of Silver Nanoparticles on the Soil Nematode Caenorhabditis elegans Using Functional Ecotoxicogenomics." Environmental Science & Technology **43**(10): 3933-3940.

Römer, I., T. A. White, M. Baalousha, K. Chipman, M. R. Viant and J. R. Lead (2011). "Aggregation and dispersion of silver nanoparticles in exposure media for aquatic toxicity tests." Journal of Chromatography A **1218**(27): 4226-4233.

Rosenkranz, P., Q. Chaudhry, V. Stone and T. F. Fernandes (2009). "A comparison of nanoparticle and fine particle uptake by Daphnia magna." Environmental Toxicology and Chemistry **28**(10): 2142-2149.

Rotello, V. (2003). Nanoparticles: Building Blocks for Nanotechnology. New York, Springer.

Ruden, C. and S. O. Hansson (2010). "Registration, Evaluation, and Authorization of Chemicals (REACH) Is but the First Step-How Far Will It Take Us? Six Further Steps to Improve the European Chemicals Legislation." Environmental Health Perspectives **118**(1): 6-10.

Rujitanaroj, P. O., N. Pimpha, P. Supaphol and Ieee (2007). Preparation of ultrafine poly(ethylene oxide)/poly(ethylene glycol) fibers containing silver nanoparticles as antibacterial coating. New York, Ieee.

Ruozi, B., G. Tosi, E. Leo and M. A. Vandelli (2007). "Application of atomic force microscopy to characterize liposomes as drug and gene carriers." Talanta **73**(1): 12-22.

Scheffer, A., C. Engelhard, M. Sperling and W. Buscher (2008). "ICP-MS as a new tool for the determination of gold nanoparticles in bioanalytical applications." Analytical and Bioanalytical Chemistry **390**(1): 249-252.

Schimpf, M., K. Caldwell and J. C. Giddings (2000). Field-Flow Fractionation Handbook. New York, Wiley-Interscience.

Scown, T. M., E. M. Santos, B. D. Johnston, B. Gaiser, M. Baalousha, S. Mitov, J. R. Lead, V. Stone, T. F. Fernandes, M. Jepson, R. van Aerle and C. R. Tyler (2010). "Effects of Aqueous Exposure to Silver Nanoparticles of Different Sizes in Rainbow Trout." Toxicological Sciences **115**(2): 521-534.

Shaw, B. J. and R. D. Handy (2011). "Physiological effects of nanoparticles on fish: A comparison of nanometals versus metal ions." Environment International **37**(6): 1083-1097.

Shkilnyy, A., M. Souce, P. Dubois, F. Warmont, M. L. Saboungi and I. Chourpa (2009). "Poly(ethylene glycol)-stabilized silver nanoparticles for bioanalytical applications of SERS spectroscopy." Analyst **134**(9): 1868-1872.

Silvert, P. Y., R. HerreraUrbina, N. Duvauchelle, V. Vijayakrishnan and K. T. Elhsissen (1996). "Preparation of colloidal silver dispersions by the polyol process .1. Synthesis and characterization." Journal of Materials Chemistry **6**(4): 573-577.

Silvert, P. Y., R. HerreraUrbina and K. TekaiaElhsissen (1997). "Preparation of colloidal silver dispersions by the polyol process .2. Mechanism of particle formation." Journal of Materials Chemistry **7**(2): 293-299.

Simkiss, K. (1990). "Surface effects in ecotoxicology." Functional Ecology **4**(3): 303-308.

Som, C., M. Berges, Q. Chaudhry, M. Dusinska, T. F. Fernandes, S. I. Olsen and B. Nowack (2010). "The importance of life cycle concepts for the development of safe nanoproducts." Toxicology **269**(2-3): 160-169.

Sondi, I. and B. Salopek-Sondi (2004). "Silver nanoparticles as antimicrobial agent: a case study on E-coli as a model for Gram-negative bacteria." Journal of Colloid and Interface Science **275**(1): 177-182.

Stebounova, L., E. Guio and V. Grassian (2011). "Silver nanoparticles in simulated biological media: a study of aggregation, sedimentation, and dissolution." Journal of Nanoparticle Research **13**(1): 233-244.

Stirred_Ultrafiltration_Cells_User_Guide (2008). Stirred Ultrafiltration Cells. Models 8003, 8010, 8050, 8200, 8400. User Guide.

Stolpe, B. and M. Hassellov (2007). "Changes in size distribution of fresh water nanoscale colloidal matter and associated elements on mixing with seawater." Geochimica Et Cosmochimica Acta **71**(13): 3292-3301.

Stone, V., B. Nowack, A. Baun, N. van den Brink, F. von der Kammer, M. Dusinska, R. Handy, S. Hankin, M. Hassellov, E. Joner and T. F. Fernandes (2010). "Nanomaterials for environmental studies: Classification, reference material issues, and strategies for physico-chemical characterisation." Science of the Total Environment **408**(7): 1745-1754.

Sun, Y. and Y. Xia (2002). "Shape-Controlled Synthesis of Gold and Silver Nanoparticles." Science **298**(5601): 2176-2179.

Taylor, N. S., R. J. M. Weber, A. D. Southam, T. G. Payne, O. Hrydziuszko, T. N. Arvanitis and M. R. Viant (2009). "A new approach to toxicity testing in Daphnia magna: application of high throughput FT-ICR mass spectrometry metabolomics." Metabolomics **5**(1): 44-58.

Tejamaya, M., I. Römer, R. C. Merrifield and J. R. Lead (2012). "Stability of Citrate, PVP, and PEG Coated Silver Nanoparticles in Ecotoxicology Media." Environmental Science & Technology.

Tian, N., Z.-Y. Zhou and S.-G. Sun (2008). "Platinum Metal Catalysts of High-Index Surfaces: From Single-Crystal Planes to Electrochemically Shape-Controlled Nanoparticles." The Journal of Physical Chemistry C **112**(50): 19801-19817.

Tielemans, M., P. Roose, P. De Groote and J. C. Vanovervelt (2006). "Colloidal stability of surfactant-free radiation curable polyurethane dispersions." Progress in Organic Coatings **55**(2): 128-136.

Tumer, Y. T. A., C. J. Roberts and M. C. Davies (2007). "Scanning probe microscopy in the field of drug delivery." Advanced Drug Delivery Reviews **59**(14): 1453-1473.

Turkevich, J., P. Stevenson and J. Hillier (1951). "A study of the nucleation and growth processes in the synthesis of colloidal gold." Discuss. Faraday. Soc. **11**: 55-75.

Turner, A., D. Brice and M. T. Brown (2012). "Interactions of silver nanoparticles with the marine macroalga, Ulva lactuca." Ecotoxicology **21**(1): 148-154.

USEPA (2002). Methods for measuring the acute toxicity of effluents and receiving waters to freshwater and marine organisms. Washington, DC, U.S. Environmental Protection Agency**:** 266.

Wang, Z. L. (2000). "Transmission Electron Microscopy of Shape-Controlled Nanocrystals and Their Assemblies." The Journal of Physical Chemistry B **104**(6): 1153-1175.

Ward, J. E. and D. J. Kach (2009). "Marine aggregates facilitate ingestion of nanoparticles by suspension-feeding bivalves." Marine Environmental Research **68**(3): 137-142.

Wijnhoven, S. W. P., W. Peijnenburg, C. A. Herberts, W. I. Hagens, A. G. Oomen, E. H. W. Heugens, B. Roszek, J. Bisschops, I. Gosens, D. Van de Meent, S. Dekkers, W. H. De Jong, M. Van Zijverden, A. Sips and R. E. Geertsma (2009). "Nano-silver - a review of available data and

knowledge gaps in human and environmental risk assessment." Nanotoxicology **3**(2): 109-U178.

Wilenzick, R., D. Russell, R. Morriss and S. Marshall (1967). "Uniform micro-crystals of platinum and gold." J. Chem. Phys. **47**(2): 533-536.

Wiley, B., Y. G. Sun, B. Mayers and Y. N. Xia (2005). "Shape-controlled synthesis of metal nanostructures: The case of silver." Chemistry-a European Journal **11**(2): 454-463.

Williams, D. B. and C. B. Carter (1996). Transmission Electron Microscopy. A textbook for materals science. . New York, Springer

Williams, S. K. R., J. R. Runyon and A. A. Ashames (2010). "Field-Flow Fractionation: Addressing the Nano Challenge." Analytical Chemistry **83**(3): 634-642.

Willis, R. C. (2002). "When size matters " Today's Chemist at work 21-23.

Woodrow_Wilson_database. (2011). Retrieved September 2011, 2011, from http://www.nanotechproject.org/inventories/consumer/analysis_draft/.

Wu, Y. A., Q. F. Zhou, H. C. Li, W. Liu, T. Wang and G. B. Jiang (2010). "Effects of silver nanoparticles on the development and histopathology biomarkers of Japanese medaka (Oryzias latipes) using the partial-life test." Aquatic Toxicology **100**(2): 160-167.

Wurl, O. and J. P. Obbard (2004). "A review of pollutants in the sea-surface microlayer (SML): a unique habitat for marine organisms." Marine Pollution Bulletin **48**(11–12): 1016-1030.

Wyatt, P. J. (1998). "Submicrometer Particle Sizing by Multiangle Light Scattering following Fractionation." Journal of Colloid and Interface Science **197**(1): 9-20.

Xia, Y., Y. J. Xiong, B. Lim and S. E. Skrabalak (2009). "Shape-Controlled Synthesis of Metal Nanocrystals: Simple Chemistry Meets Complex Physics?" Angewandte Chemie-International Edition **48**(1): 60-103.

Xiu, Z.-M., J. Ma and P. J. J. Alvarez (2011). "Differential Effect of Common Ligands and Molecular Oxygen on Antimicrobial Activity of Silver Nanoparticles versus Silver Ions." Environmental Science & Technology **45**(20): 9003-9008.

Yang, J., Q. Zhang, J. Y. Lee and H.-P. Too (2007). "Dissolution-recrystallization mechanism for the conversion of silver nanospheres to triangular nanoplates." Journal of Colloid and Interface Science **308**(1): 157-161.

Yang, K., D. Lin and B. Xing (2009). "Interactions of Humic Acid with Nanosized Inorganic Oxides." Langmuir **25**(6): 3571-3576.

Yang, X., A. P. Gondikas, S. M. Marinakos, M. Auffan, J. Liu, H. Hsu-Kim and J. N. Meyer (2011). "Mechanism of Silver Nanoparticle Toxicity Is Dependent on Dissolved Silver and Surface Coating in Caenorhabditis elegans." Environmental Science & Technology **46**(2): 1119-1127.

Yeo, M. K. and S. W. Pak (2008b). "Exposing Zebrafish to Silver Nanoparticles during Caudal Fin Regeneration Disrupts Caudal Fin Growth and p53 Signaling." Molecular & Cellular Toxicology **4**(4): 311-317.

Yeo, M. K. and J. W. Yoon (2009). "Comparison of the Effects of Nano-silver Antibacterial Coatings and Silver Ions on Zebrafish Embryogenesis." Molecular & Cellular Toxicology **5**(1): 23-31.

Zetasizer-manual (2003-2004). Zetasizer nano series user manual, Malvern Instruments Ltd.

Zhang, W., Y. Yao, N. Sullivan and Y. S. Chen (2011). "Modeling the Primary Size Effects of Citrate-Coated Silver Nanoparticles on Their Ion Release Kinetics." Environmental Science & Technology **45**(10): 4422-4428.

Zhao, C.-M. and W.-X. Wang (2012). "Importance of surface coatings and soluble silver in silver nanoparticles toxicity to Daphnia magna." Nanotoxicology **6**(4): 361-370.

Zhao, C. M. and W. X. Wang (2011). "Comparison of acute and chronic toxicity of silver nanoparticles and silver nitrate to Daphnia magna." Environmental Toxicology and Chemistry **30**(4): 885-892.

Zhao, C. M. and W. X. Wang (2012). "Importance of surface coatings and soluble silver in silver nanoparticles toxicity to Daphnia magna." Nanotoxicology **6**(4): 361-370.

APPENDIX A

Additional results

CD Rom

APPENDIX B

Published work

Published papers:

- Tejamaya, M; **Römer, I**; Merrifield, R. C; Lead, J. R. Stability of citrate, PVP and PEG coated silver nanoparticles in ecotoxicology media, *Environ. Sci. & Tech*. (2012).

- Römer, I; Pettitt M.E. and Lead J.R. Environmental fate and transport of nanoparticles. Encyclopedia of Environmetrics. 2012 (in press).

- Pettitt M.E.; **Römer, I** and Lead J.R. Nanoparticles, Environmental effects. Encyclopedia of Environmetrics. 2012 (in press).

- **Römer, I**.; White T.A.; Baalousha M; Chipman K; Viant M.R.; Lead J.R. Aggregation and dispersion of silver nanoparticles in exposure media for aquatic toxicity tests*, J. Chrom. A*, 2011, 1228 (27), 4226-4233.

Journal of Chromatography A, 1218 (2011) 4226–4233

Contents lists available at ScienceDirect

Journal of Chromatography A

journal homepage: www.elsevier.com/locate/chroma

Aggregation and dispersion of silver nanoparticles in exposure media for aquatic toxicity tests

Isabella Römer[a], Thomas A. White[b], Mohammed Baalousha[a], Kevin Chipman[b], Mark R. Viant[b], Jamie R. Lead[a,*]

[a] School of Geography Earth, and Environmental Sciences, University of Birmingham, Edgbaston, Birmingham B15 2TT, UK
[b] School of Biosciences, University of Birmingham, Edgbaston, Birmingham B15 2TT, UK

ARTICLE INFO

Article history:
Available online 24 March 2011

Keywords:
Flow field-flow fractionation
FFF
Daphnia magna
Nanomaterial
Nanoscience

ABSTRACT

Silver nanoparticles (AgNPs) are currently being very widely used in industry, mainly because of their anti-bacterial properties, with applications in many areas. Once released into the environment, the mobility, bioavailability, and toxicity of AgNPs in any ecosystem are dominated by colloidal stability. There have been studies on the stability or the aggregation of various nanoparticles (NPs) under a range of environmental conditions, but there is little information on fully characterised AgNPs in media used in (eco)toxicity studies. In this study, monodisperse 7, 10 and 20 nm citrate-stabilised AgNPs were synthesised, characterised and then fractionated and sized by flow field-flow fractionation (FFF) and measured with dynamic light scattering (DLS) in different dilutions of the media recommended by OECD for *Daphnia magna* (water flea) toxicity testing. Stability of NPs was assessed over 24 h, and less so over 21 days, similar time periods to the OECD acute and chronic toxicity tests for *D. magna*. All particles aggregated quickly in the media with high ionic strength (media1), resulting in a loss of colour from the solution. The size of particles could be measured by DLS in most cases after 24 h, although a fractogram by FFF could not be obtained due to aggregation and polydispersity of the sample. After diluting the media by a factor of 2, 5 or 10, aggregation was reduced, although the smallest NPs were unstable under all media conditions. Media diluted up to 10-fold in the absence of AgNPs did not induce any loss of mobility or fecundity in *D. magna*. These results confirm that standard OECD media causes aggregation of AgNPs, which result in changes in organism exposure levels and the nature of the exposed particles compared to exposure to fully dispersed particles. Setting aside questions of dose metrics, significant and substantial reduction in concentration over exposure period suggests that literature data are in the main improperly interpreted and nanoparticles are likely to have far greater biological effects than suggested thus far by poorly controlled exposures. We recommend that the standard OECD media is diluted by a factor of ca. 10 for use with these NPs and this test media, which reduces AgNP aggregation without affecting the viability of the text organism.

1. Introduction

Nanoparticles (NPs) are usually defined as those particles that have at least one dimension between 1 and 100 nm in size [1,2]. Metal NPs are easily prepared by traditional aqueous synthesis routes and can be chemically modified by a variety of capping agents providing monodisperse, high purity NPs suitable for (eco)toxicological studies [3]. Silver nanoparticles (AgNPs) are very widely used currently in industry [1], mainly because of their anti-bacterial properties, with applications in cosmetics and as bacteriocides in fabrics and other consumer products [2,4–6]. This increasing popularity means that these particles are currently being released to the environment [7,8] and their toxicity must be assessed. They have been shown to be toxic to microbes and invertebrates although somewhat less so to fish and humans [9].

Once released into the environment, the mobility, bioavailability, and toxicity of AgNPs are dominated by their colloidal stability [10]. Many factors can affect colloidal stability, including the type of capping agent, the local environmental conditions, such as pH, ionic strength, and the background electrolyte composition [11–14]. There have been a number of studies on the stability or the aggregation of various NPs under a range of environmental conditions [1,10], but there is little information on AgNPs [10,12,15,16] and almost none investigating the impacts of ecotoxicological exposure media on stability.

* Corresponding author. Tel.: +44 121 414 8147.
E-mail address: j.r.lead@bham.ac.uk (J.R. Lead).

0021-9673/$ – see front matter © 2011 Elsevier B.V. All rights reserved.
doi:10.1016/j.chroma.2011.03.034

Environmental Science & Technology

Article

pubs.acs.org/est

Stability of Citrate, PVP, and PEG Coated Silver Nanoparticles in Ecotoxicology Media

Mila Tejamaya,[†,‡] Isabella Römer,[†] Ruth C. Merrifield,[†] and Jamie R. Lead*[†]

[†]School of Geography, Earth and Environmental Sciences, University of Birmingham, Edgbaston, Birmingham, B15 2TT United Kingdom

[‡]School of Public Health, University of Indonesia, Kampus Baru UI Depok 16424, Jawa Barat, Indonesia

Supporting Information

ABSTRACT: Silver nanoparticles (AgNPs) are present in the environment and a number of ecotoxicology studies have shown that AgNPs might be highly toxic. Nevertheless, there are little data on their stability in toxicology media. This is an important issue as such dynamic changes affect exposure dose and the nature of the toxicant studied and have a direct impact on all (eco)toxicology data. In this study, monodisperse citrate, PVP, and PEG coated AgNPs with a core size of approximately 10 nm were synthesized and characterized; their behavior was examined in standard OECD media used for *Daphnia* sp. acute and chronic tests (in the absence of Daphnia). Surface plasmon resonance, size, aggregation, and shape were monitored over 21 days, comparable to a chronic exposure period. Charge stabilized particles (citrate) were more unstable than sterically stabilized particles. Replacement of chloride in the media (due to concerns over chloride-silver interactions) with either nitrate or sulfate resulted in increased shape and dissolution changes. PVP-stabilized NPs in a 10-fold diluted OECD media (chloride present) were found to be the most stable, with only small losses in total concentration over 21 days, and no shape, aggregation, or dissolution changes observed and are recommended for exposure studies.

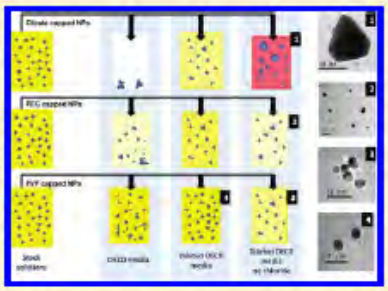

INTRODUCTION

Nanoparticles (NPs) can be defined as material with at least one dimension between 1 and 100 nm[1] or particles with novel properties that differ from its bulk material.[2] NPs have been exploited in many consumer products such as in sunscreens, cosmetics, paint, appliances, computer devices, etc. Currently there are likely to be many thousands of nanoenabled products on the market, and this number is rapidly increasing.[3] Due to their broad range of antimicrobial properties, silver nanoparticles (AgNPs) have become perhaps the most commonly used NP type. The rapid growth in commercialization has increased environmental exposure. For instance, AgNPs can be rapidly released from fabrics by washing and from building facades after rainfall events;[4,5] exposure models have indicated measurable amounts in the environment (with predicted environmental concentration (PEC) in water of tens and perhaps hundreds of ng·L^{-1}).[6]

In addition, AgNPs are potentially toxic both to humans and the environment as has been presented in a number of review papers.[7−10] As with exposure, there are many uncertainties about mechanisms of action, dose measurement, dose−response relationships, and the physicochemical form of the AgNPs during and after exposure in a complex media. In particular, the change in exposure dose and the nature of the toxicant in (eco)toxicological media, due to aggregation, dissolution, shape, and surface chemistry changes, is poorly quantified.[11,12] For AgNPs, there is little information about changes such as aggregation, dissolution, and shape at high ionic strengths and chloride concentrations relevant to such media.

Understanding both the dynamics of exposure concentration changes and the alteration in physicochemical properties of NPs during (eco)toxicology exposures is essential in the interpretation of dose−response relationships. Those changes, which are likely to occur over relevant exposure periods, are poorly accounted for in the literature to date.[13,14] A few studies have shown that aggregation[15,16] and dissolution[17,18] of AgNPs have occurred in toxicology media with consequent changes in bioavailability and toxicity.[8,19] Systematic investigations of temporal changes over exposure are required, and changes may be influenced by factors such as solution chemistry[20,21] and light.[22]

This study examined the influence of media composition and concentration to the AgNPs stability. Three different capping agents which are representative and have been frequently used in other studies[23] were utilized. They are citrate, which stabilizes by charge repulsion[23] and is weakly bound to the

Special Issue: Transformations of Nanoparticles in the Environment

Received: November 2, 2011
Revised: February 8, 2012
Accepted: March 6, 2012

   dx.doi.org/10.1021/es2038396 | Environ. Sci. Technol. XXXX, XXX, XXX−XXX

Posters presented in conferences:

- Römer, I; Wang, Z-W; Merrifield, R; Lead J. R. “Surface analysis of silver nanoparticles after being exposed to environmentally relevant conditions”. Environmental Effects of Nanoparticles and Nanomaterials, London, UK, September 2011. Poster earned 3rd prize in the poster competition.

- **Römer, I**.; White T.A.; Baalousha M; Chipman K; Viant M.R.; Lead J.R. “Aggregation and dispersion of silver nanoparticles in exposure media for aquatic toxicity tests”, 241st National Meeting and Exposition of the American-Chemical-Society (ACS), Anaheim, California, USA, March 2011.

- **Römer, I.**; Lead J. R.; “Synthesis and characterization of silver nanoparticles for fish exposures”, Environmental Effects of Nanoparticles and Nanomaterials, Clemson, South Carolina, USA, August 2010. Earned travel award worth 500$.

- Römer, I.; Lead J. R.; “Synthesis and characterization of silver nanoparticles for fish exposures”, Nanotox 2010, Napier University, Edinburgh, UK, June 2010.

- Römer, I.; Lead J. R.; “Synthesis and characterization of silver nanoparticles for fish exposures”, CEFAS student day, Weymouth, UK, May 2010.

Presentations in conferences:

- Römer, I.; White, T.A.; Gavin, A; Baalousha, M; Wang, Z-W.; Merrifield, R.C.; Chipman, K; Viant, M. R.; Lead, J. R.; “Synthesis and characterisation of silver nanoparticles for ecotoxicology applications”, CEFAS student day, Weymouth, UK, May 2012.

Surface analysis of silver nanoparticles after being exposed to environmentally relevant conditions

Isabella Römer[a], Zhi Wei Wang[b], Ruth Merrifield[a] and Jamie Lead[a]*

a School of Geography, Earth and Environmental Sciences. University of Birmingham, B15 2TT UK. IXR961@bham.ac.uk

a School of Physics and Astronomy, University of Birmingham

INTRODUCTION: Silver nanoparticles (AgNPs) are currently being very widely used in industry, mainly because of their anti-bacterial properties, with applications in many areas [1]. Once released into the environment, the mobility, bioavailability, and toxicity of AgNPs in any ecosystem are dominated by colloidal stability [2]. AgNPs released in wastewater may be converted into Ag^+ ions, complexed with ligands, agglomerated or still be present as nanoparticles [3]. By using HR-STEM and electron energy-loss spectroscopy (EELS) we have assessed the surface changes of citrate stabilized AgNPs prepared in the lab after being exposed to conditions similar to those in the environment, using fulvic acid and the presence of light.

Silver nanoparticles in citrate (as prepared)

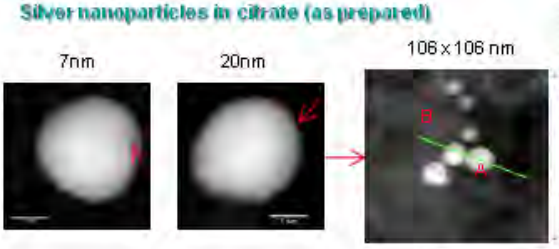

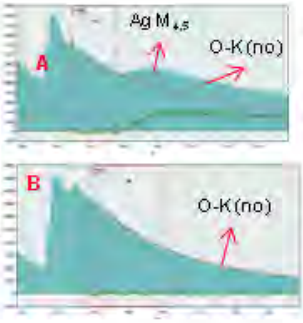

Lattices are still visible in some cases for the 20nm particles. The 7nm particle displays a <110> FCC like structure but with some defects visible in the region marked with the arrow.

No clear O core-loss edge are observed in any of the following cases, (i) when the beam goes through the Ag particles (marked A), and (ii) when the beam passes only through carbon substrate (marked B)

20nm particles + fulvic acid → 24 hours in light

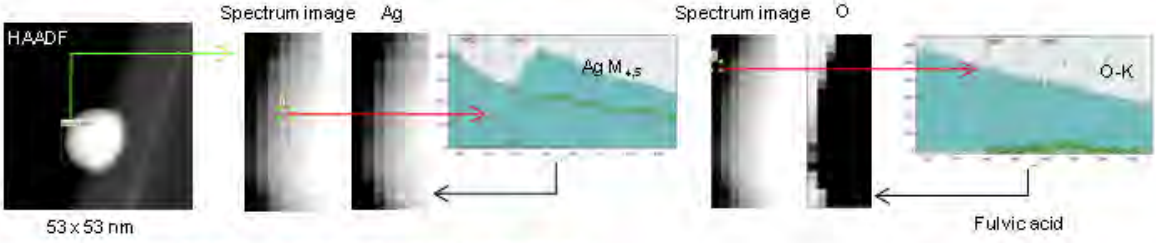

20nm particles + fulvic acid → 2 months and a half in light

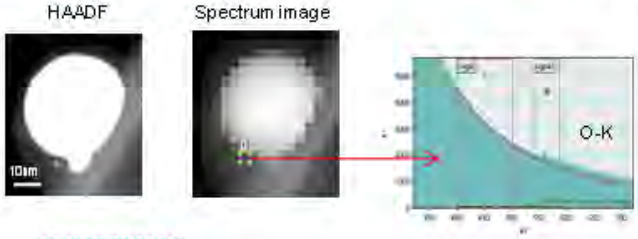

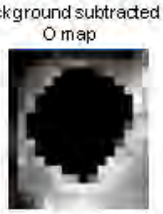

Comparing HAADF and the O map, we can see that the O signal only exists in the shell surrounding the particle.
The Ag signal could also be seen from EELS spectrum and Ag mapping of the particle.

CONCLUSIONS:

Preliminary results show that particles in fulvic acid remain stable and unchanged for months, while citrate coated particles exposed to light change in size and form but show no oxidation. Future work will include other environmentally relevant conditions, such as those similar to sewage treatment.

Citrate–stabilized 20nm particles exposed to light

REFERENCES:

[1] Y.J. Nam, Lead J. Sci. Total Environ. 400 (2008) 396. [2] A. M. El Badawy, T. P. Luxton, R. G. Silva, K. G. Scheckel, M. T. Suidan, T. M. Tolaymat. Environ. Sci. Technol. 44 (2010) 1260. [3] O. Choi, T. E. Clevenger, B. L. Deng, R. Y. Surampalli, L. Ross, Z. Q. Hu, Z. Q. Water Res. 43, 7 (2009) 1879.